Aus dem Adolf-Butenandt-Institut
Lehrstuhl für Stoffwechselbiochemie im Biomedizinischen Centrum der
Ludwig-Maximilians-Universität München
Vorstand: Prof. Dr. rer. nat. Dr. h. c. Christian Haass

Modulation des Progranulin-abhängigen FTLD-Risikos durch TMEM106B

Dissertation
zum Erwerb des Doktorgrades der Naturwissenschaften
an der Medizinischen Fakultät der
Ludwig-Maximilians-Universität zu München

vorgelegt von
Georg Werner
aus
Berlin

2021

Mit Genehmigung der Medizinischen Fakultät
der Universität München

Betreuer:	Prof. Dr. rer. nat. Dr. h.c. Christian Haass
Zweitgutachter(in):	Prof. Dr. rer. nat. Magdalena Götz
Dekan:	Prof. Dr. med. Thomas Gudermann
Tag der mündlichen Prüfung:	14.12.2021

Meinen Eltern

Inhaltsverzeichnis

INHALTSVERZEICHNIS **4**

ABKÜRZUNGSVERZEICHNIS **6**

EIGENE PUBLIKATIONEN **8**

Bestandteil dieser kumulativen Dissertation 8

Weitere Publikationen 8

ZUSAMMENFASSUNG **10**

SUMMARY **12**

I. EINLEITUNG **15**

1 NEURODEGENERATIVE ERKRANKUNGEN **15**

2 FRONTOTEMPORALE DEMENZ **15**

2.1 Die Rolle des RNA/DNA-bindenden Proteins TDP-43 in FTLD **16**

2.2 Funktion und Dysfunktion der Proteindegradation **18**

2.3 Funktion und Dysfunktion von Mikroglia in AD und FTLD **20**

3 FUNKTION UND DYSFUNKTION VON TREM2 ..... **22**

3.1 Mutationen im *TREM2*-Gen in neurodegenerativen Erkrankungen **22**

3.2 TREM2-abhängige Regulation der Aktivität von Mikroglia **22**

3.3 TREM2-abhängige Regulation der Proteindegradation **24**

4 FUNKTION UND DYSFUNKTION VON PROGRANULIN **25**

4.1 Mutationen im *GRN*-Gen in neurodegenerativen Erkrankungen **25**

4.2 Progranulin-abhängige Regulation der Proteindegradation **25**

4.3 Progranulin-abhängige Regulation der Inflammation **28**

5 FUNKTION UND DYSFUNKTION DES TRANSMEMBRANPROTEINS 106B **30**

5.1 Mutationen im *TMEM106B*-Gen in neurodegenerativen Erkrankungen **30**

5.2 TMEM106B-abhängige Regulation der Proteindegradation 32

5.3 TMEM106B-abhängige Regulation der Inflammation 35

II. ZIELSETZUNG DIESER ARBEIT 36

III. MEINE BEITRÄGE ZU DEN PUBLIKATIONEN DIESER KUMULATIVEN DISSERTATION 37

1 BEITRAG ZUR PUBLIKATION I 37

2 BEITRAG ZUR PUBLIKATION II 38

3 BEITRAG ZUR PUBLIKATION III 38

IV. ERGEBNISSE 40

1 PUBLIKATION I 40

2 PUBLIKATION II 66

3 PUBLIKATION III 98

V. LITERATURVERZEICHNIS: 116

DANKSAGUNG 138

CURRICULUM VITAE 140

AFFIDAVIT / EIDESSTATTLICHE VERSICHERUNG 143

Abkürzungsverzeichnis

Abkürzung	Bedeutung	Englischer Ursprung
AD	Alzheimer-Demenz	Alzheimer's disease
ADAM10/17	Desintegrin/Metalloproteinase-Domäne enthaltendes Protein 10 / 17	A disintegrin and metalloproteinase domain-containing protein 10 / 17
ALS	Amyotrophe Lateralsklerose	
APOE	Apolipoprotein E	
APP	Amyloid-Vorläuferprotein	Amyloid precursor protein
ATG	Autophagie	AuTophaGy
ATP	Adenosintriphosphat	
Aβ	Amyloid-β Protein	
bvFTD	Verhaltens-Form der Frontotemporalen Demenz	Behavioral variant FTD
C1QA	Komplement C1Q Untereinheit A	
CHMP2B	Geladenes multivesikuläres Protein 2b	Charged multivesicular body protein 2b
CBS	Kortikobasale Degeneration	Corticobasal syndrom
CD68	Cluster der Differenzierung 68	Cluster of Differentiation 68
CSF	Cerebrospinalflüssigkeit	
DAM	Krankheits-assoziierte Mikroglia	Disease-associated microglia
DAP12	DNAX aktivierendes Protein	DNAX activation protein 12
DNA	Desoxyribonukleinsäure	Deoxyribonucleic acid
EOAD	AD mit frühem Ausbruch	Early onset AD
ER	Endoplasmatischen Retikulum	
EWS	Ewing Sakom	Ewing sarcoma
FAD	Familiäre Form der Alzheimer Demenez	Familial Alzheimer's disease
FDG	Fluordesoxyglucose	Fluoro-2-deoxy-D-glucose
FET	FUS, EWS, und TAF15	
FIG4	Faktor induziertes Gen 4	
FTD	Frontotemporale Demenz	
FTLD	Frontotemporale Lobärdegeneration	
FUS	Fusioniert in Sarkom	Fused in sarcoma
GWAS	Genomweite Assoziationsstudien	Genome wide association studies
HM	Homöostatische-Mikroglia	Homeostatic-microglia
IBA1	Ionisiertes Kalzium-bindendes Adaptermolekül 1	Ionized calcium-binding adapter molecule 1
ITAM	Immunorezeptor mit Tyrosin-basierten Aktivierungsmotiv	Immunoreceptor tyrosine-based activation motif

MAP1LC3 / LC3	Mikrotubuli-assoziiertes Protein der Leichtenkette 3	Microtubule-associated protein light chain 3
LAMP1/2	Lysosomen-assoziiertes Membran-Protein 1/2	Lysosomal-associated membrane protein 1/2
LATE	Limbische altersbedingte TDP-43-Enzephalopathie	Limbic-predominant Age-related TDP-43 Encephalopathy
LOAD	AD mit spätem Beginn	Late onset AD
MAP	Mitogen-aktiviertes Protein	Mitogen-activated protein kinase
MBP	Basisches Myelin-Protein	Myelin basic protein
MMP	Matrix-Metalloproteasen	Matrix metallo proteinase
mRNA	Boten-Ribonukleinsäure	Messenger ribonucleic acid
mTOR	Ziel von Rapamycin	Mammalian target of rapamycin
NLS	Kernlokalisierungssequenz	Nuclear localization sequence
PET	Positronen-Emissions-Tomographie	
PGRN	Progranulin - Protein	
GRN	Progranulin Humanes-*Gen*	
Grn	*Mus-Musculus-Gen*	
PPA	Primär-Progrediente-Aphasien	
PSP	Progressive Supranukleäre Blickparese	
RNA	Ribonukleinsäure	Ribonucleic acid
SAD	Sporadische Form der Alzheimer Demenez	
SNP	Einzelnukleotid-Polymorphismus	Single nucleotide polymorphism
SPPL2a	Signal-Peptid-ähnliche Peptidase-2a	Signal Peptide Peptidase-like 2a
SQSTM1	Sequestosom 1	Sequestosome 1
sTREM2	Geschnittenes, lösliches und sezerniertes TREM2	Soluble TREM2
SYK	Milz-assoziierte Tyrosin-Kinase	Spleen associated tyrosine kinase
TAF-15	TATA-Box-bindendes Protein-assoziierter Faktor 15	TATA-box binding protein associated factor 15
TDP-43	Transaktives Anwort-DNA-Bindungsprotein 43 kDa	Transactive response DNA binding protein 43 kDa
TREM2	Von myeloischen Zellen exprimiert Rezeptor 2	Triggering receptor expressed on myeloid cells 2
TRN1	Transportin 1	
TMEM106B	Transmembranprotein 106 b - Protein	
TMEM106B	TMEM106B Humanes-Gen	
Tmem106b	TMEM106B Mus-Musculus-Gen	
TYROBP	TYRO Protein-Tyrosin-Kinase-bindendes Protein	TYRO protein tyrosine kinase-binding protein
V-ATPase	vakuläre ATPase	
VCP	Valosin-enthaltendes Protein	Valosin-Containing Protein

Eigene Publikationen

Bestandteil dieser kumulativen Dissertation

Loss of TMEM106B potentiates lysosomal and FTLD-like pathology in progranulin-deficient mice.
G. Werner, M. Damme, M. Schludi, J. Gnorich, K. Wind, K. Fellerer, B. Wefers, W. Wurst, D. Edbauer, M. Brendel, C. Haass and A. Capell 2020.
EMBO Reports, 21(10):e50241.

The FTLD Risk Factor TMEM106B Regulates the Transport of Lysosomes at the Axon Initial Segment of Motoneurons.
P. Lüningschrör*, G. Werner*, S. Stroobants, S. Kakuta, B. Dombert, D. Sinske, R. Wanner, R. Lullmann-Rauch, B. Wefers, W. Wurst, R. D'Hooge, Y. Uchiyama, M. Sendtner, C. Haass, P. Saftig, B. Knoll, A. Capell and M. Damme 2020.
Cell Reports, 30(10):3506-3519.e6. * Geteilte Erstautorenschaft

Opposite microglial activation stages upon loss of PGRN or TREM2 result in reduced cerebral glucose metabolism.
J. K. Götzl*, M. Brendel*, G. Werner*, S. Parhizkar, L. S. Monasor, G. Kleinberger, A. V. Colombo, M. Deussing, M. Wagner, J. Winkelmann, J. Diehl-Schmid, J. Levin, K. Fellerer, A. Reifschneider, S. Bultmann, P. Bartenstein, A. Rominger, S. Tahirovic, S. T. Smith, C. Madore, O. Butovsky, A. Capell and C. Haass 2019.
EMBO Molecular Medicine, 11(6):e9711. * Geteilte Erstautorenschaft

Weitere Publikationen

Enhancing protective microglial activities with a dual function TREM2 antibody to the stalk region.
K. Schlepckow, K. M. Monroe, G. Kleinberger, L. Cantuti-Castelvetri, S. Parhizkar, D. Xia, M. Willem, G. Werner, N. Pettkus, B. Brunner, A. Sulzen, B. Nuscher, H. Hampel, X. Xiang, R. Feederle, S. Tahirovic, J. I. Park, R. Prorok, C. Mahon, C. C. Liang, J. Shi, D. J. Kim, H. Sabelstrom, F. Huang, G. Di Paolo, M. Simons, J. W. Lewcock and C. Haass 2020.
EMBO Molecular Medicine, 12(4):e11227.

Poly-glycine-alanine exacerbates C9orf72 repeat expansion-mediated DNA damage via sequestration of phosphorylated ATM and loss of nuclear hnRNPA3.
Y. Nihei, K. Mori, G. Werner, T. Arzberger, Q. Zhou, B. Khosravi, J. Japtok, A. Hermann, A. Sommacal, M. Weber, D. German Consortium for Frontotemporal Lobar, A. Bavarian Brain Banking, F. Kamp, B. Nuscher, D. Edbauer and C. Haass 2020.
Acta Neuropathologica, 139(1):99-118.

Early lysosomal maturation deficits in microglia triggers enhanced lysosomal activity in other brain cells of progranulin knockout mice.
J. K. Götzl, A. V. Colombo, K. Fellerer, A. Reifschneider, G. Werner, S. Tahirovic, C. Haass and A. Capell 2018.
Molecular Neurodegeneration, 13(1):48.

TREM2 deficiency impairs chemotaxis and microglial responses to neuronal injury.
F. Mazaheri, N. Snaidero, G. Kleinberger, C. Madore, A. Daria, G. Werner, S. Krasemann, A. Capell, D. Trumbach, W. Wurst, B. Brunner, S. Bultmann, S. Tahirovic, M. Kerschensteiner, T. Misgeld, O. Butovsky and C. Haass 2017.
EMBO Reports, 18(7):1186-1198.

TREM2 deficiency reduces the efficacy of immunotherapeutic amyloid clearance.
X. Xiang, G. Werner, B. Bohrmann, A. Liesz, F. Mazaheri, A. Capell, R. Feederle, I. Knuesel, G. Kleinberger and C. Haass 2016.
EMBO Molecular Medicine, 8(9):992-1004.

Zusammenfassung

Im Fokus meiner Dissertation stehen die mit Frontotemporaler Demenz (FTD) -assoziierten Proteine Progranulin (PGRN) und Transmembranprotein106b (TMEM106B). Heterozygote Mutationen in dem PGRN-kodierenden Gen (*GRN*), haben eine reduzierte Expression und einen Funktionsverlust zur Folge und führen zur FTD. Pathologische Merkmale der *GRN*-assoziierten FTD sind die Frontotemporale Lobärdegeneration (FTLD) und TDP-43 (engl.: Transactive response DNA binding protein 43 kDa) Aggregate. Einzel-Nukleotid-Polymorphismen (SNP) in *TMEM106B* wurden im Zusammenhang mit *GRN*-Mutationen als Risikofaktor für die Entwicklung der FTD identifiziert. Es war jedoch unklar, ob ein Funktionsverlust, oder eine erhöhte Aktivität von TMEM106B, das Risiko an FTD zu erkranken erhöht.

Um die Funktion von TMEM106B besser zu verstehen, habe ich zunächst *Tmem106b*$^{-/-}$ Mauszelllinien generiert. In diesen Zellen konnte ich beobachten, dass der Funktionsverlust von TMEM106B zu einer generellen Reduktion der lysosomalen Kapazität und damit verbunden zu einem Problem in der Autophagie führt. In einem weiteren Schritt wurde eine *Tmem106b*$^{-/-}$ Mauslinie etabliert und in Zusammenarbeit mit Dr. Markus Damme (Universität Kiel) charakterisiert. Mit Hilfe dieser Mäuse konnte ich bestätigen, dass ein Funktionsverlust von TMEM106B zu einer Beeinträchtigung der lysosomalen Kapazität führt. Interessanterweise wiesen die Motoneuronen dieser Mäuse vergrößerte lysosomale Kompartimente auf. Diese Anhäufung von Vesikeln trat vor allem im Bereich des Axon-Initiationssegments auf. Proteinexpressions-Analysen von Mausgehirnproben ergaben, dass TMEM106B die Maturierung von Cathepsin D beeinflusst und somit auch die Proteindegradation in Lysosomen. Eine Akkumulation der Autophagie-Marker Ubiquitin, p62 und LC3 in diesen Proben deutet darauf hin, dass TMEM106B das Zusammenspiel von Autophagosomen und Lysosomen durch den Transport der Lysosomen reguliert **(Lüningschrör et al., 2020).**

Für das hauptsächlich von Mikroglia-Zellen exprimierte PGRN, war nicht geklärt, ob es die Aktivität der Mikroglia beeinflusst. Daher habe ich in meiner Doktorarbeit Mikroglia-Zellen aus *Grn*$^{-/-}$ Mäusen isoliert und diese auf charakteristische krankheitsassoziierte Mikroglia (DAM) Proteine analysiert. Ich konnte zeigen, dass diese Mikroglia-Zellen eine erhöhte Protein-Expression von CLEC7A, CD68, APOE und TREM2 aufweisen. Diese erhöhte Expression der typischen DAM-Proteine führte zu einer erhöhten Phagozytose-Kapazität in aus *Grn*$^{-/-}$ Mäusen isolierten Mikroglia und in von mir generierten *Grn*$^{-/-}$ Mikroglia-Zelllinien. Es war bekannt, dass der TREM2-Funktionsverlust (engl.: Triggering receptor expressed on myeloid cells 2) zu homöostatischen Mikroglia (HM) führt. Außerdem war beschrieben, dass der TREM2-Funktionsverlust im Mausgehirn eine starke Reduktion im Glukose-Metabolismus, gekennzeichnet durch ein reduziertes Fluordesoxyglucose-Signal (FDG) in der Positronen-Emissions-Tomographie (PET), bewirkt. Überraschenderweise, verursachten auch die hyperaktiven DAM in *Grn*$^{-/-}$ Mäusen eine starke Reduktion des FDG-PET Signals, damit haben sowohl hypo- als auch hyperaktive Mikroglia einen negativen Einfluss auf Neuronen **(Götzl et al., 2019).**

Um zu untersuchen, welchen Effekt die Reduktion der TMEM106B-Level auf die *GRN*-abhängige FTD-Pathologie haben könnte, etablierte ich eine *Grn*$^{-/-}$/*Tmem106b*$^{-/-}$ Mauslinie. Diese charakterisierte ich bezüglich Genexpression, Proteinexpression und Verhaltensauffälligkeiten im Vergleich zu den Wildtyp und Einzel-Defizienten *Grn*$^{-/-}$ und *Tmem106b*$^{-/-}$ Mäusen. Während eine Reduktion der PGRN-Expression, in älteren Tieren, mit einer Hyperaktivierung der Mikroglia einherging, kam es durch den Verlust der TMEM106B-Aktivität zu dem oben beschriebenen, lysosomalen Phänotyp in Neuronen. Bei vier Monaten alten Tieren beobachtete ich sowohl in den *Grn*$^{-/-}$ und als auch in *Tmem106b*$^{-/-}$ Mäusen eine geringe Aktivierung der Mikroglia, gekennzeichnet durch eine erhöhte Expression von TREM2, APOE, C1Q sowie CD68. Der kombinierte Verlust beider Proteine führte zum Auftreten einiger FTLD-TDP Merkmale, wie zum Beispiel zur Phosphorylierung und Aggregation von TDP-43, gepaart mit einer signifikanten Astrogliose und Mikrogliose. Die zusätzliche Akkumulation von p62, LC3 und Ubiquitin deutete auf eine beeinträchtigte Fähigkeit der Proteindegradation in Lysosomen und dem Abbau über das Autophagie-System hin. Die p62 Aggregate waren hauptsächlich in Neuronen und teilweise in Mikroglia lokalisiert. Daraus folgt, dass ein TMEM106B-Funktionsverlust, durch eine gestörte Funktion der Lysosomen und dem Autophagie-System, das *GRN*-abhängige FTD-Risiko erhöht.
Die Hypothese, dass ein Verlust der TMEM106B-Expression einen positiven Effekt auf die *GRN*-abhängige FTD-Pathologie hat, konnte ich widerlegen. Es ist mir gelungen ein FTD-Mausmodell mit prominenter TDP-43 Pathologie zu generieren, welches zusätzlich eine starke Neuroinflammation und Probleme in der Proteindegradation aufweist. (Werner et al., 2020).

Summary

My dissertation focuses on the frontotemporal dementia (FTD) associated proteins progranulin (PGRN) and transmembraneprotein106b (TMEM106B). Mutations in the gene encoding for PGRN (*GRN*), result in reduced expression and lead to FTD. Pathological features of *GRN*-associated FTD include aggregation of TDP-43 (transactive response DNA binding protein 43 kDa) and frontotemporal lobar degeneration (FTLD). Single nucleotide polymorphisms (SNP) in *TMEM106B* have been identified as a risk factor for the development of FTD especially in association with *GRN* mutations. However, it was unclear whether a TMEM106B loss or gain of function, increases the risk of developing FTD. In addition, the physiological function of TMEM106B in vivo has not been clearly elucidated.

In order to get a better understanding of the TMEM106B function, I first generated a mouse cell line with a genetic deletion of TMEM106B expression. I observed that a TMEM106B loss of function leads to a reduction in lysosomal capacity and an impairment in autophagy. To study the function *in vivo*, I established a *Tmem106b*$^{-/-}$ mouse line and characterized it in collaboration with Markus Damme (University of Kiel) and others. Using these mice, I observed that TMEM106B loss of function leads to impaired lysosomal capacity. Interestingly, the motoneurons of these mice exhibited enlarged lysosomal vesicles. This accumulation of vesicles occurred primarily in the axon initiation segment. I discovered that without TMEM106B the maturation of cathepsin D and thus protein degradation in lysosomes might be impaired. The accumulation of the autophagy markers ubiquitin, p62, and LC3 suggests that TMEM106B regulates the interplay of autophagosomes and lysosomes through lysosomal transport **(Lüningschrör et al., 2020).**

For PGRN, which is mainly expressed by microglial cells, it was unclear how it affects microglial activity. Therefore, I isolated microglia cells from *Grn*$^{-/-}$ mice and analyzed them for characteristic proteins of disease-associated microglia (DAM). I observed an increased expression of CLEC7A, CD68, APOE and TREM2 in these microglia. This increased expression of the DAM signature resulted in increased phagocytosis capacity in microglia isolated from *Grn*$^{-/-}$ mice and in *Grn*$^{-/-}$ microglia cell lines generated by me. It was known that the TREM2 (triggering receptor expressed on myeloid cells 2) loss of function leads to homeostatic microglia (HM). Moreover, TREM2 loss of function in mouse brain was described to cause a strong reduction in glucose metabolism, characterized by a reduced FDG (fluoro-2-deoxy-D-glucose) signal in positron emission tomography (PET). Surprisingly, hyperactive DAM in *Grn*$^{-/-}$ mice also caused a strong reduction in FDG-PET signal, thus both hypo- and hyperactive microglia have a negative impact on neurons **(Götzl et al., 2019).**

To investigate the potential effect of reduced TMEM106B expression on the *GRN*-dependent FTD pathology, I established a *Grn*$^{-/-}$/*Tmem106b*$^{-/-}$ mouse line. I characterized this line in respect to gene as well as protein expression, and analyzed behavioral abnormalities in comparison to wild-type and single-deficient mice. While a reduction in PGRN expression led to a hyperactivation of microglia in older animals, loss of TMEM106B activity resulted in the lysosomal phenotype in neurons, mentioned above. In four-month-old animals, I observed low activation of microglia in both *Grn*$^{-/-}$ and *Tmem106b*$^{-/-}$ mice, characterized by increased

expression of TREM2, APOE, C1Q, as well as CD68. The combined loss of both proteins led to the appearance of some FTLD-TDP features, such as phosphorylation and aggregation of TDP-43, coupled with significant astrogliosis and microgliosis. The additional accumulation of p62, LC3, and ubiquitin indicated an impaired capacity for protein degradation in lysosomes and degradation via the autophagy system in neurons and microglia. Therefore, the *GRN*-dependent FTD risk, might be increased due to a TMEM106B loss of function.

I could disprove the hypothesis that complete loss of TMEM106B expression has a positive effect on the *GRN*-dependent FTD pathology. I have succeeded in generating an animal model which recapitulates some features of FTD, such as a prominent TDP-43 pathology, severe neuroinflammation and an impairment in protein degradation (Werner et al., 2020).

I. Einleitung

1 Neurodegenerative Erkrankungen

Weltweit leiden ca. 50 Millionen Menschen an einer Form von Demenz. Ein Großteil davon, etwa 60 bis 70 %, entfällt auf die Alzheimer-Demenz (AD). Eine andere neurodegenerative Erkrankung, die Frontotemporale Demenz (FTD), macht in etwa 10 % aller Demenzerkrankungen aus und ist die zweithäufigste Form von Demenz in der Bevölkerung unter 65 Jahren (Forman et al., 2006, Harvey et al., 2003, Seelaar et al., 2011, Hogan et al., 2016). Eine effektive Behandlung ist im Moment weder für AD noch für FTD möglich. Proteinaggregation, Dysfunktion der Proteindegradation und Neuroinflammation sind krankheitsübergreifende Kennzeichen und Ursache zugleich für diese neurodegenerativen Erkrankungen (Guerreiro et al., 2015, Wong and Holzbaur, 2015, Ferrari et al., 2019).

2 Frontotemporale Demenz

Die Frontotemporale Lobärdegeneration (FTLD) ist eine Pathologie, die eine Familie von neurodegenerativen Erkrankungen vereint, die als FTD bezeichnet wird (Forman et al., 2006, Harvey et al., 2003, Seelaar et al., 2011, Hogan et al., 2016, Neumann and Mackenzie, 2019). FTLD ist gekennzeichnet durch eine Atrophie in großen Bereichen des frontalen und temporalen Lappen des Gehirns und führt zu unterschiedlichsten Verhaltensauffälligkeiten bei den betroffenen Personen (Rosen et al., 2002). Klinische Symptome umfassen progressive Verhaltensänderungen, sprachliche Beeinträchtigungen und motorische Probleme (Rascovsky et al., 2011, Neary et al., 2005). Einstufungen basierend auf dem weitgefächerten, heterogenen Spektrum an Symptomen sind schwierig und wurden bereits mehrfach überarbeitet (Rascovsky et al., 2011, Neary et al., 2005). Grundsätzlich lassen sich klinisch folgende Krankheitsbilder abgrenzen, die jedoch im späteren Krankheitsverlauf überlappen: die Verhaltens-Form der Frontotemporalen Demenz (bvFTD), die Primär-Progrediente-Aphasien (PPA), sowie die motorischen Varianten der Frontotemporalen Demenz, mit den Formen der progressiven supranukleären Blickparese (PSP) und der kortikobasalen Degeneration (CBS) (Olney et al., 2017).

Aufgrund der überlappenden Krankheitsbilder in FTLD Patienten ist eine pathologische Einteilung, basierend auf einer molekularen Klassifizierung sinnvoll (Neumann and Mackenzie, 2019) **Abbildung 1**. In Gehirnen von FTLD-Patienten wurden Ablagerungen mit unterschiedlicher Zusammensetzung festgestellt. Darunter wurden die in **Abbildung 1** dargestellten Proteine identifiziert: Ubiquitin, TDP-43, Tau, C9orf72-DPRs, FET (FUS, EWS, und TAF15) und TRN1 (Petkau and Leavitt, 2014, Neumann and Mackenzie, 2019). Bei etwa 45 % der Patienten ist eine TDP-43 Pathologie vorhanden (FTLD-TDP), gefolgt von einer Tau Pathologie (FTLD-Tau) bei etwas unter 45 % der Patienten. Lediglich in 9 % der Fälle, ist die FUS Pathologie (FTLD-FUS) die bestimmende Komponente, ausschließlich Ubiquitin ist lediglich in 1 % bei *CHMP2B* Mutations-Trägern zu finden (FTLD-UPS) (Petkau and Leavitt, 2014, Ferrari et al., 2019, Neumann and Mackenzie, 2019). Nur durch eine Hirnbiopsie kann abschließend geklärt werden, ob es sich um eine Tau- oder TDP-43 basierte Form der FTLD handelt.

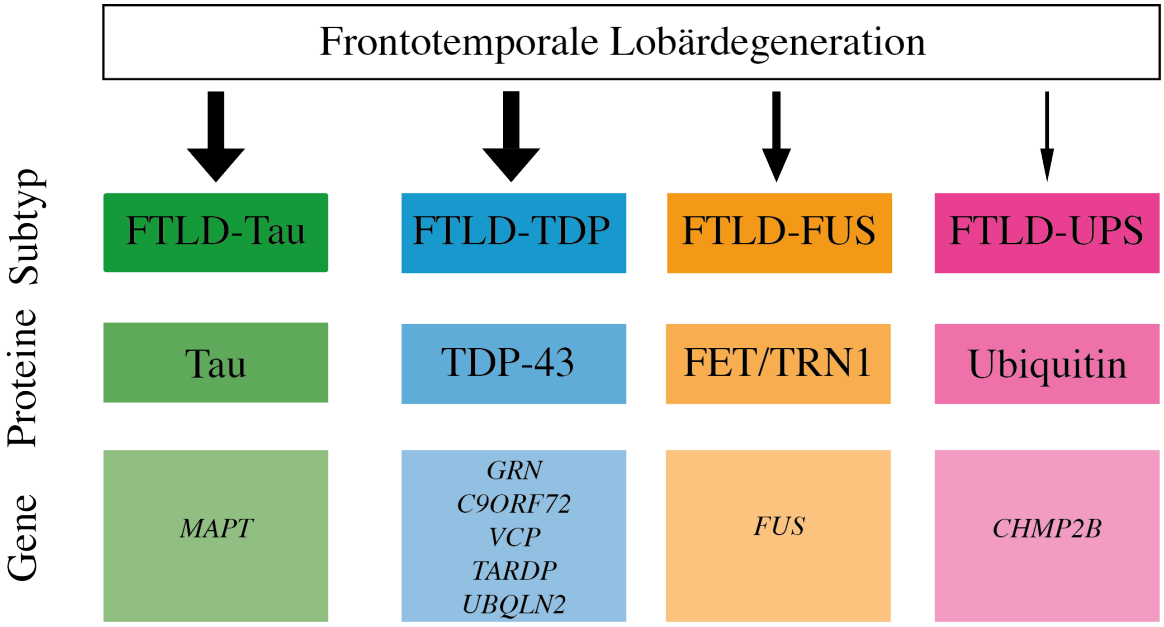

Abbildung 1: Molekulare Einteilung der Subtypen der FTLD. Die neurodegenerative Erkrankung lässt sich basierend auf den aggregierten Proteinen in verschiedene Subtypen unterteilen (in unterschiedlichen Farben). Die häufigsten Subtypen sind FTLD-TDP und FTLD-Tau (Pfeilgröße symbolisiert die Häufigkeit). Ubiquitin positive Aggregate finden sich sowohl bei FTLD-TDP als auch bei FTLD-FUS und treten nur bei FTLD-UPS ohne weitere Proteinaggregate auf. Pathologie-auslösende Genmutationen sind kursiv in der untersten Zeile des Diagramms dargestellt. Angepasst aus (Neumann and Mackenzie, 2019).

Interessanterweise haben 30 bis 50 % der FTLD Patienten eine familiäre Krankengeschichte, was eine hohe genetische Komponente vermuten lässt (Seelaar et al., 2011). Bisher wurden zahlreiche erbliche Mutationen, in den in **Abbildung 1** aufgeführten Genen, gefunden (Van Langenhove et al., 2012, Neumann and Mackenzie, 2019). Bei FTLD-TDP Patienten der familiären Variante wurden, neben seltenen Mutationen in Genen, die mit dem Proteinabbau (*VCP*, *UBQLN2* und *CHMP2B*) assoziiert sind, am häufigsten Mutationen in den beiden Genen *GRN* und *C9ORF72* detektiert (Ferrari et al., 2019). Die meisten Mutationen in *GRN* führen bei FTLD-Patienten durch Haploinsuffizienz zu einer reduzierten Expression (Cruts et al., 2006, Baker et al., 2006, Gass et al., 2006). Bei *C9ORF72*-assoziierten FTLD-Patienten wurden Vervielfältigung des Hexanukleotids GGCCCC im nicht-kodierenden Bereich des Gens *C9ORF72* entdeckt (Renton et al., 2011, DeJesus-Hernandez et al., 2011). Diese Vervielfältigung, auf mehrere 100 Kopien, führt bei Patienten zu FTLD, oder Amyotropher Lateralsklerose (ALS) (Ferrari et al., 2019). Genetische Analysen in FTLD-Patienten und ALS-Patienten ergaben, dass beide Krankheiten, neben Symptomen auch einige Gen-Mutationen gemeinsam haben (Renton et al., 2011, Ferrari et al., 2019). Mutationen in *C9ORF72*, *FUS*, *UBQLN2* und *CHMP2B* sowie die TDP-43 Proteinaggregate deuten darauf hin, dass ähnliche Mechanismen dieses Krankheitsspektrum aus ALS und FTLD verbindet (Ferrari et al., 2019, Kawakami et al., 2019, Neumann and Mackenzie, 2019).

2.1 Die Rolle des RNA/DNA-bindenden Proteins TDP-43 in FTLD

TDP-43 (engl.: Transactive response DNA binding protein 43 kDa) Aggregate sind bei FTLD-TDP namensgebend (Tome et al., 2020, Nag et al., 2018, Mackenzie and Rademakers, 2008). In FTLD-TDP Patienten wurden TDP-43 Aggregate im Nukleus und Zytoplasma von Nervenzellen festgestellt (Neumann et al., 2006, Hasegawa et al., 2008, Arai et al., 2006)

(Abbildung 2). Die Form und Lokalisation der TDP-43 Aggregate wurde zur Einteilung in 4 verschiedene Subtypen (A, B, C und D) genutzt. *GRN* abhängige FTLD-TDP Patienten sind immer als Typ A klassifiziert, gekennzeichnet durch TDP-43 positive Aggregate in Zytoplasma und in dystrophen Neuriten, sowie typische linsenförmige Aggregate im Nukleus **(Abbildung 2)** (Neumann and Mackenzie, 2019). Teilweise, ist die nukleäre Lokalisation bei einzelnen Zellen mit TDP-43-Aggregaten nahezu komplett aufgehoben und die Aggregate sind häufig zusätzlich Ubiquitin positiv (Neumann et al., 2006, Hasegawa et al., 2008, Arai et al., 2006).

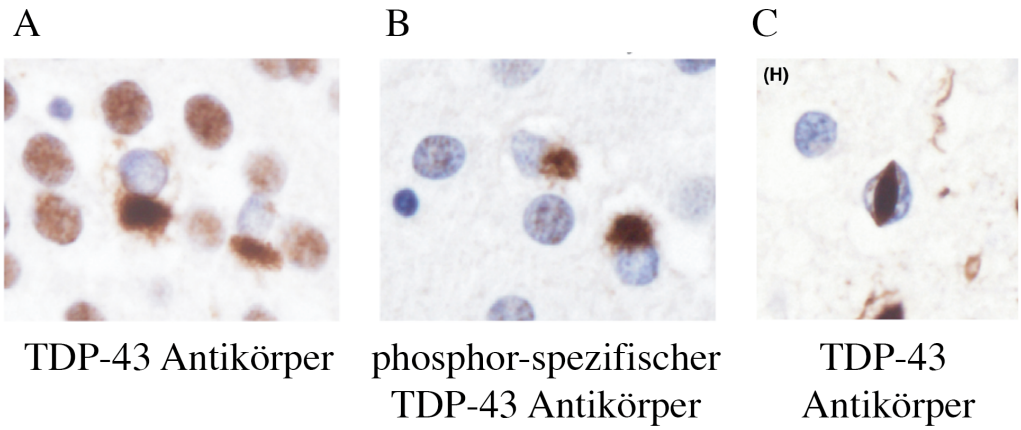

Abbildung 1: TDP-43-Pathologie in FTLD Patienten. Neuronale TDP-43 Aggregate im Kortex (A) bei FTLD-Patienten. Sowie Färbung mit einem phoshor-TDP-43 spezifischen Antikörper (B). Linsenförmige TDP-43 Aggregate im Nukleus (C). **Abbildung teilweise übernommen aus (Neumann and Mackenzie, 2019).**

Unter physiologischen Bedingungen ist TDP-43 vor allem im Nukleus lokalisiert, und als RNA-bindendes Protein im mRNA-Metabolismus involviert (Buratti and Baralle, 2008, Budini et al., 2017, Nagano et al., 2020, Briese et al., 2020). Die Funktion von TDP-43 umfasst Stabilisierung, Transport und das Spleißen der mRNA (Buratti and Baralle, 2008, Budini et al., 2017, Ling et al., 2013). Zusätzlich ist es nicht nur im Zellkern für die Regulation der Transkription von mRNA zuständig, sondern auch im Axon, wo ein TDP-43 Funktionsverlust zu einer reduzierten Verfügbarkeit von ribosomalen Proteinen führt, diese bewirkt eine reduzierte lokale Proteinsynthese und führt zu axonalen Beeinträchtigungen in Motoneuronen (Nagano et al., 2020, Briese et al., 2020).

Bei FTLD-Patienten ist neben der Lokalisation von TDP-43 auch die Prozessierung verändert. Als TDP-43-prozessierende Proteine wurden Caspase 3 & 4 sowie lysosomale Proteasen beschrieben (Zhang et al., 2007, Dormann et al., 2009, Herskowitz et al., 2012, Baralle et al., 2013, Li et al., 2015). In sequenziell extrahierten Gehirnlysaten von FTLD-Patienten liegt TDP-43 in der Harnstoff-löslichen-Fraktion in 35 & 25 kDa Fragmenten vor (Neumann et al., 2006). Diese Fragmente sind mit hoher Wahrscheinlichkeit die Spezies, die zur Aggregation außerhalb des Zellkerns neigt, da diesen die Kernlokalisierungssequenz (NLS) fehlt und TDP-43 im Zytoplasma akkumuliert (Woerner et al., 2016). Diese aggregierte Form von TDP-43 weist zusätzlich noch Phosphorylierungen an der Aminosäure Serin in den Positionen 379, 403/404 und 409/410 auf (Hasegawa et al., 2008, Neumann et al., 2009).

Zur Analyse der PGRN-assoziierten FTLD-TDP-Pathologie werden PGRN-Defiziente Mauslinien als Modell verwendet. Diese zeigten mit 21 Monaten ein geringes Ausmaß an phosphoryliertem TDP-43, jedoch fehlte die TDP-43 Mislokalisation und Aggregation im Zytoplasma gänzlich (Guo et al., 2010, Kleinberger et al., 2010, Wils et al., 2012, Yin et al., 2010, Götzl et al., 2014). Zur Untersuchung der Konsequenzen einer TDP-43 Pathologie wurde ein Mausmodell mit einer induzierbaren Expression von humanem TDP-43-ΔNLS Mutanten generiert. Die gezielte Überexpression TDP-43-ΔNLS in Neuronen, führte bei Mäusen zu einer verstärkten Aggregation und Phosphorylierung an der Position Serin 409/410 (Wils et al., 2010). TDP-43-ΔNLS-Mäuse weisen zusätzlich zur TDP-43 Pathologie eine Mikrogliose im Rückenmark und eine starke Beeinträchtigung der motorischen Fähigkeiten auf (Walker et al., 2015). Eine Induktion der Autophagie konnte in TDP-43-ΔNLS-Mäusen die TDP-43 Pathologie sowie die damit einhergehende Mikrogliose teilweise blockieren (Kumar et al., 2021). Durch zusätzliche Injektion von Gehirnextrakten von FTLD-TDP-Patienten in TDP-43-ΔNLS-Mäusen wurde die TDP-43 Pathologie verstärkt induziert. Dabei wurden eine TDP-43 Phosphorylierung, Mislokalisation und Aggregation im Zytoplasma beobachtet, zusätzlich wurde eine Zell zu Zell Transmission beschrieben (Porta et al., 2018).
Zum gegenwärtigen Stand gibt es keine Tiermodelle, die ohne eine gezielte Überexpression oder Injektion von humanem TDP-43, die TDP-43 Pathologie von FTLD-Patienten reproduzieren (Porta et al., 2018, Chang et al., 2017, Winton et al., 2008).

2.2 Funktion und Dysfunktion der Proteindegradation

Heterozygote Mutationen in mehreren Genen mit einer Funktion in der Proteindegradation wurden mit FTLD und ALS in Verbindung gebracht, darunter *C9ORF72, OPTN, UBQLN2, SQSTM1, VCP* und *TBK1* (Haack et al., 2016, Sanchez-Martin and Komatsu, 2018, Dooley et al., 2014, Wong and Holzbaur, 2014, Cirulli et al., 2015, Sellier et al., 2016, Lee et al., 2018, Wu et al., 2018, Casterton et al., 2020).
Zusätzlich konnten, krankheitsspezifische intrazelluläre Proteinaggregate in Verbindung mit den Autophagie-Adapter-Proteinen (Ubiquitin, p62 und Optineurin) nachgewiesen werden. Diese Akkumulation von Adapter-Proteinen deutet auf eine Beeinträchtigung in der Proteindegradation hin (Atkin and Paulson, 2014, Ciechanover and Kwon, 2015, Budini et al., 2017, Darios and Stevanin, 2020). Während die zelluläre Proteindegradation für kurzlebige Proteine über das Proteasomen erfolgt, werden langlebige Proteinstrukturen und beschädigte Organellen über den Prozess der Autophagie von Zellen abgebaut (Budini et al., 2017, Darios and Stevanin, 2020, Sanchez-Martin and Komatsu, 2018, Kimura et al., 2015, Huber et al., 2012, Andre et al., 1998). Dabei wird das Zielprotein mit einem Adapter-Protein markiert und anschließend von einer Lipid-Membran vollständig umschlossen, diese Autophagosomen fusionieren mit Proteasen enthaltenden Lysosomen (**Abbildung 3**) (Budini et al., 2017, Takeshige et al., 1992, Rusten and Stenmark, 2010, Darios and Stevanin, 2020).

Durch Ubiquitin zum Abbau markierte Proteine werden von Autophagie-Adapter-Proteinen gebunden. Die Adapter Proteine Optineurin (*OPTN*) und p62 binden über ihre Ubiquitin-Binde Domänen. Gleichzeitig, wird eine Lipid-Membran das Phagophore / Omegasom gebildet. Dieser Prozess wird durch mehrere Proteinkomplexe vermittelt und reguliert, darunter die

Kinasen ULK1 (engl.: Unc-51-like-kinase1) und PI3K (engl.: phosphatidyl-inositol 3-kinase) (Schmelzle and Hall, 2000, Laplante and Sabatini, 2009). ULK1 phosphoryliert PI3K, daraus resultiert die Bildung des Omegasomen am Endoplasmatischen Retikulum (ER) **(Abbildung 3)** (Kim et al., 2011, Hosokawa et al., 2009, Strohm and Behrends, 2020). Die Lipid Bindung von ATG18/WIPI2 an das Omegasomen führt zur weiteren Rekrutierung von mehreren Autophagie-Proteinen, darunter ATG5, ATG7, ATG12 und ATG16L1 (Polson et al., 2010, Sakoh-Nakatogawa et al., 2013, Dooley et al., 2014). Dieser Autophagosomen-Komplex führt zur ATG3 vermittelten Lipidierung von dem ATG8-Verwandten Protein LC3 (MAP1LC3; engl.: microtubule-associated protein light chain 3) (Polson et al., 2010, Strohm and Behrends, 2020, Dancourt and Melia, 2014).

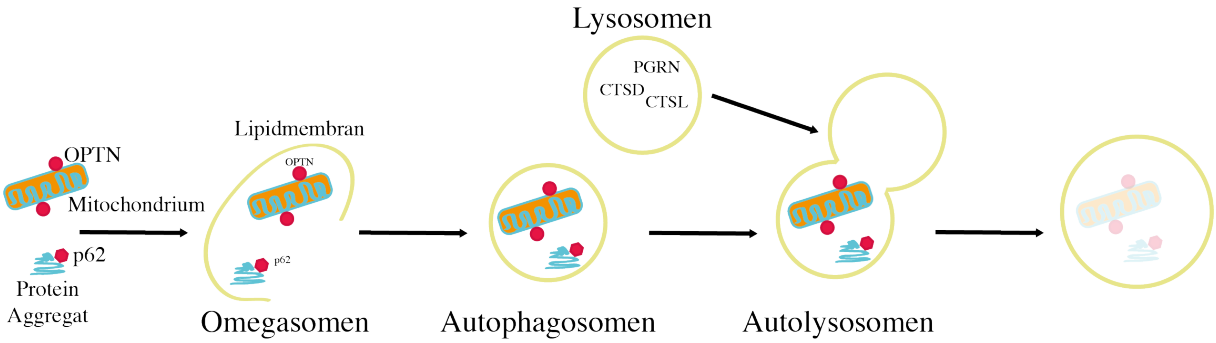

Abbildung 3: Schematische Darstellung der Autophagie. Fehlerhaft gefaltete oder beschädigte Protein-Strukturen durch Autophagie-Adapterproteine markiert. Eine Lipiddoppelmembran wird rekrutiert, und umschließt vollständig die Protein-Struktur. Durch die Fusion mit Lysosomen werden Hydrolasen und Ko-Faktoren freigegeben und aktiviert. Der Protein-Abbau führt zur Rückgewinnung der zugrunde liegenden Metaboliten. Angepasst aus (Budini et al., 2017)

Die Fusion von Autophagosomen mit Lysosomen zu Autolysosomen wird durch die Proteine CHMP2B (engl.: charged multivesicular body protein 2b), FIG4 (engl.: factor-induced gene), VCP (engl.: valosin-containing protein) und dem PIKFYVE-Komplex reguliert (Chow et al., 2009, Shatz et al., 2016, Strohm and Behrends, 2020, Filimonenko et al., 2007, Urwin et al., 2010, Vaccari et al., 2015).

Der Transport von Autophagosomen und Lysosomen ist für die Fusion unerlässlich (Farias et al., 2017, Pu et al., 2015). Interessanterweise, wird der Transport von LAMP1-positiven Lysosomen/Endosomen entlang der Axone auch zum assoziierten Transport von mRNA Granule (engl.: messenger ribonucleic acid) genutzt, dadurch können Proteine lokal translatiert werden (Zheng et al., 2001, Glock et al., 2017, Liao et al., 2019). Das ALS-assoziierte Protein ANXA11 vermittelt den Kontakt zwischen LAMP1-positiven Vesikeln und RNA Granule (Liao et al., 2019). Defizite im neuronalen Transport von Lysosomen führen damit nicht nur zu Störungen in der Autophagie, sondern möglicherweise auch zu Defiziten in der lokalen Protein-Synthese. Mutationen in TDP-43 führten ebenfalls zu Beeinträchtigungen im Transport der Lysosomen in den Axonen und veränderten die Maturierung der Lysosomalen Proteasen Cathepsin B & L (Alami et al., 2014, Roczniak-Ferguson and Ferguson, 2019). Gleichzeitig reguliert TDP-43 die Expression vieler Autophagie-Gene, unteranderem ATG7 und ATXN2 (Ling et al., 2013). Für TDP-43 wurden ein Abbau über das Proteasomen und eine Prozessierung in Lysosomen und der Abbau durch Autophagie beschrieben (Kim et al., 2009). TDP-43-Aggregate könnten sowohl den eigenen Abbau, als auch den allgemeinen Abbau über

das Proteasomen inhibieren (Guo et al., 2018). Der Autophagie vermittelte Abbau von TDP-43 benötigt p62 und VCP. Die zentrale Rolle der Autophagie in FTLD-Patienten wurde durch die Identifikation von heterozygoten Mutationen in *SQSTM1* (kodiert für p62) zusätzlich unterstrichen (Haack et al., 2016, Rusten and Stenmark, 2010, Sanchez-Martin and Komatsu, 2018).

2.3 Funktion und Dysfunktion von Mikroglia in AD und FTLD

Mikroglia nehmen als phagozytierende Zellen im Gehirn eine Schlüsselfunktion in der Eliminierung von Zellschäden und in der Abwehr von pathogenen Organismen ein (Lewcock et al., 2020, Song and Colonna, 2018b). Zusätzlich übernehmen Mikroglia eine fundamentale Funktion in der korrekten Entwicklung und Regulation der Vernetzung des Nervensystems (Stevens et al., 2007, Epelman et al., 2014). Im Mausmodell wurde gezeigt, dass ungenutzte Synapsen durch das Komplementsystem markiert und von Mikroglia eliminiert werden (Stevens et al., 2007).

Möglicherweise spielt das Komplementsystem auch bei der Degeneration von Neuronen in AD und FTLD-Patienten eine Rolle. Bei FTLD-Patienten wurden die Komplement-Faktoren C1 und C3 an Motor-Neuronen, Astrozyten und Mikroglia detektiert (Dalakas et al., 2020, Bright et al., 2019). Komplement-Faktoren lagern sich bei AD-Patienten in der Umgebung der Aβ-Plaques ab (Eikelenboom and Stam, 1982). Auch im AD-Mausmodell wurden erhöhte Mengen an Komplement-Faktoren detektiert und durch die Deletion von C3, konnte die Eliminierung der Synapsen blockiert werden (Hong et al., 2016, Shi et al., 2017). Dieser Zusammenhang konnte in einem FTLD-Mausmodell (*Grn*$^{-/-}$) bestätigt werden, indem sowohl die Aktivierung der Mikroglia als auch die Eliminierung der Synapsen, durch C3 Deletion blockiert wurde (Zhang et al., 2020, Lui et al., 2016). Die Aktivierung von Mikroglia kann damit zu erhöhter Komplement Expression führen, welche mit einer Eliminierung von Synapsen verbunden ist (Zhang et al., 2020, Lui et al., 2016).

Die Identifikation von Mutationen in den überwiegend von Mikroglia exprimierten Genen *GRN* und *TREM2* als krankheitsauslösende Gene bzw. Risikofaktoren verdeutlicht die Bedeutung der Mikroglia in FTLD und AD (Baker et al., 2006, Cruts et al., 2006, Guerreiro et al., 2013b, Cuyvers et al., 2014, Borroni et al., 2014, Tesi et al., 2020). Die Analyse des Aktivierungszustandes von Mikroglia, in Abhängigkeit von der Umgebung, Exposition und der genetischen Situation, ist damit für das Verständnis von neurodegenerativen Erkrankungen essenziell. Mit dem Fortschritt in der RNA-Sequenzierung, können nach der Isolation von Zellpopulationen aus dem Gewebe, verlässliche Informationen über das Expressionsmuster bis hin zur Einzel-Zell-Ebene gewonnen werden (Macosko et al., 2015). So verändern einzelne Mikroglia, abhängig von Entwicklungsstadium, Lokalisation im Gehirn, Alter und während der Demyelinisierung signifikant ihr Transkriptom (Hammond et al., 2019, Matcovitch-Natan et al., 2016). In Bezug auf neurodegenerative Erkrankungen wurden unterschiedliche Mausmodelle untersucht, darunter AD, Multiple Sklerose (MS) und ALS-Modelle. So führen die extrazellulären Aβ-Plaques zur Rekrutierung der Mikroglia, die Injektion von Myelin-assoziierten Proteinen induziert eine Demyelinisierung im EAE-Modell (Experimentelle autoimmune Enzephalomyelitis) und Mutationen in SOD1 (Superoxiddismutase1) gehen im

ALS-Modell mit einer Mikrogliose einher (Keren-Shaul et al., 2017, Hammond et al., 2019, Krasemann et al., 2017, Butovsky et al., 2015, Frakes et al., 2014). Doch obwohl unterschiedliche Stimuli vorlagen, kam es durch neuronale Verletzungen und Aggregation von Krankheits-assoziierten Proteinen teilweise zu ähnlichen Expressionsänderungen in Mikroglia (Macosko et al., 2015, Matcovitch-Natan et al., 2016, Keren-Shaul et al., 2017, Butovsky et al., 2015, Krasemann et al., 2017, Hammond et al., 2019).

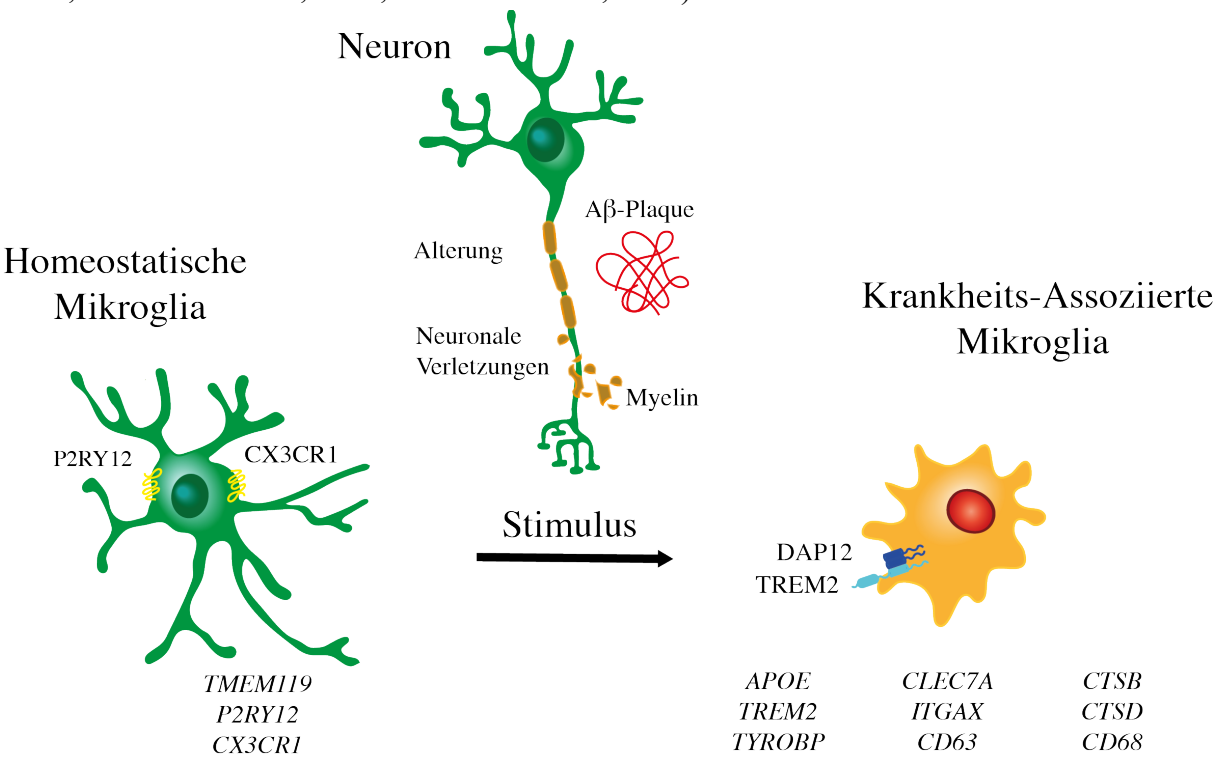

Abbildung 4: Aktivierungszustände der Mikroglia. Werden Mikroglia durch Stimuli aktiviert, beispielsweise, durch Aβ-Plaque Ablagerungen oder Alterung, reagieren diese mit einer erhöhten Expression von sogenannten DAM-Genen (DAM engl.: Disease-associated microglia). Charakteristische DAM-Gene: *APOE, TREM2, TYROBP, CLEC7A, ITGAX, CD63, CTSB, CTSD* und *CD68*. Gleichzeitig wird die Expression von Genen, die charakteristisch für homeostatische Mikroglia sind (*P2RY12, CX3CR1* und *TMEM119*), reduziert. Die morphologische Veränderung, die eine homeostatische Mikroglia-Zelle (grün), nach Kontakt mit einem Stimulus, hin zu einem reaktiven, amöboiden Zustand (orange) durchläuft ist schematisch dargestellt. Angepasst aus (Deczkowska et al., 2018).

Die Mikroglia, die einem Stimulus ausgesetzt wurden, regulierten die Expression einer Vielzahl von Genen, im Folgenden als Krankheits-assoziierte Mikroglia (DAM, engl.: Disease-associated microglia) Gene bezeichnet, stark hoch, während homöostatische Gene in ihrer Expression reduziert wurden (**Abbildung 4**). Zu den für homöostatische Mikroglia typischen Genen gehören *P2RY12, CX3CR1* und *TMEM119*. Charakteristische DAM-Gene sind: *APOE, TREM2, TYROBP, CLEC7A, ITGAX, CD63* sowie die lysosomalen Gene *CD68, CTSB* und *CTSD*. Viele dieser Gene wurden bereits mit unterschiedlichen Signalwegen und zellulären Funktionen in Verbindung gebracht, dazu gehören unter anderem: Migration, Zytoskelett-Aufbau, Phagozytose und lysosomale Aktivität (Mazaheri et al., 2017, Butovsky and Weiner, 2018, Song and Colonna, 2018a, Hickman et al., 2018). Die permanente Stimulation, unter anderem durch extrazelluläre Protein-Aggregate, könnte dazu führen, dass Mikroglia in ihrem aktivierten Zustand gefangen sind und dann ihrer ursprünglichen Funktion nicht mehr nachgehen können. APOE, das ursprünglich nur als Lipid-Transporter betrachtet wurde, der von Astrozyten sezerniert wird, wurde kürzlich als zentrales Marker-Protein für aktivierte

Mikroglia identifiziert (Keren-Shaul et al., 2017, Krasemann et al., 2017, Parhizkar et al., 2019). Zusammen mit APOE spielt TREM2 eine entscheidende Rolle für die Aktivierung von Mikroglia und der damit verbundenen Migration, Phagozytose und Zellproliferation (Keren-Shaul et al., 2017, Krasemann et al., 2017, Parhizkar et al., 2019).

3 Funktion und Dysfunktion von TREM2

3.1 Mutationen im *TREM2*-Gen in neurodegenerativen Erkrankungen

Im *TREM2* (engl.: Triggering receptor expressed on myeloid cells 2) Gen wurden bereits mehr als 60 Mutationen identifiziert, die im Zusammenhang mit AD, FTD und anderen neurodegenerativen Erkrankungen stehen (Guerreiro et al., 2013a, Cuyvers et al., 2014, Slattery et al., 2014, Sirkis et al., 2016, Tan et al., 2016, Sims et al., 2017, Zhou et al., 2019, Kunkle et al., 2019). Die in AD-Patienten identifizierten TREM2-Mutationen, die zu einem Aminosäureaustausch an Position 47 oder 62 führen (R47H & R62H) erhöhen das Risiko an LOAD (engl.: late-onset AD) sowie an FTD zu erkranken erhöhen (Guerreiro et al., 2013b, Guerreiro et al., 2013a, Jonsson et al., 2013). Die TREM2-Mutationen R47C und T66M erhöhen in einer heterozygoten Vererbung das Risiko für FTD (Guerreiro et al., 2013b, Borroni et al., 2014). TREM2-Mutationen führen zu einer fehlerhaften TREM2-Prozessierung und einer verminderten Verfügbarkeit auf der Zelloberfläche (Kleinberger et al., 2014, Kleinberger et al., 2017, Schlepckow et al., 2017, Sirkis et al., 2016). Homozygote Mutationen in *TREM2* oder in *TYROBP* (engl.: TYRO protein tyrosine kinase-binding protein) kommen selten vor und führen zu einer sehr aggressiven Leukoenzephalopathie (Degeneration der weißen Substanz im Gehirn). Diese Form der Leukoenzephalopathie, wird als Nasu-Hakola Erkrankung beschrieben (Hakola et al., 1970, Nasu T, 1970, Paloneva et al., 2000, Klünemann et al., 2005, Kaneko et al., 2010).

3.2 TREM2-abhängige Regulation der Aktivität von Mikroglia

Der Rezeptor TREM2 ist ein Typ-I Transmembran Protein, dass im Gehirn ausschließlich von Mikroglia exprimiert wird (Takahashi et al., 2005). TREM2 wird zur Zellmembran transportiert, wo der Rezeptor zusammen mit TYROBP/DAP12 (engl.: DNAX activation protein 12), einen Signal-kompetenten Komplex ausbildet. DAP12 besitzt eine ITAM (engl.: Immunoreceptor tyrosine-based activation motif) Domäne, welche nach der Dimerisierung phosphoryliert wird. Eine Stimulation von TREM2 und DAP12 über unterschiedliche Liganden führt zur Rekrutierung und Signalweiterleitung über den SYK-Signaltransduktionsweg (engl.: spleen associated tyrosine kinase) **(Abbildung 5)** (Takahashi et al., 2005, Peng et al., 2010). Unter den beschriebenen TREM2-Liganden finden sich APOE, Lipide, Myelin und Bakterien-Partikel sowie extrazelluläre Protein-Aggregate, z.B.: Aβ-Plaques (Kleinberger et al., 2014, Atagi et al., 2015, Bailey et al., 2015, Yeh et al., 2016, Wang et al., 2015, Song et al., 2017). Die Rekrutierung und Phosphorylierung der Tyrosin-Kinase SYK (engl.: spleen tyrosine kinase), führt über PLCγ2 (engl.: 1-Phosphatidylinositol-4,5-bisphosphate phosphodiesterase gamma-2), zur PKB (engl.: Protein kinase B) Aktvierung. PKB ist an die Energieschaltstelle der Zelle, dem mTORC1 Komplex, angebunden. Zusätzlich ist über PLCγ2 der MAP-Kinase Weg (engl.: mitogen-activated protein kinase) verknüpft (**Abbildung 5)** (Peng et al., 2010, Ulrich and Holtzman, 2016, Ulrich et al., 2017). TREM2 wird nach der Signalweiterleitung

durch die Metalloproteasen ADAM10 oder ADAM17 (engl.: A disintegrin and metalloproteinase domain-containing protein 10 / 17) gespalten und in Form von löslichem TREM2 (sTREM2, engl.: solubleTREM2) sezerniert (Kleinberger et al., 2014).

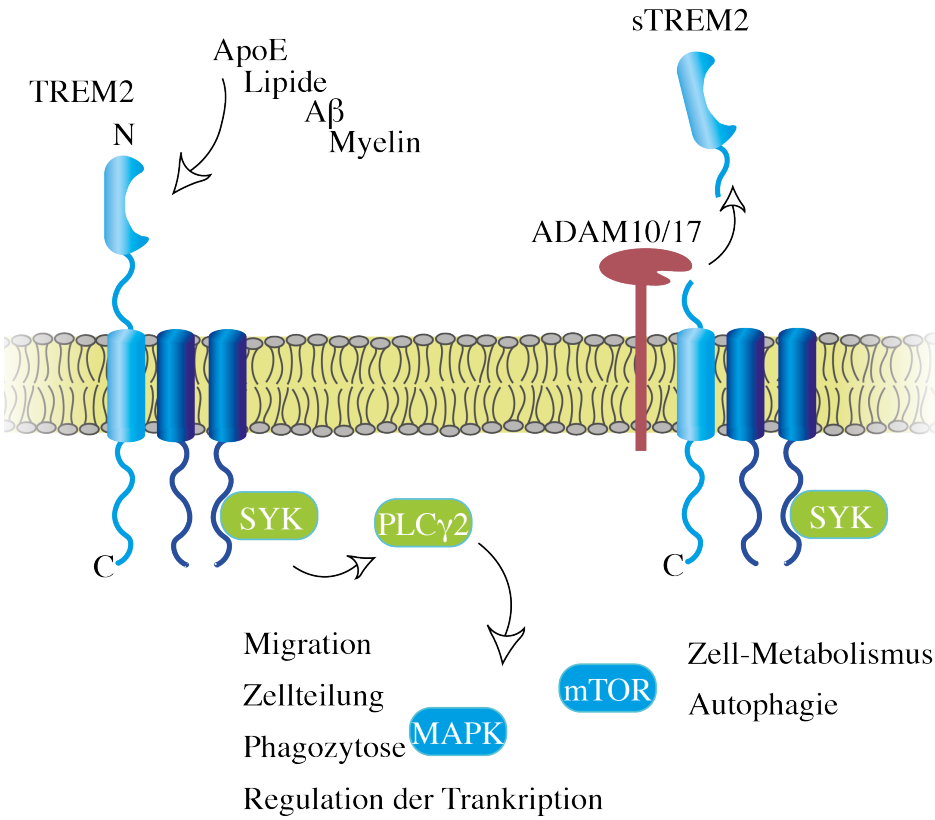

Abbildung 5: Signalkaskade ausgehend von TREM2. Zusammen mit DAP12 bildet TREM2 einen Signal-kompetenten Komplex, welcher über unterschiedliche Liganden (z.B.: APOE, Lipide, Aβ-Plaques oder Myelin) aktiviert werden kann. Dies führt zur Rekrutierung und Signalweiterleitung über SYK, welches phosphoryliert wird und schließlich mit Hilfe von PLCγ2 eine Aktivierung von PKB/AKT auslöst. Über PKB/AKT und PLCγ2 werden letztlich mTOR und MAPK aktiviert. Die Proteasen ADAM10 & ADAM17 sind schematisch in Rot dargestellt. Angepasst aus (Lewcock et al., 2020)

Mäuse ohne TREM2-Expression sind in ihren motorischen Fähigkeiten Verhaltens-unauffällig und weisen keine Unterschiede in Bezug auf ihre Lebenserwartung auf (Turnbull et al., 2006, Poliani et al., 2015, Kang et al., 2018). Die Isolation von Mikroglia, aus Mäusen mit einer genetischen Deletion der TREM2-Expression, offenbarte ein verändertes Gen-Expressionsmuster. Gene, wie *CLEC7A* und *APOE*, die für aktivierte Mikroglia charakteristisch sind, werden reduziert exprimiert, während homeostatische Gene, wie *P2RY12*, verstärkt exprimiert werden. Diese Veränderungen in der mikroglialen Signatur, führen zu einer funktionellen Einschränkung der Mikroglia (Mazaheri et al., 2017). Durch den Expressionsverlust, ist die TREM2 abhängige Phagozytose-Fähigkeit von Zellen als Reaktion auf Aβ, Bakterien und Lipide beeinträchtigt (Wang et al., 2015, Song et al., 2017, Kleinberger et al., 2014). Die Fähigkeit zur Aktivierung der Mikroglia, als Reaktion auf Extrazelluläre Protein-Aggregate, wie Aβ-Plaques, oder neuronale Verletzungen durch Laser-Strahlung, ist bei einem TREM2 Expressionsverlust ebenfalls blockiert (Mazaheri et al., 2017, Krasemann et al., 2017). Zusätzlich weisen *Trem2*$^{-/-}$ Mikroglia eine reduzierte Migration *in vitro* als auch *in vivo* auf (Mazaheri et al., 2017, Wang et al., 2016).

Die in FTD-Patienten identifizierte heterozygote Mutation T66M wurde in Mäusen durch Genom-Manipulation eingefügt (Guerreiro et al., 2013b, Borroni et al., 2014, Kleinberger et al., 2017). Die Analysen von Mäusen mit T66M Mutation, zeigten, wie auch erste Zellkultur Experimente, eine reduzierte Maturierung und Prozessierung von TREM2 (Kleinberger et al., 2014, Kleinberger et al., 2017). *In vivo* kann die mikrogliale Aktivierung durch Messung des radioaktiv markierten Tracers (engl.: trace; Spur), für das in Mitochondrien exprimierte Protein TSPO (engl.: translocator protein) analysiert werden. Die TSPO-Signalstärke wird im PET (engl.: positron emission tomography) als Zeichen für mikrogliale Aktivität verwendet (Brendel et al., 2016, Brendel et al., 2017). Bei TREM2 T66M Mäusen ist bereits ab einem Alter von 8 Monate eine starke Reduktion des TSPO-Signals zu erkennen (Kleinberger et al., 2017). Gleichzeitig kommt es zu einer starken Reduktion der Glukose-Aufnahme im Gehirn, gekennzeichnet durch ein reduziertes FDG-PET Signal (Kleinberger et al., 2017, Brendel et al., 2016). Diese starke Reduktion der Glukose-Aufnahme deutet auf einen reduzierten neuronalen Energieumsatz hin. In AD-Maus-Modellen kommt es als Folge der Amyloid-Ablagerung ebenfalls zu einem Anstieg der TREM2-Expression und einem erhöhten Mikroglia TSPO-Signal (Brendel et al., 2016, Brendel et al., 2017, Parhizkar et al., 2019).

Mutationen in TREM2 führen damit zu einem Funktionsverlust, gekennzeichnet durch eine beeinträchtigte Regulation und Aufrechterhaltung vieler Funktionen der Mikroglia, wie Phagozytose und Migration. Im Gegensatz zum Funktionsverlust durch Mutationen, führt eine gezielte Stabilisierung des TREM2-Signalkomplexes durch Antikörper, zu einer erhöhten TREM2 abhängigen verbesserten Myelin-Aufnahme sowie Aβ-Phagozytose durch Mikroglia, und einem gesteigerten Zellüberleben unter Stressbedingungen (Schlepckow et al., 2020, Cignarella et al., 2020, Price et al., 2020, Wang et al., 2020).

3.3 TREM2-abhängige Regulation der Proteindegradation

Die Fähigkeit zur Aufnahme und zum Abbau von Myelin ist TREM2 abhängig (Safaiyan et al., 2021, Monroe and Di Paolo, 2021, Dong et al., 2021). In primären Mikroglia wurde beobachtet, dass die Myelin Zugabe die Expression von Cathepsin L induziert, diese Induktion ist, durch eine Deletion der TREM2-Expression, blockiert (Safaiyan et al., 2021). TREM2 ist damit für die Aufnahme und die Lysosomale Degradation von Myelin wichtig (Safaiyan et al., 2021). Isolierte *Trem2*$^{-/-}$ Mikroglia reagieren auf eine Aβ-Exposition mit einer reduzierten Aktivität des mTORC1-Komplexes (Ulland et al., 2017). Diese Reduktion des mTORC1-Komplex (engl.: mammalian target of rapamycin) ist gekennzeichnet durch reduzierte Phosphor-S6-Kinase Mengen, gefolgt von einer Reduktion der Autophagie Proteine LC3 und p62. Daraus ergibt sich, dass TREM2, über DAP12 und PLCγ2, mit der lysosomalen Schaltzentrale mTORC1 direkt Einfluss auf viele Zellfunktionen nehmen kann und die Expression von Lysosomalen Proteasen reguliert (Ulland et al., 2017, Safaiyan et al., 2021).

4 Funktion und Dysfunktion von Progranulin

4.1 Mutationen im *GRN*-Gen in neurodegenerativen Erkrankungen

PGRN ist ein 593 Aminosäuren langes, glykosyliertes und lösliches Protein (Bateman and Bennett, 2009, Lui et al., 2016). Bei FTD-Patienten sind Mutationen in dem Progranulin-Gen *GRN* neben *C9ORF72* der häufigste genetische Faktor (Cruts et al., 2006, Baker et al., 2006, Gass et al., 2006). Es wurden bis heute über 140 Mutationen in dem *GRN* Gen nachgewiesen (Moore et al., 2020, Greaves and Rohrer, 2019). Wobei nur ein nicht kodierender SNP (rs5848) in *GRN* mit AD in Verbindung gebracht wurde (Brouwers et al., 2008). In äußerst seltenen Fällen haben Patienten Mutationen auf beiden Allelen. Bei diesen Patienten kommt es zu einer adulten Form der Lysosomalen Speichererkrankung, der Neuronalen Ceroid-Lipofuszinose (NCL) (Smith et al., 2012, Almeida et al., 2016). Die meisten Mutationen in *GRN* sind sogenannte „loss-of-function" Mutationen, die zu einer Verschiebung des Lesemusters oder zu einer Veränderung von Splice- Erkennungsmotiven führen und damit zu einem vorzeitigen Stopp-Codon. Dadurch kommt es zum Abbau der mRNA, oder einem nicht funktionellen Protein, in der Konsequenz weisen Patienten in diesem Fall eine um 50 % reduzierte PGRN Expression auf (Cruts et al., 2006, Baker et al., 2006, Gass et al., 2006, Moore et al., 2020, Zhou et al., 2021). Punktmutationen in *GRN*, die nicht zu einem Funktionsverlust führen, reduzieren die PGRN Expression in einem geringeren Ausmaß (Shankaran et al., 2008, Paushter et al., 2018, Zhou et al., 2021).

4.2 Progranulin-abhängige Regulation der Proteindegradation

Das Protein PGRN ist über verschiedenen Spezies relativ konserviert und wird von allen Zellen exprimiert, im Gehirn ist PGRN jedoch hauptsächlich mikroglialen Ursprungs (Bateman and Bennett, 2009, Lui et al., 2016, Götzl et al., 2018). Zunächst wurden Prozessierungsprodukte vom PGRN isoliert und vor allem die Funktion als Wachstumsfaktor analysiert (Bateman et al., 1990, Bhandari et al., 1992, Shoyab et al., 1990). Interessanterweise kann PGRN sowohl in Lysosomen als auch im extrazellulären Bereich zu 6kDa Peptiden, den Granulinen (P,G,F,B,A,C,D und E), prozessiert werden (Paushter et al., 2018). Als PGRN prozessierende Proteasen im extrazellulären Bereich wurden NE (Neutophile Elastase), MMP-9 & MMP-12 (engl.: Matrix metalloproteinase) und ADAMTS-7 (A Disintegrin and metalloproteinase with thrombospondin motifs 7) beschrieben **(Abbildung 6)** (Zhu et al., 2002, Suh et al., 2012, Paushter et al., 2018). SLPI (engl.: Secretory leukocyte protease inhibitor) hingegen wirkt stabilisierend auf PGRN. Zu den intrazellulär PGRN prozessierenden Lysosomalen Protease gehören die Aspartat Protease Cathepsin D (CTSD) und die Cysteine-Proteasen Cathepsin B (CTSB) und Cathepsin L (CTSL) **(Abbildung 6)** (Holler et al., 2017, Lee et al., 2017, Zhou et al., 2017b, Laurent-Matha et al., 2006). Eine Inhibition der Ansäuerung von Lysosomen stabilisiert die PGRN-Level und zeigt, dass die Prozessierung und der Abbau von PGRN über pH-abhängige Enzyme geschehen muss (Capell et al., 2011, Tanaka et al., 2017).

Sezerniertes PGRN kann über C-terminale Bindung an Sortilin wieder in die Zelle aufgenommen und zu Lysosomen transportiert werden **(Abbildung 7)** (Hu et al., 2010, Prudencio et al., 2012, Zhou et al., 2015). Der lysosomale Transport kann auch gemeinsam mit Prosaposin (PSAP) über den Mannose-6-Phosphat Weg erfolgen (Zhou et al., 2017c). Das ebenfalls sekretierte und prozessierte Glycoprotein PSAP, ist ein wichtiger Faktor für den lysosomalen Abbau von Sphingolipiden (Schulze and Sandhoff, 2014). PSAP wird in vier

Saposin-Fragmente prozessiert (A-D), genetische Mutationen in *PSAP* führen zu unterschiedlichen lysosomalen Speichererkrankungen (Schulze and Sandhoff, 2014). Eine potentielle Funktion von PGRN und den Granulinen in Lysosomen ist die Bindung an CTSD und die Beta-Glucocerebrosidase (GCase) (Zhou et al., 2017a, Beel et al., 2017, Jian et al., 2016, Butler et al., 2019). Rekombinantes humanes PGRN bindet *in vitro* an Cathepsin D und erhöht die Aktivität (Beel et al., 2017). In Abwesenheit von PGRN wurde eine erhöhte CTSD Expression beobachtet, während gleichzeitig eine reduzierte CTSD Aktivität vorlag (Beel et al., 2017). Ob PGRN, oder die Granuline eine Chaperon-ähnliche Funktion für CTSD und GCase durch eine direkte Interaktion und Stabilisierung der Enzyme haben, ist noch nicht abschließend geklärt (Zhou et al., 2017a, Beel et al., 2017, Jian et al., 2016, Butler et al., 2019).

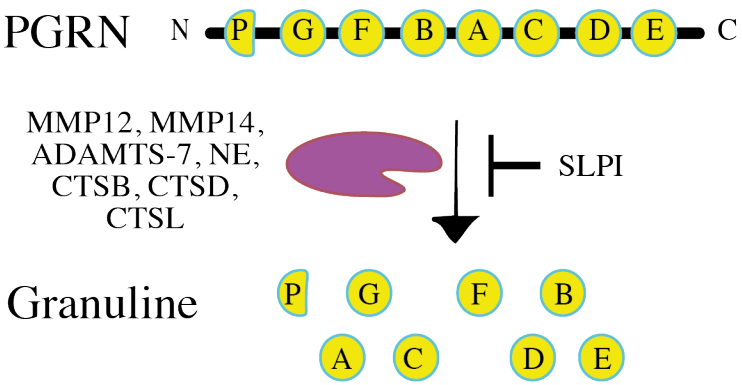

Abbildung 6: Schematische Darstellung der Progranulin Domänenstruktur und Zellulären Funktion. Die Großbuchstaben bezeichnen die Granulin-Domänen. PGRN kann sowohl extrazellulär als auch Lysosomen vorkommen und in sogenannte Granuline prozessiert werden.

Die Reduktion der PGRN Expression führt in *GRN*-FTLD-Patienten, zu einer veränderten Expression lysosomaler Hydrolasen und Transmembranproteinen (Götzl et al., 2014, Ward et al., 2017). Darüber hinaus akkumuliert die Untereinheit-C der mitochondrialen ATP-Synthase und SaposinD, die Akkumulation beider Proteine ist für NCL-Patienten charakteristisch (Götzl et al., 2014). Ein Hinweis dafür, dass die Lysosomen, funktionell beeinträchtigt sind ist auch die Akkumulation von Ubiquitin und Lipofuszin in den Neuronen von FTLD-Patienten (Götzl et al., 2014, Ward et al., 2017, Ahmed et al., 2010, Hafler et al., 2014, Petkau et al., 2017). Lipofuszin ist eine Anhäufung von unlöslich gewordenen, autofluoreszierenden Lipiden und Proteinen. Da PGRN im Gehirn hauptsächlich von Mikroglia exprimiert wird, deutet die neuronale Lipofuszin Anhäufung, auf eine Lysosomale Funktion in Mikroglia und Neuronen hin.

Bei einem Verlust der PGRN-Expression verändern sich die Lysosomen, und ihre Proteinzusammensetzung in Zellkultur, sowie in Mäusen. In der Folge detektierten einige Arbeitsgruppen erhöhte Expression von Cathepsinen, während andere eine Reduktion beobachteten (Götzl et al., 2014, Wils et al., 2012, Chang et al., 2017, Ward et al., 2017, Huang et al., 2020). Es konnte nicht abschließend geklärt werden, ob der pH-Wert der Lysosomen sich PGRN-abhängig verändert (Tanaka et al., 2017, Klein et al., 2017).

Das bei PGRN-Defizienz ebenfalls gehäufte Auftreten von Ubiquitin sowie p62, spricht jedoch dafür, dass Proteine, die zum Abbau markiert wurden, nicht korrekt über das Autophagie-System abgebaut werden **(Abbildung 7)** (Wils et al., 2012, Seibenhener et al., 2007, Tanaka et al., 2014, Rusten and Stenmark, 2010, Foster and Rea, 2020, Chang et al., 2017). Der PGRN

Expressionsverlust, bewirkt zusätzlich eine Akkumulation der lysosomalen Transmembranproteine LAMP1 und 2 (engl.: Lysosomal associated membrane protein 1/2) (Götzl et al., 2014, Tanaka et al., 2017, Götzl et al., 2018). Die glykosylierten Proteine LAMP1/2 sind wichtig für die Lysosomale Biogenese und ein Expressionsverlust bewirkte eine Akkumulation von p62-positiven Autophagie Vesikeln *in vivo* (Eskelinen, 2006, Rothaug et al., 2015). Damit könnte der PGRN Funktionsverlust, durch eine Fehlfunktion in LAMP1/2, die Proteindegradation in Lysosomen und die Autophagie negativ beeinträchtigen (Götzl et al., 2014, Tanaka et al., 2017, Götzl et al., 2018).

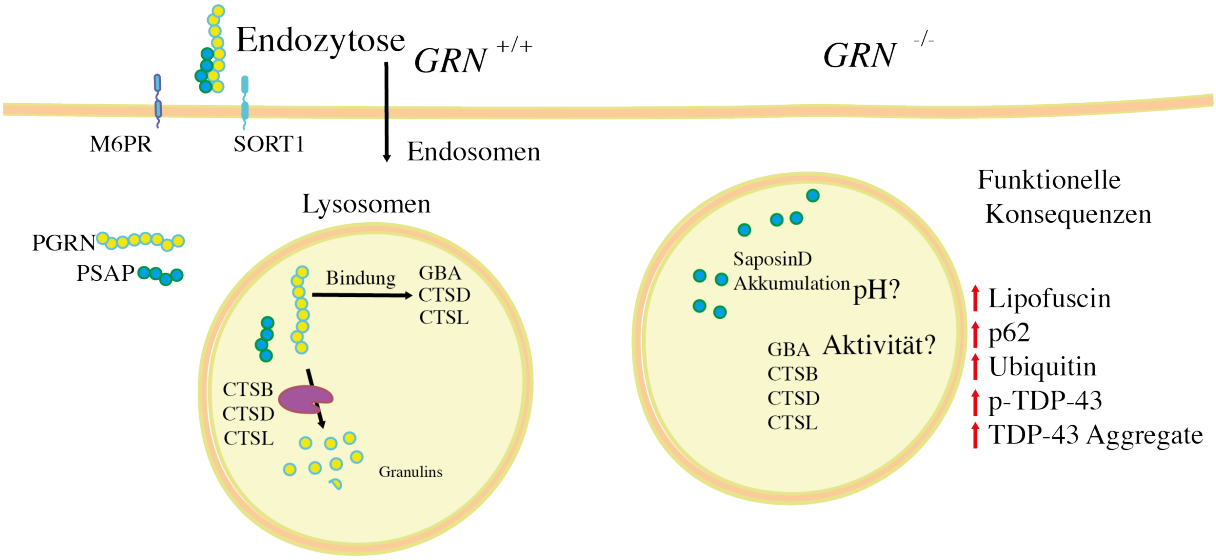

Abbildung 7: Schematische Darstellung der Lysosomalen Funktion von Progranulin. Sezerniertes Progranulin (blau-gelbe Kette) wird zusammen mit Prosaposin (blaue Kette) Rezeptor vermittelt endozytiert (M6PR und SORT1). PGRN bindet in Lysosomen an GBA, CTSD sowie CTSL. CTSB, CTSD und CTSL prozessieren PGRN in die Granuline (blau-gelbe Punkte). Der PGRN Expressionsverlust führt zu einer Beeinträchtigung der Lysosomalen Aktivität, gekennzeichnet durch eine Akkumulation von p62, Ubiquitin, Lipofuscin und phosphorylierter TDP-43 Aggregate. Angepasst aus (Root et al., 2021)

Da Mikroglia im Gehirn eine Schlüsselfunktion im Proteinabbau einnehmen ist ein Verständnis der Funktion von PGRN auf Zelltyp spezifischer Ebene wichtig. Während der Verlust der PGRN Expression eine reduzierte Maturierung der Cathepsine in Mikroglia bewirkt, wurde ein Anstieg an lysosomalen Proteasen im gesamten Gehirn auf Protein und mRNA Ebene detektiert (Götzl et al., 2014, Götzl et al., 2018, Chang et al., 2017). Dem gegenüber wurde, in einigen *Grn*$^{-/-}$ Mikroglia eine erhöhte Fähigkeit zum Abbau von Lysosomalen-Substraten wie fluoreszierendem Serum gemessen (Lui et al., 2016). PGRN könnte damit unter physiologischen Bedingungen die lysosomale Aktivität regulieren (Götzl et al., 2018). Interessanterweise genügt die PGRN-Expression in einem Zelltyp, Mikroglia oder Neuronen, um die *Grn*$^{-/-}$ abhängigen lysosomalen Phänotypen komplett zu eliminieren (Petkau et al., 2017, Arrant et al., 2019). PGRN kann damit sowohl von Mikroglia als auch Neuronen sezerniert, endozytiert und in Lysosomen transportiert werden.

Die für den Lipidstoffwechel in Lysosomen wichtige Interaktion zwischen PGRN und PSAP oder Sortilin führt bei PGRN-Funktionsverlust zur Akkumulation von Lipiden und Lipid-assoziierten Proteinen (Hu et al., 2010, Tayebi et al., 2020, Zhou et al., 2015, Prudencio et al., 2012, Tanaka et al., 2017, Marschallinger et al., 2020, Götzl et al., 2014, Götzl et al., 2018). Bei einem PGRN-abhängigen Funktionsverlust im Lipidstoffwechsel akkumulieren die Lipide

zunächst in Makrophagen und Mikroglia und später in Neuronen (Kojima et al., 2009, Marschallinger et al., 2020, Ahmed et al., 2010). Die Lipid Ansammlungen in *Grn*$^{-/-}$ Mikroglia führen zu einer veränderten Expression vieler DAM Gene, jedoch ohne eine Induktion der TREM2 und APOE Expression (Marschallinger et al., 2020). Zusätzlich wiesen diese LDAM (engl.: lipid-associated macrophages) eine Beeinträchtigung der Phagozytose Kapazität auf (Marschallinger et al., 2020).

4.3 Progranulin-abhängige Regulation der Inflammation

Zusätzlich, zu dem lysosomalen Phänotyp, kommt es, sowohl bei FTD-Patienten als auch in *Grn*$^{-/-}$ Mäusen, zu einer starken Aktivierung der Astrozyten (Astrogliose) und Mikroglia (Mikrogliose), die bei 12 Monate alten Tieren beginnt (Ahmed et al., 2010, Yin et al., 2010, Martens et al., 2012, Wils et al., 2012, Götzl et al., 2014). Neuroinflammation, gekennzeichnet durch einen Anstieg von CD68 (engl.: Cluster of Differentiation 68) und IBA1 (engl.: Ionized calcium-binding adapter molecule 1) in Gewebeschnitten, tritt bei allen FTD-Patienten und NCL-Patienten auf (Cagnin et al., 2004, Lant et al., 2014, Castaneda et al., 2008, Bright et al., 2019). Die Mikrogliose in FTD-Patienten wurde durch Messung des TSPO-PET Signals untersucht, dabei wurde festgestellt, dass die Aktivierung der Mikroglia vor dem Eintreten der Atrophie beginnt (Cagnin et al., 2004, Lant et al., 2014, Castaneda et al., 2008, Bright et al., 2019). Der Zustand der Mikroglia ist damit von hoher Relevanz für die Pathogenese.

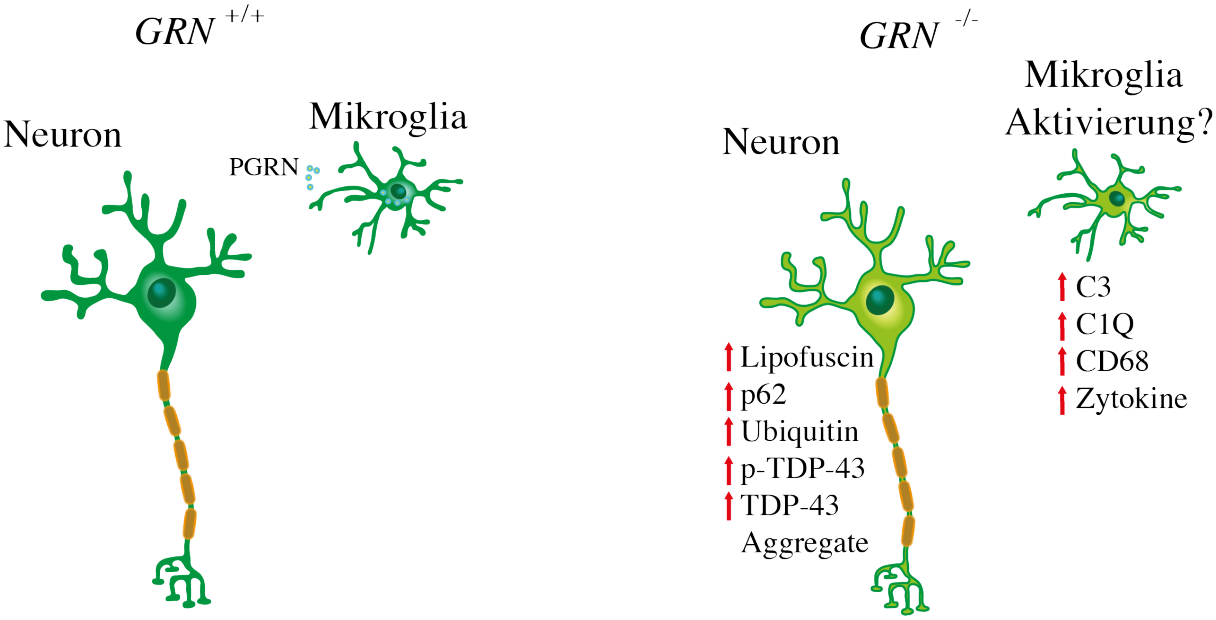

Abbildung 8: Schematische Darstellung der Progranulin-Defizienz. Progranulin (blau-gelbe Punkte) wird von Mikroglia exprimiert und sezerniert. Der PGRN Expressionsverlust führt in Mikroglia zu einer erhöhten Expression von CD68 sowie einer Freisetzung von C3, C1Q und Proinflammatorischer Zytokine. In Neuronen kommt es zu einer Akkumulation von p62, Ubiquitin, Lipofuscin und phosphorylierter TDP-43 Aggregate. Angepasst aus (Petkau and Leavitt, 2014).

Im Mausmodell führte die Induktion einer neuronalen Verletzung zu einer Rekrutierung von Mikroglia und einer erhöhten PGRN-Expression in Mikroglia (Moisse et al., 2009, Beel et al., 2018, Tanaka et al., 2013). Bei Verlust der PGRN-Expression verstärkte und verlängerte sich die Aktivierung von Mikroglia nach der Verletzung (Tanaka et al., 2013, Martens et al., 2012). Eine Änderung der Anzahl der IBA1-positiven Mikroglia war lediglich lokal zu beobachten (Yin et al., 2010). Die Expressionsänderungen durch die Lipidakkumulation in *Grn*$^{-/-}$ Mikroglia

überlappen teilweise mit den Änderungen durch Stimulation der Zellen mit dem Bakterien-Bestandteil LPS (Lipopolysaccharide) (Marschallinger et al., 2020). Der PGRN Expressionsverlust führt bei einer zusätzlichen Stimulation der Zellen mit LPS zur Dysregulation der Zytokine Ausschüttung (Yin et al., 2010). In *Grn*$^{-/-}$ Mäusen wurden erhöhte neurotoxische Zytokine wie der Tumornekrosefaktor (TNF) gemessen, während das Entzündungshemmende Interleukin-10 (IL-10) herunterreguliert wurde (Yin et al., 2010). PGRN hingegen inhibiert die Freisetzung von Zytokinen durch Bindung an, die im Entzündungsprozess wichtigen Rezeptoren, TLR-9 (engl.: Toll Like Receptor), TNF-Rezeptor und EphA2 (Wei et al., 2014, Pickford et al., 2011). Zusätzlich führt die LPS-Exposition von Mikroglia zu einer erhöhten Expression von MMP12 (engl.: Matrix Metallo Proteinase) (Suh et al., 2012). MMP12 gehört, neben MMP9 und der Neutorphilen Elastase, zu den PGRN prozessierenden Proteasen im Extrazellulären Raum (Zhu et al., 2002, Suh et al., 2012, Paushter et al., 2018). Diese Proteasen werden vor allem von Astrozyten und Mikroglia exprimiert (Suh et al., 2012, Mendsaikhan et al., 2019). Die Stimulation von Astrozyten und Mikroglia, könnte damit zu einer zusätzlichen Regulation von PGRN im Extrazellulären Raum führen (Suh et al., 2012, Mendsaikhan et al., 2019, Paushter et al., 2018).

Das Komplementsystem spielt eine entscheidende Rolle in der Abwehr und Beseitigung von Pathogenen. Der klassische Komplementweg führt nach initialer Bindung von C1Q an die Zielzelle durch die Anlagerung mehrere Komplementfaktoren zur Rekrutierung und Konvertierung von C3 (Dalakas et al., 2020). Die Konvertierung von C3 führt zur Initiation der Zell-Lyse durch Ausbildung des MAC (Membran Angriff Complex) (Dalakas et al., 2020). Zusätzlich zur PGRN-abhängigen Dysregulation der Zytokine, wurden bei FTD-Patienten erhöhte Konzentrationen der Komplementfaktoren C1Q und C3 detektiert (Dalakas et al., 2020, Bright et al., 2019). Diese übermäßige Komplement-Produktion wird durch das *Grn*$^{-/-}$ Mausmodell rekapituliert (Lui et al., 2016). Während die Aktivierung der Mikroglia durch genetische Deletion von C3 blockiert wurde, ist die der Einfluss auf die schwache TDP-43 Pathologie in Neuronen bei 20 Monate alten Tieren noch umstritten (Lui et al., 2016, Zhang et al., 2020). Wie PGRN neben dem Aktivitätszustand der Mikroglia auch die Produktion von verschiedenen proinflammatorischen Faktoren reguliert ist noch nicht abschließend geklärt. Zusätzlich stellt sich die Frage, wie der PGRN Funktionsverlust in Mikroglia, die TDP-43 Pathologie in Neuronen auslöst **(Abbildung 8)**.

5 Funktion und Dysfunktion des Transmembranproteins 106B

5.1 Mutationen im *TMEM106B*-Gen in neurodegenerativen Erkrankungen

Das Gen *TMEM106B* kodiert für das 274 Aminosäuren lange Transmembranprotein 106B (**Abbildung 10**) (Lang et al., 2012). Im Gehirn wird TMEM106B von Neuronen, Mikroglia, Astrozyten und Endothelzellen konstitutiv exprimiert (Busch et al., 2013). FTLD-TDP Patienten wurden in Genomweite Assoziationsstudien (GWAS) auf SNP untersucht, um genetische Risiko-Faktoren zu identifizieren (Van Deerlin et al., 2010, Cruchaga et al., 2011) (van der Zee et al., 2011). Dabei wurde festgestellt, dass sich die Häufigkeit von drei SNPs (rs1990622, rs6966915, rs1020004) in dem Bereich des Gens *TMEM106B* zwischen FTLD-Patienten von Kontrollpatienten unterschieden (Van Deerlin et al., 2010). Bis heute wurden viele weitere SNPs in den nicht-kodierenden Bereichen von *TMEM106B* in unterschiedlichen Patienten-Kohorten identifiziert, nur zwei Mutationen in Exon 6 und 9 liegen im kodierenden Bereich des Gens. Am häufigsten wurde der SNP rs1990622 nach der 3`UTR (Untranslatierte Region) detektiert, die meisten anderen krankheitsrelevanten SNPs in *TMEM106B* treten mit diesem gemeinsam auf **(Abbildung 9)** (Van Deerlin et al., 2010, Cruchaga et al., 2011, van der Zee et al., 2011). In Bezug auf den SNP rs1990622 ist das T-Allel, die Risikovariante mit rund 60 %, die häufigere Form und das C-Allel die protektive Variante. Interessanterweise, wurde die protektive Variante auf beiden Allelen (Homozygot für (C)) in *GRN*-FTD-Patienten besonders selten festgestellt, in 2,6 % der *GRN*-Patienten gegenüber 19,1 % in der Kontrollgruppe (Finch et al., 2011, van der Zee et al., 2011). In anderen FTD-Patienten Kohorten unterschied sich die Häufigkeit der protektiven Variante nicht signifikant, dennoch korrelierte das protektive Allele mit einer erhöhten PGRN Expression und mit einem um bis zu 13 Jahre späteren Beginn der FTD-Pathologie in *GRN*-Mutationsträgern (Cruchaga et al., 2011). Neben der FTLD-Assoziation hat, das verbreite Risiko-Allel (rs1990622) gleichzeitig einen Effekt auf das Volumen des linken Frontallappens (Adams et al., 2014).

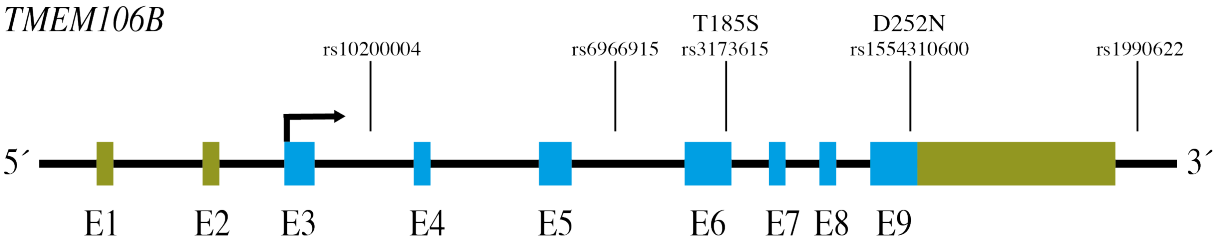

Abbildung 9: Schematische Darstellung der genomischen Region von *TMEM106B*. Kodierende Bereiche sind in Blau, untranslatierte in Grün dargestellt. Die Translation beginnt in Exon 3 und ist durch einen Pfeil gekennzeichnet. Zusätzlich ist die protektive Mutation T185S und die mit Leukodystrophie-assoziierte Mutation D252N gekennzeichnet. E1 bis 9: Exon 1 bis 9. In rs Nummern sind die Positionen ausgewählter SNPs im *TMEM106B* Gen-Lokus dargestellt, angepasst aus (Nicholson and Rademakers, 2016, Hunt et al., 2018).

Im kodierenden Bereich von *TMEM106B* wurde eine Mutation in Exon 6 (rs3173615) an korrespondierender Aminosäureposition 185 entdeckt, die zu einem Aminosäureaustausch von Threonin zu Serin führt **(Abbildung 9 & 10 & Tabelle 1)** (Nicholson et al., 2013)**.** Die S185 Variante tritt meistens in Verbindung mit dem protektiven Allel (C) in SNP rs1990622 auf (Cruchaga et al., 2011, Nicholson et al., 2013). Die S185-Form führt möglicherweise zu einer reduzierten Proteinstabilität und Expression von TMEM106B in Zellkulturexperimenten,

gegenüber der erhöhten Expression der T185-Form (Nicholson et al., 2013). Aufgrund der geringeren Häufigkeit der S185 Variante in FTD-Patienten, geht man von einem protektiven Effekt aus (Nicholson et al., 2013). Ein TMEM106B rs3173615 Varianten-abhängiger Einfluss auf die PGRN-Expression wird diskutiert (Nicholson et al., 2013, Nicholson and Rademakers, 2016, Feng et al., 2021).

Die zweite Mutation in Exon 9 (rs1554310600) führt zu einem Aminosäureaustausch an der Aminosäureposition 252, von Asparaginsäure zu Asparagin **(Abbildung 9 & 10)**. Die heterozygote D252N Mutation wurde bei Patienten mit Leukodystrophie mit Hypomyelinisierung entdeckt (Simons et al., 2017, Yan et al., 2018). Eine Hypomyelinisierung wurde in Patienten und in *Tmem106b*$^{-/-}$ Mäusen nach der Induktion einer neuronalen Verletzung beobachtet (Simons et al., 2017, Zhou et al., 2020, Feng et al., 2020).

Auch *C9ORF72*-FTLD Patienten wurden auf SNPs in *TMEM106B* untersucht. Dabei wurde festgestellt, dass das protektive Allel (C) in SNP rs1990622 in *TMEM106B,* im homozygoten Zustand, mit einer reduzierten TDP-43 Pathologie-assoziiert sind (van Blitterswijk et al., 2014, Gallagher et al., 2014, Ferrari et al., 2019). Jedoch konnte in Mausexperimenten kein TMEM106B-abhängiger, modulierender Effekt auf die C9ORF72-Pathologie festgestellt werden (Nicholson et al., 2018).

Gleichzeitig wurde eine Interaktion mit dem APOE Genotyp im Kontext der Alzheimer-Erkrankung untersucht (Lu et al., 2014). Dabei wurde entdeckt, dass bei gesunden APOE e4 Trägern das protektive Allel (C) in *TMEM106B* (21,4 %) häufiger vorkommt als in APOE e4 Trägern mit AD-Pathologie (13,6 %) (Lu et al., 2014). In AD-Patienten mit TDP-43 Pathologie wurde das protektive Allel (C) in SNP rs1990622 seltener detektiert, als in AD-Patienten ohne TDP-43 Pathologie (Rutherford et al., 2012). Es wurde vorgeschlagen, späte Formen der Demenz mit TDP-43 Pathologie, die bei 25 % der Autopsie-Proben bei über 85-Jährigen festgestellt werden konnten, als LATE zu klassifizieren (engl.; Limbic-predominant Age-related TDP-43 Encephalopathy) (Nelson et al., 2019). Genau in diesen Patienten wurde das Risiko Allel (T) in SNP rs1990622 in *TMEM106B* als Faktor identifiziert der mit erhöhtem neuronalen Zellverlust und Expressionsänderungen, von Oligodendrozyten, Lysosom und Myelin-assoziierten Genen, korreliert (Nelson et al., 2019, Hokkanen et al., 2020, Yang et al., 2020).

Krankheitsbild	SNP	Risiko Allele	Protektive Allele	Assoziierter Phänotyp	Referenzen
FTLD-TDP	rs1990622	T	C	Erhöhtes Risiko für FTLD-TDP	(Van Deerlin et al., 2010, van der Zee et al., 2011, Finch et al., 2011, Cruchaga et al., 2011, Deming and Cruchaga, 2014, Lattante et al., 2014, Gallagher et al., 2017, Harding et al., 2017, Pottier et al., 2018)
GRN **Mutationen**	rs3173615 (T185S)	C (T185)	G (S185)	Alle anderen SNPs sind im Verkupplungsungleichgewicht mit rs1990622	
	rs1990621	C	G		
	rs1990620	A	G	Protektive SNP sind selten, vor allem bei *GRN* Mutationsträgern	
	rs1020004	A	G		
	rs6966915	C	T		
FTLD-TDP	rs1990622	T	C	Risiko Varianten assoziiert mit verstärktem kognitivem Abbau	(Lattante et al., 2014, van Blitterswijk et al., 2014, Deming and Cruchaga, 2014, Gallagher et al., 2014, Vass et al., 2011)
C9ORF72 **Hexanukleotid**	rs3173615	C	G		
AD	rs1595014	T	A	Risiko Varianten erhöhen AD-Risiko, abhängig vom *APOE* Allele	(Jun et al., 2016)
APOE	rs1990622	T	C		
AD / LATE TDP-43	rs1990622	T	C	Risiko Variante korreliert mit verstärkter TDP-43 Pathologie	(Rutherford et al., 2012, Josephs et al., 2019, Nelson et al., 2019, Hokkanen et al., 2020) ,
AD	rs1990622	T	C	Protektive Variante korreliert mit reduziertem Inflammationsprofil	(Lu et al., 2014, Milind et al., 2020)
Alterung des Gehirns	rs1990622	T	C	Protektive Variante korreliert mit reduziertem Inflammationsprofil	(Rhinn and Abeliovich, 2017, Li et al., 2020),
Leukodystrophie	rs1554310600 (D252N)	c.754G>A		Sehr seltene Kodierende Mutation Starke Hypomyelisierung, Verlangsamte Entwicklung der motorischen Fähigkeiten	(Simons et al., 2017, Yan et al., 2018)

Tabelle 1: SNPs in dem *TMEM106B* Gen Lokus in verschiedenen neurodegenerativen Krankheitsbildern. Angepasst aus: (Feng et al., 2021).

5.2 TMEM106B-abhängige Regulation der Proteindegradation

TMEM106B ist ein Typ 2 Transmembranprotein mit fünf Glykosylierungsstellen und kann von SPPL2a (engl.: Signal Peptide Peptidase-like 2a) innerhalb der Transmembranproteine prozessiert werden (**Abbildung 8**) (Lang et al., 2012, Brady et al., 2013). Die Expression von TMEM106B ist sowohl in FTD-Patienten als auch in *Grn*$^{-/-}$ Mäusen erhöht (Götzl et al., 2014). Interessanterweise ist TMEM106B auch in Mausmodellen für lysosomale Speicherkrankheiten (*Ctsd*$^{-/-}$) um ein vielfaches erhöht (Götzl et al., 2014).

Das Risiko Allel (T) in SNP rs1990622 in *TMEM106B* führt zu einer erhöhten Expression (Van Deerlin et al., 2010, Cruchaga et al., 2011, van der Zee et al., 2011, van Blitterswijk et al., 2014). In *GRN*-FTD, *C9ORF72*-FTD und AD-Patienten wurde das Risiko Allel (T) SNP rs1990622 mit erhöhtem Aufkommen der TDP-43 Pathologie korreliert (Van Deerlin et al., 2010, Cruchaga et al., 2011, van der Zee et al., 2011, van Blitterswijk et al., 2014, Gallagher et al., 2014, Nelson et al., 2019, Hokkanen et al., 2020, Yang et al., 2020). Ob TMEM106B einen direkten Einfluss auf die Entstehung der TDP-43 Pathologie hat, ist nicht untersucht. TDP-43 wird sowohl über das Proteasom als auch über die Autophagie abgebaut, deshalb ist ein Verständnis über die TMEM106B-abhängige Regulation der Proteindegradation essenziell.

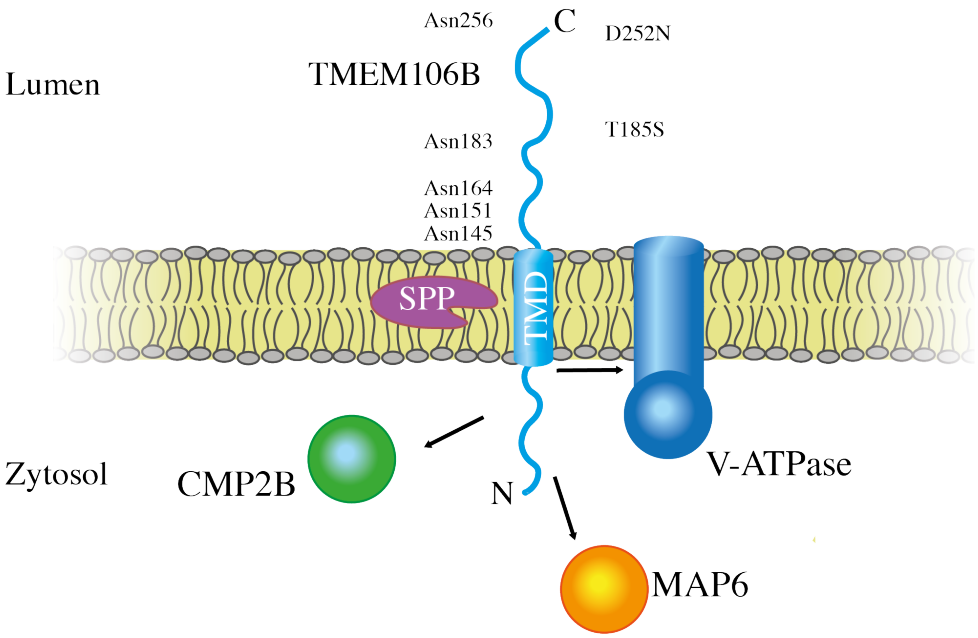

Abbildung 10: Schematische Darstellung der Topologie von TMEM106B. Abgebildet sind der luminale C-terminus (C), die Transmembrandomäne (TMD) und der zytoplasmatische N-terminus (N). Die Gylskosylierungsstellen sind links gekennzeichnet (Asn145 - Asn256). Rechts sind die beiden einzigen Krankheit-assoziierten kodierenden Mutation T185S (Threonin zu Serin) und D252N (Asparaginsäure zu Asparagin) gekennzeichnet. Angepasst aus (Nicholson and Rademakers, 2016, Ware et al., 2020)

Überexpressionsexperimente zeigten, dass TMEM106B sowohl in Lysosomen als auch in Endosomen lokalisiert ist (Lang et al., 2012). In kultivierten Zellen führt eine erhöhte Expression von TMEM106B zu vergrößerten Lysosomalen-Kompartimenten (LAMP1-postiv) (Brady et al., 2013, Stagi et al., 2014, Busch et al., 2016, Kundu et al., 2018). Eine erhöhte TMEM106B Expression bewirkte, dass der mTOR abhängige Transkriptionsfaktor-EB (TFEB) in den Kern wandert (Stagi et al., 2014). TFEB wurde als ein Transkriptionsfaktor identifiziert der die Expression von vielen Lysosomalen-Hydrolasen, Lysosomalen-Membranproteinen und Autophagie-assoziierter Gene induziert (Stagi et al., 2014, Palmieri et al., 2011). Zu den TFEB induzierten Genen gehören unter anderem die Lysosomen-assoziierten Gene *CTSA, CTSB, CTSD, CTSF* und *PSAP*. Auch die Expression der V-ATPase (Vakuläre ATPase) Untereinheiten wird von TFEB induziert und gehört damit zu den TFEB-abhängigen CLEAR-Genen (engl.: Coordinated Lysosomal Expression and Regulation) (Palmieri et al., 2011, Tanaka et al., 2017).

In kultivierten Zellen bewirkte eine verstärkte TMEM106B Expression, eine erhöhte Sezernierung der Proteasen CTSA und CTSB (Ou et al., 2015, Kundu et al., 2018). Demgegenüber führte die TMEM106B Mutation D252N, vermutlich zu einem TMEM106B Funktionsverlust (Simons et al., 2017, Yan et al., 2018). So wurde in Fibroblasten von diesen Patienten eine stark verminderte Maturierung der lysosomalen Proteasen CTSB & CTSL nachgewiesen (Ito et al., 2018, Simons et al., 2017, Zhou et al., 2020, Feng et al., 2020). Damit bewirkt eine erhöhte Expression von TMEM106B in Zellulären-Systemen eine erhöhte Maturierung und Sezernierung, während eine Reduktion mit einer verminderten Maturierung der lysosomalen Proteasen einhergeht **(Abbildung 11)**. Zugleich wurde eine, im Gegensatz zu *Grn* $^{-/-}$ Mäusen, reduzierte CTSA, CTSB, CTSD und CTSL Expression in *Tmem106b* $^{-/-}$ Mäusen

festgestellt (Klein et al., 2017, Feng et al., 2020). Damit würden PGRN und TMEM106B einen entgegengesetzten Effekt auf einige lysosomale Proteasen haben. Die entgegengesetzte Regulation der Expression und der Maturierung einiger Cathepsine, würde eine Normalisierung der *GRN*-Pathologie durch einen TMEM106B Funktionsverlust bewirken (Klein et al., 2017).

Die Maturierung und Prozessierung der Cathepsine ist pH-abhängig, weshalb die beschriebene reduzierte Expression der V-ATPase Untereinheiten (V0, V0a1, V0c, und V0d1) durch den TMEM106B Funktionsverlust umso bedeutender ist (Klein et al., 2017). Zusätzlich wurde eine direkte Interaktion des mit der V-ATPase assoziierten Adapter Proteins (AP-1) mit TMEM106B beschrieben (Klein et al., 2017). Diese Regulation der V-ATPase Expression und Interaktion würde eine TMEM106B-abhängige Ansäuerung der Lysosomen bewirken (Klein et al., 2017). Der TMEM106B Funktionsverlust führte in Zellen zu einer reduzierten Ansäuerung der Lysosomen (Klein et al., 2017). Es wurde diskutiert, ob sowohl PGRN als auch TMEM106B den pH der Lysosomen regulieren **(Abbildung 11)** (Tanaka et al., 2017, Klein et al., 2017). Darauf basierend entstand die Hypothese, dass die PGRN-Defizienz zu einer lysosomalen Hyperfunktion führt, welche durch eine TMEM106B-Defizienz blockiert und normalisiert wird (Klein et al., 2017).

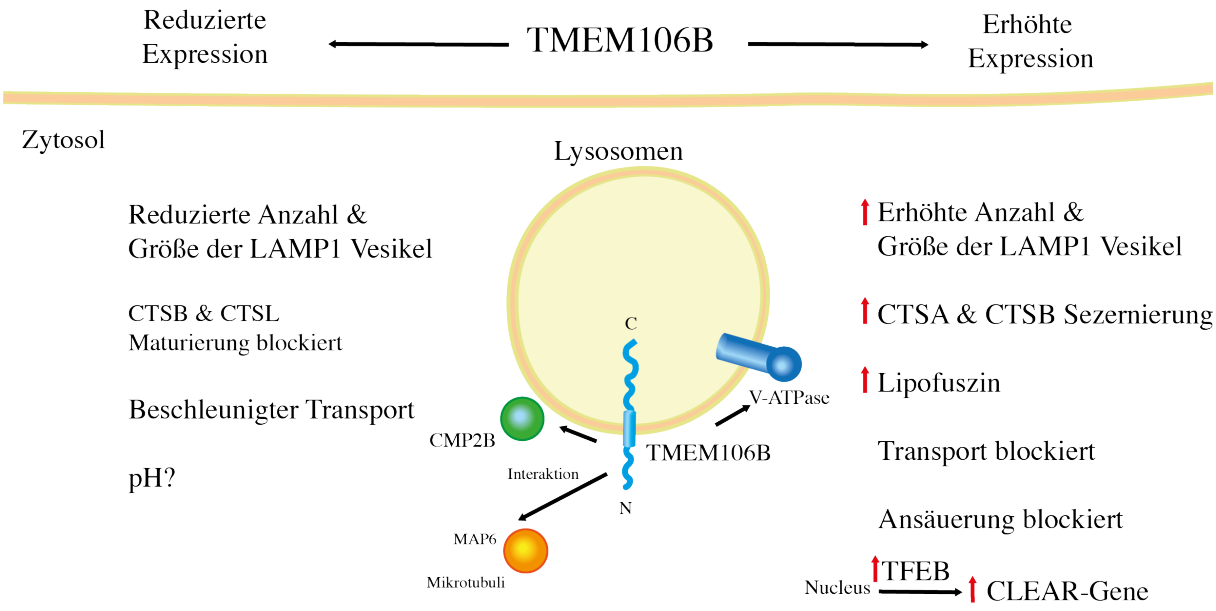

Abbildung 11: Schematische Darstellung der TMEM106B abhängigen Lysosomalen Prozesse. Abgebildet sind die TMEM106B Interaktionspartner CHMP2B, MAP6 und V-ATPase. Die Folgen einer veränderten TMEM106B-Expression sind dargestellt. Angepasst aus (Root et al., 2021).

Eine reduzierte TMEM106B Expression bewirkte, einen verstärkten retrograden lysosomalen Transport in Dendriten von kultivierten Neuronen (Schwenk et al., 2014, Stagi et al., 2014). Deshalb könnte es sein, dass eine endogene Funktion von TMEM106B darin besteht, den Transport von Lysosomen entlang der Mikrotubuli zu regulieren (Schwenk et al., 2014, Stagi et al., 2014). Zu den bekannten TMEM106B Interaktionsproteinen gehören zwei mit den Endosomen/Lysosomen-Transport assoziierte Proteine. Darunter das Mikrotubuli-assoziierte Protein (MAP6) und das Autophagie-assoziierte CHMP2B (engl.: Charged Multivesicular Body Protein 2B) **(Abbildung 11)** (Schwenk et al., 2014, Jun et al., 2015).

5.3 TMEM106B-abhängige Regulation der Inflammation

Bei der Expressionsanalyse von *post mortem* Gehirngewebe von AD-Patienten, die einen späten Krankheitsbeginn haben, wurde das protektive Allel (C) in SNP rs1990622 mit einer reduzierten Entzündung in Verbindung gebracht (Milind et al., 2020). Eine Studie hat die mRNA-Expressionsdaten von Autopsie-Proben von über 7000 Probanden miteinander verglichen und mit dem Alter der Probanden korreliert (Rhinn and Abeliovich, 2017). Dabei wurde festgestellt, dass einige Probanden, ab einem Alter von 65 Jahren, von ihrem Expressionsmuster eher älteren Probanden entsprachen als ihrer eigenen Altersgruppe. Gene die von Mikroglia, Astrozyten und Oligodendrozyten exprimiert werden, waren in ihrer Expression vom Alter der Probanden abhängig (Rhinn and Abeliovich, 2017). GWAS in diesen Probanden, zeigten genetische Variationen in den Genloci *GRN* und *TMEM106B*. Jedoch waren nur SNPs in *TMEM106B* signifikant assoziiert. Die SNPs in *TMEM106B* haben, ab einem Alter von 65 Jahren, einen Effekt auf das Transkriptom im Gehirn und verschieben vor allem die Expression von Genen die mit Entzündungspprozessen assoziiert sind. Zu den differenziell regulierten Genen gehörten unter anderem Komplementfaktor *C1QA* sowie *TREM2, CSTL* und *GFAP*. Träger der Risiko-Variante SNP rs1990622(T) glichen von ihrem Expressionsmuster damit eher älteren als gleichaltrigen Personen (Rhinn and Abeliovich, 2017).

II. Zielsetzung dieser Arbeit

In *GRN*-FTLD-Patienten wurden SNPs in *TMEM106B* als Risikofaktor identifiziert (Van Deerlin et al., 2010, Cruchaga et al., 2011, van der Zee et al., 2011). Zusätzlich wurden in *GRN*-Patienten und in FTLD-Patienten, ohne Mutation in *GRN,* erhöhte Protein-Mengen an TMEM106B detektiert.
Der Einfluss der Expression von TMEM106B auf die PGRN-Pathologie wird kontrovers diskutiert. Unter anderem wurde die Hypothese aufgestellt, dass eine Reduktion der TMEM106B-Proteinmenge, die PGRN-Pathologie positiv beeinflussen kann (Nicholson and Rademakers, 2016, Klein et al., 2017). Diese Hypothese wollte ich in einem Mausmodell überprüfen. Das Ziel dieses Projektes war es zu klären, wie die beiden lysosomalen Proteine TMEM106B und PGRN funktionell zusammenhängen und ob sich die lysosomalen Veränderungen gegenseitig nivellieren. Wie ändern sich die Neuronen und Astrozyten und werden die Mikroglia in ihrem Aktivierungsprofil verändert? Wie ändert sich die TDP-43 Pathologie von alten $Grn^{-/-}$ Mäusen, wenn TMEM106B nicht mehr exprimiert wird **(Publikation I)**? Das Verständnis darüber wie PGRN und TMEM106B interagieren ist von enormer Bedeutung, da TMEM106B Risiko-SNPs vor allem als zusätzlicher Faktor in neurodegenerativen Erkrankungen im Zusammenhang mit TDP-43 Pathologie auftreten.

TMEM106B wurde in Zellkultur Experimenten mit dem Transport von Lysosomen in Verbindung gebracht (Lang et al., 2012, Schwenk et al., 2014). Daher wollte ich zusätzlich in meiner Doktorarbeit die physiologische Funktion von TMEM106B *in vivo* genauer untersuchen. Das Ziel war es, zu verstehen, in welchen zellulären Prozessen und in welchen Zelltypen das Transmembranprotein TMEM106B eine Rolle spielt. Welche Folgen hätte der Expressionsverlust von TMEM106B für die Lysosomen in ihrer Zusammensetzung und Funktion *in vivo* **(Publikation II)**?

PGRN wird hauptsächlich von Mikroglia exprimiert. Welche Auswirkungen ein Funktionsverlust von PGRN auf den Aktivierungszustand der Mikroglia hat, war jedoch noch nicht untersucht. Julia Götzl konnte in Zusammenarbeit mit dem Labor von Dr. Oleg Butovsky zeigen, dass akut isolierte Mikroglia eine charakteristische Krankheits-assoziierte Mikroglia mRNA Signatur aufweisen. Mein Ziel für dieses Teilprojektes war somit die biochemische und funktionelle Analyse von primären Mikroglia und von Mikroglia-Zelllinien. Welche Folgen hat der Expressionsverlust von PGRN für isolierte und kultivierte Mikroglia **(Publikation III)**?

III. Meine Beiträge zu den Publikationen dieser kumulativen Dissertation

Loss of TMEM106B potentiates lysosomal and FTLD-like pathology in progranulin-deficient mice.
G. Werner, M. Damme, M. Schludi, J. Gnorich, K. Wind, K. Fellerer, B. Wefers, W. Wurst, D. Edbauer, M. Brendel, C. Haass and A. Capell 2020.
EMBO Reports 21(10):e50241.

The FTLD Risk Factor TMEM106B Regulates the Transport of Lysosomes at the Axon Initial Segment of Motoneurons.
P. Luningschror*, G. Werner*, S. Stroobants, S. Kakuta, B. Dombert, D. Sinske, R. Wanner, R. Lullmann-Rauch, B. Wefers, W. Wurst, R. D'Hooge, Y. Uchiyama, M. Sendtner, C. Haass, P. Saftig, B. Knoll, A. Capell and M. Damme 2020.
Cell Reports 30(10):3506-3519.e6. * Geteilte Erstautorenschaft

Opposite microglial activation stages upon loss of PGRN or TREM2 result in reduced cerebral glucose metabolism.
J. K. Götzl*, M. Brendel*, G. Werner*, S. Parhizkar, L. S. Monasor, G. Kleinberger, A. V. Colombo, M. Deussing, M. Wagner, J. Winkelmann, J. Diehl-Schmid, J. Levin, K. Fellerer, A. Reifschneider, S. Bultmann, P. Bartenstein, A. Rominger, S. Tahirovic, S. T. Smith, C. Madore, O. Butovsky, A. Capell and C. Haass 2019.
EMBO Molecular Medicine 11(6):e9711. * Geteilte Erstautorenschaft

1 Beitrag zur Publikation I

Im Rahmen dieser Publikation etablierte ich *Grn*$^{-/-}$*/ Tmem106b*$^{-/-}$ Defiziente Mäuse. Diese Mäuse untersuchte ich auf Verhaltensauffälligkeiten, Genexpressionsänderungen und auf weitere biochemische und immunhistologische Veränderungen. Meine Ergebnisse legen nahe, dass ich das erste Tiermodell etabliert habe, welches zumindest einige der charakteristischen FTLD-TDP-Merkmale rekapituliert. Darunter TDP-43 Phosphorylierung und Aggregation, gepaart mit einer massiven Astrogliose und Mikrogliose. Somit konnte ich die Hypothese widerlegen und zeigen, dass eine Reduktion der TMEM106B Level die GRN-abhängige FTLD-Pathologie weiter verstärkt (Publikation I).

Als Erstautor, dieser Veröffentlichung habe ich, gemeinsam mit Anja Capell und Christian Haass, die Studie erarbeitet und geplant. Ich habe das Mausmodell etabliert, alle biochemischen und immunhistologischen Untersuchungen durchgeführt und ausgewertet. Des Weiteren habe ich die Verhaltenstests, nach dem Training durch Martin Schludi, vollständig durchgeführt und analysiert. Die PET-Scans wurden durch die Gruppe von Matthias Brendel durchgeführt. Die RNA-Extraktion wurde von Katrin Fellerer durchgeführt, Aufbereitung und Auswertung der Expressionsdaten wurden von mir umgesetzt. Alle Abbildungen (außer der TSPO-PET und der Rückenmark-Daten) wurden von mir erstellt.

Alle von mir beigetragenen Ergebnisse sind in den Abbildungen 1 A-E, 2 A-E, 3A-E, 4 A-D, 5 A-E, 6 A-C, 7A-F, 8 A-D und EV1, EV2, EV4, EV5 gezeigt (Werner et al., 2020).

2 Beitrag zur Publikation II

In von mir per CRISPR/Cas9 generierten *Tmem106b*$^{-/-}$ Zellen konnte ich eine generelle Reduktion der lysosomalen Kapazität und, infolgedessen, ein Autophagie-Problem beobachten. Ich generierte eine *Tmem106b*$^{-/-}$ Mauslinie durch Verpaarung, einer bestehenden *Tmem106b*-LoxP-Linie, mit einer Cre-Recombinase-Linie. Die initialen Beobachtungen, in den von mir generierten zellulären Modellen, konnte ich in der von mir etablierten Mauslinie bestätigen. Zusätzlich konnte ich in einem komplett unabhängig generierten Mausmodell von Markus Damme die gleichen Lysosomalen Veränderungen mittels Biochemie detektieren. Meine biochemischen Analysen in den beiden Mausmodellen zu unterschiedlichen Zeitpunkten zeigten, dass TMEM106B die Maturierung verschiedener Cathepsine beeinflusst und somit auch den Protein-Abbau in den Lysosomen. Zusätzlich konnte ich auf biochemischer Ebene eine Akkumulation der Autophagie Marker p62 und LC3 zu beobachten. Die Funktion von TMEM106B ist damit im Zusammenspiel von Autophagie und Lysosomen zu verorten. Diese Ergebnisse könnten erklären, warum SNPs in *TMEM106B* in unterschiedlichen neurodegenerativen Erkrankungen zu finden sind (Publikation II).

Begründung für eine geteilte Erstautorenschaft (Publikation II):
Als einer der Erstautoren habe ich ein Mausmodell etabliert und zusammen mit einem weiteren Mausmodell biochemisch charakterisiert. Diese Veröffentlichung beantwortet unterschiedlichste Aspekte der physiologischen Funktion von TMEM106B in *vivo*. Markus Damme entdeckte vergrößerte lysosomale Kompartimente in Motoneuronen im *Nucleus facialis*. Patrick Lüningschrör bestätigte diese lysosomalen Beeinträchtigungen in isolierten und kultivierten Motoneuronen. Durch die kombinierte Expertise konnten wir, in dem von mir etablierten *Tmem106b*$^{-/-}$ Mäusen und einem zweiten unabhängigen Tiermodellen, die Funktion von TMEM106B untersuchen und validieren.

Alle von mir beigetragenen Ergebnisse sind in den Abbildungen 1F, 5C, S3A, S3B, S3F, S7A, S7B gezeigt (Lüningschrör et al., 2020).

3 Beitrag zur Publikation III

Im Rahmen dieser Veröffentlichung konnte ich belegen, dass sich die erhöhte Transkription von DAM-Genen, in isolierten *Grn*$^{-/-}$ Mikroglia, auch auf Ebene der Protein-Expression widerspiegelt. Dafür habe ich erfolgreich Mikroglia aus Mausgehirnen isoliert und biochemisch analysiert. Die isolierten *Grn*$^{-/-}$ Mikroglia weisen erhöhte Protein Level für mehrere DAM Marker Proteine auf, unter diesen, TREM2, CLEC7A, CD68, sowie APOE. Zusätzlich konnte ich bei isolierten und anschließend kultivierten Mikroglia von Wiltdtyp, *Grn*$^{-/-}$ und *Trem2*$^{-/-}$ Mäusen Phagozytose Messungen mit *E.coli*-Bakterien-Partikeln durchführen. So konnte ich belegen, dass auch kultivierte *Grn*$^{-/-}$ Mikroglia eine erhöhte Phagozytose-Rate als funktionelle Konsequenz der DAM-Signatur aufweisen. Gleichzeitig konnte ich die von mir etablierte Technik, zur genetischen Modifikation der BV-2 Zelllinie, für dieses Projekt nutzen. Der Verlust der PGRN-Expression führt auch in den von mir per CRISPR/Cas9 generierten *Grn*$^{-/-}$ Mikroglia-Zelllinie zu der ähnlich erhöhten Expression von DAM-Genen. Diese Verschiebung hin zu einem überaktivierten Zustand, äußerte sich ebenso in einer erhöhten Phagozytose-Kapazität. Somit konnte ich zeigen, dass sowohl in akut isolierten Mikroglia, als auch in

genetisch modifizierten mikroglialen Zelllinien, ein Verlust der PGRN-Expression zu einer funktionalen Hyperaktivierung der Zellen führt (Publikation I).

Begründung für eine geteilte Erstautorenschaft (Publikation I):
Als einer der Erstautoren, habe ich primäre Mikroglia isoliert sowie biochemisch und funktionell analysiert. Zusätzlich konnte ich in von mir etablierten *Grn*$^{-/-}$ Mikroglia-Zelllinie funktionelle Konsequenzen analysieren. Dieses umfangreiche Projekt wurde mit unterschiedlichster Methodik experimentell von mehreren Personen getragen. Julia Götzl führte die Isolation und Gen-Expression-Analyse von Mikroglia durch. Matthias Brendel untersuchte die Aktivierungszustände der Mikroglia und den Glukose-Metabolismus *in vivo*. Erst durch diese interdisziplinäre Zusammenarbeit war es möglich, die verschiedenen funktionellen Konsequenzen eines PGRN-Expressionsverlustes zu untersuchen.

Alle von mir beigetragenen Ergebnisse sind in den Abbildungen 2 A,B,G,H, 3 A, EV1 A und EV1 B dargestellt (Götzl et al., 2019).

IV. Ergebnisse

1 Publikation I

Loss of TMEM106B potentiates lysosomal and FTLD-like pathology in progranulin-deficient mice.
G. Werner, M. Damme, M. Schludi, J. Gnorich, K. Wind, K. Fellerer, B. Wefers, W. Wurst, D. Edbauer, M. Brendel, C. Haass and A. Capell 2020.
EMBO Reports 21(10):e50241.

Alle von mir beigetragenen Ergebnisse sind in den Abbildungen 1 A-E, 2 A-E, 3A-E, 4 A-D, 5 A-E, 6 A-C, 7A-F, 8 A-D und EV1, EV2, EV4, EV5 gezeigt (Werner et al., 2020).

Article

SOURCE DATA | TRANSPARENT PROCESS | OPEN ACCESS

EMBO reports

Loss of TMEM106B potentiates lysosomal and FTLD-like pathology in progranulin-deficient mice

Georg Werner[1], Markus Damme[2], Martin Schludi[3], Johannes Gnörich[4], Karin Wind[4], Katrin Fellerer[1], Benedikt Wefers[3,5], Wolfgang Wurst[3,5,6], Dieter Edbauer[3], Matthias Brendel[4], Christian Haass[1,3,6,*] & Anja Capell[1,**]

Abstract

Single nucleotide polymorphisms (SNPs) in *TMEM106B* encoding the lysosomal type II transmembrane protein 106B increase the risk for frontotemporal lobar degeneration (FTLD) of *GRN* (progranulin gene) mutation carriers. Currently, it is unclear if progranulin (PGRN) and TMEM106B are synergistically linked and if a gain or a loss of function of TMEM106B is responsible for the increased disease risk of patients with *GRN* haploinsufficiency. We therefore compare behavioral abnormalities, gene expression patterns, lysosomal activity, and TDP-43 pathology in single and double knockout animals. $Grn^{-/-}$/$Tmem106b^{-/-}$ mice show a strongly reduced life span and massive motor deficits. Gene expression analysis reveals an upregulation of molecular signature characteristic for disease-associated microglia and autophagy. Dysregulation of maturation of lysosomal proteins as well as an accumulation of ubiquitinated proteins and widespread p62 deposition suggest that proteostasis is impaired. Moreover, while single $Grn^{-/-}$ knockouts only occasionally show TDP-43 pathology, the double knockout mice exhibit deposition of phosphorylated TDP-43. Thus, a loss of function of TMEM106B may enhance the risk for *GRN*-associated FTLD by reduced protein turnover in the lysosomal/autophagic system.

Keywords FTD; neurodegeneration; progranulin; TDP-43; TMEM106B
Subject Categories Molecular Biology of Disease; Neuroscience
DOI 10.15252/embr.202050241 | Received 17 February 2020 | Revised 5 August 2020 | Accepted 10 August 2020
EMBO Reports (2020) e50241

Introduction

Frontotemporal lobar degeneration (FTLD) is the second most common pre-senile neurodegenerative disease after Alzheimer's disease and is predominantly characterized by either tau or TAR DNA-binding protein 43 (TDP-43) depositions. Clinically, FTLD-TDP patients present with behavior and personality changes as well as speech disabilities (Snowden *et al*, 2006). In addition, many patients show an overlap with motor neuron diseases like amyotrophic lateral sclerosis (ALS) (Hardy & Rogaeva, 2014). A strong family history of dementia is present in FTD patients, implicating a significant genetic component. *C9orf72* repeat expansions (DeJesus-Hernandez *et al*, 2011; Renton *et al*, 2011) and progranulin (PGRN) haploinsufficiency are common causes of familial FTLD with TDP-43 pathology (FTLD-TDP) (Baker *et al*, 2006; Cruts *et al*, 2006; Gass *et al*, 2006). PGRN appears to exhibit neurotrophic and anti-inflammatory activities (Bateman *et al*, 2018). In addition, loss of PGRN is linked to dysfunctional lysosomal degradation and autophagy (Chang *et al*, 2017; Kao *et al*, 2017). While patients with PGRN haploinsufficiency show lysosomal abnormalities and present with some biochemical phenotypes of neuronal ceroid lipofuscinosis (NCL) (Gotzl *et al*, 2014; Ward *et al*, 2017), homozygous mutations leading to total loss of PGRN result in classical NCL (Smith *et al*, 2012; Almeida *et al*, 2016). PGRN is upregulated upon lysosomal dysfunction (Capell *et al*, 2011) and co-regulated with other lysosomal genes (Sardiello *et al*, 2009; Belcastro *et al*, 2011). Furthermore, PGRN is transported to lysosomes (Hu *et al*, 2010; Zhou *et al*, 2015) where it is processed by lysosomal proteases to granulin peptides (Holler *et al*, 2017; Lee *et al*, 2017; Zhou *et al*, 2017b). Lysosomal gene expression in *Grn* knockout mice is upregulated during aging (Gotzl *et al*, 2014; Klein *et al*, 2017) or injury (Tanaka *et al*, 2013, 2017; Beel *et al*, 2017). In line with lysosomal dysfunction in *GRN*-associated FTLD, aged *Grn* knockout mice are characterized by accumulation of lipofuscin, saposin D, the autophagy markers SQSTM1/p62 and ubiquitin. It is still puzzling that TDP-43 pathology is abundant in *GRN* patients, but only occasionally observed in aged *Grn* knockout mice (Ahmed *et al*, 2010; Yin *et al*, 2010a; Ghoshal *et al*, 2012; Petkau *et al*, 2012; Wils *et al*, 2012; Gotzl *et al*, 2014; Tanaka *et al*, 2014).

1 Metabolic Biochemistry, Biomedical Center (BMC), Faculty of Medicine, Ludwig-Maximilians-Universität München, Munich, Germany
2 Institute of Biochemistry, Kiel University, Kiel, Germany
3 German Center for Neurodegenerative Diseases (DZNE), Munich, Germany
4 Department of Nuclear Medicine, University Hospital, Ludwig-Maximilians-Universität München, Munich, Germany
5 Institute of Developmental Genetics, Helmholtz Zentrum München, German Research Center for Environmental Health, Neuherberg, Germany
6 Munich Cluster for Systems Neurology (SyNergy), Munich, Germany
*Corresponding author. Tel: +49 89440046550; E-mail: christian.haass@mail03.med.uni-muenchen.de
**Corresponding author. Tel: +49 89440046534; E-mail: anja.capell@mail03.med.uni-muenchen.de

The high variability in age of onset as well as the incomplete penetrance of *GRN* mutations led to the search for genetic risk factors in a genome-wide association study (GWAS), which identified single nucleotide polymorphisms (SNPs) in the *TMEM106B* locus that segregate with *GRN*-associated FTLD (Van Deerlin *et al*, 2010). *TMEM106B* risk variants are also associated with *C9orf72* repeat mutations (van Blitterswijk *et al*, 2014; Gallagher *et al*, 2014), TDP-43 pathology, severity of *GRN* independent FTLD, and other neurodegenerative disorders (Rutherford *et al*, 2012; Murray *et al*, 2014; Nelson *et al*, 2015; Yu *et al*, 2015). The most significant SNPs are in high linkage disequilibrium with a SNP that leads to a threonine to serine exchange at amino acid 185. The minor protective S185 allele is underrepresented in FTLD and may thus reduce the risk of *GRN* mutation carriers (Cruchaga *et al*, 2011; Finch *et al*, 2011; van der Zee *et al*, 2011). However, contradictory findings make it difficult to understand how TMEM106B and PGRN functionally interact to increase the risk for FTLD-TDP. There is some evidence that the risk haplotype enhances inflammatory gene expression (Rhinn & Abeliovich, 2017; Ren *et al*, 2018), whereas the protective variant provides neuroprotection (Li *et al*, 2020). Functionally, TMEM106B is linked to the lysosomal protein degradation pathway and autophagy suggesting an interaction with similar functions of PGRN. TMEM106B is an endo-lysosomal type 2 transmembrane protein and plays a crucial role in regulating lysosomal size, morphology, subcellular trafficking, and acidification (Chen-Plotkin *et al*, 2012; Lang *et al*, 2012; Brady *et al*, 2013; Schwenk *et al*, 2014; Stagi *et al*, 2014). In neurons, TMEM106B overexpression leads to enlarged lysosomes, inhibits their acidification and transport, and results in accumulation of LAMP1-positive structures at the cell soma (Stagi *et al*, 2014). This may be in line with increased mRNA and protein levels (Van Deerlin *et al*, 2010; Nicholson *et al*, 2013; Gallagher *et al*, 2017) in FTLD-TDP patients (Van Deerlin *et al*, 2010; Chen-Plotkin *et al*, 2012; Gotzl *et al*, 2014). This would also be consistent with the observation that a *Tmem106b* knockout rescues lysosomal deficits in *Grn* knockout mice (Klein *et al*, 2017). However, knockdown of TMEM106B also results in clustering of lysosomes in nuclear proximity and enhanced retrograde transport in dendrites (Schwenk *et al*, 2014; Clayton *et al*, 2018). Moreover, similar to TMEM106B overexpression, TMEM106B deficiency in mice also results in impaired lysosomal acidification and reduced lysosomal enzyme activities (Klein *et al*, 2017; Arrant *et al*, 2018) and altered axonal transport accompanied by accumulation of lipofuscin and autophagosomes (Luningschror *et al*, 2020). Thus, it is currently unclear if a loss or a gain of function contributes to the elevated risk for FTLD.

To understand a potential pathological consequence and synergistic effects of PGRN and TMEM106B loss of function, we investigated single knockout and double knockout animals. Surprisingly, we found that loss of TMEM106B strongly enhanced age-related PGRN phenotypes resulting in robust TDP-43 pathology, early lysosomal dysfunction accompanied by an accumulation of ubiquitinated proteins, severe microgliosis/astrogliosis, and dramatically reduced life span. This suggests that the *TMEM106B* risk alleles may modulate *GRN*-associated FTLD via a loss-of-function mechanism.

Results

Loss of PGRN and TMEM106B leads to early motor deficits in mice

To understand the contribution of a loss of function of TMEM106B to FTLD pathology, we generated *Grn/Tmem106b* double knockout animals. The *Tmem106b*$^{-/-}$ mouse line was generated by injection of targeted ES cells (KOMP clone EPD0047_1_E02) into BALB/C blastocysts. Germline transmission of the tm2a allele (Wtsi lacZ genetrap "knockout first" cassette between exon3 and exon4) was verified, and the mice were bred with constitutively *Cre* recombinase expressing mice to delete exon 4 and generate the *Tmem106b*$^{-/-}$ (tm2b) founder generation (Fig 1A) (see also (Luningschror *et al*, 2020)). *Grn*$^{-/-}$/*Tmem106b*$^{-/-}$ mice were generated by crossing *Tmem106b*$^{-/-}$ mice with *Grn*$^{-/-}$ mice (Kayasuga *et al*, 2007). All genotypes were verified by Western blotting (Fig 1B). In contrast to the single knockout lines, double knockout *Grn*$^{-/-}$/*Tmem106*b$^{-/-}$ mice showed a reduced life expectancy. According to animal welfare practices, we had to sacrifice these mice at 16–18 weeks of age when they reached pre-defined endpoint criteria. The hind-leg clasping reflex test revealed an overt phenotypic difference between 3-month-old *Grn*$^{-/-}$/*Tmem106b*$^{-/-}$ mice and single knockout littermates or wild-type (WT) mice. *Grn*$^{-/-}$/*Tmem106b*$^{-/-}$ mice showed sustained hind limb clasping associated with trunk flexion while single knockout and WT mice held their hind limbs apart with paw external rotation (Fig 1C). Furthermore, the rotarod test confirmed motor incoordination in *Grn*$^{-/-}$/*Tmem106b*$^{-/-}$ mice (Fig 1D). The motor deficits of the *Grn*$^{-/-}$/*Tmem106b*$^{-/-}$ mice, visible by shaking-like movements and paresis

Figure 1. Early motor deficits in *Grn*$^{-/-}$/*Tmem106b*$^{-/-}$ mice.

A Schema of the mouse wild-type and mutant *Tmem106b* locus. The *tm2a* allele carries a *LacZ-Neo* selection cassette in intron 3 and a loxP-flanked exon 4. Upon *Cre* recombinase expression in the germline, exon 4 is deleted and *Tmem106b* expression abolished (*tm2b allele*).

B Western blot analysis of total brain lysates of wild-type, *Tmem106b*$^{-/-}$, *Grn*$^{-/-}$ and *Grn*$^{-/-}$/*Tmem106b*$^{-/-}$ mice using antibody 6F2 to detect TMEM106B. (4.5-month-old mice with the given genotype; n = 3 biological replicates per genotype).

C Hind limb clasping test wild-type, *Tmem106b*$^{-/-}$, *Grn*$^{-/-}$, *Grn*$^{+/-}$/*Tmem106b*$^{-/-}$ and *Grn*$^{-/-}$/*Tmem106b*$^{-/-}$ mice. Representative pictures are shown of three mice analyzed for each genotype at 3 months of age.

D Rotarod performance of wild-type, *Tmem106b*$^{-/-}$, *Grn*$^{-/-}$, *Grn*$^{+/-}$/*Tmem106b*$^{-/-}$ and double knockout animals at 3–4 months of age. Number of animals used for analysis, 10 wild-type, 12 *Tmem106b*$^{-/-}$, five *Grn*$^{-/-}$, seven *Grn*$^{+/-}$/*Tmem106b*$^{-/-}$, three *Grn*$^{-/-}$/*Tmem106b*$^{-/-}$ mice.

E Representative picture of a 4.5-month-old double knockout (*Grn*$^{-/-}$/*Tmem106b*$^{-/-}$) mouse after manual flip.

Data information: For statistical analysis (D), one-way ANOVA with Tukey's *post hoc* test was used to compare the mean ± SD of the individual genotypes. Significance is indicated; *P < 0.05; **P < 0.01; and ****P < 0.0001.
Source data are available online for this figure.

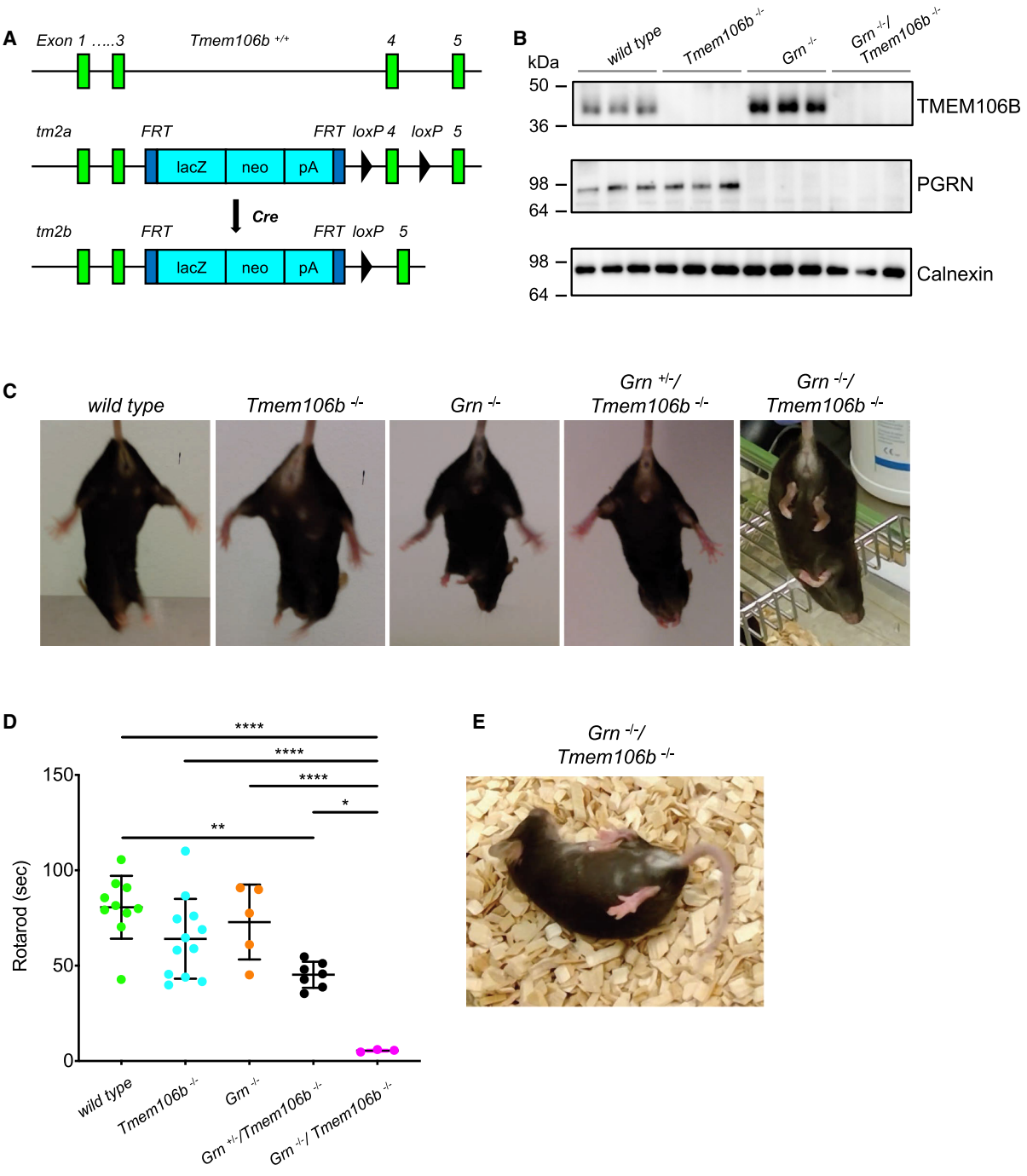

Figure 1.

of hind limbs, increased with age to a stage in which the mice could not turn back, when they were manually flipped over (Fig 1E and Movie EV1). To investigate whether the total loss of TMEM106B and PGRN is required for developing such a strong phenotype, we analyzed $Grn^{-/+}/Tmem106b^{-/-}$ mice. Although the hind-leg clasping reflex was normal (Fig 1C) and the mice could not be turned on their back, rotarod performance was significantly impaired compared to WT but significantly improved compared to double

knockout mice (Fig 1D). Thus, reduced PGRN levels in combination with TMEM106B loss of function exacerbate the rather mild phenotypes of the individual knockouts. However, the strong effect on life expectancy only occurred upon total loss of both proteins PGRN and TMEM106B.

Enhanced dysregulation of genes in the double knockout is associated with microglia and astrocyte function

To specify functional changes in $Grn^{-/-}/Tmem106b^{-/-}$ mice, we analyzed the expression of genes associated with neurodegenerative diseases using the nCounter® Neuropathology panel (NanoString Technologies) in total brain of 4.5-month-old mice. Genes expressed in neurons, astrocytes, microglia, oligodendrocytes, and endothelial cells, addressing six fundamental themes of neurodegeneration including neurotransmission, neuron–glia interaction, neuroplasticity, cell structure integrity, neuroinflammation, and metabolism, were analyzed. Gene expression levels of 760 genes in each sample were normalized against the geometric mean of 10 housekeeping genes. The most significant dysregulation of genes was found in $Grn^{-/-}/Tmem106b^{-/-}$ mice (Fig 2A–C). While in single knockout mice expression of genes was altered no more than two-fold up or 0.5-fold down, in the double knockout mice 23 genes were dysregulated above/below these values. Overlap in gene expression was considered if a gene was significantly changed in the respective mouse models with more than 20% change in at least one mouse model. Most overlap exists between $Tmem106b^{-/-}$ and $Grn^{-/-}/Tmem106b^{-/-}$ mice (15 genes, 10 up, five down), while the strongest modulation occurs in a gene cluster associated with activated microglia in $Grn^{-/-}$ and $Grn^{-/-}/Tmem106b^{-/-}$ mice (Cd68, C1qc) or in all three mouse models (Trem2, C1qa, C1qb; Fig 2D). Notably, almost all overlapping genes are regulated in the same direction. The double knockout mice show the strongest effects, and the changes in gene expression are not simply the additive effects of single knockout mice (Fig 2D). In line with previous findings, pathway analyses revealed upregulation of gene clusters associated with activated microglia, autophagy (Lui *et al*, 2016; Gotzl *et al*, 2019), and angiogenesis in $Grn^{-/-}$ mice and in $Tmem106b^{-/-}$ mice (Fig 2E). Scores of these gene clusters were strongly elevated in the double knockout animals (Fig 2E), suggesting severe microgliosis and deficits in protein degradation. Moreover, all downregulated genes in $Grn^{-/-}/Tmem106b^{-/-}$ mice are associated with "axon and dendrite structure" and "neural connectivity". The strongest downregulation in $Grn^{-/-}/Tmem106b^{-/-}$ mice was observed for genes affecting "myelination" (Fa2h, Mog, Mag, Ugt8a, Mal; Fig 2C). Note that downregulation of myelination-associated genes could be confirmed on the protein level (Fig EV1). Interestingly, in several pathways associated with neuronal function like "neuronal cytoskeleton", "myelination", "axon and dendrite structure", and "vesicle trafficking", a high score is only observed in double knockout mice, while single knockout mice show no changes (Fig 2E).

Besides upregulated genes associated with hyperactivated microglia, Gfap is 6.5-fold upregulated and therefore after Cd68, which is eight-fold upregulated, the second strongest upregulated gene in the double knockout mice (Fig 2C). Thus, we also addressed glial pathology by analyzing gene expression using the nCounter® Neuroinflammation panel (NanoString Technologies) covering 757 genes and 13 housekeeping in total brain of 4.5-month-old mice. Gene expression levels were analyzed as described for the nCounter® Neuropathology panel. As expected expression changes in the single knockout mice are low, no gene reaches a two-fold or 0.5-fold change in expression (Fig 3A and B). The double knockout mice show again the strongest effects with 27 genes either with a two-fold or 0.5-fold change, and 126 genes with more than 20% change (Fig 3C). Changes in gene expression are not simply additive (Fig 3D). Ninteen genes were altered in all three mouse models and 17 genes altered in the double knockout together with either single knockout (Fig 3D). As observed for the Neuropathology panel, almost all overlapping genes are regulated in the same direction. Downregulation overlapped only in $Tmem106b^{-/-}$ and $Grn^{-/-}/Tmem106b^{-/-}$ mice, while upregulation overlapped more between $Grn^{-/-}$ and $Grn^{-/-}/Tmem106b^{-/-}$ mice in astrocytic and microglial expressed genes (Fig 3D). Furthermore, all inflammation-associated pathways, like "innate and adaptive", "immune response", "inflammatory signaling", and "astrocyte and microglia function", were slightly upregulated in $Grn^{-/-}$ mice and strongly increased in $Grn^{-/-}/Tmem106b^{-/-}$ mice (Fig 3E). Thus, the hyperactivated microglial state identified in the Neuropathology panel was confirmed with the Neuroinflammation panel. In line with expression changes of genes associated with myelination, detected in the Neuropathology panel,

Figure 2. Expression analysis reveals global dysregulation of gene clusters associated with autophagy and microglial activation in double knockout mice.

A–C Volcano plot of differentially expressed brain mRNAs of 4.5-month-old mice (n = 3 biological replicates per genotype) detected by the Neuropathology panel of NanoString. Expression changes were only taken into consideration when the extent of change was above 20% as indicated by vertical lines for all volcano plots. Gliosis- and myelination-related genes are highlighted if changes are above 20%. Fold changes are displayed after $\log_2$ transformation. (A) Comparison of differentially expressed brain mRNAs from $Tmem106b^{-/-}$ and wild-type mice. From 680 detected genes, 21 are significantly upregulated, while 10 are significantly reduced. (B) Comparison of $Grn^{-/-}$ and wild-type mice. From 680 detected genes, 12 are significantly upregulated, while six are significantly reduced. (C) Volcano plot for $Grn^{-/-}/Tmem106b^{-/-}$ and wild-type mice. From 680 detected genes, 79 are significantly upregulated, while 24 are significantly reduced.

D Display of differently expressed genes overlapping between the analyzed genotypes from (A–C). Overlap was considered if a gene was significantly changed in the respective mouse models with more than 20% change in at least one mouse model. Note that nine genes are significantly altered in all three genotypes in comparison to the wild type. Seven genes are exclusively overlapping between the $Grn^{-/-}$ and the $Grn^{-/-}/Tmem106b^{-/-}$ mice. $Tmem106b^{-/-}$ and $Grn^{-/-}/Tmem106b^{-/-}$ mice share 15 significantly altered genes. $Tmem106b^{-/-}$ and $Grn^{-/-}$ mice share one significant altered gene. Data represent the mean ± SD.

E Gene set analysis based on NanoString advanced analysis R-script included in the Neuropathology panel.

Data information: For statistical analysis of volcano plot data, unpaired two-tailed Student's t-test was performed between individual genotypes and the wild-type control condition. Significance was accepted when $P < 0.05$ as indicated by the dotted line.
Source data are available online for this figure.

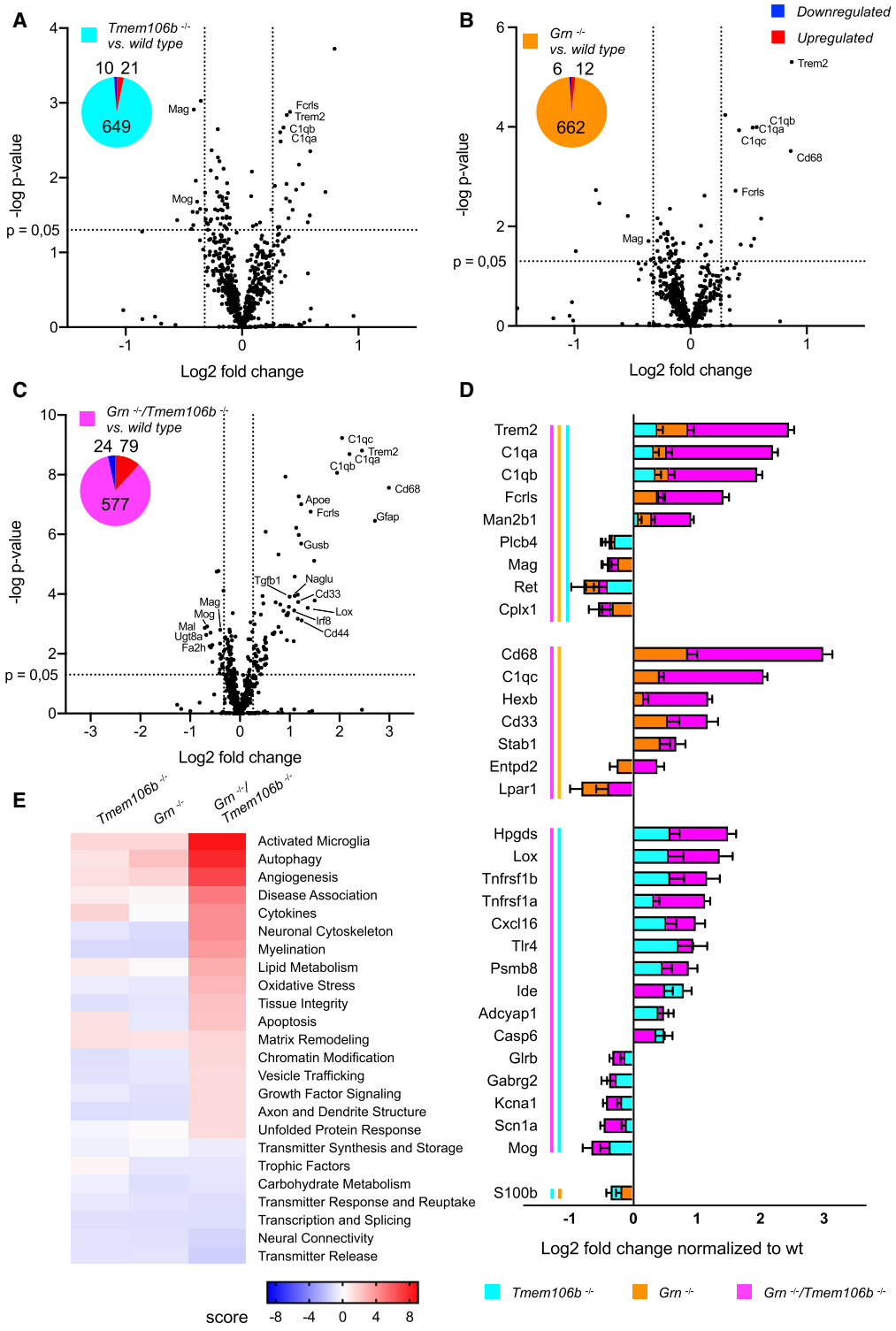
A
Tmem106b -/- vs. wild type
10 21
649
Mag
Fcrls
Trem2
C1qb
C1qa
Mog
-log p-value
p = 0,05
Log2 fold change
B
Grn -/- vs. wild type
6 12
662
Downregulated
Upregulated
Trem2
C1qb
C1qa
C1qc
Cd68
Fcrls
Mag
-log p-value
p = 0,05
Log2 fold change
C
Grn -/-/Tmem106b -/- vs. wild type
24 79
577
C1qc
Trem2
C1qa
C1qb
Cd68
Apoe
Fcrls
Gfap
Gusb
Tgfb1
Naglu
Cd33
Lox
Irf8
Cd44
Mag
Mog
Mal
Ugt8a
Fa2h
-log p-value
p = 0,05
Log2 fold change
D
Trem2
C1qa
C1qb
Fcrls
Man2b1
Plcb4
Mag
Ret
Cplx1
Cd68
C1qc
Hexb
Cd33
Stab1
Entpd2
Lpar1
Hpgds
Lox
Tnfrsf1b
Tnfrsf1a
Cxcl16
Tlr4
Psmb8
Ide
Adcyap1
Casp6
Glrb
Gabrg2
Kcna1
Scn1a
Mog
S100b
Log2 fold change normalized to wt
Tmem106b -/-
Grn -/-
Grn -/-/Tmem106b -/-
E
Tmem106b -/-
Grn -/-
Grn -/-/ Tmem106b -/-
Activated Microglia
Autophagy
Angiogenesis
Disease Association
Cytokines
Neuronal Cytoskeleton
Myelination
Lipid Metabolism
Oxidative Stress
Tissue Integrity
Apoptosis
Matrix Remodeling
Chromatin Modification
Vesicle Trafficking
Growth Factor Signaling
Axon and Dendrite Structure
Unfolded Protein Response
Transmitter Synthesis and Storage
Trophic Factors
Carbohydrate Metabolism
Transmitter Response and Reuptake
Transcription and Splicing
Neural Connectivity
Transmitter Release
score

Figure 2.

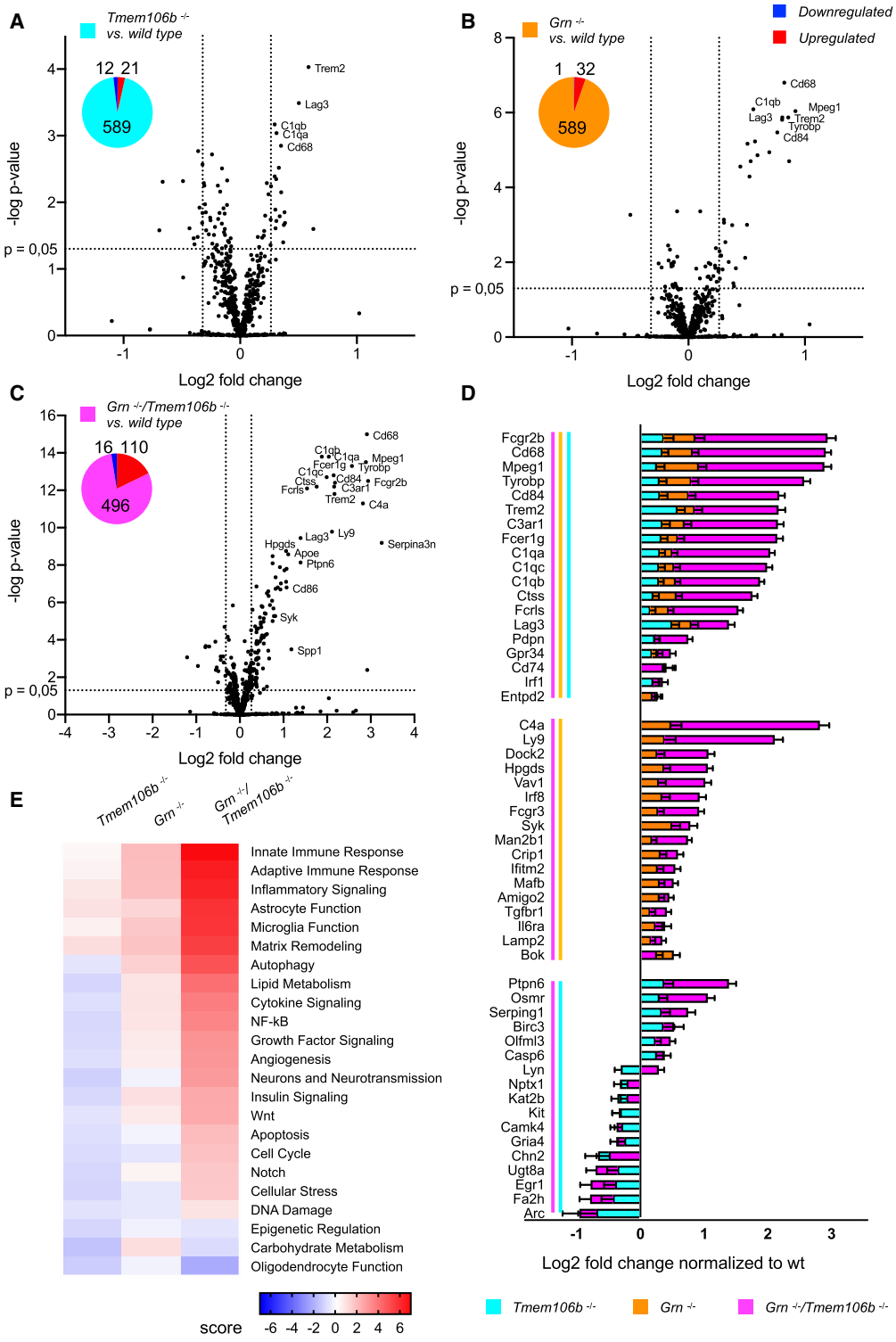

Figure 3.

Figure 3. Expression analysis reveals enhanced dysregulation of genes associated with microglia and astrocyte function.

A–C Analysis of brain mRNA expression of 4.5-month-old mice (five wild-type, four *Grn*$^{-/-}$, four *Tmem106b*$^{-/-}$, five *Grn*$^{-/-}$/*Tmem106b*$^{-/-}$ mice) detected by the Neuroinflammation panel by NanoString. Expression changes were only taken into consideration when the extent of change was above 20% as indicated by vertical lines for in all volcano plots. Gliosis-related genes are highlighted if changes are above 20%. Fold changes are displayed after $\log_2$ transformation. (A) Comparison of differentially expressed mRNA of *Tmem106b*$^{-/-}$ mice in comparison to wild-type mice. From 622 detected genes, 21 are significantly upregulated, while 12 are significantly reduced. (B) Comparison of differentially expressed mRNA in *Grn*$^{-/-}$ and wild-type mice. From 622 detected genes, 32 are significantly upregulated, while only one is significantly reduced. (C) Volcano plot of differentially expressed brain mRNAs from *Grn*$^{-/-}$/*Tmem106b*$^{-/-}$ mice in comparison to wild-type mice. From 622 detected genes, 110 are significantly upregulated, while 16 are significantly reduced.

D Display of differently expressed genes overlapping between the analyzed genotypes from (A–C). Overlap was considered if a gene was significantly changed in the respective mouse models with more than 20% change in at least one mouse model. Note that 19 genes are significantly altered in all three genotypes in comparison to the wild type. Seventeen genes are exclusively overlapping between the *Grn*$^{-/-}$ and the *Grn*$^{-/-}$/*Tmem106b*$^{-/-}$ mice. *Tmem106b*$^{-/-}$ and *Grn*$^{-/-}$/*Tmem106b*$^{-/-}$ mice share 17 significantly altered genes. Data represent the mean ± SD.

E Gene set analysis based on NanoString advanced analysis R-script included in the Neuroinflammation panel.

Data information: For statistical analysis of volcano plot data, unpaired two-tailed Student's *t*-test was performed between individual genotypes and the wild-type control condition. Significance was accepted when $P < 0.05$ as indicated by the dotted line.
Source data are available online for this figure.

"oligodendrocyte function" is also strongly reduced in the double knockout (Fig 3E).

Exaggerated gliosis in young *Grn*$^{-/-}$/*Tmem106b*$^{-/-}$ mice

To validate the changes of the mRNA signature at the protein level, we performed biochemical analyses of total brain homogenate from 4.5-month-old mice. This confirmed a significant 3.4- to 4.7-fold increase of GFAP and IBA1 expression in *Grn*$^{-/-}$/*Tmem106b*$^{-/-}$ mice (Fig 4A and B) which is in line with strong astrogliosis and microgliosis in the double knockout. Importantly and consistent with our previous findings in *Grn*$^{-/-}$ mice (Gotzl *et al*, 2014), at this age no microgliosis and astrogliosis was apparent in the single knockouts (Fig 4A and B). Next, we investigated by immunohistochemistry which brain regions were particularly affected by gliosis. Astrogliosis and microgliosis were most prominent in the thalamus, pons and medulla, midbrain, cerebellum, and cerebral cortex of the double knockout mice (Figs 4C and D, and EV2A and B). To confirm enhanced microgliosis in double knockout mice *in vivo*, we performed previously established TSPO-μPET (Brendel *et al*, 2016; Gotzl *et al*, 2019). A higher increase of TSPO signals between 2- and 3.5-month-old *Grn*$^{-/-}$/*Tmem106b*$^{-/-}$ mice compared to WT was detected in the regions of accelerated astro- and microgliosis, like thalamus, pons and medulla, midbrain, and cerebellum (Fig 4E). To further investigate microglial activation in the different mouse lines, we analyzed protein expression of CD68, CLEC7A, TREM2, and ApoE in total brain extracts of 4.5-month-old mice (Fig 5A). Quantification revealed a significant increase of all four proteins in *Grn*$^{-/-}$/*Tmem106b*$^{-/-}$ mice (Fig 5B). Only TREM2 was also significantly elevated in *Grn*$^{-/-}$ mice (Fig 5B). In *Grn*$^{-/-}$/*Tmem106b*$^{-/-}$ mice, most IBA1-positive microglia are also positive for CLEC7A, CD68, and to a lower extent for TREM2 confirming activated microglia already at the age of 4.5 months (Fig 5C–E).

The strong motor phenotype together with the gliosis in regions of the brainstem let us additionally analyze the spinal cord for astrogliosis and microgliosis. Again, only *Grn*$^{-/-}$/*Tmem106b*$^{-/-}$ mice show a strongly increased expression of GFAP and CD68, a microglial lysosomal membrane protein, in both white and gray matter (Fig EV3).

Enhanced lysosomal and autophagic dysfunction in *Grn*$^{-/-}$/*Tmem106b*$^{-/-}$ mice

Activation of microglia is accompanied by elevated expression of lysosomal cathepsins, which was described for aged *Grn*$^{-/-}$ mice (Ahmed *et al*, 2010; Wils *et al*, 2012; Tanaka *et al*, 2013; Gotzl *et al*, 2014; Klein *et al*, 2017). In line with these observations, *Grn*$^{-/-}$/*Tmem106b*$^{-/-}$ mice show elevated levels of the cathepsin D, cathepsin B, and cathepsin L compared to WT and single knockout mice (Fig 6A and B). The elevated CatD and CatL expression levels result in significantly increased enzymatic activities compared to WT and single knockout mice (Fig 6C). Elevated lysosomal protease expression and lysosomal activity often indicate impaired protein degradation and accumulation of autophagy cargo as observed in NCL mouse models (Gotzl *et al*, 2014) and in aged *Grn* knockout mice (Ahmed *et al*, 2010; Wils *et al*, 2012; Gotzl *et al*, 2014). Furthermore, autophagy is among the strongest hits in the pathway analysis

Figure 4. Astrogliosis and microgliosis in different brain regions of *Grn*$^{-/-}$/*Tmem106b*$^{-/-}$ mice.

A Western blot analysis of GFAP and IBA1 in total brain lysates from 4.5-month-old mice with the given genotype (n = 3 biological replicates per genotype).

B Quantification of (A). Protein expression was normalized to levels in wild-type animals. Data represent the mean ± SD.

C Expression of GFAP in sagittal brain sections. Representative images of indicated brain regions (CBX, cerebellum; CTX, cortex; MY, medulla; TH, thalamus). Scale bar indicates 100 μm.

D Expression of IBA1 in sagittal brain sections. Representative images of indicated brain regions (CBX, cerebellum; CTX, cortex; MY, medulla; TH, thalamus). Scale bar indicates 100 μm.

E *In vivo* ^{18}F-GE180 TSPO μPET imaging. Two female *Grn*$^{-/-}$/*Tmem106b*$^{-/-}$ and five female wild-type mice underwent longitudinal TSPO μPET at 2.0 and 3.5 months of age. All analyses were performed by PMOD (V3.5, PMOD technologies). Normalization of injected activity was performed by the previously validated myocardium correction method.

Data information: (B), one-way ANOVA with Tukey's *post hoc* test was used to compare individual genotypes. Significance is indicated; ***$P < 0.001$; and ****$P < 0.0001$.
Source data are available online for this figure.

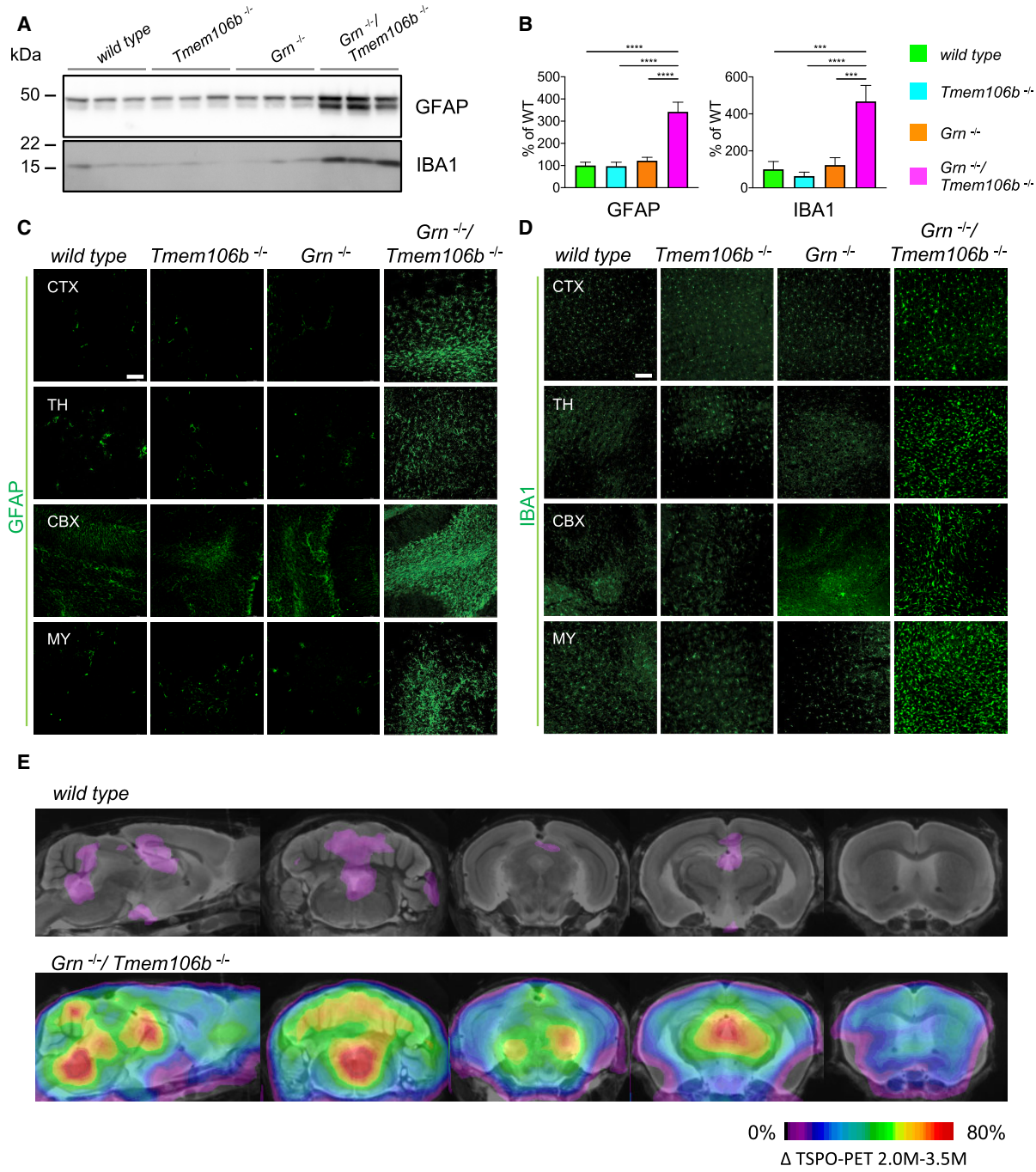

Figure 4.

of both NanoString panels (Figs 2E and 3E); therefore, we next investigated accumulation of autophagic cargo. Since the complete loss of PGRN results in a NCL-like storage phenotype with exaggerated deposition of lipofuscin in aged mice (Kleinberger *et al*, 2013), we investigated the autofluorescence signal in single and double knockout mice. Lipofuscin is detectable predominantly in the thalamus of the double knockout mice, while the single knockout mice show weak (*Tmem106b*$^{-/-}$) or no lipofuscin deposition (*Grn*$^{-/-}$) at

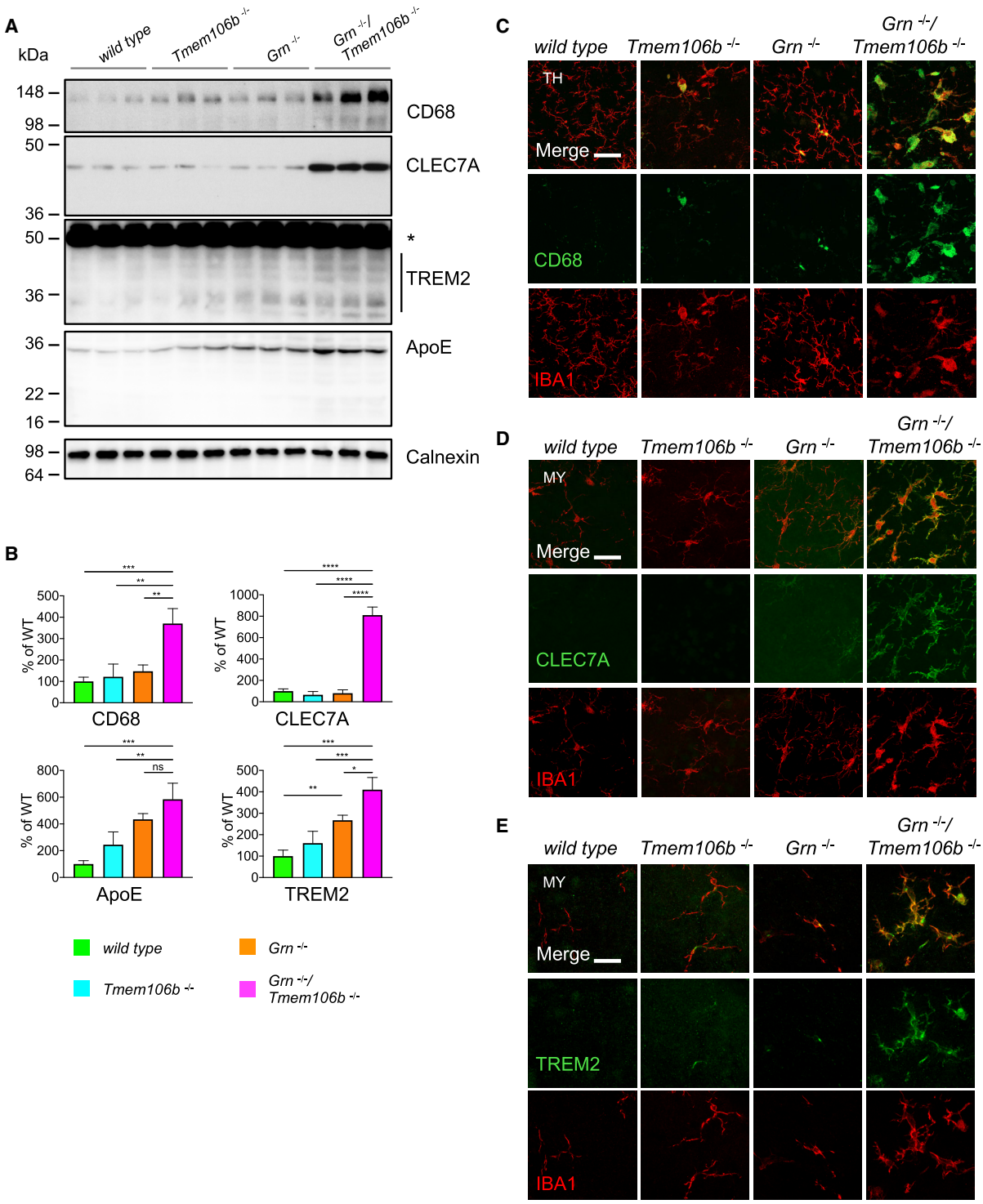

Figure 5.

Figure 5. Enhanced expression of proteins associated with activated microglia in $Grn^{-/-}/Tmem106b^{-/-}$ mice.

A Western blot analysis of CD68, CLEC7A, TREM2, and ApoE in total brain lysates from 4.5-month-old mice with the given genotype. Asterisk indicates unspecific band (n = 3 biological replicates per genotype).

B Quantification of (A). Protein expression was normalized to levels in wild-type animals. Data represent the mean ± SD.

C Expression of CD68 and the microglial marker IBA1 in sagittal brain sections. Representative images of indicated brain regions (TH, thalamus). Scale bar indicates 25 μm.

D Expression of CLEC7A and the microglial marker IBA1 in sagittal brain sections. Representative images of indicated brain regions (MY, medulla). Scale bar indicates 25 μm.

E Expression of TREM2 and the microglial marker IBA1 in sagittal brain sections. Representative images of indicated brain regions (MY, medulla). Scale bar indicates 25 μm.

Data information: For statistical analysis of protein levels (B), one-way ANOVA with Tukey's *post hoc* test was used to compare individual genotypes. Significance is indicated; *$P < 0.05$; **$P < 0.01$; ***$P < 0.001$; and ****$P < 0.0001$.
Source data are available online for this figure.

4.5 months of age (Fig 7A). Interestingly, in $Grn^{-/-}/Tmem106b^{-/-}$ mice lipofuscin accumulation partially overlaps with the microglia marker IBA1, which may suggest early degradation deficits in microglia (Fig 7A). Lipofuscin accumulation indicates a dysfunction in protein degradation as described for NCL (Palmer *et al*, 2013) and *GRN*-associated FTLD (Ward *et al*, 2017). Since protein aggregates and long-lived proteins are normally cleared by autophagy, we investigated the multifunctional adaptor protein p62/sequestosome1 (p62/SQSTM1), which directs ubiquitinated cargos for autophagy. Indeed, $Grn^{-/-}/Tmem106b^{-/-}$ mice show robustly elevated p62/SQSTM1 levels in RIPA and urea lysates compared to single knockout and WT mice (Fig 7B and C). The accumulation of p62/SQSTM1 in the urea lysate reflects reduced solubility and indicates elevated protein aggregation. Furthermore, p62/SQSTM1 accumulates in all brain regions associated with elevated astrogliosis and microgliosis of $Grn^{-/-}/Tmem106b^{-/-}$ mice including the spinal cord (Figs 7D and EV3). Co-staining of p62/SQSTM1 with NeuN, Iba1, or GFAP shows that most p62/SQSTM1 accumulates in neurons and not in microglia or astrocytes (Figs 7E and F). The minor co-localization of p62 with microglia is also supported by little overlay in the cerebellar staining (Fig EV4). In line with accumulation of the p62/SQSTM1, ubiquitinated proteins are significantly increased and autophagosomes are accumulated, as indicated by elevated LC3II levels, in double knockout mice compared to single knockout mice (Fig 7B and C).

Accelerated TDP-43 aggregation and phosphorylation in $Grn^{-/-}/Tmem106b^{-/-}$ mice

The pathological hallmarks of *GRN*-associated FTLD are nuclear and cytoplasmic, ubiquitin positive inclusions composed of phosphorylated TDP-43 and its proteolytically generated C-terminal fragments. In aged *Grn* knockout mice, cytoplasmic TDP-43 depositions were only occasionally detected (Guo *et al*, 2010; Kleinberger *et al*, 2010; Yin *et al*, 2010b). To address the question if the additional loss of TMEM106B promotes TDP-43 pathology in the *Grn* knockout mice, we performed immunohistochemistry. Small cytoplasmic TDP-43 inclusions were detected throughout the brain of $Grn^{-/-}/Tmem106b^{-/-}$ mice (Figs 8A and EV5). They were less frequent in the cortex and most abundant in the midbrain (Fig 8A). Some of the inclusions also contain TDP-43 phosphorylated at amino acids 409/410, a specific hallmark of FTLD-TDP (Hasegawa *et al*, 2008; Neumann *et al*, 2009) (Fig 8B). Sequential high salt (HS), RIPA, and urea extraction of total brain homogenate revealed slightly reduced levels of TDP-43 holoprotein in the HS fraction of the $Grn^{-/-}/Tmem106b^{-/-}$ mice compared to WT and $Tmem106b^{-/-}$ mice (Fig 8C and D), but elevated levels of a RIPA-extracted C-terminal TDP-43 fragments of approximately 35 kDa (Fig 8C and D). Moreover, phosphorylated TDP-43, specifically detected in the urea fraction, is significantly elevated in the double knockout mice (Fig 8C and D).

Discussion

In this study, we demonstrate that the combined knockout of *Tmem106b* and *Grn* accelerates the phenotypes of the individual knockout mice suggesting that a loss of function of TMEM106B further promotes *Grn*-associated FTLD.

Motor impairment is an early and very prominent phenotype detected in $Grn^{-/-}/Tmem106b^{-/-}$ mice and to a much lesser extent in $Grn^{+/-}/Tmem106b^{-/-}$ mice already at 3 months of age (Fig 1C–E). Hind limb clasping and paralysis has been observed in a number of mouse models for neurodegenerative diseases like Alzheimer's disease, Parkinson's disease, and other tauopathies (http://www.inf

Figure 6. Elevated lysosomal enzyme levels and activity in $Grn^{-/-}/Tmem106b^{-/-}$ mice.

A Western blot analysis of cathepsin (Cat) D, B, and L in total brain lysates from 4.5-month-old mice with the indicated genotype. Different maturation variants are indicated (hc, heavy chain; p, preform; sc, single chain; n = 3 biological replicates per genotype).

B Quantification of proteolytically generated variants of cathepsin D, B, and L normalized to levels in wild-type animals from (A). Data represent the mean ± SD.

C Catalytic activity of cathepsin D, B, and L. Total brain lysates from 4.5-month-old mice were incubated with quenched fluorogenic substrate for Cat D, Cat B, and Cat L. The linear increase of fluorescence signal was measured and then normalized to wild type. Data represent the mean normalized activity ± SD (n = 3 biological replicates per genotype).

Data information: For statistical analysis of normalized data (B, C), one-way ANOVA with Tukey's *post hoc* test was used to compare individual genotypes. Significance is indicated; ns $P > 0.05$; *$P < 0.05$; **$P < 0.01$; ***$P < 0.001$; and ****$P < 0.0001$.
Source data are available online for this figure.

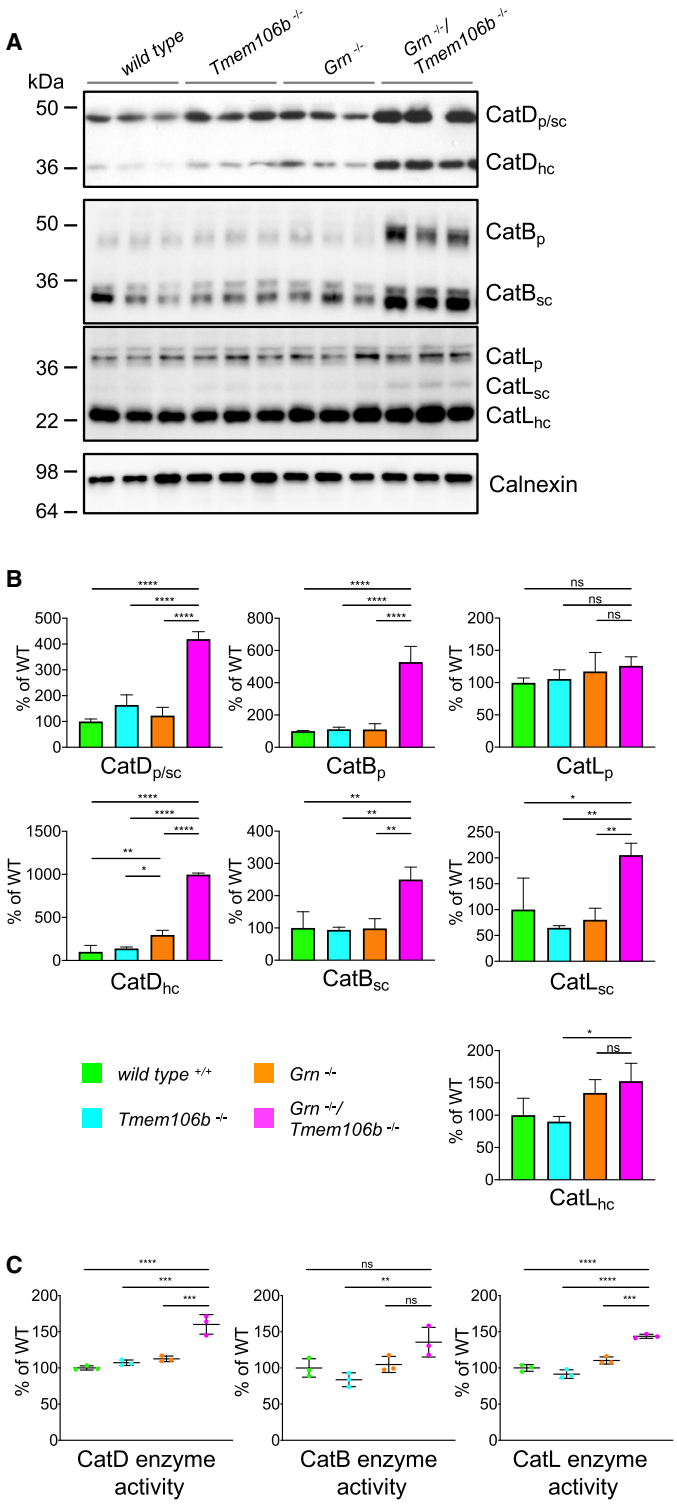

Figure 6.

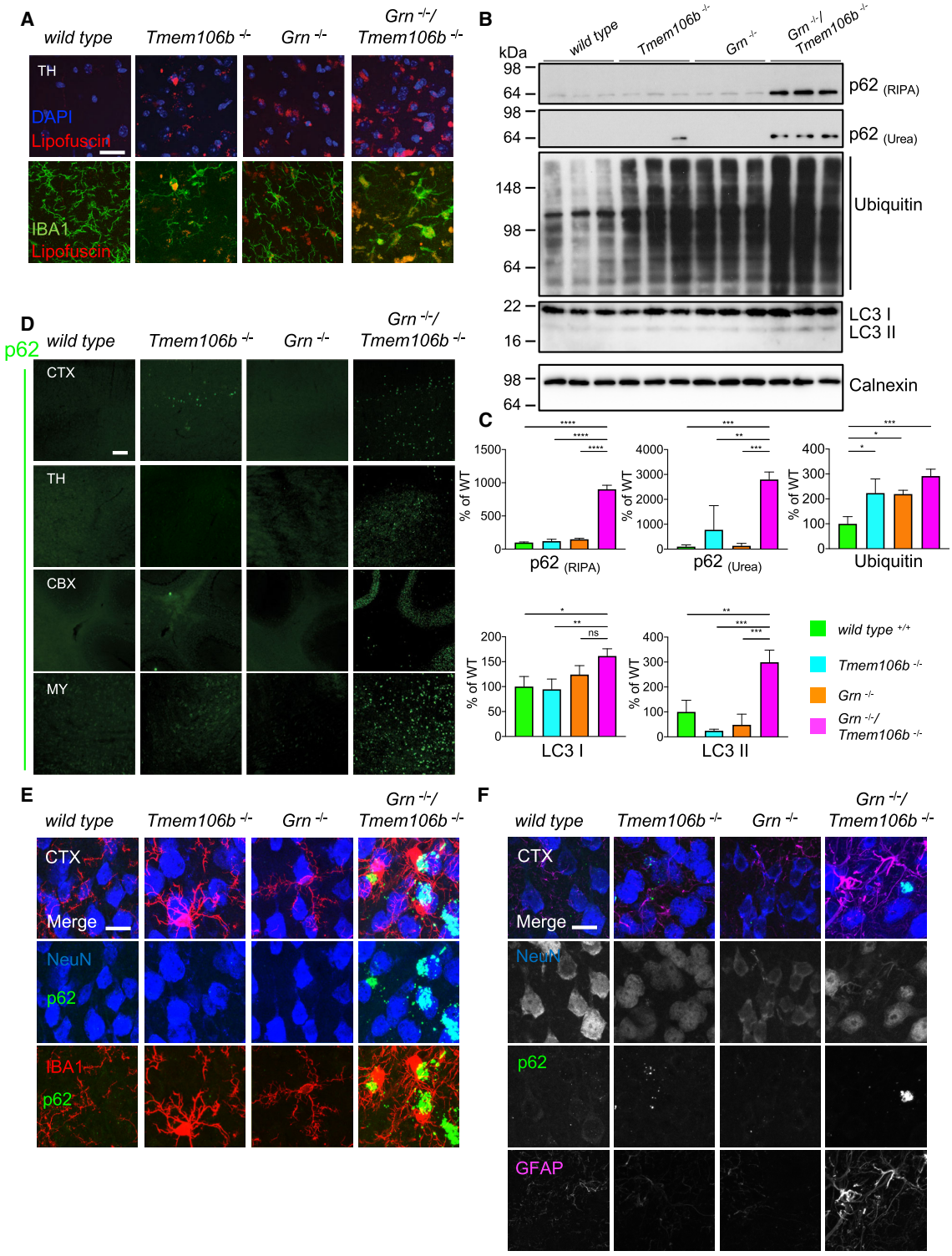

Figure 7.

Figure 7. Widespread impairment of autophagy and protein degradation in $Grn^{-/-}/Tmem106b^{-/-}$ mice.

A Immunofluorescence analysis of lipofuscin (red) and IBA1 (green) in sagittal brain sections. Representative images of the thalamus (TH). Scale bar indicates 25 μm.

B Western blot analysis of ubiquitin and the autophagy marker LC3 in RIPA, and p62 in RIPA and urea total brain lysates from 4.5-month-old mice with the indicated genotype. Calnexin used as a loading control. (n = 3 biological replicates per genotype).

C Quantification of (B). Protein expression was normalized to levels in wild-type animals. Data represent the mean ± SD.

D Immunofluorescence analysis of p62 in sagittal brain sections. Representative images of indicated brain regions (CBX, cerebellum; CTX, cortex; MY, medulla; TH, thalamus). Scale bar indicates 100 μm.

E Localization of p62 mainly in NeuN-positive cells in the cortex (CTX) of 4.5-month-old mice. Minor overlap of aggregates with microglial marker IBA1. Scale bar indicates 15 μm.

F Complete overlap of co-staining of p62 with NeuN in the cortex (CTX) and not with the reactive astrocyte marker GFAP. Scale bar indicates 15 μm.

Data information: For statistical analysis of normalized data (C), one-way ANOVA with Tukey's *post hoc* test was used to compare individual genotypes. Significance is indicated; ns $P > 0.05$; *$P < 0.05$; **$P < 0.01$; ***$P < 0.001$; and ****$P < 0.0001$.
Source data are available online for this figure.

ormatics.jax.org/mp/annotations/MP:0001513) and may indicate progression of neurodegeneration, including cerebellar ataxia. In addition, several FTD/ALS mouse models (Wils *et al*, 2010; Le *et al*, 2016; Liu *et al*, 2016) as well as autophagy-related mouse models (Komatsu *et al*, 2005; Hara *et al*, 2006) present with similar motor deficits. Impaired autophagy has been associated with many neurodegenerative diseases (Nixon, 2013) including FTD/ALS (Gotzl *et al*, 2016). In *Tmem106b* and *Grn* double knockout mice, dysfunction in the lysosomal/autophagic degradation is indicated by accumulation of lipofuscin, ubiquitinated proteins, and the cargo adaptor protein p62 (Fig 6A–E). P62 interacts with autophagic substrates and delivers them to autophagosomes for degradation. Since p62 is also degraded during this process, accumulation of p62 suggests that the turnover of autophagosomes may be delayed which is also indicated by LC3II accumulation. Elevated autophagy associated with an increase of autophagosomes and cargo adaptor proteins is unlikely since mRNA expression of autophagy initiating genes and cargo adaptors is not elevated. However, we cannot distinguish between a failure of autophagosome/lysosome fusion or lysosomal degradation of engulfed autolysosome since both would result in cargo, p62 and LC3II accumulation.

A significant contribution of dysfunctional autophagy to the prominent phenotype of the double knockout mice is further supported by "autophagy" being one of the strongest hits in the pathway analysis of the nCounter® Neuropathology gene expression panel (Fig 2E). Indicators of impaired protein degradation are also detected in single knockout mice, albeit to a much lesser extent. In line with our earlier findings (Gotzl *et al*, 2018), "autophagy" was also one of the strongest hits in the pathway analysis in $Grn^{-/-}$ mice (Fig 2E). Furthermore, in line with previous findings (Ahmed *et al*, 2010; Ghoshal *et al*, 2012; Wils *et al*, 2012; Petkau *et al*, 2016; Beel *et al*, 2017; Tanaka *et al*, 2017; Zhou *et al*, 2017a; Gotzl *et al*, 2018) $Grn^{-/-}$ mice also showed impaired protein degradation but recognizable effects occur after the age 6 months.

Besides PGRN, the lysosomal transmembrane protein TMEM106B is linked to lysosomal integrity and function (Chen-Plotkin *et al*, 2012; Lang *et al*, 2012; Brady *et al*, 2013; Schwenk *et al*, 2014; Stagi *et al*, 2014). In cell culture, loss of TMEM106B affects lysosomal positioning and trafficking (Schwenk *et al*, 2014; Stagi *et al*, 2014) leading to reduced stress resistance (Stagi *et al*, 2014). However, overexpression also results in dysfunctional and enlarged lysosomes (Chen-Plotkin *et al*, 2012; Brady *et al*, 2013; Stagi *et al*, 2014) causing a translocation of the autophagy regulation transcription factor EB (TFEB) to nuclei (Stagi *et al*, 2014). Since such prominent phenotypes were detected in cellular systems, it is surprising that some *Tmem106b* knockout mouse models revealed only minor changes in lysosomal integrity (Klein *et al*, 2017; Arrant *et al*, 2018; Nicholson *et al*, 2018). We demonstrate that 4.5-month-old *Tmem106b* knockout mice show ubiquitin accumulation and few p62-positive inclusions in cortex and cerebellum (Fig 6A and C). Additionally, it was recently demonstrated that these mice show vacuolization in thalamus and facial motor nucleus accompanied by large LAMP1-positive membrane structures (Luningschror *et al*, 2020). Mechanistically, this could be explained by an enhanced retrograde axonal transport of lysosomes followed by an accumulation of endo-/lysosomal membrane structures at the axon initial segment, which may result in reduced fusion of lysosomes with autophagosomes. Reduced fusion may lead to impaired autophagic degradation in *Tmem106b* mice (Luningschror *et al*, 2020). Therefore, the strong phenotype of the $Grn^{-/-}/Tmem106b^{-/-}$ mice could be the consequence of disturbed lysosomal (Beel *et al*, 2017; Tanaka *et al*, 2017; Zhou *et al*, 2017a) and autophagic activities (Chang *et al*, 2017) in neurons and microglia.

In clear contrast to our observations, additional loss of TMEM106B has recently been reported to protect against the FTLD-like phenotypes in $Grn^{-/-}$ mice (Klein *et al*, 2017), while our findings and those published independently by two other research teams in this issue of EMBO Reports (Feng *et al*, 2020a; Zhou *et al*, 2020a) even demonstrate prominent gliosis, premature death, and exacerbated FTLD-like pathology. Klein *et al* report an increase in several lysosomal enzymes and their activity in 2-month-old $Grn^{-/-}$ mice. These enhanced activities of lysosomal enzymes are reduced upon additional TMEM106B knockout. However, lipofuscin accumulation is not reduced, which indicates that dysfunction in protein degradation is not improved. One may speculate that the elevated lysosomal enzyme levels and activities in $Grn^{-/-}$ mice, which predominantly occur in non-microglial cells (Gotzl *et al*, 2018), could be a rescue attempt in response to the lysosomal dysfunction. Lysosomal dysfunction shows the strongest effects in microglia since these cells have the highest PGRN expression (Lui *et al*, 2016; Gotzl *et al*, 2018) and are the degradation hub in the brain. Thus, with additional loss of TMEM106B the ability to upregulate such rescue mechanisms may be lost or overcome by factors released from malfunctional microglia. In line with the idea that TMEM106B plays a role in regulating a lysosomal rescue mechanism, it has been shown that TMEM106B knockdown reduces the signaling of TFEB (Stagi *et al*, 2014), a master regulator of the lysosomal autophagic pathway (Settembre & Ballabio, 2011; Settembre *et al*, 2011).

Loss of TMEM106B in $Grn^{-/-}$ mice dramatically enhanced astrogliosis and microgliosis (Fig 4). Note, that 7- to 18-month-old $Grn^{-/-}$ mice show similar progressive astrogliosis and microgliosis (Ahmed *et al*, 2010; Yin *et al*, 2010b; Ghoshal *et al*, 2012; Petkau *et al*, 2012; Wils *et al*, 2012) but the double knockout mice develop these phenotypes already before 4.5 months of age. Furthermore,

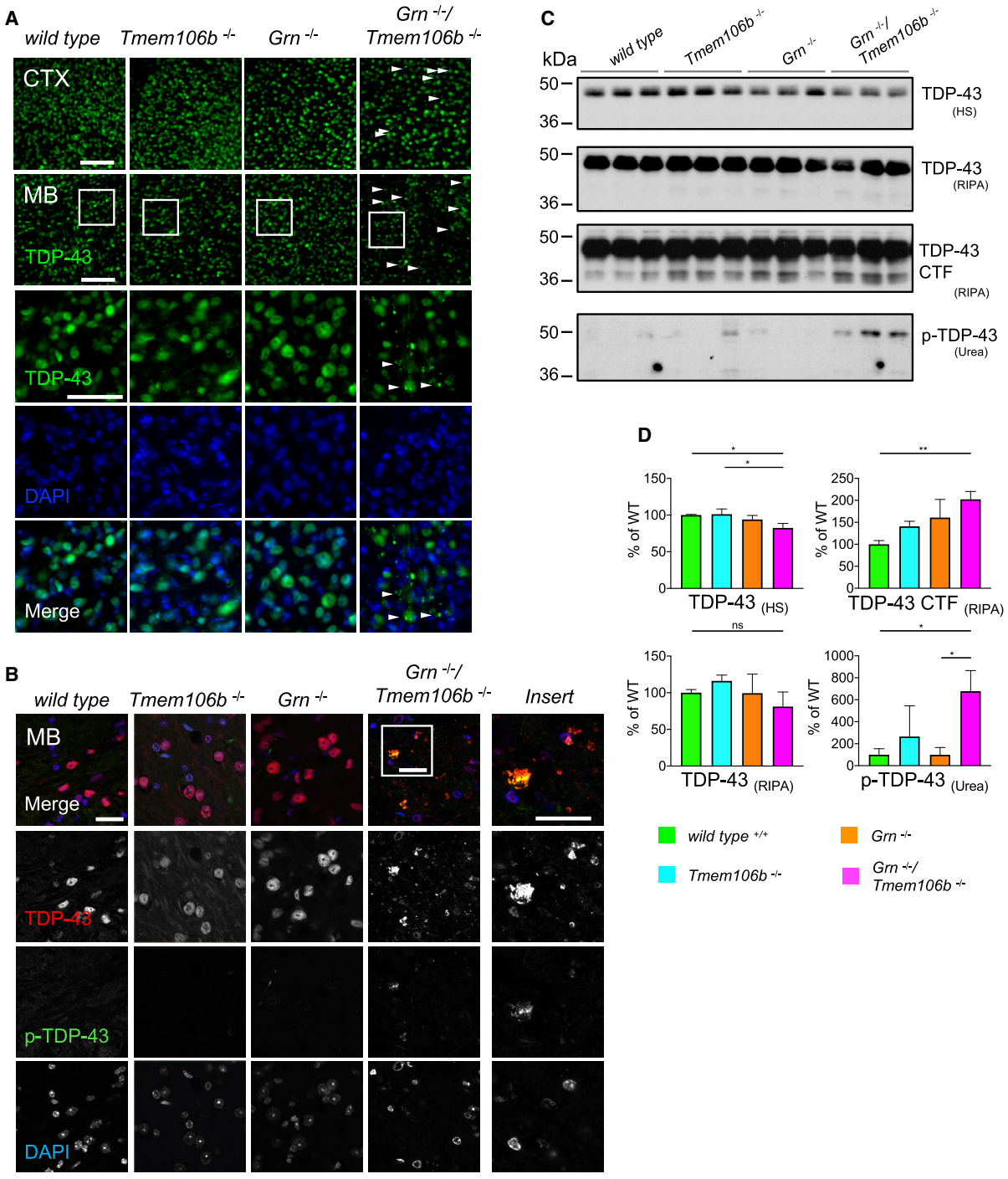

Figure 8.

Figure 8. Enhanced TDP-43 aggregation and phosphorylation in $Grn^{-/-}/Tmem106b^{-/-}$ mice.

A Immunofluorescence analysis of TDP-43 in sagittal brain sections. Representative images of indicated brain regions (CTX, cortex; MB, midbrain). White arrow heads indicate TDP-43 aggregation. Scale bar indicates 100 μm. Zoom in on TDP-43 aggregation in double knockout mouse brain sections of the midbrain, scale bar zoom in indicates 50 μm (animals 4.5 months of age).

B Immunofluorescence analysis of total TDP-43 and phosphorylated TDP-43 (p-TDP-43) in sagittal brain sections by confocal microscopy. Representative images of one confocal layer in the midbrain. Zoom in on TDP-43 aggregation in double knockout mouse brain sections of the midbrain. Scale bar indicates 25 μm (animals 4.5 months of age).

C Western blot analysis of TDP-43 and phosphorylated TDP-43 (p-TDP-43) in sequential high salt (HS)/RIPA/Urea fractionations of total brain lysates from 4.5-month-old mice with the indicated genotype. Analysis of C-terminal fragments of TDP-43 (CTF) in RIPA fraction. p-TDP-43 analyzed in Urea fraction (n = 3 biological replicates per genotype).

D Quantification of (C). Protein expression was normalized to levels in wild-type animals. Data represent the mean ± SD.

Data information: For statistical analysis of normalized data (D), one-way ANOVA with Tukey's *post hoc* test was used to compare individual genotypes. Significance is indicated; ns $P > 0.05$; *$P < 0.05$; **$P < 0.01$.

"activated microglia", "innate and adaptive immune response", "inflammatory signaling", and "astrocyte function" are the strongest hits in the gene expression pathway analysis (Figs 2E and 3E). Several genes related to inflammation and disease-associated microglia (DAM) are already slightly upregulated in the brain of $Grn^{-/-}$ mice (Figs 2B and 3B) and further increased in $Grn^{-/-}/Tmem106b^{-/-}$ mice (Figs 2C and 3C). Of note, the double knockout of $Grn^{-/-}/Tmem106b^{-/-}$ shifts the change in the mRNA signature to a much earlier time point as observed in $Grn^{-/-}$ alone (Lui *et al*, 2016; Gotzl *et al*, 2019). Among the strongest hits in double knockouts are mostly microglial expressed genes such as Cd68, Trem2, Tyrobp, Apoe, and complement factors but also genes associated with astrocyte activation such as Gfap, Serpina3n, and C4a (Figs 2C and 3C). Additionally, we detect in 4.5-month-old double knockouts reduced gene expression of myelination-associated genes (Fa2h, Mog, Mag, Ugt8a, Mal) and reduced protein levels of MOG and MAP (Fig EV1) which is in line with recent publications describing myelination deficits upon TMEM106B deficiency or loss of function (Feng *et al*, 2020b; Ikemoto *et al*, 2020; Zhou *et al*, 2020b).

Finally, the question arises how PGRN and TMEM106B deficiency results in lysosomal dysfunction affecting mainly microglia, which initiates autophagic cargo protein accumulation and pathological TDP-43 deposition in neurons. Since PGRN is mainly expressed in microglia, whereas TMEM106b is ubiquitously expressed within the brain (with the lowest expression in microglia), it is tempting to speculate that microglia lacking PGRN may initiate a pathological crosstalk to neurons. Another option would be that TMEM106B-deficient neurons required protective support from microglia, which could not be provided upon additional PGRN deficiency. In the same vein, malfunctioned oligodendrocytes may not receive support in the absence of PGRN. These scenarios suggest that dysfunctional microglia cannot appropriately communicate with other brain cells or are unable to compensate neuronal or oligodendrocyte defects.

Materials and Methods

Animal experiments

All animal experiments were performed according to German animal welfare law and approved by the government of upper Bavaria. Mice were kept under standard housing conditions including standard pellet food and water provided *ad libitum*. Recombinant mouse ES cells carrying *loxP* sites flanking *Exon 4* of *Tmem106b (tm2a allele)* were provided by the KOMP consortium (Clone EPD0047_1_E02). Blastocyst injection of the *tm2a* allele carrying ES cells leads to chimeric mice that were further bread with *Cre* deleter mice after germline transmission to obtain the $Tmem106b^{-/-}$ mouse line. The $Grn^{-/-}$ mouse line was kindly provided by Dr. M. Nishihara. Breeding and behavior tests were performed under the animal license: ROB-55.2-2532.Vet_02-17-106. Mice were perfused with PBS after deep/lethal anesthesia.

Rotarod behavior test

The rotarod test was conducted in accordance with European and national guidelines, and all experiments were performed with the researcher blinded to the genotype. The spindle speed was accelerated from 5 to 50 rpm over 5 min. The test finished either when the mouse dropped down or after the time limit of 5 min. After three rounds of training on three individual days, the average time of three trials with 1-h break in between was used.

In vivo μPET imaging

Small animal positron emission tomography (μPET) procedures followed an established standardized protocol for radiochemistry, acquisition, and post-processing (Brendel *et al*, 2016). In brief, ^{18}F-GE180 TSPO μPET with an emission window of 60–90 min post-injection was used to measure cerebral microglial activity. Two female $Grn^{-/-}$ &$Tmem106b^{-/-}$ and five female wild-type mice underwent longitudinal TSPO μPET at 2.0 and 3.5 months of age. All analyses were performed by PMOD (V3.5, PMOD technologies, Basel, Switzerland). Normalization of injected activity was performed by the previously validated myocardium correction method (Deussing *et al*, 2018). TSPO μPET estimates (percentage changes over time) deriving from a brainstem target VOI (7 mm³) were extracted and compared descriptively between the two age and genotype groups. Percentage difference maps were calculated for the changes between baseline and follow-up for the averaged images of $Grn^{-/-}/Tmem106b^{-/-}$ and wild type.

Gene expression profiling and data analysis

Snap-frozen brain hemispheres were mechanically powdered in liquid nitrogen. Following total RNA isolation with the Qiagen RNeasy Mini Kit, 80 ng total RNA per sample was used for gene

expression profiling with the nCounter® Neuropathology panel from NanoString (NanoString Technologies). Expression analysis on the nCounter® Neuroinflammation panel was conducted using 60 ng of total RNA per sample. NanoString reads for all samples were analyzed and normalized using the nSolver software including the R plugin for advanced gene set analysis (NanoString Technologies). The geometric mean of the on-chip housekeeping genes was used for normalization of reads. The mean of each group was used for calculation of the fold changes. For the Neuropathology panel, each group contained an n of three animals. The Neuroinflammation panel was conducted on six wild-type, four $Grn^{-/-}$ and four $Tmem106b^{-/-}$ single knockout, and five double knockout $Grn^{-/-}/Tmem106b^{-/-}$ mice. Detailed information on mice used is listed in Table EV1. Volcano plots were generated by plotting the $\log_2$-transformed changes between wild-type and individual groups, against the calculated values of significance with the software GraphPad Prism 8.

Western blotting and antibodies

Mice were PBS perfused, and for biochemically analysis, each brain hemisphere was snap-frozen in liquid nitrogen and mechanically ground to powder. Brain powder was lysed in RIPA buffer (150 mM NaCl, 20 mM Tris–HCl pH 7.4, 1% NP40, 0.05% Triton X-100, 0.5% sodium deoxycholate, 2.5 mM ETDA) using the Precellys lysing kit (Ref.: P00933-LYSK0-A; Bertin Technologies). Supernatants were collected after centrifugation at 17,000 *g*, 4°C, and protein concentration was determined using the bicinchoninic acid assay (Interchim Bioscience). For analysis of TDP-43 and p62, proteins were sequentially isolated as described previously (Gotzl *et al*, 2014). All samples were boiled in Laemmli buffer, and proteins were separated on Tris-glycine gels. Proteins were transferred onto polyvinylidene difluoride membranes or nitrocellulose membranes (both GE Healthcare Life Science). HRP-conjugated antibodies and Pierce™ ECL Plus Western Blotting Substrate (Thermo Fisher Scientific) were used for visualization. The following antibodies were used for Western blotting: TMEM106B (clone 6F2, (Lang *et al*, 2012)), GFAP (DAKO, Z0334), IBA1 (GeneTex, GTX100042), CD68 (Abcam, ab125212), CLEC7A (R&D Systems, AF1756), TREM2 (clone 5F4, (Xiang *et al*, 2016), p62 (MBL, PM045), LC3 (Novusbio, NB100), Ubiquitin (Santa Cruz, clone P4D1), Cathepsin D (Santa Cruz, sc-6486), Cathepsin B (R&D Systems, AF965), Cathepsin L (R&D Systems, AF1515), TDP-43 (Proteintech, 12892-2AP), and Phospho-TDP-43 409/410 (Cosmo Bio Co, CAC-TIP-PTD-M01).

Immunofluorescence and image acquisition

Following deep/lethal anesthesia, animals were PBS perfused. One brain hemisphere was fixed overnight in 4% PFA in PBS (pH = 7.4) and transferred to 30% sucrose in PBS. Brains were processed into 35-µm-thick sagittal sections. Sections were blocked in 4% goat serum and incubated with indicated antibodies of the bellow listed primary antibodies. After several washing steps, sections were incubated with fluorophore conjugated secondary antibodies as indicated (Alexa 488, 594, 647; Thermo Fisher Scientific). After additional washing steps, nuclei were visualized with DAPI. Sections were embedded in Fluoromount™ (Sigma-Aldrich, Merck). Image acquisition was performed on a LEICA DMI-8 with a DFC9000GT camera and the following objectives: (HC PL FL L 20×/0.40 CORR PH1; HC PL APO 40×/0.95 CORR). Confocal Images were acquired on Zeiss LSM 800 Microscope Axio Observer 7 (Objective Plan-Apochromat 63×/1,4 Oil M27). The following antibodies were used for immunofluorescence: GFAP (DAKO, Z0334), IBA1 (GeneTex, GTX100042), CD68 (Abcam, ab125212), CLEC7A (R&D Systems, AF1756), TREM2 (R&D Systems, AF1729), p62 (MBL, PM045), p62 (Progen Biotech GP62C), NeuN (Millipore, MAB377), TDP-43 (Proteintech, 12892-2AP), and Phospho-TDP-43 409/410 (Cosmo Bio Co, CAC-TIP-PTD-M01).

Enzyme activity assay

Fluorescence-based activity assays (Abnova) were used to asses enzyme activity of cathepsin D, cathepsin B, and cathepsin L. Mouse brain powder was homogenized in the recommended lysis buffer and subsequently centrifuged. Cleavage of the quenched fluorescence substrate was continuously measured using the Fluoroskan Ascent FL plate reader (Labsystems).

Statistical analysis

Data were analyzed using GraphPad Prism 8. The rotarod performance is displayed as mean duration on the rotarod from three rounds of testing for each tested animal with standard deviation (SD) of the respective group. Differences between groups were tested by one-way ANOVA with Tukey's *post hoc* test (Figs 1D, 4B, 5B, 6B and C, 7C and 8D). For the analysis of gene expression, the mean of the individual group is compared to the mean of the wild-type controls by two-tailed, unpaired Student's *t*-test (Figs 2A–C and 3A–C). For multiple comparison expression analysis and enzyme activity, all data were normalized to wild type.

Significant differences are indicated as follows in all diagrams: $*P < 0.05$; $**P < 0.01$; $***P < 0.001$; and $****P < 0.0001$.

Data availability

Data sets of raw and processed data produced in this study are available in the following database:

NanoString gene sequence, raw, and processed data:
Gene Expression Omnibus accession number (GSE155065) at https://www.ncbi.nlm.nih.gov/geo/query/acc.cgi?acc = GSE155065
Gene Expression Omnibus accession number (GSE155066) at https://www.ncbi.nlm.nih.gov/geo/query/acc.cgi?acc = GSE155066

Expanded View for this article is available online.

Acknowledgements
This work is supported by the Deutsche Forschungsgemeinschaft (DFG) within the framework of the Munich Cluster for Systems Neurology (EXC 2145 SyNergy; ID 390857198). CH is supported by the Koselleck Project HA1737/16-1 of the DFG (Helmholtz-Gemeinschaft, Zukunftsthema "Immunology and Inflammation" (ZT-0027)). We thank Ramona Rodde for excellent technical assistance. We would like to acknowledge the NanoString EMEA grant program for providing a Neuropathology panel. We would like to thank Dr. M. Nishihara (Department of Veterinary Physiology, The University of Tokyo) for providing the $Grn^{-/-}$ founder mouse strain. Open access funding enabled and organized by ProjektDEAL.

Author contributions

AC, CH, and GW conceived the study and analyzed the results. AC and CH wrote the manuscript with input from all co-authors. GW performed all Western blot assays and immunofluorescence experiments. DE conducted and GW and MS performed behavioral experiments. MD performed the staining of the spinal cord and provided support on immunofluorescence techniques. JG, KW, and MB performed and analyzed TSPO-PET imaging. KF performed RNA isolation and enzyme activity assays. WW consulted and BW generated the *Tmem106b*$^{-/-}$ founder mouse from ES cells.

Conflict of interest

CH collaborates with Denali Therapeutics, participated on one advisory board meeting of Biogen, and received a speaker honorarium from Novartis and Roche. CH is chief advisor of ISAR Bioscience.

References

Ahmed Z, Sheng H, Xu YF, Lin WL, Innes AE, Gass J, Yu X, Wuertzer CA, Hou H, Chiba S *et al* (2010) Accelerated lipofuscinosis and ubiquitination in granulin knockout mice suggest a role for progranulin in successful aging. *Am J Pathol* 177: 311 – 324

Almeida MR, Macario MC, Ramos L, Baldeiras I, Ribeiro MH, Santana I (2016) Portuguese family with the co-occurrence of frontotemporal lobar degeneration and neuronal ceroid lipofuscinosis phenotypes due to progranulin gene mutation. *Neurobiol Aging* 41: 200.e201 – 200

Arrant AE, Nicholson AM, Zhou X, Rademakers R, Roberson ED (2018) Partial Tmem106b reduction does not correct abnormalities due to progranulin haploinsufficiency. *Mol Neurodegener* 13: 32

Baker M, Mackenzie IR, Pickering-Brown SM, Gass J, Rademakers R, Lindholm C, Snowden J, Adamson J, Sadovnick AD, Rollinson S *et al* (2006) Mutations in progranulin cause tau-negative frontotemporal dementia linked to chromosome 17. *Nature* 442: 916 – 919

Bateman A, Cheung ST, Bennett HPJ (2018) A brief overview of progranulin in health and disease. *Methods Mol Biol* 1806: 3 – 15

Beel S, Moisse M, Damme M, De Muynck L, Robberecht W, Van Den Bosch L, Saftig P, Van Damme P (2017) Progranulin functions as a cathepsin D chaperone to stimulate axonal outgrowth *in vivo*. *Hum Mol Genet* 26: 2850 – 2863

Belcastro V, Siciliano V, Gregoretti F, Mithbaokar P, Dharmalingam G, Berlingieri S, Iorio F, Oliva G, Polishchuck R, Brunetti-Pierri N *et al* (2011) Transcriptional gene network inference from a massive dataset elucidates transcriptome organization and gene function. *Nucleic Acids Res* 39: 8677 – 8688

van Blitterswijk M, Mullen B, Nicholson AM, Bieniek KF, Heckman MG, Baker MC, DeJesus-Hernandez M, Finch NA, Brown PH, Murray ME *et al* (2014) TMEM106B protects C9ORF72 expansion carriers against frontotemporal dementia. *Acta Neuropathol* 127: 397 – 406

Brady OA, Zheng Y, Murphy K, Huang M, Hu F (2013) The frontotemporal lobar degeneration risk factor, TMEM106B, regulates lysosomal morphology and function. *Hum Mol Genet* 22: 685 – 695

Brendel M, Probst F, Jaworska A, Overhoff F, Korzhova V, Albert NL, Beck R, Lindner S, Gildehaus FJ, Baumann K *et al* (2016) Glial activation and glucose metabolism in a transgenic amyloid mouse model: a triple-tracer PET study. *J Nucl Med* 57: 954 – 960

Capell A, Liebscher S, Fellerer K, Brouwers N, Willem M, Lammich S, Gijselinck I, Bittner T, Carlson AM, Sasse F *et al* (2011) Rescue of progranulin deficiency associated with frontotemporal lobar degeneration by alkalizing reagents and inhibition of vacuolar ATPase. *J Neurosci* 31: 1885 – 1894

Chang MC, Srinivasan K, Friedman BA, Suto E, Modrusan Z, Lee WP, Kaminker JS, Hansen DV, Sheng M (2017) Progranulin deficiency causes impairment of autophagy and TDP-43 accumulation. *J Exp Med* 214: 2611 – 2628

Chen-Plotkin AS, Unger TL, Gallagher MD, Bill E, Kwong LK, Volpicelli-Daley L, Busch JI, Akle S, Grossman M, Van Deerlin V *et al* (2012) TMEM106B, the risk gene for frontotemporal dementia, is regulated by the microRNA-132/212 cluster and affects progranulin pathways. *J Neurosci* 32: 11213 – 11227

Clayton EL, Milioto C, Muralidharan B, Norona FE, Edgar JR, Soriano A, Jafar-Nejad P, Rigo F, Collinge J, Isaacs AM (2018) Frontotemporal dementia causative CHMP2B impairs neuronal endolysosomal traffic-rescue by TMEM106B knockdown. *Brain* 141: 3428 – 3442

Cruchaga C, Graff C, Chiang HH, Wang J, Hinrichs AL, Spiegel N, Bertelsen S, Mayo K, Norton JB, Morris JC *et al* (2011) Association of TMEM106B gene polymorphism with age at onset in granulin mutation carriers and plasma granulin protein levels. *Arch Neurol* 68: 581 – 586

Cruts M, Gijselinck I, van der Zee J, Engelborghs S, Wils H, Pirici D, Rademakers R, Vandenberghe R, Dermaut B, Martin JJ *et al* (2006) Null mutations in progranulin cause ubiquitin-positive frontotemporal dementia linked to chromosome 17q21. *Nature* 442: 920 – 924

DeJesus-Hernandez M, Mackenzie IR, Boeve BF, Boxer AL, Baker M, Rutherford NJ, Nicholson AM, Finch NA, Flynn H, Adamson J *et al* (2011) Expanded GGGGCC hexanucleotide repeat in noncoding region of C9ORF72 causes chromosome 9p-linked FTD and ALS. *Neuron* 72: 245 – 256

Deussing M, Blume T, Vomacka L, Mahler C, Focke C, Todica A, Unterrainer M, Albert NL, Lindner S, von Ungern-Sternberg B *et al* (2018) Coupling between physiological TSPO expression in brain and myocardium allows stabilization of late-phase cerebral [(18)F]GE180 PET quantification. *NeuroImage* 165: 83 – 91

Feng T, Mai S, Roscoe JM, Sheng RR, Ullah M, Zhang J, Iscol Katz I, Yu H, Xiong W, Hu F (2020a) Loss of TMEM106B and PGRN leads to severe lysosomal abnormalities and neurodegeneration in mice. *EMBO Rep* https://doi.org/10.15252/embr.202050219

Feng T, Sheng RR, Sole-Domenech S, Ullah M, Zhou X, Mendoza CS, Enriquez LCM, Katz II, Paushter DH, Sullivan PM *et al* (2020b) A role of the frontotemporal lobar degeneration risk factor TMEM106B in myelination. *Brain* 143: 2255 – 2271

Finch N, Carrasquillo MM, Baker M, Rutherford NJ, Coppola G, Dejesus-Hernandez M, Crook R, Hunter T, Ghidoni R, Benussi L *et al* (2011) TMEM106B regulates progranulin levels and the penetrance of FTLD in GRN mutation carriers. *Neurology* 76: 467 – 474

Gallagher MD, Suh E, Grossman M, Elman L, McCluskey L, Van Swieten JC, Al-Sarraj S, Neumann M, Gelpi E, Ghetti B *et al* (2014) TMEM106B is a genetic modifier of frontotemporal lobar degeneration with C9orf72 hexanucleotide repeat expansions. *Acta Neuropathol* 127: 407 – 418

Gallagher MD, Posavi M, Huang P, Unger TL, Berlyand Y, Gruenewald AL, Chesi A, Manduchi E, Wells AD, Grant SFA *et al* (2017) A dementia-associated risk variant near TMEM106B alters chromatin architecture and gene expression. *Am J Hum Genet* 101: 643 – 663

Gass J, Cannon A, Mackenzie IR, Boeve B, Baker M, Adamson J, Crook R, Melquist S, Kuntz K, Petersen R *et al* (2006) Mutations in progranulin are a major cause of ubiquitin-positive frontotemporal lobar degeneration. *Hum Mol Genet* 15: 2988 – 3001

Ghoshal N, Dearborn JT, Wozniak DF, Cairns NJ (2012) Core features of frontotemporal dementia recapitulated in progranulin knockout mice. *Neurobiol Dis* 45: 395 – 408

Gotzl JK, Mori K, Damme M, Fellerer K, Tahirovic S, Kleinberger G, Janssens J, van der Zee J, Lang CM, Kremmer E *et al* (2014) Common pathobiochemical hallmarks of progranulin-associated frontotemporal lobar degeneration and neuronal ceroid lipofuscinosis. *Acta Neuropathol* 127: 845 – 860

Gotzl JK, Lang CM, Haass C, Capell A (2016) Impaired protein degradation in FTLD and related disorders. *Ageing Res Rev* 32: 122 – 139

Gotzl JK, Colombo AV, Fellerer K, Reifschneider A, Werner G, Tahirovic S, Haass C, Capell A (2018) Early lysosomal maturation deficits in microglia triggers enhanced lysosomal activity in other brain cells of progranulin knockout mice. *Mol Neurodegener* 13: 48

Gotzl JK, Brendel M, Werner G, Parhizkar S, Sebastian Monasor L, Kleinberger G, Colombo AV, Deussing M, Wagner M, Winkelmann J *et al* (2019) Opposite microglial activation stages upon loss of PGRN or TREM2 result in reduced cerebral glucose metabolism. *EMBO Mol Med* 11: e9711

Guo A, Tapia L, Bamji SX, Cynader MS, Jia W (2010) Progranulin deficiency leads to enhanced cell vulnerability and TDP-43 translocation in primary neuronal cultures. *Brain Res* 1366: 1 – 8

Hara T, Nakamura K, Matsui M, Yamamoto A, Nakahara Y, Suzuki-Migishima R, Yokoyama M, Mishima K, Saito I, Okano H *et al* (2006) Suppression of basal autophagy in neural cells causes neurodegenerative disease in mice. *Nature* 441: 885 – 889

Hardy J, Rogaeva E (2014) Motor neuron disease and frontotemporal dementia: sometimes related, sometimes not. *Exp Neurol* 262(Pt B): 75 – 83

Hasegawa M, Arai T, Nonaka T, Kametani F, Yoshida M, Hashizume Y, Beach TG, Buratti E, Baralle F, Morita M *et al* (2008) Phosphorylated TDP-43 in frontotemporal lobar degeneration and amyotrophic lateral sclerosis. *Ann Neurol* 64: 60 – 70

Holler CJ, Taylor G, Deng Q, Kukar T (2017) Intracellular proteolysis of progranulin generates stable, lysosomal granulins that are haploinsufficient in patients with frontotemporal dementia caused by GRN mutations. *eNeuro* 4: ENEURO.0100-17.2017

Hu F, Padukkavidana T, Vaegter CB, Brady OA, Zheng Y, Mackenzie IR, Feldman HH, Nykjaer A, Strittmatter SM (2010) Sortilin-mediated endocytosis determines levels of the frontotemporal dementia protein, progranulin. *Neuron* 68: 654 – 667

Ikemoto S, Hamano SI, Kikuchi K, Koichihara R, Hirata Y, Matsuura R, Hiraide T, Nakashima M, Inoue K, Kurosawa K *et al* (2020) A recurrent TMEM106B mutation in hypomyelinating leukodystrophy: a rapid diagnostic assay. *Brain Dev* 42: 603 – 606

Kao AW, McKay A, Singh PP, Brunet A, Huang EJ (2017) Progranulin, lysosomal regulation and neurodegenerative disease. *Nat Rev Neurosci* 18: 325 – 333

Kayasuga Y, Chiba S, Suzuki M, Kikusui T, Matsuwaki T, Yamanouchi K, Kotaki H, Horai R, Iwakura Y, Nishihara M (2007) Alteration of behavioural phenotype in mice by targeted disruption of the progranulin gene. *Behav Brain Res* 185: 110 – 118

Klein ZA, Takahashi H, Ma M, Stagi M, Zhou M, Lam TT, Strittmatter SM (2017) Loss of TMEM106B ameliorates lysosomal and frontotemporal dementia-related phenotypes in progranulin-deficient mice. *Neuron* 95: 281 – 296

Kleinberger G, Wils H, Ponsaerts P, Joris G, Timmermans JP, Van Broeckhoven C, Kumar-Singh S (2010) Increased caspase activation and decreased TDP-43 solubility in progranulin knockout cortical cultures. *J Neurochem* 115: 735 – 747

Kleinberger G, Capell A, Haass C, Van Broeckhoven C (2013) Mechanisms of granulin deficiency: lessons from cellular and animal models. *Mol Neurobiol* 47: 337 – 360

Komatsu M, Waguri S, Ueno T, Iwata J, Murata S, Tanida I, Ezaki J, Mizushima N, Ohsumi Y, Uchiyama Y *et al* (2005) Impairment of starvation-induced and constitutive autophagy in Atg7-deficient mice. *J Cell Biol* 169: 425 – 434

Lang CM, Fellerer K, Schwenk BM, Kuhn PH, Kremmer E, Edbauer D, Capell A, Haass C (2012) Membrane orientation and subcellular localization of transmembrane protein 106B (TMEM106B), a major risk factor for frontotemporal lobar degeneration. *J Biol Chem* 287: 19355 – 19365

Le NT, Chang L, Kovlyagina I, Georgiou P, Safren N, Braunstein KE, Kvarta MD, Van Dyke AM, LeGates TA, Philips T *et al* (2016) Motor neuron disease, TDP-43 pathology, and memory deficits in mice expressing ALS-FTD-linked UBQLN2 mutations. *Proc Natl Acad Sci USA* 113: E7580 – E7589

Lee CW, Stankowski JN, Chew J, Cook CN, Lam YW, Almeida S, Carlomagno Y, Lau KF, Prudencio M, Gao FB *et al* (2017) The lysosomal protein cathepsin L is a progranulin protease. *Mol Neurodegener* 12: 55

Li Z, Farias FHG, Dube U, Del-Aguila JL, Mihindukulasuriya KA, Fernandez MV, Ibanez L, Budde JP, Wang F, Lake AM *et al* (2020) The TMEM106B FTLD-protective variant, rs1990621, is also associated with increased neuronal proportion. *Acta Neuropathol* 139: 45 – 61

Liu Y, Pattamatta A, Zu T, Reid T, Bardhi O, Borchelt DR, Yachnis AT, Ranum LP (2016) C9orf72 BAC mouse model with motor deficits and neurodegenerative features of ALS/FTD. *Neuron* 90: 521 – 534

Lui H, Zhang J, Makinson SR, Cahill MK, Kelley KW, Huang HY, Shang Y, Oldham MC, Martens LH, Gao F *et al* (2016) Progranulin deficiency promotes circuit-specific synaptic pruning by microglia via complement activation. *Cell* 165: 921 – 935

Luningschror P, Werner G, Stroobants S, Kakuta S, Dombert B, Sinske D, Wanner R, Lullmann-Rauch R, Wefers B, Wurst W *et al* (2020) The FTLD risk factor TMEM106B regulates the transport of lysosomes at the axon initial segment of motoneurons. *Cell Rep* 30: 3506 – 3519

Murray ME, Cannon A, Graff-Radford NR, Liesinger AM, Rutherford NJ, Ross OA, Duara R, Carrasquillo MM, Rademakers R, Dickson DW (2014) Differential clinicopathologic and genetic features of late-onset amnestic dementias. *Acta Neuropathol* 128: 411 – 421

Nelson PT, Wang WX, Partch AB, Monsell SE, Valladares O, Ellingson SR, Wilfred BR, Naj AC, Wang LS, Kukull WA *et al* (2015) Reassessment of risk genotypes (GRN, TMEM106B, and ABCC9 variants) associated with hippocampal sclerosis of aging pathology. *J Neuropathol Exp Neurol* 74: 75 – 84

Neumann M, Kwong LK, Lee EB, Kremmer E, Flatley A, Xu Y, Forman MS, Troost D, Kretzschmar HA, Trojanowski JQ *et al* (2009) Phosphorylation of S409/410 of TDP-43 is a consistent feature in all sporadic and familial forms of TDP-43 proteinopathies. *Acta Neuropathol* 117: 137 – 149

Nicholson AM, Finch NA, Wojtas A, Baker MC, Perkerson RB 3rd, Castanedes-Casey M, Rousseau L, Benussi L, Binetti G, Ghidoni R *et al* (2013) TMEM106B p. T185S regulates TMEM106B protein levels: implications for frontotemporal dementia. *J Neurochem* 126: 781 – 791

Nicholson AM, Zhou X, Perkerson RB, Parsons TM, Chew J, Brooks M, DeJesus-Hernandez M, Finch NA, Matchett BJ, Kurti A *et al* (2018) Loss of Tmem106b is unable to ameliorate frontotemporal dementia-like phenotypes in an AAV mouse model of C9ORF72-repeat induced toxicity. *Acta Neuropathol Commun* 6: 42

Nixon RA (2013) The role of autophagy in neurodegenerative disease. *Nat Med* 19: 983 – 997

Palmer DN, Barry LA, Tyynela J, Cooper JD (2013) NCL disease mechanisms. *Biochim Biophys Acta* 1832: 1882 – 1893

Petkau TL, Neal SJ, Milnerwood A, Mew A, Hill AM, Orban P, Gregg J, Lu G, Feldman HH, Mackenzie IR *et al* (2012) Synaptic dysfunction in progranulin-deficient mice. *Neurobiol Dis* 45: 711 – 722

Petkau TL, Hill A, Leavitt BR (2016) Core neuropathological abnormalities in progranulin-deficient mice are penetrant on multiple genetic backgrounds. *Neuroscience* 315: 175 – 195

Ren Y, van Blitterswijk M, Allen M, Carrasquillo MM, Reddy JS, Wang X, Beach TG, Dickson DW, Ertekin-Taner N, Asmann YW *et al* (2018) TMEM106B haplotypes have distinct gene expression patterns in aged brain. *Mol Neurodegener* 13: 35

Renton AE, Majounie E, Waite A, Simon-Sanchez J, Rollinson S, Gibbs JR, Schymick JC, Laaksovirta H, van Swieten JC, Myllykangas L *et al* (2011) A hexanucleotide repeat expansion in C9ORF72 is the cause of chromosome 9p21-linked ALS-FTD. *Neuron* 72: 257 – 268

Rhinn H, Abeliovich A (2017) Differential aging analysis in human cerebral cortex identifies variants in TMEM106B and GRN that regulate aging phenotypes. *Cell Syst* 4: 404 – 415

Rutherford NJ, Carrasquillo MM, Li M, Bisceglio G, Menke J, Josephs KA, Parisi JE, Petersen RC, Graff-Radford NR, Younkin SG *et al* (2012) TMEM106B risk variant is implicated in the pathologic presentation of Alzheimer disease. *Neurology* 79: 717 – 718

Sardiello M, Palmieri M, di Ronza A, Medina DL, Valenza M, Gennarino VA, Di Malta C, Donaudy F, Embrione V, Polishchuk RS *et al* (2009) A gene network regulating lysosomal biogenesis and function. *Science* 325: 473 – 477

Schwenk BM, Lang CM, Hogl S, Tahirovic S, Orozco D, Rentzsch K, Lichtenthaler SF, Hoogenraad CC, Capell A, Haass C *et al* (2014) The FTLD risk factor TMEM106B and MAP6 control dendritic trafficking of lysosomes. *EMBO J* 33: 450 – 467

Settembre C, Ballabio A (2011) TFEB regulates autophagy: an integrated coordination of cellular degradation and recycling processes. *Autophagy* 7: 1379 – 1381

Settembre C, Di Malta C, Polito VA, Garcia Arencibia M, Vetrini F, Erdin S, Erdin SU, Huynh T, Medina D, Colella P *et al* (2011) TFEB links autophagy to lysosomal biogenesis. *Science* 332: 1429 – 1433

Smith KR, Damiano J, Franceschetti S, Carpenter S, Canafoglia L, Morbin M, Rossi G, Pareyson D, Mole SE, Staropoli JF *et al* (2012) Strikingly different clinicopathological phenotypes determined by progranulin-mutation dosage. *Am J Hum Genet* 90: 1102 – 1107

Snowden JS, Pickering-Brown SM, Mackenzie IR, Richardson AM, Varma A, Neary D, Mann DM (2006) Progranulin gene mutations associated with frontotemporal dementia and progressive non-fluent aphasia. *Brain* 129: 3091 – 3102

Stagi M, Klein ZA, Gould TJ, Bewersdorf J, Strittmatter SM (2014) Lysosome size, motility and stress response regulated by fronto-temporal dementia modifier TMEM106B. *Mol Cell Neurosci* 61: 226 – 240

Tanaka Y, Matsuwaki T, Yamanouchi K, Nishihara M (2013) Increased lysosomal biogenesis in activated microglia and exacerbated neuronal damage after traumatic brain injury in progranulin-deficient mice. *Neuroscience* 250: 8 – 19

Tanaka Y, Chambers JK, Matsuwaki T, Yamanouchi K, Nishihara M (2014) Possible involvement of lysosomal dysfunction in pathological changes of the brain in aged progranulin-deficient mice. *Acta Neuropathol Commun* 2: 78

Tanaka Y, Suzuki G, Matsuwaki T, Hosokawa M, Serrano G, Beach TG, Yamanouchi K, Hasegawa M, Nishihara M (2017) Progranulin regulates lysosomal function and biogenesis through acidification of lysosomes. *Hum Mol Genet* 26: 969 – 988

Van Deerlin VM, Sleiman PM, Martinez-Lage M, Chen-Plotkin A, Wang LS, Graff-Radford NR, Dickson DW, Rademakers R, Boeve BF, Grossman M *et al* (2010) Common variants at 7p21 are associated with frontotemporal lobar degeneration with TDP-43 inclusions. *Nat Genet* 42: 234 – 239

Ward ME, Chen R, Huang HY, Ludwig C, Telpoukhovskaia M, Taubes A, Boudin H, Minami SS, Reichert M, Albrecht P *et al* (2017) Individuals with progranulin haploinsufficiency exhibit features of neuronal ceroid lipofuscinosis. *Sci Transl Med* 9: eaah5642

Wils H, Kleinberger G, Janssens J, Pereson S, Joris G, Cuijt I, Smits V, Ceuterick-de Groote C, Van Broeckhoven C, Kumar-Singh S (2010) TDP-43 transgenic mice develop spastic paralysis and neuronal inclusions characteristic of ALS and frontotemporal lobar degeneration. *Proc Natl Acad Sci USA* 107: 3858 – 3863

Wils H, Kleinberger G, Pereson S, Janssens J, Capell A, Van Dam D, Cuijt I, Joris G, De Deyn PP, Haass C *et al* (2012) Cellular ageing, increased mortality and FTLD-TDP-associated neuropathology in progranulin knockout mice. *J Pathol* 228: 67 – 76

Xiang X, Werner G, Bohrmann B, Liesz A, Mazaheri F, Capell A, Feederle R, Knuesel I, Kleinberger G, Haass C (2016) TREM2 deficiency reduces the efficacy of immunotherapeutic amyloid clearance. *EMBO Mol Med* 8: 992 – 1004

Yin F, Banerjee R, Thomas B, Zhou P, Qian L, Jia T, Ma X, Ma Y, Iadecola C, Beal MF *et al* (2010a) Exaggerated inflammation, impaired host defense, and neuropathology in progranulin-deficient mice. *J Exp Med* 207: 117 – 128

Yin F, Dumont M, Banerjee R, Ma Y, Li H, Lin MT, Beal MF, Nathan C, Thomas B, Ding A (2010b) Behavioral deficits and progressive neuropathology in progranulin-deficient mice: a mouse model of frontotemporal dementia. *FASEB J* 24: 4639 – 4647

Yu L, De Jager PL, Yang J, Trojanowski JQ, Bennett DA, Schneider JA (2015) The TMEM106B locus and TDP-43 pathology in older persons without FTLD. *Neurology* 84: 927 – 934

van der Zee J, Van Langenhove T, Kleinberger G, Sleegers K, Engelborghs S, Vandenberghe R, Santens P, Van den Broeck M, Joris G, Brys J *et al* (2011) TMEM106B is associated with frontotemporal lobar degeneration in a clinically diagnosed patient cohort. *Brain* 134: 808 – 815

Zhou X, Sun L, Bastos de Oliveira F, Qi X, Brown WJ, Smolka MB, Sun Y, Hu F (2015) Prosaposin facilitates sortilin-independent lysosomal trafficking of progranulin. *J Cell Biol* 210: 991 – 1002

Zhou X, Paushter DH, Feng T, Pardon CM, Mendoza CS, Hu F (2017a) Regulation of cathepsin D activity by the FTLD protein progranulin. *Acta Neuropathol* 134: 151 – 153

Zhou X, Paushter DH, Feng T, Sun L, Reinheckel T, Hu F (2017b) Lysosomal processing of progranulin. *Mol Neurodegener* 12: 62

Zhou X, Brooks M, Jiang P, Koga S, Zuberi AR, Baker MC, Parsons TM, Castanedes-Casey M, Phillips V, Librero AL *et al* (2020a) Loss of Tmem106b exacerbates FTLD pathologies and causes motor deficits in progranulin deficient mice. *EMBO Rep* https://doi.org/10.15252/embr.202050197

Zhou X, Nicholson AM, Ren Y, Brooks M, Jiang P, Zuberi A, Phuoc HN, Perkerson RB, Matchett B, Parsons TM *et al* (2020b) Loss of TMEM106B leads to myelination deficits: implications for frontotemporal dementia treatment strategies. *Brain* 143: 1905 – 1919

Expanded View Figures

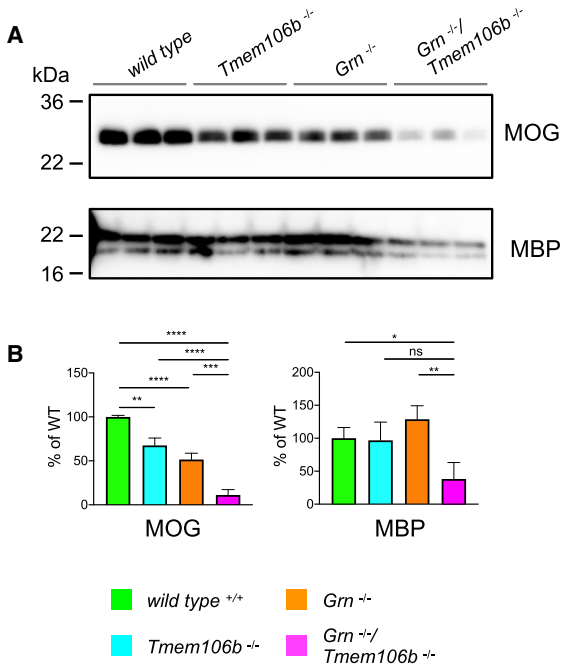

Figure EV1. Reduced abundance of myelination-related proteins in *Grn*$^{-/-}$/*Tmem106b*$^{-/-}$ mice.

A Western blot analysis of the myelin basic protein (MBP) and the myelin oligodendrocyte glycoprotein (MOG) in RIPA total brain lysates from 4.5-month-old mice with the indicated genotype (n = 3 biological replicates per genotype).

B Quantification of (A). Protein expression was normalized to levels in wild-type animals. Data represent the mean ± SD.

Data information: For statistical analysis of normalized data, one-way ANOVA with Tukey's *post hoc* test was used to compare individual genotypes. Significance is indicated; *P < 0.05; **P < 0.01; ***P < 0.001; and ****P < 0.0001.

Source data are available online for this figure.

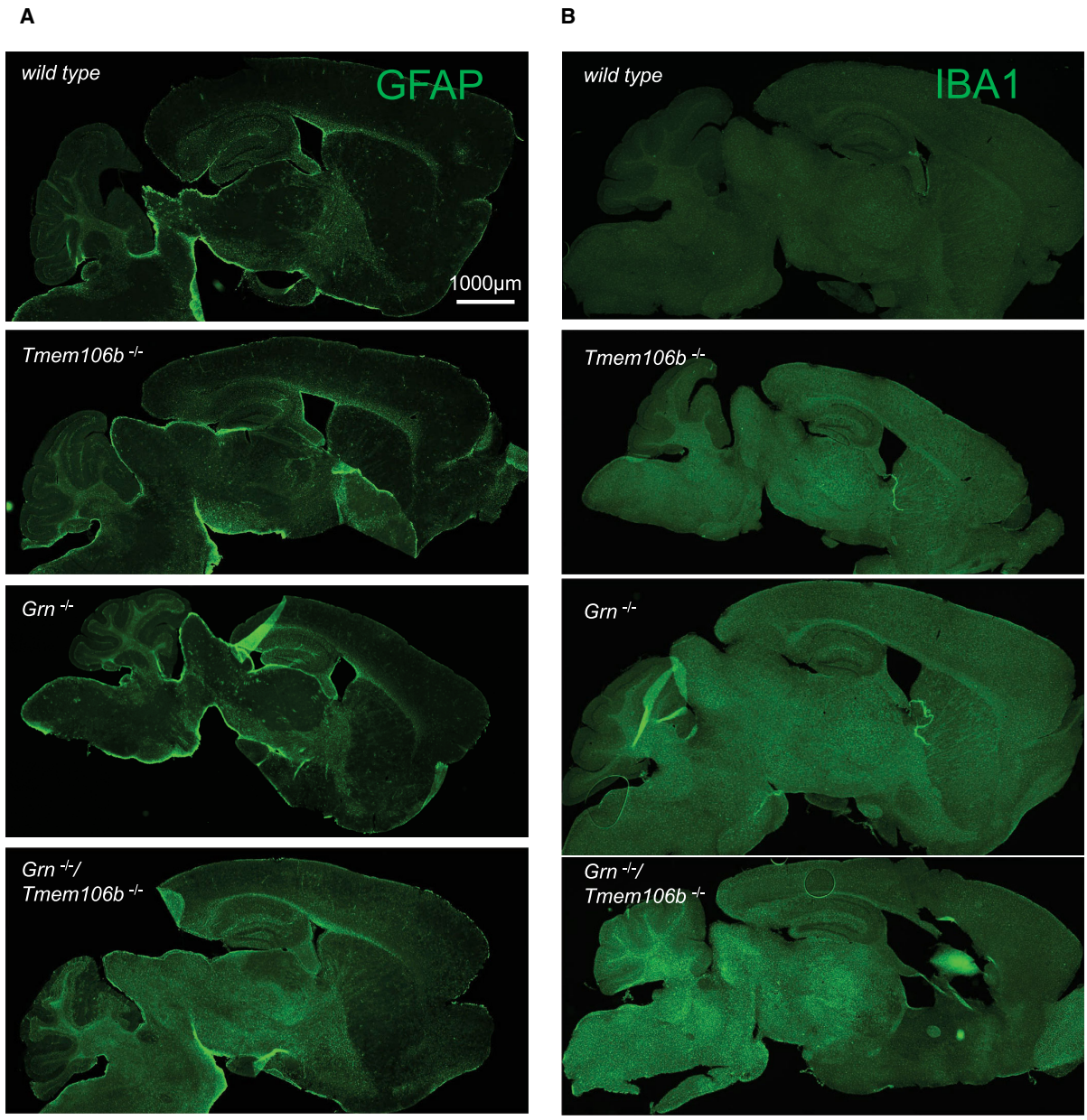

Figure EV2. Increased gliosis in sagittal brain sections of *Grn*$^{-/-}$/*Tmem106b*$^{-/-}$ mice.

A, B Gliosis analyzed by immunofluorescence staining of GFAP (A) and IBA1 (B) in sagittal brain sections. Whole brain section of 4.5-month-old mice, all genotypes acquired by same acquisition conditions. Scale bar indicates 1,000 µm.

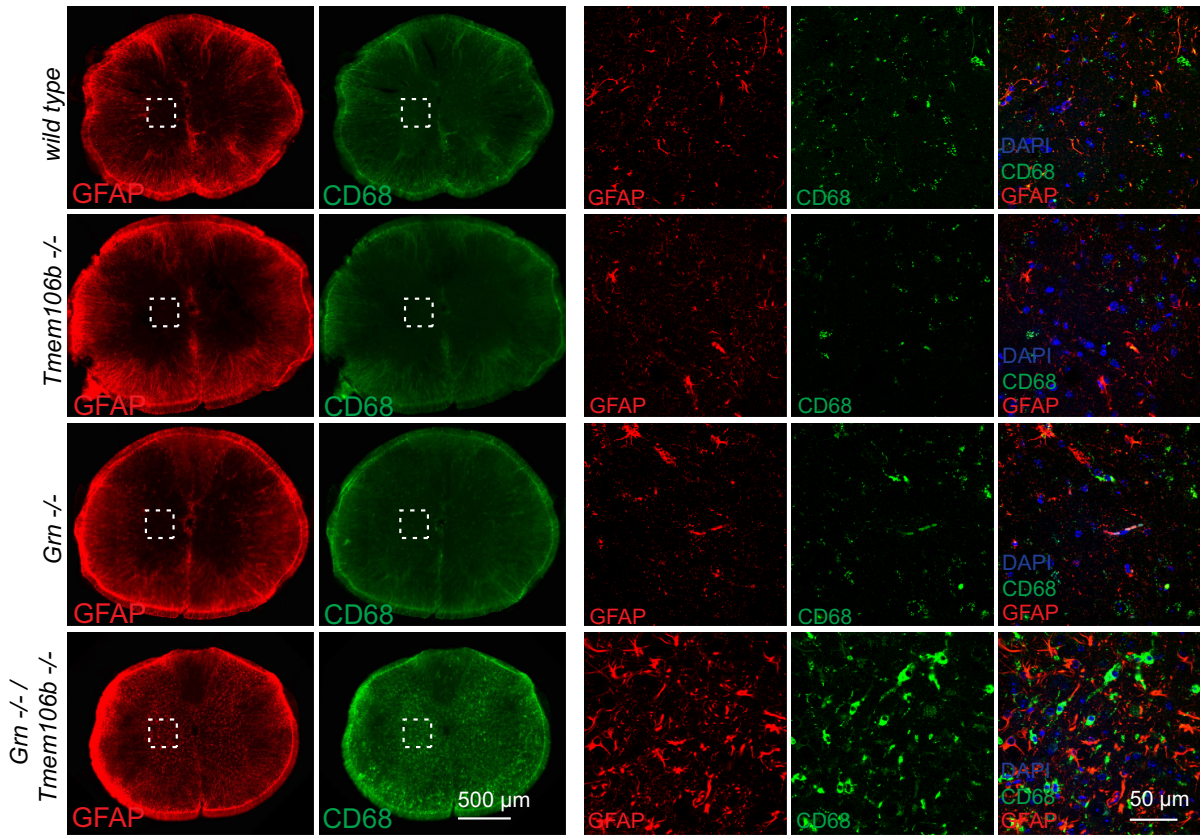

Figure EV3. Increased gliosis in the spinal cord of *Grn*$^{-/-}$/*Tmem106b*$^{-/-}$ mice.

Astrogliosis and microgliosis in spinal cord sections analyzed by immunofluorescence staining of GFAP and CD68. Scale bar indicates 500 µm in overview and 50 µm in insert.

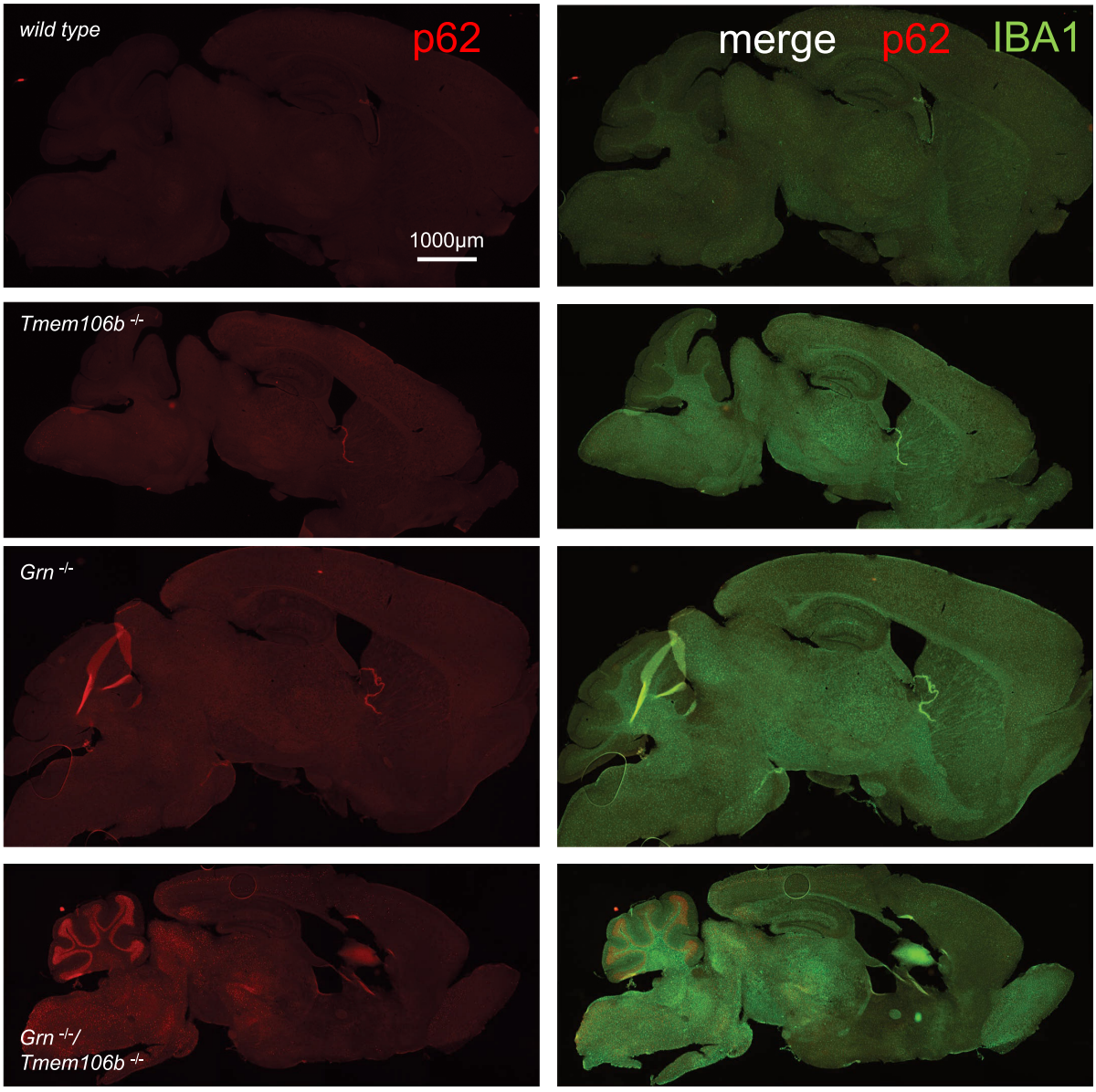

Figure EV4. Overview of brain regions with p62-positive aggregates.

Immunofluorescence staining of p62 in sagittal brain sections. Merge of p62 and IBA1 staining from EV2. Whole brain section of 4.5-month-old mice, all images acquired by identical acquisition conditions. Scale bar indicates 1,000 µm.

Figure EV5. Enhanced TDP-43 aggregation in different brain regions of *Grn*$^{-/-}$/*Tmem106b*$^{-/-}$ mice.

Immunofluorescence analysis of TDP-43 in sagittal brain sections of 4.5-month-old mice. Representative images of indicated brain regions (CBX, cerebellum; CTX, cortex; MB, midbrain; MY, medulla; TH, thalamus). White arrow heads indicate TDP-43 aggregates. Scale bar indicates 100 µm. Zoom in on TDP-43 aggregates in double knockout mouse brain sections of the midbrain, scale bar zoom in indicates 50 µm.

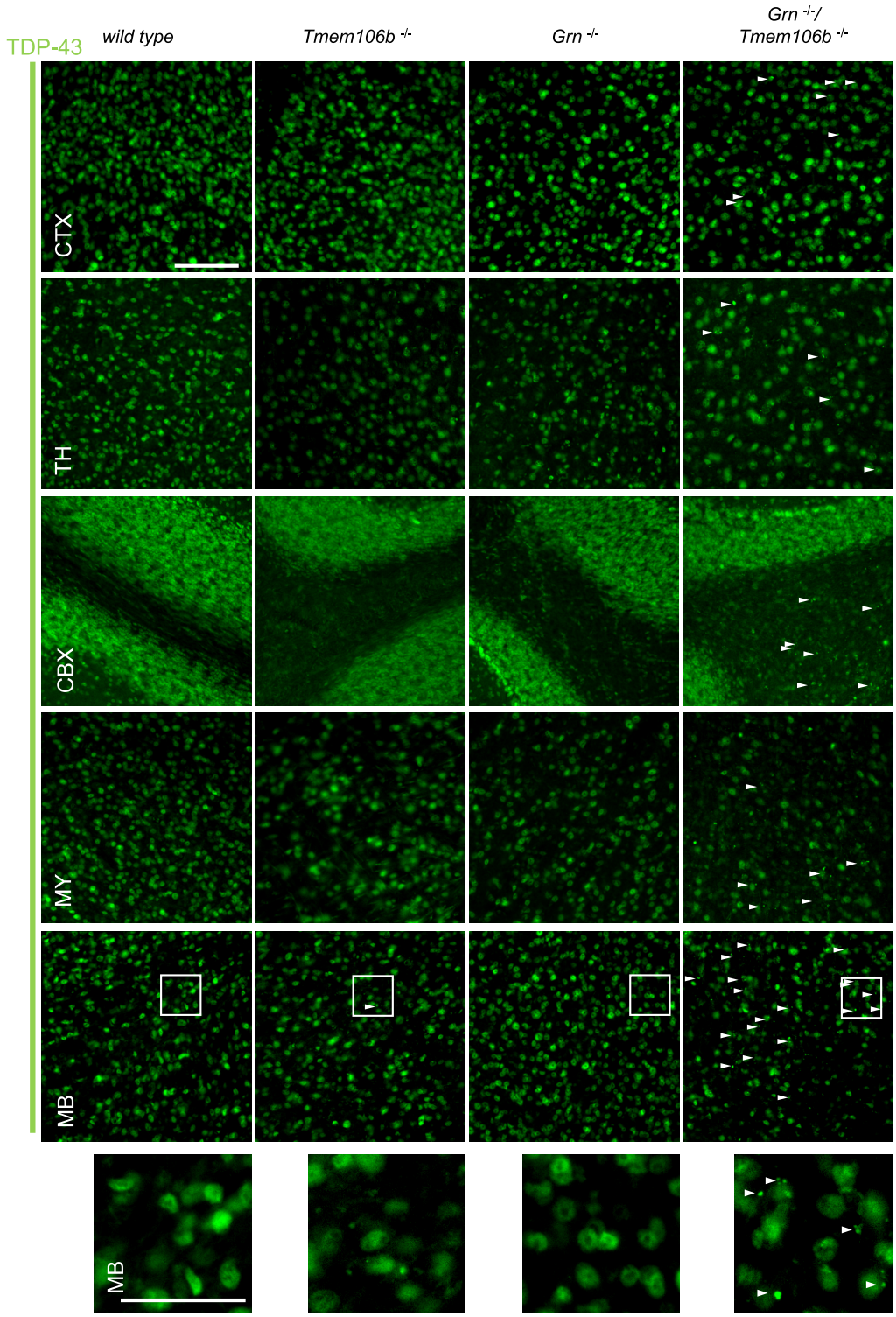

Figure EV5.

2 Publikation II

The FTLD Risk Factor TMEM106B Regulates the Transport of Lysosomes at the Axon Initial Segment of Motoneurons.
P. Luningschror*, G. Werner*, S. Stroobants, S. Kakuta, B. Dombert, D. Sinske, R. Wanner, R. Lullmann-Rauch, B. Wefers, W. Wurst, R. D'Hooge, Y. Uchiyama, M. Sendtner, C. Haass, P. Saftig, B. Knoll, A. Capell and M. Damme 2020.
Cell Reports 30(10):3506-3519.e6. * Geteilte Erstautorenschaft

Alle von mir beigetragenen Ergebnisse sind in den Abbildungen 1F, 5C, S3A, S3B, S3F, S7A, S7B gezeigt (Lüningschrör et al., 2020).

Article

Cell Reports

The FTLD Risk Factor TMEM106B Regulates the Transport of Lysosomes at the Axon Initial Segment of Motoneurons

Graphical Abstract

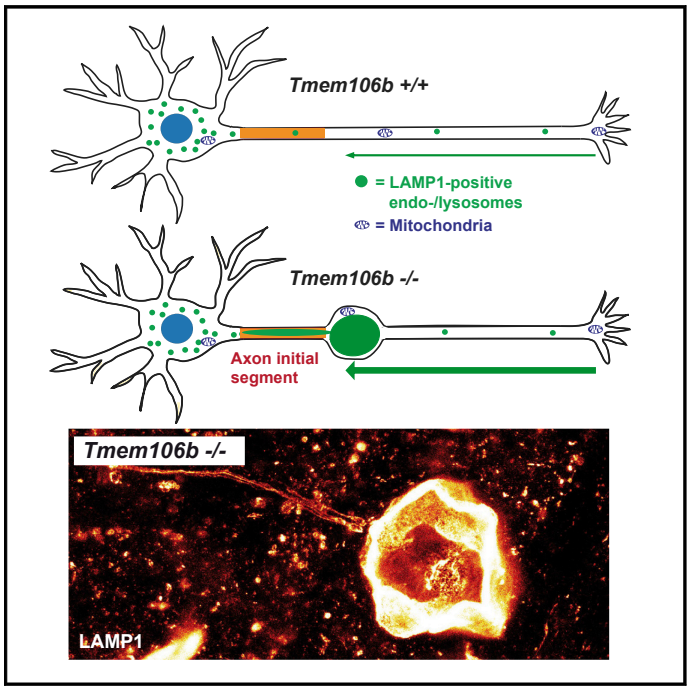

Authors

Patrick Lüningschrör, Georg Werner, Stijn Stroobants, ..., Bernd Knöll, Anja Capell, Markus Damme

Correspondence

mdamme@biochem.uni-kiel.de

In Brief

Genetic variants in the *TMEM106B* gene, coding for a lysosomal transmembrane protein, are linked to various neurodegenerative diseases. The function of TMEM106B remains enigmatic. Lüningschrör et al. analyze *Tmem106b*-knockout mice and find drastically enlarged LAMP1-positive vacuoles in proximal axons of selected motoneuron nuclei. Vacuolization is caused by impaired axonal transport.

Highlights

- *Tmem106b* knockout leads to LAMP1-positive vacuoles at the axon initial segment
- Vacuolization is mostly confined to motoneurons
- Vacuoles develop due to impaired axonal trafficking of LAMP1-positive organelles
- Degradation of autophagic cargo is impaired due to TMEM106B deficiency

Lüningschrör et al., 2020, Cell Reports *30*, 3506–3519
March 10, 2020
https://doi.org/10.1016/j.celrep.2020.02.060

CellPress

Cell Reports
Article

The FTLD Risk Factor TMEM106B Regulates the Transport of Lysosomes at the Axon Initial Segment of Motoneurons

Patrick Lüningschrör,[1,12] Georg Werner,[2,12] Stijn Stroobants,[3] Soichiro Kakuta,[4] Benjamin Dombert,[1] Daniela Sinske,[5] Renate Wanner,[5] Renate Lüllmann-Rauch,[6] Benedikt Wefers,[7,8,9,10] Wolfgang Wurst,[7,8,9,10] Rudi D'Hooge,[3] Yasuo Uchiyama,[4] Michael Sendtner,[1] Christian Haass,[2,7,10] Paul Saftig,[11] Bernd Knöll,[5] Anja Capell,[2] and Markus Damme[11,13,*]

[1]Institute of Clinical Neurobiology, University Hospital Wuerzburg, University of Wuerzburg, 97078 Wuerzburg, Germany
[2]Chair of Metabolic Biochemistry, Biomedical Center (BMC), Faculty of Medicine, Ludwig-Maximilians-Universität München, 81377 Munich, Germany
[3]Laboratory of Biological Psychology, KU Leuven, 3000 Leuven, Belgium
[4]Department of Cellular and Molecular Neuropathology, Juntendo University Graduate School of Medicine, Tokyo, Japan
[5]Institute of Physiological Chemistry, Ulm University, 89081 Ulm, Germany
[6]Institute for Anatomy, Kiel University, 24098 Kiel, Germany
[7]German Center for Neurodegenerative Diseases (DZNE) Munich, Munich, Germany
[8]Institute of Developmental Genetics, Helmholtz Zentrum München, German Research Center for Environmental Health, 85764 Neuherberg, Germany
[9]Technische Universität München-Weihenstephan, 85764 Neuherberg/Munich, Germany
[10]Munich Cluster for Systems Neurology (SyNergy), 81377 Munich, Germany
[11]Institute of Biochemistry, Kiel University, 24098 Kiel, Germany
[12]These authors contributed equally
[13]Lead Contact
*Correspondence: mdamme@biochem.uni-kiel.de
https://doi.org/10.1016/j.celrep.2020.02.060

SUMMARY

Genetic variations in *TMEM106B*, coding for a lysosomal membrane protein, affect frontotemporal lobar degeneration (FTLD) in *GRN*- (coding for progranulin) and *C9orf72*-expansion carriers and might play a role in aging. To determine the physiological function of TMEM106B, we generated TMEM106B-deficient mice. These mice develop proximal axonal swellings caused by drastically enlarged LAMP1-positive vacuoles, increased retrograde axonal transport of lysosomes, and accumulation of lipofuscin and autophagosomes. Giant vacuoles specifically accumulate at the distal end and within the axon initial segment, but not in peripheral nerves or at axon terminals, resulting in an impaired facial-nerve-dependent motor performance. These data implicate TMEM106B in mediating the axonal transport of LAMP1-positive organelles in motoneurons and axonal sorting at the initial segment. Our data provide mechanistic insight into how TMEM106B affects lysosomal proteolysis and degradative capacity in neurons.

INTRODUCTION

Genetic variants in TMEM106B have been linked with differential aging and various neurodegenerative diseases, including frontotemporal lobar degeneration (FTLD), limbic-predominant age-related TDP-43 encephalopathy (LATE), and Parkinson's disease (Nelson et al., 2019; Tropea et al., 2019; van der Zee et al., 2011). The precise molecular function of TMEM106B is, however, still enigmatic. *TMEM106B* encodes a glycosylated lysosomal membrane protein with one transmembrane domain and type II topology (Lang et al., 2012). While the larger glycosylated carboxy-terminus faces the lysosomal lumen, the 96-amino-acid-long amino-terminus is localized in the cytosol. TMEM106B may play a role in the transport of lysosomes, based on studies in HeLa cells and cultured neurons (Clayton et al., 2018; Schwenk et al., 2014; Stagi et al., 2014). Overexpression of TMEM106B in neuronal and non-neuronal cells leads to TMEM106B dose-dependent enlarged dysfunctional lysosomes, as shown in several studies (Brady et al., 2013; Busch et al., 2016; Chen-Plotkin et al., 2012; Lang et al., 2012), though the molecular mechanism(s) explaining this effect remains to be determined. Acute knockdown of TMEM106B in HeLa cells causes a redistribution of lysosomes from the cell periphery to the perinuclear region (Schwenk et al., 2014) and a reduced number of lysosomes per cell (Stagi et al., 2014). In cultured primary hippocampal neurons, knockdown of TMEM106B affects the transport of lysosomes in dendrites, ultimately leading to reduced dendritic branching (Schwenk et al., 2014; Stagi et al., 2014). TMEM106B-deficient mice were generated and characterized previously (Arrant et al., 2018; Klein et al., 2017; Nicholson et al., 2018). Generally, no spontaneous phenotype in the basal TMEM106B-deficient situation was found except for subtle changes of lysosomal proteins, a downregulation of subunits of the V-ATPase, and decreased LysoTracker staining in primary cortical neurons (Klein et al., 2017).

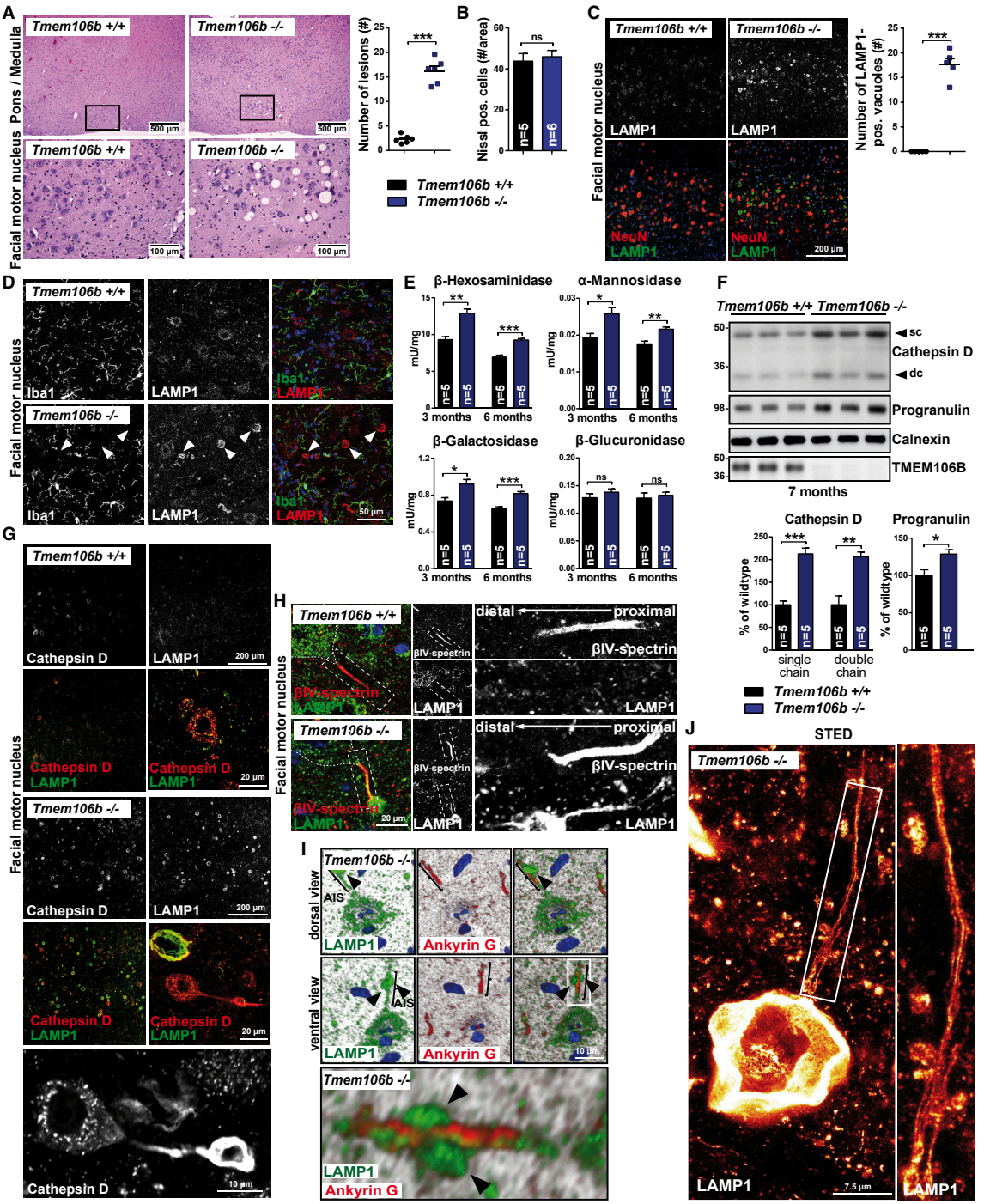

(legend on next page)

Genetic variants were first linked genetically with FTLD (Van Deerlin et al., 2010), the second most common form of presenile dementia, affecting up to 15 in 100,000 people at 45–64 years of age (Ratnavalli et al., 2002). Even though the precise mechanisms leading to neuronal dysfunction and, finally, cell death remain poorly understood, accumulating evidence hints to a dysfunctional endo-/lysosomal pathway (Ghazi-Noori et al., 2012; Götzl et al., 2014; Shi et al., 2018). The second most common cause of familial FTLD are heterozygous missense and nonsense mutations in *GRN*, coding for progranulin. Progranulin haploinsufficiency considerably increases the risk of developing FTLD (Baker et al., 2006; Cruts et al., 2006; Gass et al., 2006). Genetic approaches aiming to identify risk factors and modifiers for disease onset and severity by genome-wide association studies (GWASs) revealed the *TMEM106B* locus that segregates with the disease (Van Deerlin et al., 2010). Stratification of the patients highlighted a significantly reduced association of the *TMEM106B* "protective" allele with *GRN* carriers compared to non-*GRN* carriers. This genetic linkage of *TMEM106B* with FTLD and *GRN*-mutation carriers was validated in follow-up studies (Finch et al., 2011; Pottier et al., 2018; Premi et al., 2017; van der Zee et al., 2011). Subsequently, the *TMEM106B* protective allele was shown to be significantly associated with lower disease risk in *C9orf72* carriers (Gallagher et al., 2014; Premi et al., 2017; van Blitterswijk et al., 2014). In conclusion, *TMEM106B* is a bona fide risk factor and modulator for FTLD.

To gain insight into TMEM106B-dependent cellular processes, we generated *Tmem106b* knockout (KO) mice by CRISPR/Cas9 and independently by the homologous recombination of targeted embryonic stem cells (ESCs). TMEM106B-deficient mice present features affecting primarily motoneurons (MNs) of the facial motor nucleus (FMN) and other brain stem motor nuclei. MNs of *Tmem106b* KO mice show dramatically enlarged LAMP1-positive vacuoles specifically at the axon initial segment (AIS) and an increased retrograde axonal transport of lysosomes, implicating a pivotal role for TMEM106B in axonal transport in distinct neuronal populations and, as a consequence, impaired axonal autophagy. This phenotype was also observed in a second, fully independent *Tmem106b* KO mouse strain. Our results provide mechanistic insight into how TMEM106B may affect lysosomal proteolysis.

RESULTS

Deficiency of TMEM106B in Mice Leads to Vacuolization of Brain Stem Nuclei

Using CRISPR/Cas9-mediated genome editing, we generated TMEM106B-deficient mice by introducing short frameshift mutations in exon 3, the first coding exon (Figures S1A–S1D). Immunoblotting of brain and spinal cord lysates validated the complete absence of the detectable TMEM106B protein in homozygous KO mice and a reduction to ~50% in heterozygous animals (Figure S1E). Homozygous *Tmem106b* KO mice were born according to Mendelian frequencies after mating heterozygotes (Figure S1F). Adult *Tmem106b* KO mice had a similar weight to wild-type mice at an age of 10 weeks (Figure S1G). The major peripheral organs were unremarkable. Histologic analysis revealed spongiform vacuolization of selected brain areas at 10 weeks of age (Figures 1A and S2A). Spongiform vacuolization was particularly pronounced in the FMN but was also detectable in subregions of the thalamus, the trigeminal motor nucleus, and the hypoglossal nucleus. Vacuoles were regularly, but less frequently, seen in the anterior horn of the spinal cord (Figure S2A). The number of MNs in the FMN did not reveal differences between KO animals and controls even at 22 weeks of age (Figure 1B). Since TMEM106B is a lysosomal protein and TMEM106B overexpression leads to enlarged lysosomes in cultured cells (Brady et al., 2013; Chen-Plotkin et al., 2012; Gallagher et al., 2017; Stagi et al., 2014), we analyzed lysosomes in more detail. Immunofluorescence staining for the lysosomal marker LAMP1 revealed intensely stained, large round or infolded structures in the FMN, trigeminal motor nucleus, and thalamus of *Tmem106b* KO mice resembling the number, distribution, and size of the vacuoles seen by hematoxylin/eosin (H&E) staining (Figures 1C and S2B). Analysis of *Tmem106b* KO animals at different ages revealed first a solid appearance at 4 weeks of age, while 2-week-old animals barely showed any vacuoles, indicating that vacuoles are not due to defects in embryonic development (Figure S2C). The vacuoles stained negatively for the mitochondrial-marker Cox-IV (Figure S2D). Furthermore, these vacuoles did not represent phagosomes of microglia/macrophage origin, as revealed by Iba-1 co-staining. Neither signs of microgliosis nor astrogliosis were observed in

Figure 1. Accumulation of Drastically Enlarged Vacuoles of Lysosomal Origin in the AIS of the FMN

(A) H&E staining of the hindbrain and the FMN of 5-month-old control and *Tmem106b* KO mice. The number of vacuoles per FMN of individual animals is plotted (mean ± SEM, n = 6).

(B) Number of FMN Nissl-positive MNs in 6-month-old control and *Tmem106b* KO mice (mean ± SEM, n = 5–6).

(C) Immunofluorescence staining of the FMN with antibodies against LAMP1 (white, top panel; green, bottom panel) and NeuN (red, bottom panel) in 4-month-old mice.

(D) Immunofluorescence of Iba1 (green) and LAMP1 (red) of the FMN. Maximum intensity *Z*-projection of confocal stacks. Nuclei are stained with DAPI (blue). Age: 4 months.

(E) Enzymatic activity of the lysosomal hydrolases β-hexosaminidase, α-mannosidase, β-galactosidase, and β-glucuronidase in brain extracts of 3- and 6-month-old control and *Tmem106b* KO mice (mean ± SEM, n = 5).

(F) Immunoblots from brain lysates of 6-month-old mice for CatD progranulin, TMEM106B to confirm the KO, and calnexin to confirm equal loading. CatD and progranulin levels were quantified and normalized to wild-type mice (mean ± SEM, n = 5). dc, double-chain CatD; sc, single-chain CatD.

(G) Immunofluorescence of LAMP1 (green) and CatD (red) of the FMN. Nuclei are stained with DAPI (blue). Age: 4 months.

(H) Immunofluorescence of LAMP1 (green) and βVI Spectrin (red) of the FMN. The dashed box is shown enlarged. The soma of the MN is encircled with a dashed line. Nuclei are stained with DAPI (blue). Age: 4 months.

(I) Maximum intensity *Z*-projection of confocal stacks of LAMP1 (green) and AnkyrinG (red) staining of the FMN. Vacuolated lysosomes are marked by arrowheads. Nuclei are stained with DAPI (blue). Age: 4 months.

(J) LAMP1 immunofluorescence STED-microscopy image of an FMN vacuole. Age: 4 months.

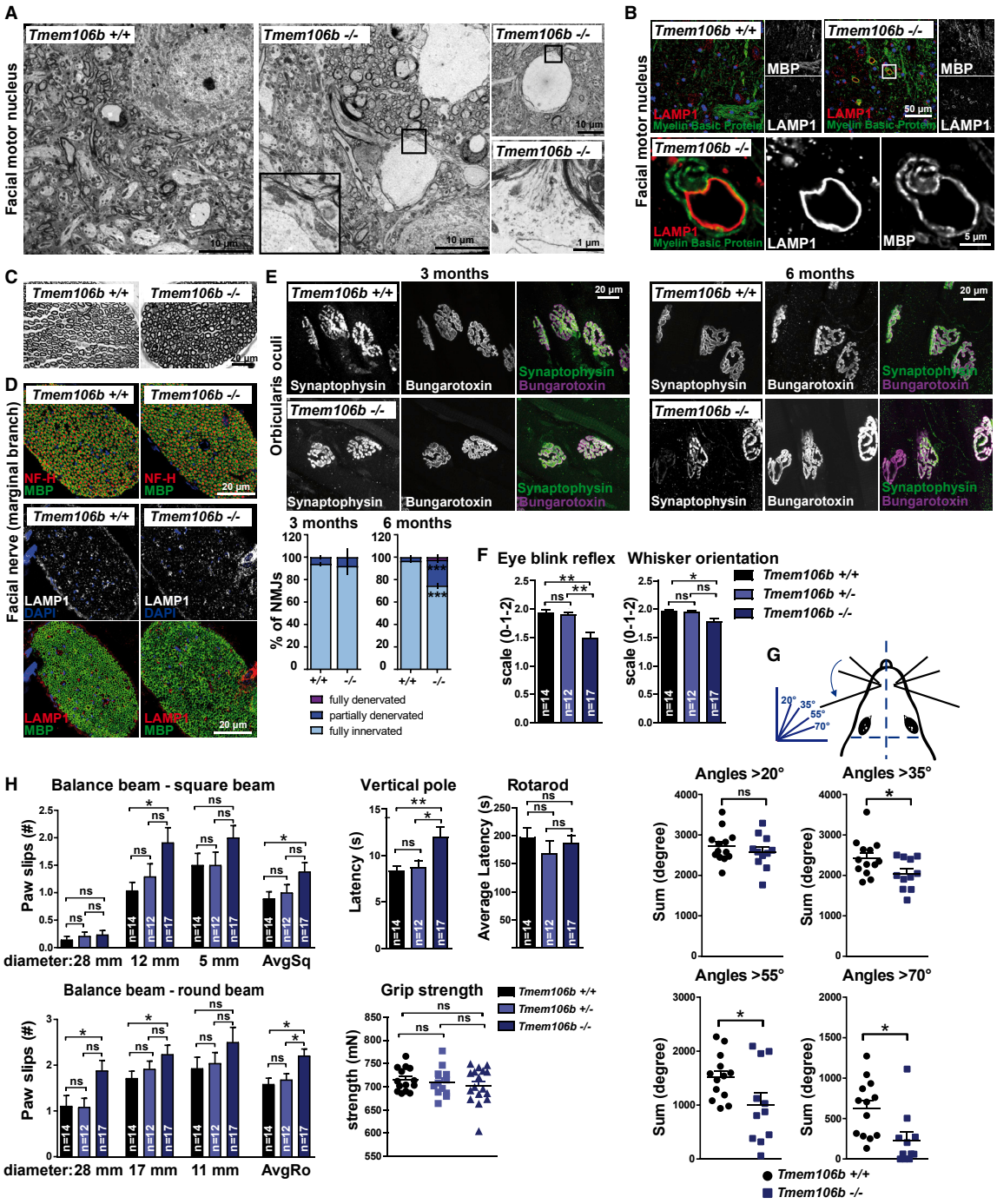

Figure 2. Axonal Vacuolization of the Facial MN Is Restricted to the Proximal Axon and Leads to Functional Facial Motor Deficits

(A) Electron micrographs of the FMN of 4-month-old wild-type and *Tmem106b* KO mice. Representative axons are shown. The boxed area is shown enlarged.

(B) Immunofluorescence staining of the FMN with antibodies against LAMP1 (red) and MBP (green). Nuclei are stained with DAPI (blue). Age: 4 months. The boxed area is shown enlarged.

(legend continued on next page)

the heavily vacuolated FMN at 4 months of age, as detected by immunofluorescence staining for Iba-1, CD68, and GFAP (Figures 1D and S2E). LAMP1-positive vacuoles in the FMN varied in size ranging from 1 μm to 35 μm, thus even partially exceeding the average size of MN somata. The activity of the lysosomal hydrolases β-hexosaminidase, α-mannosidase, and β-galactosidase, but not that of β-glucuronidase, was significantly increased in brain extracts of both 3- and 6-month-old *Tmem106b* KO animals (Figure 1E), while their transcript levels were unchanged (Figure S2F). Cathepsin D (CatD) levels in brain extracts were 2-fold increased in the *Tmem106b* KO animals, and progranulin expression was also significantly increased (Figure 1F). Since LAMP1 is not only present on lysosomes, but also found on other organelles from the endocytotic pathway, we further examine the identity of the LAMP1-positive vacuoles by staining with CatD as a marker of mature lysosomes. Co-staining of CatD and LAMP1 revealed a similar but not completely overlapping pattern of the vacuoles within the FMN (Figure 1G). Notably, CatD staining was also ring-like and did not fill the lumen of the vacuoles, but it often contained a "shaft"-like projection (Figure 1G, bottom panel). Most vacuoles showed immunoreactivity for both CatD and LAMP1 to a variable extent, but LAMP1-negative vacuoles were generally rare. We observed a general tendency of LAMP1-positive vacuoles being larger than CatD-positive vacuoles (Figure 1G). Next to the CRISPR/Cas9-mediated KO strain, we generated a second, independent *Tmem106b* KO mouse line by blastocyst injection of *Tmem106b*-targeted (ESCs) containing an artificial splice-acceptor site and β-galactosidase-containing reporter construct under the control of the endogenous *Tmem106b* promoter targeting exon 4, which is flanked by Cre- and flippase recombinase sites (tm2a allele). The KO in tm2a mice is based on efficient usage of the splice acceptor site, which is often leaky, leading to hypomorphic mice (Mitchell et al., 2001). To generate full KOs, tm2a-heterozygous animals were bred with Cre-recombinase-expressing mice, leading to a deletion of exon 4 and a frameshift in the coding region after exon 4 (tm2b allele) (Figures S3A–S3G). We used heterozygote tm2b animals to follow the expression of *Tmem106b* by X-gal staining, which showed a broad and ubiquitous expression throughout the brain, with a staining pattern resembling the general distribution of neurons (Figure S3C). Consistent with the CRISPR/Cas9 *Tmem106b* KO mouse line, this second, fully independent tm2b mouse line showed LAMP1-positive vacuoles in a similar distribution, increased levels of CatD, but no changes in the transcript levels of *Ctsd*, *Hexb*, *Man2b1*, *Glb1*, and *Gusb* (Figures S3D–S3G).

The close proximity of the LAMP1-positive giant vacuoles to the soma in both *Tmem106b* KO strains prompted us to investigate a relationship to the AIS of affected MNs. Notably, the entire AIS (visualized by staining for AnkyrinG or βIV-spectrin) of facial MNs showed regularly intense LAMP1 immunoreactivity, and very often a vacuole appeared at the distal end of the AIS or bulged from the AIS (Figures 1H and 1I). The AIS of cortical neurons or hippocampal CA3-neurons, however, lacked such LAMP1-positive vacuoles (Figure S4A). Stimulated emission depletion (STED) super-resolution microscopy of MNs *in situ* revealed a single tubular LAMP1-positive organelle often filling out the entire AIS, culminating with a giant vacuole at the distal end (Figure 1J). Electron microscopy of the vacuolated FMN revealed an electron-lucent character of the vacuoles. They were limited by a single membrane and were usually localized in the AIS or in myelinated axons, squeezing the remaining axoplasm between the vacuole membrane and axolemma (Figure 2A). However, organelles like mitochondria were regularly observed between the vacuoles and the axolemma, indicating that organelles are probably still able to pass these "roadblocks" (Figure 2A). More than one vacuole in a single axon was concomitantly observed, and the axon extended after a vacuole, indicating no axonopathy due to vacuolization (Figure 2A). This finding was confirmed by co-staining of LAMP1 with Tuj1 for visualization of the axon and a 3D reconstruction of *Z* stacks (Figure S4B). Immunofluorescence staining for Myelin basic protein (MBP) and LAMP1 verified the localization of the vacuoles in myelinated axons (Figure 2B). Correlative light-electron microscopy additionally confirmed the appearance of CatD at the limiting membrane of the vacuoles (Figure S5A).

Facial-Nerve-Innervated Muscle Groups Are Functionally Impaired in TMEM106B-Deficient Mice

Since proximal FMN axons are severely affected by vacuolization, we investigated the distal facial-nerve- and FMN-innervated neuromuscular junctions (NMJs) of the *orbicularis oculi* muscle in more detail and analyzed FMN-dependent behavioral changes as a functional readout. The peripheral facial nerve of *Tmem106b* KO mice was unaffected by vacuolization and appeared normally myelinated, as revealed by histology and immunofluorescence for MBP and neurofilament H (NFH) at the age of 5 months. Moreover, LAMP1-positive vacuoles were absent in the peripheral facial nerve (Figures 2C and 2D), the compact facial nerve in the hindbrain (Figure S2G), and the corresponding NMJ (Figure S2H). NMJs revealed a normal distribution and number of

(C) Toluidine blue-stained sections of the facial nerve (buccal branch) of a 4-month-old *Tmem106b* KO mouse and wild-type control.
(D) Immunofluorescence staining of the facial nerve (buccal branch) of a 4-month-old *Tmem106b* KO mouse and wild-type control for NFH (red), MBP (green), LAMP1 alone (white), or LAMP1 (red) and MBP (green). Nuclei are stained with DAPI (blue).
(E) Immunofluorescence staining of neuromuscular junctions (NMJs) of the *orbicularis oculi* muscle of 3- and 6-month-old *Tmem106b* and control animals with fluorescently labeled Bungarotoxin (magenta) and an antibody against synaptophysin (green). Quantification depicts the number of fully innervated or partially denervated NMJs of *Tmem106b* KO mice and wild-type controls (n = 3; 15–25 NMJs/animal).
(F) Quantification of the eye blink and whisker-orienting reflex in $Tmem106b^{+/+}$, $Tmem106b^{+/-}$, and $Tmem106b^{-/-}$ mice (n = 12–17). The average of six assessments was used for analysis. Three-point scale (0: absent; – 1: reduced; – 2: normal). Age: 2–3 months.
(G) Quantification of the whisker movement expressed as the addition of angles >20°, >35°, >35°, and >70° from *Tmem106b* KO and wild-type control mice. The sum in degree is depicted (n = 11–13; each point represents one animal; age: 6 months).
(H) Quantification of neuromotor function: number of paw slips during balance beam traversal (square and round beams), vertical pole latency, average rotarod latency, and grip strength of $Tmem106b^{+/+}$, $Tmem106b^{+/-}$, and $Tmem106b^{-/-}$ mice (age 2–3 months; mean ± SEM, n = 12–17).

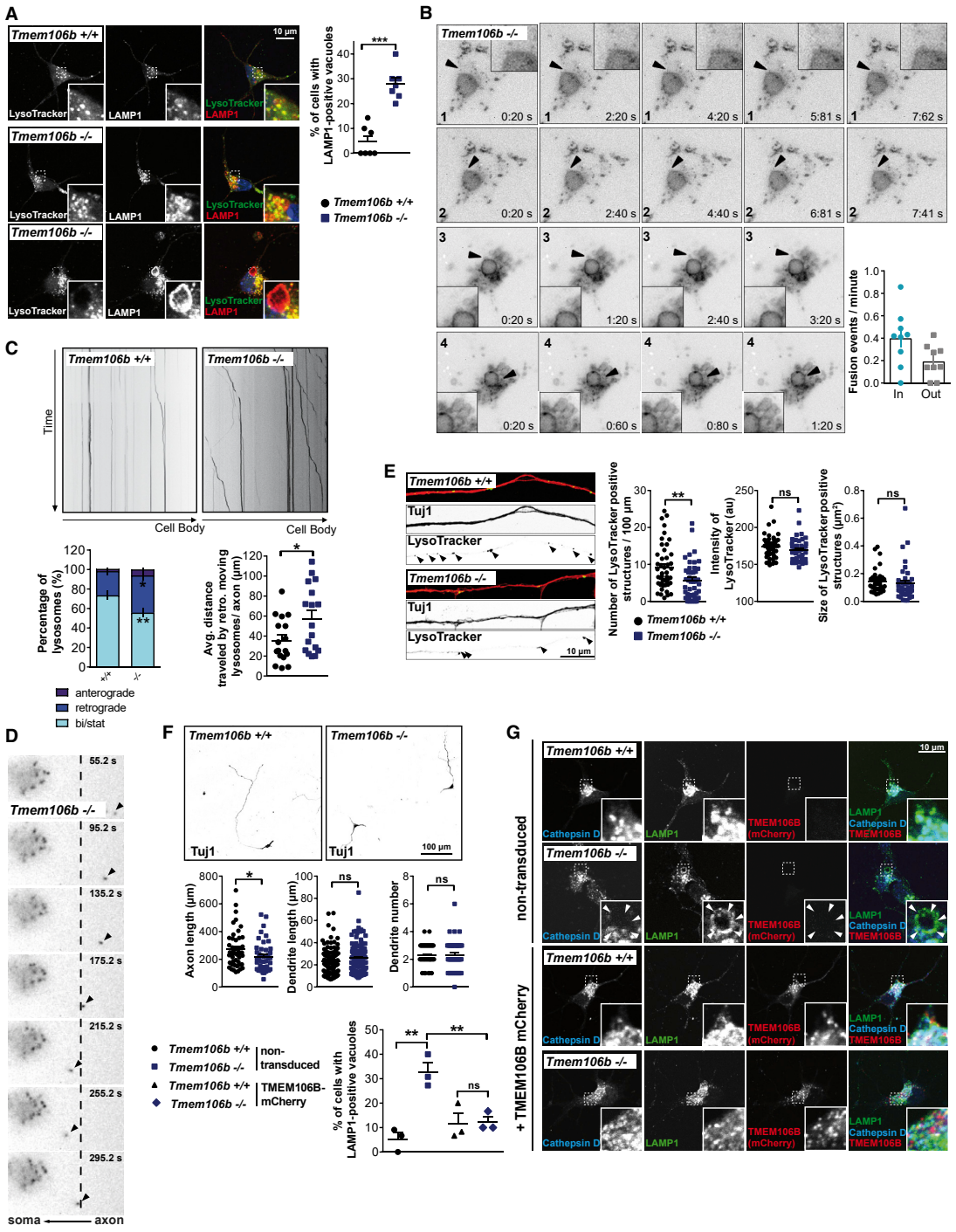

(legend on next page)

mitochondria and synaptic vesicles, as revealed by staining for Hsp60 and synaptophysin (Figure S2I). In 8- to 10-week-old mice, no signs of denervation or other pathologic alterations were observed for the NMJs within the *orbicular oculi* muscle in *Tmem106b* KO mice (Figure 2E). However, in 6-month-old animals, we detected a significantly enhanced number of partially denervated NMJs, as shown by synaptophysin staining. To a lesser extent, we also observed fully denervated axon terminals with a complete absence of synaptophysin (Figure 2E). Assessment of the eye blink reflex and whisker orientation—FMN-dependent motor groups—revealed a slight but significant reduced response of both muscle groups (Figure 2F). More sophisticated video-based tracking of the whisker movement measuring the total number of all angles and the total number of peaks (Figures 2G, S5B, and S5C) by counting the addition of angles, revealed significant differences between wild-type and *Tmem106b* KO mice at the age of 8–10 weeks for all angles >35°, implicating functional impairment of the corresponding innervating MNs. More general motor function tests revealed slightly reduced motor coordination in balance beam and vertical pole tests, but no significant differences in rotarod performance or grip strength. Heterozygous animals did not show significant differences (Figure 2H). Eye blink reflex and whisker orientation remained statistically significant between the genotypes in mice at 14 months of age, and there was a progressive decline in motor coordination, tested by the balance beam test (Figure S5D). These data indicate proximal nerve pathology in the absence of major myelination defects, leading to impaired MN function and accompanied by moderate and partially progressive behavioral deficits.

Retrograde Axonal Transport of Lysosomes Is Impaired in *Tmem106b* KO Mice

Our findings of LAMP1-positive vacuoles within proximal but not distal axons of MNs *in situ* encouraged us to investigate the axonal transport of lysosomes in primary MNs *ex vivo*. Even though vacuoles were less frequent, we routinely observed MN vacuolization *in situ* in spinal cord sections, as assessed by histology and co-staining with a ChAT antibody (Figures S2A, S2B, and S6A), implying that spinal MNs serve as a good model system.

In total, 28% of cultured MNs from TMEM106B-deficient (but not wild-type) mice showed LAMP1-positive vacuoles, mostly within the soma and to a much lesser extent in proximal axons, after 5 days *in vitro* (DIV5) (Figure 3A). Primary neurosphere-derived neurons from Tmem106b KO mice lacked such vacuoles (Figure S6B), emphasizing again that MNs are the primary affected neuronal cell type. LAMP1-positive vacuoles in primary MNs stained negative for LysoTracker and CatD, suggesting that they do not represent fully matured lysosomes (Figures 3A and S5C). Since we almost exclusively detected these vacuoles at the AIS *in situ*, we also stained for AIS markers in cultured MNs. In contrast to MNs *in situ*, cultured MNs seem not to have fully established an AIS, probably leading to the buildup of LAMP1-positive vacuoles at the soma. We wondered whether these structures are still active in terms of membrane exchange. Upon lentiviral expression of LAMP1-GFP, we specifically monitored LAMP1-positive vacuoles and analyzed fusion and/or fission events. Our data show that smaller LAMP1-GFP structures fuse with and bud off these large vacuoles (Figure 3B). Based on these experiments, we calculated the rate of fission and fusion events per minute and detected a higher number of fusing structures in comparison to structures budding off (Figure 3B). In summary, these experiments show that *in vitro*, the LAMP1-positive vacuoles still undergo membrane turnover, probably leading to the net growth of the vacuoles.

Although the LAMP1-positive vacuoles stained negative for LysoTracker, we wondered whether acidified organelles in axons were also affected in TMEM106B-deficient MNs. Live cell imaging and tracing of LysoTracker-labeled vesicles in the proximal axon of DIV7 MNs revealed a significantly higher percentage of retrograde transported LysoTracker-positive vesicles in KO cells than in wild-type control cells. Furthermore, retrograde moving LysoTracker-positive vesicles traveled an increased total distance in TMEM106B-deficient animals (Figure 3C). Intriguingly, LysoTracker-positive vesicles were frequently observed moving along the proximal axon but stopping before entering the soma and the very proximal part of the axon, implicating defects in the entry into the soma (Figure 3D; Video S1). In wild-type MNs, lysosomes traveled a shorter distance and were mostly stationary (Video S2). Furthermore, quantification of LysoTracker-positive vesicles in fixed cells revealed a similar size and LysoTracker intensity but a

Figure 3. Retrograde Axonal Sorting of Lysosomes Is Impaired *Ex Vivo* and *In Vivo*

(A) LysoTracker DND-99 (green) with LAMP1 (red) immunofluorescence-staining of DIV7 primary MNs. Two representative images of *Tmem106b* KO MNs are shown. Nuclei are stained with DAPI (blue).

(B) Single frames of two representative videos of lentiviral LAMP1-GFP-infected primary MNs of *Tmem106b* KO mice. Four representative independent fusion events of two different cells are shown. Quantification of organelles undergoing fusion or fission with the large LAMP1-positive vacuole. Single lysosomes are labeled with arrowheads.

(C) Kymographs of axonal LysoTracker-positive organelle movement in isolated MNs from control and *Tmem106b* KO mice (DIV7). Quantification of the directional movement and the total retrograde traveled distance are shown. n = 16–19 lysosomes per genotype/condition. Two representative images of *Tmem106b* KO MNs are shown.

(D) Single frames of a representative video of LysoTracker-stained MNs isolated from *Tmem106b* KO mice. A single lysosome is labeled with an arrowhead.

(E) LysoTracker DND-99 (green) with Tuj1 (red) immunofluorescence staining of axons (as in B) of DIV7 primary neurons. Quantification of the number of LysoTracker-positive organelles, intensity, and size per axon is shown (mean ± SEM, n = 12–16 cells/experiment; three experiments).

(F) Representative Tuj1 immunofluorescence-stained primary neurons (DIV7). Quantification of the axon length, dendrite length, and dendrite number. (mean ± SEM, n = 15–20 cells/experiment; three experiments).

(G) Immunofluorescence staining for LAMP1 (green) and CatD (blue) of lentiviral TMEM106B-mCherry (red) transduced or non-transduced primary cultivated MNs from control and *Tmem106b* KO mice (DIV7). A quantification of the number of cells with LAMP1-positive swelling is depicted (mean ± SEM, n = 3).

slightly decreased number in the axons of *Tmem106b* KO mice (Figure 3E). Next, we measured the dendrite number and dendrite and axon length in cultured MNs to address whether TMEM106B deficiency has any morphological consequences. We detected a slight but significantly decreased axon length but no differences in dendrite number or length in *Tmem106b* KO MNs (Figure 3F).

Finally, we performed a rescue experiment with primary MNs. Lentiviral re-expression of ubiquitin-driven mCherry-tagged TMEM106B in primary neurons fully rescued the presence of vacuoles in *Tmem106b* KO MNs, indicating that this phenotype is indeed due to a loss of function of TMEM106B (Figure 3G).

To investigate the axonal transport of endocytic organelles dynamically in facial MNs *in situ*, we applied the neuronal tracer FluoroGold (FG), which is frequently used for retrograde labeling experiments. FG is endocytosed and retrogradely transported in endo-/lysosomes finally reaching the MN soma (Schmued and Fallon, 1986). We first tested whether the endocytosis of FG differs between wild-type and *Tmem106b* KO primary MNs (Figure 4A), but we detected no difference in the endocytic uptake of FG after 15 or 60 min. Next, FG was injected into the FMN-innervated whisker pads of 4-month-old animals (Figure 4B), an age with established pathology. After perfusion and fixation of the mice 4 days after injection, sections were stained with an antibody against FG and LAMP1. In total, ~75% of all LAMP1-positive vacuoles were positive for FG, confirming our observation in cultured MNs that vacuoles are still active in terms of membrane fusion. Several LAMP1-positive vacuoles, especially small ones, stained intensively for FG, validating the axonal and endosomal origin of the vacuoles, while large vacuoles were partially FG negative (Figure 4C). Importantly, for a shorter period of 1 day after FG injection, both the number of FG-positive MNs and the total area of FG in the somata of the FMN were significantly reduced (Figure 4D). These findings provide further evidence that the accumulation of lysosomal membrane structures at the AIS is due to altered retrograde transport, resulting in an impaired delivery of lysosomes to the soma (Figure 4E). These data also suggest that TMEM106B deficiency affects MNs in a cell-autonomous manner, resulting in defective axonal transport of LAMP1-positive organelles and axonal outgrowth *in vitro* and defective retrograde transport of FG-positive vesicles *in vivo*.

TMEM106B Deficiency Causes Impaired Clearance of Lysosomal Cargo and Reduced Turnover of Autophagosomes

We next investigated in more detail whether the altered transport of LAMP1-positive organelles leads to an impaired turnover of axonal autophagosomes. To explore this in cultured MNs, we utilized a lentiviral vector coding for tandem-fluorescent-tagged RFP-GFP-LC3, allowing discrimination between acidified and non-acidified vesicles (Lüningschrör et al., 2017). Quantification of the number of autophagosomes and autolysosomes from DIV7 primary MNs showed an almost doubled number of axonal autophagosomes but a comparable number of autolysosomes in *Tmem106b* KO compared to wild-type MNs, implicating reduced fusion of autophagosomes with lysosomes (Figure 5A). As previously shown (Lüningschrör et al., 2017), in axons of primary MNs, autolysosomes were hardly detectable, suggesting that the final maturation into lysosomes takes place at the soma. To further investigate the interaction of autophagosomes with LAMP1-positive vacuoles in primary MNs, we simultaneously expressed LAMP1-GFP and RFP-LC3 in cultured MNs (Figure 5B). We specifically analyzed MNs containing LAMP1 vacuoles and found that the majority of vacuoles were LC3-RFP positive, suggesting that these vacuoles indeed fused with autophagosomes at a certain stage but failed to mature to genuine lysosomes, as shown by negative staining for CatD (Figure 3A). In this line, an increase of LC3 II (the autophagosome-bound lipidated form) was also observed in primary mouse embryonic fibroblasts (MEFs) of *Tmem106b* KO mice under basal conditions (Figure S7A). Inhibition of the fusion of lysosomes with autophagosomes in MEFs by bafilomycin A showed no further increase in LC3 II in the *Tmem106b* KO cells compared to the wild type, indicating no enhanced generation of autophagosomes, but an impaired fusion of lysosomes and autophagosomes in *Tmem106b* KO MEFs.

Immunoblots from brain extracts of 6-month-old wild-type and *Tmem106b* KO mice for LC3, p62, and ubiquitin revealed a significant increase in LC3 II, p62, and high-molecular-weight ubiquitinated proteins, further providing evidence for a pathological accumulation of autophagosomes and autophagic cargo/substrates (Figure 5C). In this line, large p62-positive aggregates were observed in the hindbrain and spinal cord of *Tmem106b* KO mice by immunofluorescence (Figure 5D). The p62-positive aggregates started to appear at 4 months of age and were very rarely seen in regions other than the hindbrain. We observed a slight but significant increase in the amount of autofluorescent neuronal lipofuscin in the thalamus (Figure 5E), an area also affected by vacuolization. Electron microscopic evaluation and quantification of the lysosomal volume density revealed a significant increase in the volume of lipofuscin-filled lysosomes in both the spinal cord and the thalamus, but not the cerebral cortex (Figure 5F). In support of the data of the CRISPR/Cas9-mediated *Tmem106b* KO mice, the *Tmem106b*^{tm2b} KO mice similarly showed an increase of LC3 II, high-molecular-weight ubiquitin aggregates, increased autofluorescence in the thalamus, and p62-positive aggregates (Figures S7B–S7D). These results point toward a reduced clearance of lysosomal substrates and autophagic cargo in *Tmem106b* KO neurons, possibly caused by altered axo-dendritic sorting of lysosomes.

DISCUSSION

The major phenotypic features of *Tmem106B* KO mice are giant LAMP1-positive vacuoles specifically occurring at the AIS of MNs. Vacuole formation ultimately leads to functional deficits of the affected motor units as a consequence of the loss of TMEM106B. The enlarged vacuoles are partially negative for CatD *in situ* and *in vitro* and negative for LysoTracker, but they are positive for LAMP1. Therefore, they do not represent genuine functional lysosomes. Even the designation of those highly non-physiological organelles as "lysosomes" should be taken with caution, as they might also represent late endosomes, autolysosomes, or hybrid organelles. However, as they bear no similarity to any physiological organelles in wild-type mice, a more precise designation is useless. In this regard, it should also be noted that

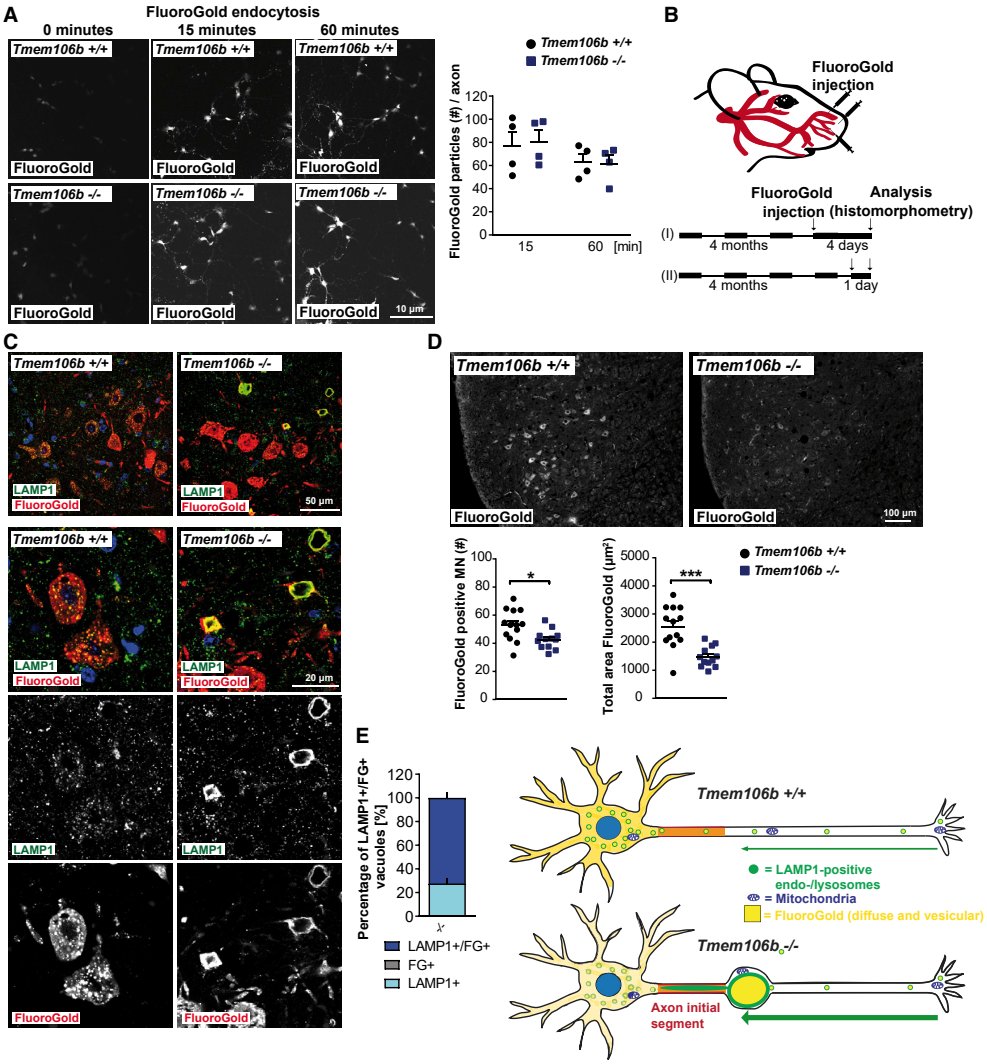

Figure 4. TMEM106B Deficiency Leads to Reduced Delivery of the Retrograde Tracer FluoroGold in MNs *In Vivo*

(A) Primary MNs from wild-type and *Tmem106b* KO mice (DIV5) were offered FluoroGold (FG) for 15 min, washed, and chased for the indicated time points. FG was stained by immunofluorescence with an FG-specific antibody. The number of FG particles in axons was counted and is depicted on the right. Somata were excluded from the analysis (mean ± SEM, n = 4).

(B) Scheme of the FG retrograde labeling experiments.

(C) Immunofluorescence of the FMN for FG (red) and LAMP1 (green) 4 days after FG injection. Nuclei are stained with DAPI (blue). Quantification of FG and/or LAMP1-positive vacuoles is depicted (n = 3).

(D) Representative image of the FMN stained for FG 1 day after injection of FG in wild-type control and *Tmem106b* KO mice (4 months). Quantification of the number of FG-positive MNs and area covered by FG staining is shown (mean ± SEM, n = 12–13).

(E) Scheme of the localization of LAMP1-positive organelles (green) in MNs of wild-type control and *Tmem106b* KO mice. The distribution of FG (yellow) is indicated.

LAMP1-positive organelles even in wild-type neurons represent a heterogeneous population of endocytotic organelles (including late endosomes and autolysosomes) that are processed toward degradative lysosomes (Cheng et al., 2018). Such LAMP1-positive organelles are enriched in axons and most likely contain retrogradely transported cargo derived from the distal axon like maturing autolysosomes/autophagosomes (Maday et al., 2014). The fact that most vacuoles in primary MNs were positive for LC3 indicates that autophagosomes significantly contribute to their biogenesis.

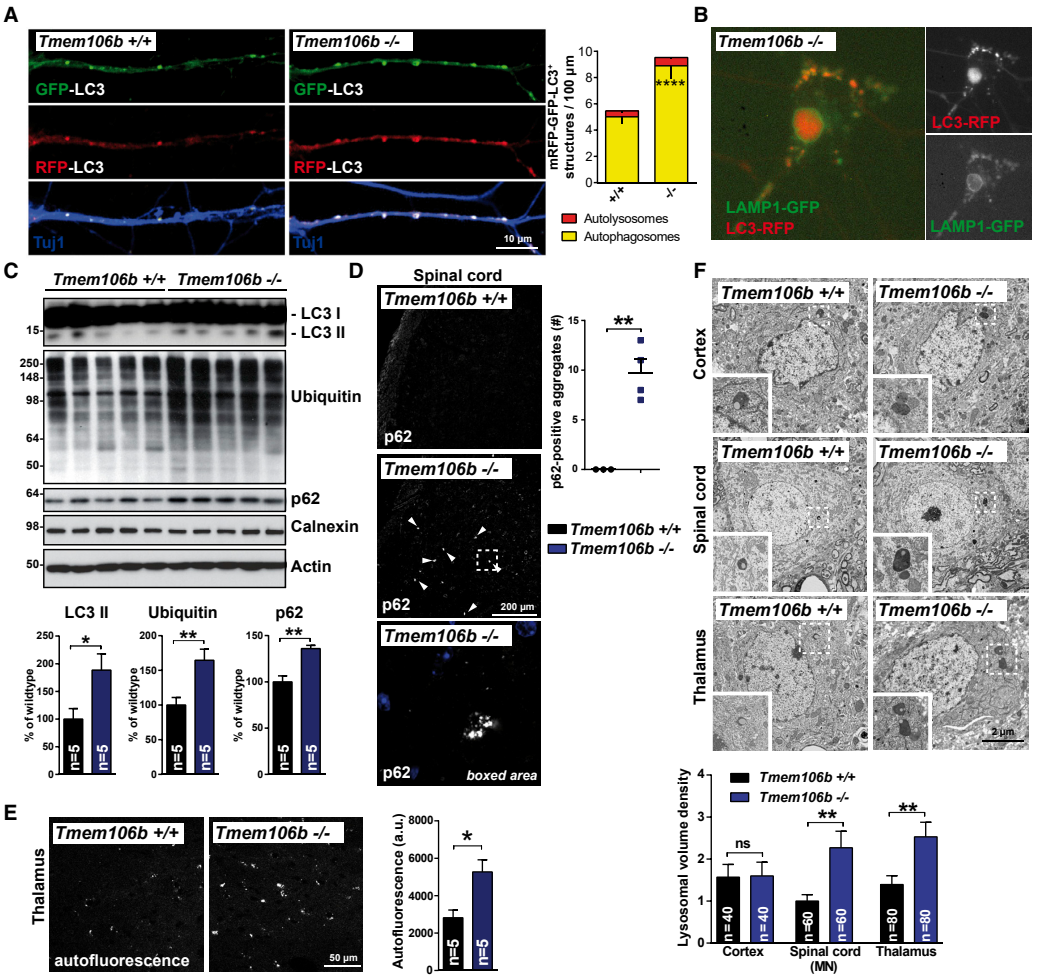

Figure 5. TMEM106B Deficiency Impairs the Degradation of Lysosomal Substrates

(A) Representative confocal images of the axon of lentivirus-infected tandem fluorescent-tagged LC3 (mRFP-EGFP-LC3)-expressing primary MNs (DIV7) of *Tmem106b* KO and control cells. RFP channel is depicted in red, GFP channel is depicted in green. The axon is stained with an antibody against Tuj1 (blue). Quantification of RFP-positive (autolysosomes) and RFP-GFP-double-positive organelles (autophagosomes) in the axon. Mean ± SEM; n = 10 neurons/experiment; three experiments; two-way ANOVA; Bonferroni post-test.

(B) Primary MNs (DIV7) of *Tmem106b* KO mice infected with lentiviruses coding for LAMP1-GFP (green) and LC3-RFP (red).

(C) Immunoblots of total-brain lysates with the indicated antibodies. Age: 6 months. Quantification is shown below. Mean ± SEM; n = 5.

(D) Immunofluorescence staining of the spinal cord for p62. p62-positive aggregates are marked with arrowheads. Quantification of the number of p62-positive aggregates/section (mean ± SEM, n = 3–4). Nuclei are stained with DAPI (blue). Age: 4 months.

(E) Representative confocal images of autofluorescence (488-nm laser excitation) in the thalamus of *Tmem106b* KO and control mice. Age: 4 months.

(F) Electron micrographs of neurons of the cortex, spinal cord, and thalamus. A quantification of lysosomal volume density is given. Mean ± SEM (n = 40–80 single neurons from two independent mice/genotype).

Three groups previously reported the generation and characterization of TMEM106B-deficient mice (Arrant et al., 2018; Klein et al., 2017; Nicholson et al., 2018). Interestingly, key phenotypic alterations described in the two KO strains described in our study (vacuolization of MNs, increased autophagosomes, and aggregates) were not reported. Generally, no spontaneous phenotype in the basal *Tmem106b* KO situation was found in previous studies except for subtle changes of lysosomal proteins like cathepsin B, cathepsin L, and DPP7; a downregulation of subunits of the V-ATPase; and decreased LysoTracker intensity in primary neurons. We, in contrast, observed an increase in the activity of several lysosomal enzymes and increased levels of

CatD. No major differences in the LysoTracker staining were observed in primary neurons. Notably, both previously published mouse models were generated by the same KO strategy: both strains are ''knock-in-/KO-first'' alleles, in which an intronic gene trap vector with an artificial splice-acceptor site abrogates the transcription of the wild-type transcript. However, this strategy might result in an incomplete KO: due to incomplete usage of the splice-acceptor site, the resulting mouse lines can be hypomorphs with residual wild-type transcript and protein instead of a full KO (Mitchell et al., 2001). In both studies, the authors crossed homozygous or heterozygous *Tmem106b* gene trap mice with progranulin KO mice and observed a partial rescue of the *Grn* KO phenotype (Klein et al., 2017; Arrant et al., 2018). If the *Tmem106b* KO was incomplete, the results of these experiments are also difficult to interpret. Alternatively, in the previous studies, the phenotype described here has not been detected because the histological characterization focused on brain regions more relevant for FTLD.

Overexpression of TMEM106B in cultured cells leads to enlarged dysfunctional lysosomes, as shown in several studies (Arrant et al., 2018; Brady et al., 2013; Chen-Plotkin et al., 2012; Gallagher et al., 2017; Lang et al., 2012), and TMEM106B knockdown leads to a reduced number of lysosomes (Chen-Plotkin et al., 2012; Stagi et al., 2014). Our observation of drastically enlarged, LAMP1-positive organelles in the KO situation appears to be counterintuitive in that regard. However, it seems to be plausible that the levels of TMEM106B need to be tightly balanced, and both reduced levels as well as increased levels cause dysregulation of lysosomal size. Whether both situations are caused by the same molecular mechanism(s), however, needs to be formally proven. In this respect, it should also be noted that the lysosome enlargement is dose dependent (Gallagher et al., 2017). These findings have relevance for TMEM106B's role in disease, given that the effect of genetic variants in different disease entities (e.g., on TMEM106B levels) is still obscure. In cultured primary hippocampal neurons, knockdown of TMEM106B affects the transport of lysosomes in dendrites (Schwenk et al., 2014). These studies were complemented by analyses with primary cortical neurons, showing a similar effect on the neuritic transport of lysosomes (Stagi et al., 2014). In both studies, an increase in the number of moving lysosomes was shown. However, it remained unclear whether TMEM106B knockdown affects the transport of moving lysosomes in the anterograde or retrograde direction in neurites, and both studies focused on moving lysosomes in dendrites. The availability of the new *Tmem106b* KO models allowed histopathological analyses of proximal and distal nerve segments and an unbiased survey of the loss-of-function effect in different terminally differentiated neuronal cell types. These *in vivo* data support a primary defect in lysosome positioning, and they clearly show that TMEM106B is particularly important in the sorting of lysosomes in the axon rather than in dendrites and that the retrograde movement is altered. The axon differs in several regards from dendrites: in contrast to dendrites, the axon contains a tight barrier, the AIS, which is preventing somatodendritic cargo from entering . If there are any gatekeeper mechanisms for retrograde cargo, controlling entry of cargo into the AIS from the distal end is unknown. Additionally, the orientation of microtubules considerably differs between the axon and dendrites: while the axon has a uniform arrangement of microtubules with plus ends distal to the cell body (plus-end out), dendrites have equal numbers of plus- and minus-end-out microtubules (Yau et al., 2016). Both features might contribute to the observed phenotype with an accumulation of large LAMP1-positive vacuoles at the distal AIS. Finally, the cargo (i.e., the LAMP1-positive organelles) differ in their microtubule-interacting motor machinery between dendrites and the axon, contributing to differences between dendritic and axonal sorting. Knockdown of TMEM106B in primary cortical neurons was previously shown to increase the retrograde transport of lysosomes in dendrites (Schwenk et al., 2014). This effect might be even more pronounced *in vivo* and in MNs with their long complex axon, ultimately explaining the observed phenotype. Interestingly, a recent study revealed altered positioning of endo-/lysosomes in dendrites of cortical neurons of CHMP2B-deficient mice (Clayton et al., 2018), which were previously shown to develop axonal degeneration as well (Ghazi-Noori et al., 2012). This altered positioning of lysosomes in dendrites of CHMP2B-deficient mice was rescued by knockdown of TMEM106B (Clayton et al., 2018). It will be interesting to determine if TMEM106B levels also affect axonal degeneration in CHMP2B-deficient mice.

The observation that cultured spinal MNs frequently show LAMP1-positive vacuoles in both the soma and the proximal axon suggests that an impaired transport of lysosomes is cell autonomous and is the primary cause for the observed phenotype, and impaired autophagy and formation of vacuoles is a secondary event. This finding is in good agreement with the increased retrograde transport rate of lysosomes in the axon of primary MNs *ex vivo*, presumably ultimately leading to a buildup of lysosomes at the distal end of the AIS, but a reduced delivery of the axonal tracer to the soma observed *in vivo*. The decreased delivery of FG to the soma at later time points seems contradictory, given a higher transport of FG-containing organelles. However, it seems reasonable that the tracer gets stuck in the vacuoles (of which the majority are FG positive), finally leading to impaired somatic delivery. Surprisingly, the observed severe vacuolization of the FMN has only small functional consequences, reflected by very mild behavioral deficits. At 2 months of age, NMJs remain intact despite clear vacuolization. Furthermore, vacuolization seems not to completely impair axonal trafficking, allowing survival of the proximal axon, the NMJ, and finally the MN itself. However, denervation of NMJs in aged animals indicates a functional decline. Notably, the AIS pathology might additionally explain the observed functional behavioral and motoric alterations despite a lack of degeneration in young animals: alterations of the AIS due to, for example, mutations in Tau were shown to affect neuronal excitability (Sohn et al., 2019). Similarly, the altered morphology of the AIS in *Tmem106b* KO mice might cause functional deficits.

It is tempting to speculate that lysosomes or retrogradely transported late endosomes accumulating within or at the distal end of the AIS undergo aberrant fusion, ultimately leading to the ballooning of the axon. These lysosomes are likely dysfunctional and unable to degrade any cargo, which might explain the slight increase in some lysosomal enzymes and soluble proteins like CatD or progranulin, considering that (active) lysosomal

proteases regulate the levels of lysosomal enzymes. This explanation is additionally supported by the unchanged transcript levels of the investigated enzymes, suggesting posttranscriptional regulation of the levels of these enzymes or modulation of their activity. We can also not rule out that TMEM106B is directly modulating their function, explaining the increased activity, and that in fact, the giant vacuoles are a consequence of such a dysregulation. The increase of progranulin is particularly interesting, given the close genetic interaction between *GRN* and *TMEM106B* in human FTLD patients. However, given an increase of other lysosomal proteins to a similar extent, we think this finding is not specific for progranulin but rather reflects the general lysosomal alterations. Nevertheless, we cannot fully rule out the possibility that TMEM106B directly affects progranulin levels by a direct physical interaction (e.g., protecting progranulin from proteolysis).

Alternatively to the suggested aberrant fusion hypothesis, TMEM106B could have a dual function, involving the cytosolic N terminus mediating the retrograde microtubule-dependent transport of lysosomes by interacting directly or indirectly with motor proteins and the luminal domain mediating fusion events and/or activity of lysosomal enzymes. This might also explain alterations in autophagy, which could lead both to defects in fusion and to indirect effects due to impaired lysosomal degradation. Of note, our study provides experimental evidence for a sorting mechanism for LAMP1-positive organelles at the distal end of the AIS and suggests the presence of ''gatekeeper'' machinery facilitating the retrograde entry of lysosomes into the AIS. Other mechanisms are also conceivable: the entry of axonal retrograde cargo into the AIS might be limiting, and through TMEM106B deficiency, too much cargo is transported to the AIS, exceeding its capacity. Microtubule modifications or motor preference might differ between the distal end of the AIS and the proximal axon and cause the disassembly of the motor and LAMP1-positive cargo. Finally, the AIS is the site where myelin sheath begins, and myelination might be critical for the formation of the vacuoles. The precise mechanism by which vacuoles develop *in situ* at the distal end of the AIS remains to be determined. Previous studies reported that the fusion between LAMP1-positive endosomes and autophagosomes in axons is an early event, taking place in the distal axon. During retrograde transport, these organelles mature, but the final maturation and acidification take place as a last step in the soma (Maday et al., 2014). It is also possible to hypothesize that the AIS is critical during this process, sorting retrograde transported autophagosomes/amphisomes to the soma for their final maturation.

An interesting observation is the very restricted occurrence of the vacuoles in selected MN nuclei. MNs show an extreme degree of polarization and are characterized by exceedingly long axons and highly complex arborization, making them susceptible to any (even subtle) alterations in the axonal transport of organelles. TMEM106B is expressed ubiquitously in neurons, and there is no pronounced higher expression in MNs compared to other neuronal subpopulations. Though we cannot finally prove this hypothesis, we speculate that the complexity in the axonal arborization and the long distances that need to be overcome by LAMP1-positive organelles in axons of MNs might explain their predominant susceptibility.

The ''protective'' effect of *TMEM106B* coding variants in humans with FTLD has been suggested to be the result of reduced expression due to decreased stability of the resulting protein bearing the T185S amino acid exchange (Nicholson et al., 2013; Van Deerlin et al., 2010). The situation in the KO with a full deletion instead of possibly slightly reduced protein levels due to the T185S variant is, however, clearly different and likely has a much higher impact on cellular function and resulting dysfunction. It should be noted that the purpose of our present study was not to generate a model for FTLD, but to get a better understanding of the physiological function of TMEM106B. Variants in *TMEM106B* were initially found to convey the highest effect on *GRN* carriers, but later studies revealed a significant effect on *C9orf72* carriers as well, implying that TMEM106B acts *in trans* to both *GRN* and *C9orf72* mutations. Our proposed model of impaired lysosomal degradation based on altered axonal trafficking leads us to the hypothesis that mutations in progranulin and perhaps C9orf72 affect lysosomal proteolysis and that alterations in TMEM106B additionally titrate disease risk and severity in a dose-dependent manner. Moreover, the observed accumulation of lipofuscin in the *Tmem106b* KO mice, presumably caused by axonal transport defects, might explain the effect of genetic *TMEM106B* variations on aging and cognition (Rhinn and Abeliovich, 2017; White et al., 2017), considering that an age-dependent lysosomal lipofuscin accumulation is one of the hallmarks of neuronal aging.

STAR★METHODS

Detailed methods are provided in the online version of this paper and include the following:

- KEY RESOURCES TABLE
- LEAD CONTACT AND MATERIALS AVAILABILITY
- EXPERIMENTAL MODEL AND SUBJECT DETAILS
  - Animal Models
  - Primary Cells
- METHOD DETAILS
  - Quantitative real time PCR (qRT-PCR)
  - Biochemical Experiments
  - Histology and electron microscopy
- *IN VIVO* LABELING WITH FLUORO-GOLD RETROGRADE TRACER
  - Behavioral Studies
  - Immunocytochemistry and live-cell imaging
  - Immunocytochemistry
- QUANTIFICATION AND STATISTICAL ANALYSIS
- DATA AND CODE AVAILABILITY

SUPPLEMENTAL INFORMATION

Supplemental Information can be found online at https://doi.org/10.1016/j.celrep.2020.02.060.

ACKNOWLEDGMENTS

We thank Dagmar Niemeier, Maike Langer, and Katrin Fellerer for excellent technical assistance and Björn Schuster, Inken Beck, and Radislav Sedlacek (Institute of Molecular Genetics, Prague) for the generation of *Tmem106b*

CRISPR KO mice. M.D. and P.S. are supported by the Deutsche Forschungsgemeinschaft (DFG) FOR2625. B.K. is supported by the DFG through SFB 1149. C.H. is supported by the DFG within the framework of the Munich Cluster for Systems Neurology (EXC 1010 SyNergy, ID 390857198) and a DFG-funded Koselleck Project (HA1737/16-1). W.W. is supported by the DFG through SFB 870 and by the "EUCOMM: Tools for Functional Annotation of the Mouse Genome" (EUCOMMTOOLS) project (FP7-HEALTH-F4-2010-261492).

AUTHOR CONTRIBUTIONS

P.L., G.W., S.S., S.K., B.D., D.S., R.W., R.L-R., and M.D. performed experimental work. P.L., G.W., S.S., B.W., W.W., R.D.H., Y.U., M.S., C.H., P.S., B.K., A.C., and M.D. were involved in experimental design and data analysis and interpretation, and they also edited the manuscript. M.D. conceived the study and wrote the manuscript.

DECLARATION OF INTERESTS

The authors declare no competing interests.

Received: February 14, 2019
Revised: October 21, 2019
Accepted: February 13, 2020
Published: March 10, 2020

REFERENCES

Arrant, A.E., Nicholson, A.M., Zhou, X., Rademakers, R., and Roberson, E.D. (2018). Partial Tmem106b reduction does not correct abnormalities due to progranulin haploinsufficiency. Mol. Neurodegener. *13*, 32.

Baker, M., Mackenzie, I.R., Pickering-Brown, S.M., Gass, J., Rademakers, R., Lindholm, C., Snowden, J., Adamson, J., Sadovnick, A.D., Rollinson, S., et al. (2006). Mutations in progranulin cause tau-negative frontotemporal dementia linked to chromosome 17. Nature *442*, 916–919.

Brady, O.A., Zheng, Y., Murphy, K., Huang, M., and Hu, F. (2013). The frontotemporal lobar degeneration risk factor, TMEM106B, regulates lysosomal morphology and function. Hum. Mol. Genet. *22*, 685–695.

Busch, J.I., Unger, T.L., Jain, N., Tyler Skrinak, R., Charan, R.A., and Chen-Plotkin, A.S. (2016). Increased expression of the frontotemporal dementia risk factor TMEM106B causes C9orf72-dependent alterations in lysosomes. Hum. Mol. Genet. *25*, 2681–2697.

Chen-Plotkin, A.S., Unger, T.L., Gallagher, M.D., Bill, E., Kwong, L.K., Volpicelli-Daley, L., Busch, J.I., Akle, S., Grossman, M., Van Deerlin, V., et al. (2012). TMEM106B, the risk gene for frontotemporal dementia, is regulated by the microRNA-132/212 cluster and affects progranulin pathways. J. Neurosci. *32*, 11213–11227.

Cheng, X.T., Xie, Y.X., Zhou, B., Huang, N., Farfel-Becker, T., and Sheng, Z.H. (2018). Characterization of LAMP1-labeled nondegradative lysosomal and endocytic compartments in neurons. J. Cell Biol. *217*, 3127–3139.

Claussen, M., Kübler, B., Wendland, M., Neifer, K., Schmidt, B., Zapf, J., and Braulke, T. (1997). Proteolysis of insulin-like growth factors (IGF) and IGF binding proteins by cathepsin D. Endocrinology *138*, 3797–3803.

Clayton, E.L., Milioto, C., Muralidharan, B., Norona, F.E., Edgar, J.R., Soriano, A., Jafar-Nejad, P., Rigo, F., Collinge, J., and Isaacs, A.M. (2018). Frontotemporal dementia causative CHMP2B impairs neuronal endolysosomal trafficrescue by TMEM106B knockdown. Brain *141*, 3428–3442.

Crawley, J.N. (2007). What's Wrong With My Mouse?: Behavioral Phenotyping of Transgenic and Knockout Mice, Second Edition (Wiley).

Cruts, M., Gijselinck, I., van der Zee, J., Engelborghs, S., Wils, H., Pirici, D., Rademakers, R., Vandenberghe, R., Dermaut, B., Martin, J.J., et al. (2006). Null mutations in progranulin cause ubiquitin-positive frontotemporal dementia linked to chromosome 17q21. Nature *442*, 920–924.

Dombert, B., Sivadasan, R., Simon, C.M., Jablonka, S., and Sendtner, M. (2014). Presynaptic localization of Smn and hnRNP R in axon terminals of embryonic and postnatal mouse motoneurons. PLoS ONE *9*, e110846.

Finch, N., Carrasquillo, M.M., Baker, M., Rutherford, N.J., Coppola, G., Dejesus-Hernandez, M., Crook, R., Hunter, T., Ghidoni, R., Benussi, L., et al. (2011). TMEM106B regulates progranulin levels and the penetrance of FTLD in GRN mutation carriers. Neurology *76*, 467–474.

Gallagher, M.D., Suh, E., Grossman, M., Elman, L., McCluskey, L., Van Swieten, J.C., Al-Sarraj, S., Neumann, M., Gelpi, E., Ghetti, B., et al. (2014). TMEM106B is a genetic modifier of frontotemporal lobar degeneration with C9orf72 hexanucleotide repeat expansions. Acta Neuropathol. *127*, 407–418.

Gallagher, M.D., Posavi, M., Huang, P., Unger, T.L., Berlyand, Y., Gruenewald, A.L., Chesi, A., Manduchi, E., Wells, A.D., Grant, S.F.A., et al. (2017). A Dementia-Associated Risk Variant near TMEM106B Alters Chromatin Architecture and Gene Expression. Am. J. Hum. Genet. *101*, 643–663.

Gass, J., Cannon, A., Mackenzie, I.R., Boeve, B., Baker, M., Adamson, J., Crook, R., Melquist, S., Kuntz, K., Petersen, R., et al. (2006). Mutations in progranulin are a major cause of ubiquitin-positive frontotemporal lobar degeneration. Hum. Mol. Genet. *15*, 2988–3001.

Gey, M., Wanner, R., Schilling, C., Pedro, M.T., Sinske, D., and Knöll, B. (2016). Atf3 mutant mice show reduced axon regeneration and impaired regeneration-associated gene induction after peripheral nerve injury. Open Biol. *6*, 160091.

Ghazi-Noori, S., Froud, K.E., Mizielinska, S., Powell, C., Smidak, M., Fernandez de Marco, M., O'Malley, C., Farmer, M., Parkinson, N., Fisher, E.M., et al. (2012). Progressive neuronal inclusion formation and axonal degeneration in CHMP2B mutant transgenic mice. Brain *135*, 819–832.

Götzl, J.K., Mori, K., Damme, M., Fellerer, K., Tahirovic, S., Kleinberger, G., Janssens, J., van der Zee, J., Lang, C.M., Kremmer, E., et al. (2014). Common pathobiochemical hallmarks of progranulin-associated frontotemporal lobar degeneration and neuronal ceroid lipofuscinosis. Acta Neuropathol. *127*, 845–860.

Gutzmann, A., Ergül, N., Grossmann, R., Schultz, C., Wahle, P., and Engelhardt, M. (2014). A period of structural plasticity at the axon initial segment in developing visual cortex. Front. Neuroanat. *8*, 11.

Klein, Z.A., Takahashi, H., Ma, M., Stagi, M., Zhou, M., Lam, T.T., and Strittmatter, S.M. (2017). Loss of TMEM106B Ameliorates Lysosomal and Frontotemporal Dementia-Related Phenotypes in Progranulin-Deficient Mice. Neuron *95*, 281–296.e286.

Lang, C.M., Fellerer, K., Schwenk, B.M., Kuhn, P.H., Kremmer, E., Edbauer, D., Capell, A., and Haass, C. (2012). Membrane orientation and subcellular localization of transmembrane protein 106B (TMEM106B), a major risk factor for frontotemporal lobar degeneration. J. Biol. Chem. *287*, 19355–19365.

Lüningschrör, P., Binotti, B., Dombert, B., Heimann, P., Perez-Lara, A., Slotta, C., Thau-Habermann, N., R von Collenberg, C., Karl, F., Damme, M., et al. (2017). Plekhg5-regulated autophagy of synaptic vesicles reveals a pathogenic mechanism in motoneuron disease. Nat. Commun. *8*, 678.

Maday, S., Twelvetrees, A.E., Moughamian, A.J., and Holzbaur, E.L. (2014). Axonal transport: cargo-specific mechanisms of motility and regulation. Neuron *84*, 292–309.

Markmann, S., Krambeck, S., Hughes, C.J., Mirzaian, M., Aerts, J.M., Saftig, P., Schweizer, M., Vissers, J.P., Braulke, T., and Damme, M. (2017). Quantitative Proteome Analysis of Mouse Liver Lysosomes Provides Evidence for Mannose 6-phosphate-independent Targeting Mechanisms of Acid Hydrolases in Mucolipidosis II. Mol. Cell. Proteomics *16*, 438–450.

Mitchell, K.J., Pinson, K.I., Kelly, O.G., Brennan, J., Zupicich, J., Scherz, P., Leighton, P.A., Goodrich, L.V., Lu, X., Avery, B.J., et al. (2001). Functional analysis of secreted and transmembrane proteins critical to mouse development. Nat. Genet. *28*, 241–249.

Nelson, P.T., Dickson, D.W., Trojanowski, J.Q., Jack, C.R., Boyle, P.A., Arfanakis, K., Rademakers, R., Alafuzoff, I., Attems, J., Brayne, C., et al. (2019). Limbic-predominant age-related TDP-43 encephalopathy (LATE): consensus working group report. Brain *142*, 1503–1527.

Nicholson, A.M., Finch, N.A., Wojtas, A., Baker, M.C., Perkerson, R.B., 3rd, Castanedes-Casey, M., Rousseau, L., Benussi, L., Binetti, G., Ghidoni, R., et al. (2013). TMEM106B p.T185S regulates TMEM106B protein levels: implications for frontotemporal dementia. J. Neurochem. *126*, 781–791.

Nicholson, A.M., Zhou, X., Perkerson, R.B., Parsons, T.M., Chew, J., Brooks, M., DeJesus-Hernandez, M., Finch, N.A., Matchett, B.J., Kurti, A., et al. (2018). Loss of Tmem106b is unable to ameliorate frontotemporal dementia-like phenotypes in an AAV mouse model of C9ORF72-repeat induced toxicity. Acta Neuropathol. Commun. *6*, 42.

Pottier, C., Zhou, X., Perkerson, R.B., III, Baker, M., Jenkins, G.D., Serie, D.J., Ghidoni, R., Benussi, L., Binetti, G., López de Munain, A., et al. (2018). Potential genetic modifiers of disease risk and age at onset in patients with frontotemporal lobar degeneration and GRN mutations: a genome-wide association study. Lancet Neurol. *17*, 548–558.

Premi, E., Grassi, M., van Swieten, J., Galimberti, D., Graff, C., Masellis, M., Tartaglia, C., Tagliavini, F., Rowe, J.B., Laforce, R., Jr., et al.; Genetic FTD Initiative (GENFI) (2017). Cognitive reserve and TMEM106B genotype modulate brain damage in presymptomatic frontotemporal dementia: a GENFI study. Brain *140*, 1784–1791.

Ratnavalli, E., Brayne, C., Dawson, K., and Hodges, J.R. (2002). The prevalence of frontotemporal dementia. Neurology *58*, 1615–1621.

Rhinn, H., and Abeliovich, A. (2017). Differential Aging Analysis in Human Cerebral Cortex Identifies Variants in TMEM106B and GRN that Regulate Aging Phenotypes. Cell Syst *4*, 404–415.e405.

Schmued, L.C., and Fallon, J.H. (1986). Fluoro-Gold: a new fluorescent retrograde axonal tracer with numerous unique properties. Brain Res. *377*, 147–154.

Schwenk, B.M., Lang, C.M., Hogl, S., Tahirovic, S., Orozco, D., Rentzsch, K., Lichtenthaler, S.F., Hoogenraad, C.C., Capell, A., Haass, C., and Edbauer, D. (2014). The FTLD risk factor TMEM106B and MAP6 control dendritic trafficking of lysosomes. EMBO J. *33*, 450–467.

Shi, Y., Lin, S., Staats, K.A., Li, Y., Chang, W.H., Hung, S.T., Hendricks, E., Linares, G.R., Wang, Y., Son, E.Y., et al. (2018). Haploinsufficiency leads to neurodegeneration in C9ORF72 ALS/FTD human induced motor neurons. Nat. Med. *24*, 313–325.

Shibata, M., Kanamori, S., Isahara, K., Ohsawa, Y., Konishi, A., Kametaka, S., Watanabe, T., Ebisu, S., Ishido, K., Kominami, E., and Uchiyama, Y. (1998). Participation of cathepsins B and D in apoptosis of PC12 cells following serum deprivation. Biochem. Biophys. Res. Commun. *251*, 199–203.

Sohn, P.D., Huang, C.T., Yan, R., Fan, L., Tracy, T.E., Camargo, C.M., Montgomery, K.M., Arhar, T., Mok, S.A., Freilich, R., et al. (2019). Pathogenic Tau Impairs Axon Initial Segment Plasticity and Excitability Homeostasis. Neuron *104*, 458–470.e5.

Stagi, M., Klein, Z.A., Gould, T.J., Bewersdorf, J., and Strittmatter, S.M. (2014). Lysosome size, motility and stress response regulated by fronto-temporal dementia modifier TMEM106B. Mol. Cell. Neurosci. *61*, 226–240.

Tropea, T.F., Mak, J., Guo, M.H., Xie, S.X., Suh, E., Rick, J., Siderowf, A., Weintraub, D., Grossman, M., Irwin, D., et al. (2019). TMEM106B Effect on cognition in Parkinson disease and frontotemporal dementia. Ann. Neurol. *85*, 801–811.

van Blitterswijk, M., Mullen, B., Nicholson, A.M., Bieniek, K.F., Heckman, M.G., Baker, M.C., DeJesus-Hernandez, M., Finch, N.A., Brown, P.H., Murray, M.E., et al. (2014). TMEM106B protects C9ORF72 expansion carriers against frontotemporal dementia. Acta Neuropathol. *127*, 397–406.

Van Deerlin, V.M., Sleiman, P.M., Martinez-Lage, M., Chen-Plotkin, A., Wang, L.S., Graff-Radford, N.R., Dickson, D.W., Rademakers, R., Boeve, B.F., Grossman, M., et al. (2010). Common variants at 7p21 are associated with frontotemporal lobar degeneration with TDP-43 inclusions. Nat. Genet. *42*, 234–239.

van der Zee, J., Van Langenhove, T., Kleinberger, G., Sleegers, K., Engelborghs, S., Vandenberghe, R., Santens, P., Van den Broeck, M., Joris, G., Brys, J., et al. (2011). TMEM106B is associated with frontotemporal lobar degeneration in a clinically diagnosed patient cohort. Brain *134*, 808–815.

Wanner, R., Gey, M., Abaei, A., Warnecke, D., de Roy, L., Dürselen, L., Rasche, V., and Knöll, B. (2017). Functional and Molecular Characterization of a Novel Traumatic Peripheral Nerve-Muscle Injury Model. Neuromolecular Med. *19*, 357–374.

White, C.C., Yang, H.S., Yu, L., Chibnik, L.B., Dawe, R.J., Yang, J., Klein, H.U., Felsky, D., Ramos-Miguel, A., Arfanakis, K., et al. (2017). Identification of genes associated with dissociation of cognitive performance and neuropathological burden: Multistep analysis of genetic, epigenetic, and transcriptional data. PLoS Med. *14*, e1002287.

Yau, K.W., Schätzle, P., Tortosa, E., Pagès, S., Holtmaat, A., Kapitein, L.C., and Hoogenraad, C.C. (2016). Dendrites In Vitro and In Vivo Contain Microtubules of Opposite Polarity and Axon Formation Correlates with Uniform Plus-End-Out Microtubule Orientation. J. Neurosci. *36*, 1071–1085.

STAR★METHODS

KEY RESOURCES TABLE

REAGENT or RESOURCE	SOURCE	IDENTIFIER
Antibodies		
Rabbit-polyclonal TMEM106B	Bethyl Antibodies	Cat# A303-439A, RRID:AB_10953337
Rat-monoclonal TMEM106B Clone 6F2	Lang et al., 2012	Clone 6F2
Rabbit polyclonal p62	MBL	Cat# PM045, RRID:AB_1279301
Rabbit-polyclonal Calnexin	Stressgen / Enzo	Cat# ADI-SPA-860, RRID:AB_10616095
Goat-polyclonal Cathepsin D C-20	Santa Cruz Biotechnology	Cat# sc-6486, RRID:AB_637896
Rabbit polyclonal cathepsin D	Shibata et al., 1998	N/A
Rabbit-monoclonal GRN Clone 8H10	Götzl et al., 2014	N/A
Mouse-monoclonal Ubiqutin (clone P4D1)	Santa Cruz Biotechnology	Cat# sc-8017, RRID:AB_628423
Rabbit-polyclonal LC3B	Novus	Cat# NB100-2220, RRID:AB_10003146
Mouse-monoclonal beta-Actin Clone AC-74	Sigma-Aldrich	Cat# A2228, RRID:AB_476697
Goat polyclonal Ankyrin G (P-20)	Santa Cruz Biotechnology	Cat# sc-31778, RRID:AB_2289736
Rabbit-polyclonal βIV-spectrin	Gutzmann et al., 2014	N/A
Rabbit-polyclonal FluoroGold	Millipore	Cat# AB153 RRID:AB_90738
Rat-monoclonal LAMP-1 Clone 1D4B	DSHB	RRID:AB_2134500
Mouse-monoclonal neurofilament (NF-M) Clone 2H3	DSHB	RRID:AB_531793
Rabbit-polyclonal Myelin basic protein antibody (MBP)	GeneTex	Cat# GTX22404, RRID:AB_370733
Mouse-monoclonal Tuj1	Neuromics	Cat# MO15013, RRID:AB_2737114
Mouse-monoclonal NeuN	Millipore	Cat# mAbA60, RRID:AB_2314891
Rabbit-polyclonal Iba1	GeneTex	Cat# GTX100042, RRID:AB_1240434
Rabbit-polyclonal COX IV	Abcam	Cat# ab16056, RRID:AB_443304
Rabbit-polyclonal ChAT	Synaptic Systems	Cat# 297 013, RRID:AB_2620040)
Rabbit-polyclonal Anti-Fluorescent Gold Antibody	Millipore	Cat# AB153-I, RRID:AB_2632408)
Goat anti-rabbit IgG Alexa Fluor 488	Invitrogen	RRID: AB_143165
Goat anti-rat IgG Alexa Fluor 594	Invitrogen	RRID: AB_10561522
Goat anti-rabbit IgG Alexa Fluor 647	Invitrogen	RRID: AB_2535812
Goat anti-rabbit IgG Alexa Fluor 488	Invitrogen	RRID: AB_143165
Goat anti-rat IgG Alexa Fluor 594	Invitrogen	RRID: AB_10561522
Goat anti-rabbit IgG Alexa Fluor 647	Invitrogen	RRID: AB_2535813
Donkey anti-sheep Alexa Fluor 594	Invitrogen	RRID: AB_2534083
Biological Samples		
ES Cell clone: Clone EPD0047_1_E02	KOMP consortium	RRID:MMRRC_050092-UCD
Chemicals, Peptides, and Recombinant Proteins		
FluoroGold	Fluorochrome	https://fluorochrome.com/flouro-gold/
α-Bungarotoxin, Alexa Fluor 488 conjugate	Invitrogen	Cat# B13422
LysoTracker Red DND-99	Invitrogen	Cat# L7528
Experimental Models: Organisms/Strains		
Mouse line: *Tmem106b*^{del2bp}	This paper	N/A
Mouse line: *Tmem106b*^{tm2a}	This paper	N/A
Oligonucleotides		
Tmem106b_ex3_F: GGTTTCCTTGTATCAGACATTAC	Sigma-Aldrich	N/A
Tmem106b_ex3_R: GCTTAACTCACTTCTATTACTGC	Sigma-Aldrich	N/A
Tmem106b_CE_F: GGCGTTACATCGACAGACAA	Sigma-Aldrich	N/A
Tmem106b_CE_R: TGAGAGACATCTCCATTTCTTCC	Sigma-Aldrich	N/A

(*Continued on next page*)

Continued

REAGENT or RESOURCE	SOURCE	IDENTIFIER
For1: TTCTCTCCATGTGCTGCATTATGAGC	Sigma-Aldrich	N/A
Rev1: ACGTGCTTCTCTCATCTACAGTTTTCC	Sigma-Aldrich	N/A
For2: GGGATCTCATGCTGGAGTTCTTCG	Sigma-Aldrich	N/A
Rev2: GAGATGGCGCAACGCAATTAATG	Sigma-Aldrich	N/A
Tmem106b: 5′-GCTGCTGCTAGCACCATGGGAAA GTCTCTTTCTCACTTACC-3′	Metabion	N/A
Tmem106b: 5′-GCTGCTACCGGTTTGTTGTGGCTGA AGGACATTTAG-3′	Metabion	N/A
mCherry: 5′- GCTGCTACCGGTGGAGGTGGT GGA TCTTCTGTGAGCAAGGGCGAGGAGGATAACATGG–3′	Metabion	N/A
mCherry: 5′-GCTGCTTCTAGATTACTTGTACAGCTCGTCC –3′	Metabion	N/A
Recombinant DNA		
FUW-Tmem106b-mCherry	this study	N/A
LAMP1-mGFP	Addgene	#21075
pmRFP-LC3	Addgene	#34831
FUW-RFP-GFP-LC3	Lüningschrör et al., 2017	PMID: 29084947
FUW-RFP-LC3	this study	N/A
FUW -Lamp1-mGFP	this study	N/A
FUW-RFP-LC3-CMV::Lamp1-mGFP	this study	N/A
Software and Algorithms		
GraphPad Prism	GraphPad	RRID:SCR_002798
Templo Software	CONTEMPLAS GmbH	N/A
Vicon Motus 2D software	CONTEMPLAS GmbH	N/A

LEAD CONTACT AND MATERIALS AVAILABILITY

Plasmids, not covered by any restrictions like MTAs generated in this study are available upon request. Further information and requests for resources and reagents should be directed to and will be fulfilled by the Lead Contact, Markus Damme (mdamme@biochem.uni-kiel.de).

EXPERIMENTAL MODEL AND SUBJECT DETAILS

Animal Models

Generation of Tmem106b knockout Mice by CRISPR/Cas9

For the generation of *Tmem106b* KO mice by CRISPR/Cas9-mediated targeting of the *Tmem106b* locus, a guide RNA (gRNA_Tmem106b F1; sequence: AGTGAAGTGCACAACGAAGACGG; protospacer adjacent motif (PAM) is underlined) was designed, that targets exon 3, the first coding exon in the *Tmem106b* gene. The gRNA overlaps with a BbsI restriction site. Single-cell embryos from C57BL/6 mice were co-injected with Cas9 mRNA and gRNA_Tmem106b F1 gRNA. The resulting mutations after non-homologous end-joining repair identified after screening of the offspring in founder mouse lines were validated by Sanger-sequencing. The two chosen founder lines contained either a 2bp deletion (#30907) or a 1bp insertion (#29772); both leading to frameshift mutations. Founder mice were mated with C57BL/6 and germline transmission of the mutation was validated again by Sanger sequencing. A founder line with a 2bp deletion was selected for further experiments, but another strain with a 1bp insertion was phenotypically indistinguishable. The following generations of mice were routinely genotyped by PCR with genomic tail DNA as a template followed by restriction enzyme digest with BbsI and agarose gel electrophoresis or capillary electrophoresis. Primers for amplification of a 552bp fragment of the wild-type locus partially covering exon 3 are: Tmem106b_ex3_F: GGTTTCCTTGTATCAGACATTAC; Tmem106b_ex3_R: GCTTAACTCACTTCTATTACTGC. Alternatively, PCR products amplifying a smaller fragment (121bp of the wild-type locus partially covering exon 3, sequences: Tmem106b_CE_F: GGCGTTACATCGACAGACAA; Tmem106b_CE_R: TGAGAGACATCTCCATTTCTTCC) were separated by capillary electrophoresis with a QIAXcel electrophoresis device (QIAGEN).

Generation of Tmem106b *KO mice with targeted embryonic stem (ES) cells*

Targeted ES cells were obtained from the KOMP consortium (Clone EPD0047_1_E02) and provided by the MMRRC consortium. Generation, breeding and analysis of mice were in line with local and national guidelines and has been approved by the local authorities. ES cells were injected into BALB/C blastocysts. The obtained chimeric mice were bred C57BL/6N wild-type mice to

obtain germline transmission. In the resulting mouse line (tm2a, Knockout-first), expression of *Tmem106b* is disrupted by a splice acceptor (SA) site in the intronic sequence between exons 3 and 4. A β-galactosidase reporter gene (lacZ) is expressed under the control of the endogenous *Tmem106b* promoter. Mice carrying the tm2a allele were bred with Cre-deleter mice which constitutively express the recombinase under the control of the Gt(ROSA)26Sor gene. Mice were genotyped with PCRs for the wild-type-allele, covering a 301 bp sequence in the intronic sequence between exon 3 and exon 4 (For1: TTCTCTCCATGTGCTGCATTATGAGC and Rev1: ACGTGCTTCTCTCATCTACAGTTTTCC) and the tm2b allele, covering partially the targeting cassette and the intronic sequence between exon 4 and exon 5 (For2: GGGATCTCATGCTGGAGTTCTTCG and Rev2: GAGATGGCGCAACGCAATTAATG). Animals for all phenotypic analyses were generated by heterozygous mating of mice with the *Tmem106b* tm2b allele.

Mice were housed at standard laboratory conditions (12 hours light/dark cycle, constant room temperature and humidity). Behavioral testing took place during the light phase of the cycle. Food and water were available *ad libitum*. Experimental protocols were approved by the ethical research committee of the KU Leuven according to EC guidelines or were approved by local german authorities (Ministerium für Energiewende, Landwirtschaft, Umwelt, Natur und Digitalisierung; AZ V242-4255/2018; Regierungspräsidium Tübingen, Germany; TVA 1368). Mice of both genders were used for histology and biochemistry experiments. For the behavioral studies, only female mice were used. The age of the animals is indicated for every experiment, generally animals between two and six months were used, with the exception of the eye blink and whisker orienting reflex tests and balance beam test, in which 14 months old animals were inlcuded.

Primary Cells

Primary MN culture

Murine embryonic spinal MNs were isolated and cultured as described (Lüningschrör et al., 2017). Briefly, after dissection of the ventrolateral part of E12.5 embryos, spinal cord tissues were incubated for 15 minutes in 0.1% trypsin in Hank's balanced salt solution. Cells were triturated and incubated in Neurobasal medium (Invitrogen, CA, USA), supplemented with 1 × Glutamax (Invitrogen, CA, USA) on Nunclon plates (Nunc) pre-coated with antibodies against the p75 NGF receptor (MLR2, kind gift of Robert Rush, Flinders University, Adelaide, Australia) for 45 minutes. Plates were washed three times with Neurobasal medium, and the remaining MN were recovered from the plate with depolarization solution (0.8% NaCl, 35 mM KCl and 2 mM $CaCl_2$) and collected in MN medium (2% horse serum, 1x B27 in Neurobasal medium with 1x Glutamax).

METHOD DETAILS

Quantitative real time PCR (qRT-PCR)

Total RNA was prepared from homogenized mouse brain using the QIAshredder and RNeasy Mini Kit (QIAGEN) according to manufacturer's instructions. 2 μg of RNA was reverse transcribed into cDNA using SuperScript IV reverse transcriptase (Thermo Fisher Scientific Termofisher) and random hexamer primers (Promega). The following primer sets from Integrated DNA Technologies were used: mouse Ctsd Mm.PT.53a.7639164 (Exon boundary 4 to 5), mouse Glb1 Mm.PT.58.8893651 (Exon boundary 4 to 6), Gusb Mm.PT.39a.22214848 (Exon boundary 1 to 2), Hexb Mm.PT.58.6976437 (Exon boundary 6 to 7) and Man2b1 Mm.PT.58.11143577 (Exon boundary 16 to 17). cDNA levels were measured in triplicates using TaqMan assays on a 7500 Fast Real-Time-PCR System (Applied Biosystems), normalized to Hrtp1 Mm.PT.39a.22214828. cDNA expression and relative transcription levels of the respective sequences were analyzed using the comparative delta Ct method (7500 Software V2.0.5, Applied Biosystems, Life Technologies).

Biochemical Experiments

Brain extracts and immunoblotting

Snap frozen brain tissue was mechanically powdered in liquid nitrogen and lysed in RIPA buffer (150 mM NaCl, 20 mM Tris–HCl pH 7.4, 1% NP40, 0.05% Triton X-100, 0.5% sodium-desoxycholate, 2.5 mM ETDA) using the Precellys lysing kit (Ref.: P00933-LYSK0-A) followed by centrifugation at 17,000 × g, 4°C for 45 minutes. Supernatants were collected and protein concentration was determined using BC assay. For SDS-PAGE samples were boiled in Laemmli sample buffer and separated on TRIS-glycine gels. Proteins were transferred onto polyvinylidene difluoride membranes (GE Healthcare Life Science; Amersham Hybond PVDF,) or nitrocellulose membranes (GE Healthcare Life Science). Membranes were blocked for one hour in I-Block™ (Thermo Fisher Scientific) and exposed to the indicated antibody. HRP-conjugated antibodies and Pierce ECL Plus Western Blotting Substrate (Thermo Fisher Scientific) were used for detection and visualization. The following antibodies were used: Cathepsin D (Santa Cruz, sc-6486), GRN (clone 8H10) (Götzl et al., 2014), TMEM106B (A303-439A, Bethyl Antibodies) (Götzl et al., 2014), TMEM106B (clone 6F2) (Lang et al., 2012), calnexin (Stressgen, SPA-860), ubiquitin (Santa Cruz; clone P4D1), p62 (MBL, PM045), LC3 (Novus Biologicals, NB100-2220), actin (Sigma-Aldrich).

Enzymatic assays for lysosomal hydrolases

Brain tissue was homogenized with a potter Elvehjem in 15 volumes (w/v) ice-cold TBS containing 0.5% Triton X-100 and protease inhibitor cocktail. After incubation on ice for 30 minutes with vortexing, lysates were cleared by centrifugation. The specific activity of lysosomal hydrolases was determined as described previously (Markmann et al., 2017) with the following 4-Nitrophenyl-conjugated

substrates (all 10 mM): p-Nitrophenyl-α-D-mannopyranoside (α-mannosidase), p-Nitrophenyl-β-D-glucuronide (β-glucuronidase), p-Nitrophenyl-β-D-glucopyranoside (β-hexosaminidase), p-Nitrophenyl-β-D-galactopyranoside (β-galactosidase).

Histology and electron microscopy

Immunofluorescence of brain and nerve tissues

Mice were deeply anaesthetized and perfused through the left heart ventricle with 0.1 M phosphate buffer (PB) (pH 7.4) followed by perfusion with 4% paraformaldehyde (PFA) in PB. After tissue removal, tissues were post-fixed for another 4 hours in 4% PFA and subsequently transferred to 30% sucrose (in PB) over night. 35 μm thick free-floating sections were cut with a sliding microtome (SM2000R, Leica). For antibody-labeling, sections were washed in PB, blocked with 4% normal goat serum and 0.5% Triton X-100 in 0.1 M PB for one hour at room temperature (RT) and subsequently incubated with the primary antibodies at 4°C over night in blocking solution. After washing three times with PB containing 0.25% Triton X-100, sections were incubated with AlexaFluor fluorophore-conjugated secondary antibodies (AlexaFluor 488, 594 or 647) (Life Technologies) for one hour at RT and washed again three times with PB containing 0.25% Triton X-100. Finally, sections were mounted in Mowiol/DABCO containing DAPI. Images were taken with an Olympus confocal microscope (FV1000, Olympus). STED images were acquired with a Stedycon STED (Abberior Instruments) microscope. The following antibodies were used: AnkyrinG (Santa Cruz, P-20), βIV-spectrin (kind gift from Maren Engelhardt, Gutzmann et al., 2014), LAMP1 (DSHB, Hybridoma Bank, clone 1D4B), cathepsin D (gift from Thomas Braulke, Claussen et al., 1997), Neurofilament H (DSHB, Hybridoma Bank, clone 2H3) Myelin Basic Protein (MBP) (Genetex, GTX22404), NeuN (Millipore, clone A60), Iba1 (Genetex, GTX100042), Cox IV (Abcam, ab16056), ChAT (#297 013, Synaptic Systems), FluoroGold™ (AB153, Millipore).

X-gal staining for β-galactosidase reporter gene expression analysis

For β-galactosidase reporter gene expression analysis, free floating sections from heterozygote tm2b-mice were permeabilized for 10 minutes in PBS containing 0.01% (w/v) Na-Deoxycholat, 0.02% (v/v) Nonidet P-40, washed with PBS and subsequently incubated in substrate solution (5 mM $K_3Fe(CN)_6$, 5 mM $K_4Fe(CN)_6$, 2 mM $MgCl_2$, in PBS containing 1 mg/ml (w/v) of the β-galactosidase substrate 5-bromo-4-chloro-indolyl-β-d-galactopyranoside (X-Gal) for 3 hours.

Electron microscopy and correlative electron/ light microscopy

After perfusion fixation with 4%PFA as described above, brains were further fixed for electron microscopy. For conventional electron microscopy, they were fixed with 2% glutaraldehyde in PB for 2 hours at 4°C, and postfixed with 2% osmium tetroxide (OsO_4) for 2 hours at 4°C. Specimens were dehydrated with graded ethanol and embedded in Epon812. For correlative light/electron microscopy, the specimens were cut into 30 μm sections with a vibratome (VT1200S, Leica Microsystems). Sections were immunolabeled with primary antibodies (cathepsin D, Shibata et al., 1998); LAMP1; Novus Biologicals; clone 1D4B) at 4°C over night. After washing with PBS, sections were incubated with secondary antibodies (anti-rabbit IgG Alexa Fluor 488 FluoroNanogold, Nanoprobes; anti-Rat IgG Cy3) and DAPI. Sections were then attached to a gridded glass-bottom dish (Matsunami) and observed with a confocal laser scanning microscope (TCS/SP5, Leica Microsystems). Sections were fixed in 2% glutaraldehyde in PBS for 1 hour at 4°C, and were subjected to gold enhancement using GoldEnhance Plus (Nanoprobes). Sections were postfixed, dehydrated, and embedded as described above. Embedded samples were cut at 80 nm with an ultramicrotome (UC6, Leica Microsystems), while ultrathin sections were stained with 4% uranyl acetate and 1% lead citrate. They were then examined with a transmission electron microscope (HT7700, Hitachi).

Immunohistochemical staining of neuromuscular junctions (NMJ)

Staining of NMJs was carried out as previously described (Dombert et al., 2014). Briefly, mice were deeply anesthetized and transcardially perfused with 4% PFA. Subsequently, the *orbicularis orbi* muscle was dissected and post-fixed in 4% PFA for at least two hours. The tissue was washed in PBS-T (0.1% Tween-20) for 20 minutes at RT and incubated with α-Bungarotoxin-Alexa488 (Invitrogen) for 25 minutes at RT. The tissue was then incubated overnight at 4°C with a blocking solution (2% BSA, 0.1% Tween-20 and 10% donkey serum), followed by incubation with the indicated primary antibodies for three days at 4°C. After washing with PBS at pH 7.4 (PAA Laboratories) three times for 15 minutes, the appropriate secondary antibodies were applied for 1 hour at RT. The tissue was washed again as above described, and embedded in Aqua Polymount (Polysciences).

IN VIVO LABELING WITH FLUORO-GOLD RETROGRADE TRACER

The application of the retrograde axonal tracer FluoroGold (FG; Fluorochrome) was previously described with minor modifications (Gey et al., 2016). Mice were injected with 4 x μl of FG (4% in H_2O) with a Hamilton syringe in the whisker pad. The animals were sacrificed and the brains were fixed in 4% PFA for one day and cut into 80 μm vibratome sections. For each animal, FG positive neurons of four sections were analyzed. Quantification was performed manually with ImageJ. All experiments were in accordance with institutional regulations by the local animal ethical committee (Regierungspräsidium Tübingen, Germany; TVA 1368).

Behavioral Studies

Eye blink reflex and whisker-orientation reflex

Facial nerve function was assessed by stimulation of facial movements (Crawley, 2007). The eye blink reflex was elicited by approaching the eye with the tip of a cotton swab. The whisker-orientation reflex was provoked by slightly stroking the whiskers

with a cotton swab tip, promoting an orientation response. Vigorousness of both responses was subsequently rated on a 3-point scale (0: absent – 1: reduced – 2: normal). The average of 6 assessments was used for analysis.

Whisker movement

Whisker movement was performed as described previously (Wanner et al., 2017). Prior to whisker movement analysis, mice were handled daily to accustom them for videotaping. For whisker movement analysis, all whiskers except the whiskers in the C row were clipped in anesthetized mice by micro scissors. Hand restraint mice were videotaped for 53 s by a high-speed camera at 100 Hz from top-view. Video sequences were reviewed and 1 s fragments were further processed in Templo Software (CONTEMPLAS GmbH, Germany). The selected video sequences were analyzed by Vicon Motus 2D software (CONTEMPLAS GmbH, Germany). The angular whisker position of the C1 whisker was determined by using a spatial model, consisting of a line between the fix points right and left eye and its corresponding midsagittal plane in a 90 degree angle. The plane for the whisker was set up by two points, the whisker shaft and a point on the vibrissae approximately 0.5 cm further out. The change of angle between the midsagittal plane and whisker was analyzed within 1 s for lesion and control side. The threshold for a peak was set to different angles (20°, 35°, 55° and 70°) and all angles for both pro- and retraction above these individual thresholds were summed up within these 100 Hz sequences (Figure 2). In addition, the peak numbers above these threshold angles were calculated in one 100 hs sequence counting one peak for each direction (Figure S4C). All experiments were in accordance with institutional regulations by the local animal ethical committee (Regierungspräsidium Tübingen, Germany; TVA 1368).

Grip strength, Balance Beam, Vertical pole, Rotarod

Forelimb grip strength was assessed by letting mice spontaneously grab a T-shaped bar connected to a digital dynamometer (Ugo Basile, Comerio, Italy). This allowed quantification of strength which was averaged over 10 trials. The rotarod test was included as a measure of motor coordination and equilibrium. All mice received 2 minutes of training at a fixed speed of 4 rpm on the apparatus (MED Associates Inc., St. Albans, Vermont, USA). Subsequently, 4 test trials (10 minutes intertrial interval) were conducted with an accelerating rotation from 4 to 40 rpm for 5 minutes. Drop latency was registered up to the 5 minutes cut-off. Motor function was further evaluated using the vertical pole test. Mice were positioned with their head upward on the top side of a vertical wooden beam, the surface of which was made rough with rope (length 55 cm, cross-section 1.5 cm). Latency to turn downward and descend was registered for every animal. Finally, the balance beam test was performed to gain further insight into sensorimotor function. Mice were trained to walk across a set of 1 m long narrow beams. Six beams were used which shape and diameter represented an increasing challenge for balance and equilibrium (square (SQ), cross-section: 28, 12 & 5 mm; round (RO), diameter: 28, 17 & 11 mm). Beams were placed 50 cm above the ground, terminating on a square escape platform. During the training phase, mice learned to traverse the 12 mm square beam until all subjects reached the predetermined criterion of 20 s traversal latency. The test phase consisted of 2 consecutive trials on each of the beams in the order described above. The average of both trials was used for analysis.

Plasmid construction and lentiviral production

FUW-Tmem106b-mCherry was generated by digestion of the FUWG plasmid by NheI and XbaI, and the resulting 10 kB fragment was purified by gel extraction. The cDNA of mCherry was amplified by PCR using the following primer: 5′- GCTGCTACCGGT GGAGGTGGT GGA TCTTCTGTGAGCAAGGGCGAGGAGGATAACATGG–3′ and 5′-GCTGCTTCTAGATTACTTGTACAGCTCGTCC –3′. The PCR product was purified, digested by AgeI and XbaI, and purified. The cDNA of *Tmem106b* was amplified by PCR using the following primer: 5′-GCTGCTGCTAGCACCATGGGAAAGTCTCTTTCTCACTTACC-3′and 5′-GCTGCTACCGGTTTGTTGTGGC TGAAGGACATTTAG-3′. The PCR product was purified, digested by NheI and AgeI, and again purified. Both fragments were simultaneously cloned into the FUGW backbone by ligation.

For the simultaneous expression of RFP-LC3 and Lamp1-GFP, we first constructed FUW-RFP-LC3. The FUGW plasmid was digested by XbaI and EcoRI, and the resulting 10 kB fragment was purified by gel extraction. pmRFP-LC3 (Addgene Plasmid #21075) was digested by NheI and EcoRI and the resulting 1.4 kB fragment was purified by gel extraction. Subsequently, both inserts were ligated into the XbaI and EcoRI sites of the backbone. The XbaI site was destroyed during cloning.

Next, FUW-RFP was digested by EcoRI, blunted, purified, and dephosphorylated. Lamp1-mGFP (Addegene Plasmid #34831) was digested by AseI and NotI, and the resulting CMV::Lamp1-mGFP fragment was purified by gel extraction, blunted and phosphorylated. Subsequently, both fragments were ligated to generate FUW-RFP-LC3-CMV::Lamp1-mGFP.

FUW-Lamp1-mGFP was generated by the digestion of FUGW by XbaI. The resulting 10kB fragment was purified by gel extraction, blunted and dephosphorylated. Lamp1-mGFP (Addegene Plasmid #34831) was digested by EcoRI and NotI and the resulting 2 kB fragment was purified by gel extraction, blunted and phosphorylated. Subsequently, both fragments were ligated.

Lentivirus was produced by co-transfecting HEK293T cells with the indicated expression and packaging plasmids using Lipofectamine 2000 (Invitrogen). The medium was replaced 24 hours after transfection and collected 24 hours later. Subsequently, the virus was concentrated by ultracentrifugation. For lentiviral transduction, MN were incubated with viral particles for 10 minutes at RT directly before plating.

Immunocytochemistry and live-cell imaging

Live-cell imaging: For live-cell imaging, 4,000 cells per cm^2 were plated on PORN/Laminin-coated coverslips and cultured for 7 days. On day 7, the cells were labeled with LysoTracker Green DND-26 (New England Biolabs) for 30 minutes and subsequently imaged for 7 minutes. The LysoTracker was applied in MN media without Phenol Red supplemented with BackDrop® Green Background

Suppressor (Cell Signaling). Lysosomal movement was monitored using an upright microscope (BXWI, Olympus), in a heated imaging chamber (Luigs & Neumann). Images (8-bit) were captured with a Rolera-XR camera (Qimaging) and StreamPix 4 software (Norpix) under continuous illumination with a 470 nm LED light source (Visitron Systems). Lysosomes moving less than 5 μm were considered as stationary or bidirectional moving, respectively.

Immunocytochemistry

For immunocytochemistry, we plated 4,000 cells per cm^2 and cultured the cells for 7 days. For stainings with LysoTracker, cells were labeled with LysoTracker Deep Red (Thermo Fisher Scientific) one hour prior to fixation. Subsequently, the cells were fixed with 4% PFA for 15 minutes at RT, followed by three washes with PBS for 5 minutes at RT. For blocking and permeabilization, the cells were incubated with blocking solution (10% Donkey Serum, 0.3% Triton X-100 in TBST) for 30 minutes at RT. Incubation with the primary antibody was carried out overnight at 4°C in the following solution: 1% Donkey Serum, 0.03% Triton X-100 in TBST. The next day, the cells were washed three times with TBST for 5 minutes at RT and the appropriate secondary antibodies were applied in TBST for 2 hours at RT. Finally, the MN were washed three times with TBST for 15 minutes. The cells were counterstained with DAPI during the first washing step after incubation with the secondary antibodies. The following primary antibodies were used: Cathepsin D (gift from Thomas Braulke, Claussen et al., 1997), Tuj1 (Neuromics, MO15013), LAMP1 (DSHB, Hybridoma Bank; clone 1D4B). Images were acquired using an Olympus Fluoview1000i confocal microscope.

FluoroGold endocytosis in primary MN

After five days in culture FluoroGold was added to the primary motoneurons at a final concentration of 0.01% (w/v) to the medium. After 15 or 60 minutes the cells were washed three times with PBS and then fixed with 4% PFA for 15 minutes at RT. The number of FluoroGold particles was analyzed using the ImageJ "Analyze Particles" plug-in. At least 90 cells were analyzed per genotype and time point.

Re-expression of TMEM106B

Expression of Tmem106b-mCherry in cultured MN: Primary MN were transduced with FUGW-Tmem106-mCherry and fixed with 4% PFA for 15 minutes at RT after 5 days in culture.

QUANTIFICATION AND STATISTICAL ANALYSIS

If not stated otherwise, a two-tailed unpaired t test was performed using GraphPad Prism Software Version 5.03. Significant values were considered at $p < 0.05$. Values are expressed as mean ± standard error of the mean (SEM) and significance is designated as *, $p < 0.05$; **, $p < 0.005$; ***, $p < 0.0001$.

Behavioral data are presented as mean + SEM. Shapiro-Wilk and Brown-Forsythe tests were used to determine normality and variance homogeneity. Violation of these assumptions was followed by non-parametric testing or (where possible) data transformation. Transformed data was retransformed for consistent visualization. Performance of *Tmem106b* wild-type, heterozygous and KO mice was compared using Kruskal-Wallis ANOVA on ranks (facial nerve reflexes), 1-way ANOVA (vertical pole, grip strength) and 2-way repeated-measures ANOVA (balance beam, rotarod). Dunn's and Holm-Sidak methods were used for multiple comparisons.

DATA AND CODE AVAILABILITY

No large datasets were produced in this study.

SUPPLEMENTAL INFORMATIONS

Figure S1

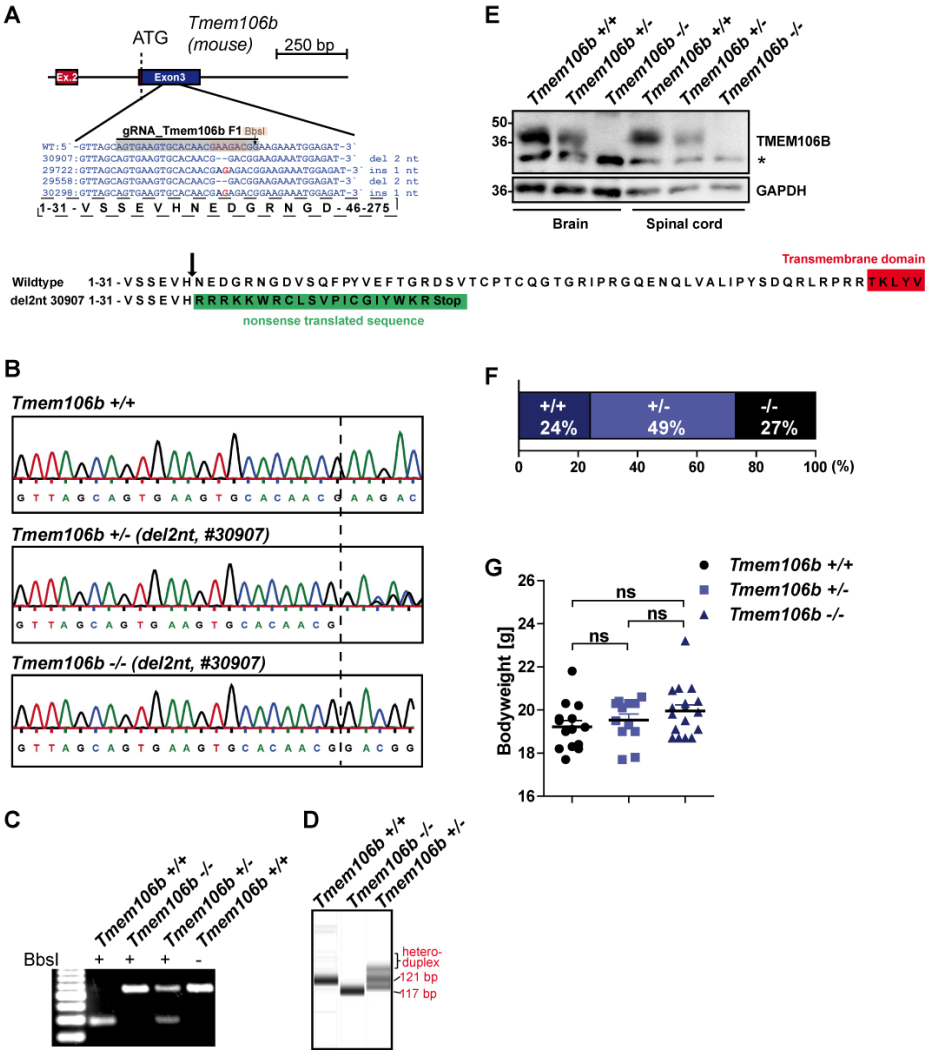

Figure S1. Related to Figure 1. CRISPR/Cas9-mediated generation and genotyping of *Tmem106b* knockout mice. (A) Schematic representation of the murine *Tmem106b* locus covering exon 2 and the first coding exon 3 containing the ATG start codon. Excerpt of the sequence of genomic tail DNA of several founder lines (30907; 29722; 29558; 30298) with the resulting genomic modifications covering the target sequence of the guide (g)RNA is shown. Recognition site of the restriction enzyme BbsI is indicated. The coded amino acid sequence is indicated below the nucleotide sequence. The predicted amino acid sequence of the strain 30907 with the 2 nucleotide deletion leading to a frameshift and premature stop-codon is depicted below in comparison to the wildtype sequence. **(B)** Representative sequencing chromatogram of founder line 30907 containing a 2

nucleotide deletion (del2nt) either heterozygous or homozygous is shown in comparison to the non-edited wildtype sequence. **(C)** Agarose gel of the PCR product for initial genotyping generating a 552bp fragment (right lane) that is further digested with the restriction enzyme BbsI. In the case of an intact recognition site for BbsI, two fragments are generated after restriction digest (274 & 276bp) (left lane). Homozygous CRISPR/Cas9-mediated genomic changes lead to the complete loss of the BbsI cleavage site. Heterozygous animals show both, undigested (552bp) and digested bands (274 and 276bp). **(D)** Electrophoresis chromatogram of the capillary-electrophoresis-based genotyping-PCR. A smaller PCR-fragment (121bp in wildtype mice) covering the CRISPR/Cas9-edited genomic sequence is generated with genomic tail-DNA as template. Capillary electrophoresis efficiently separates the 2bp size-difference between homozygous wildtype and knockout animals. In heterozygous animals, an additional band is observed, presumably due to the formation of a heteroduplex of the small fragments. **(E)** Immunoblot analysis of *Tmem106b* +/+, +/- and -/- brain- and spinal cord lysates with an antibody against TMEM106B (Bethyl-Laboratories; A303-439A) and GAPDH as loading control. **(F)** Genotype distribution of litters from *Tmem106b* heterozygote couples. (n = 102 animals in total). **(G)** Total bodyweight of 3 months old *Tmem106b* +/+, +/- and -/- animals. N = 12-17. Student's t-test; ns = not significant.

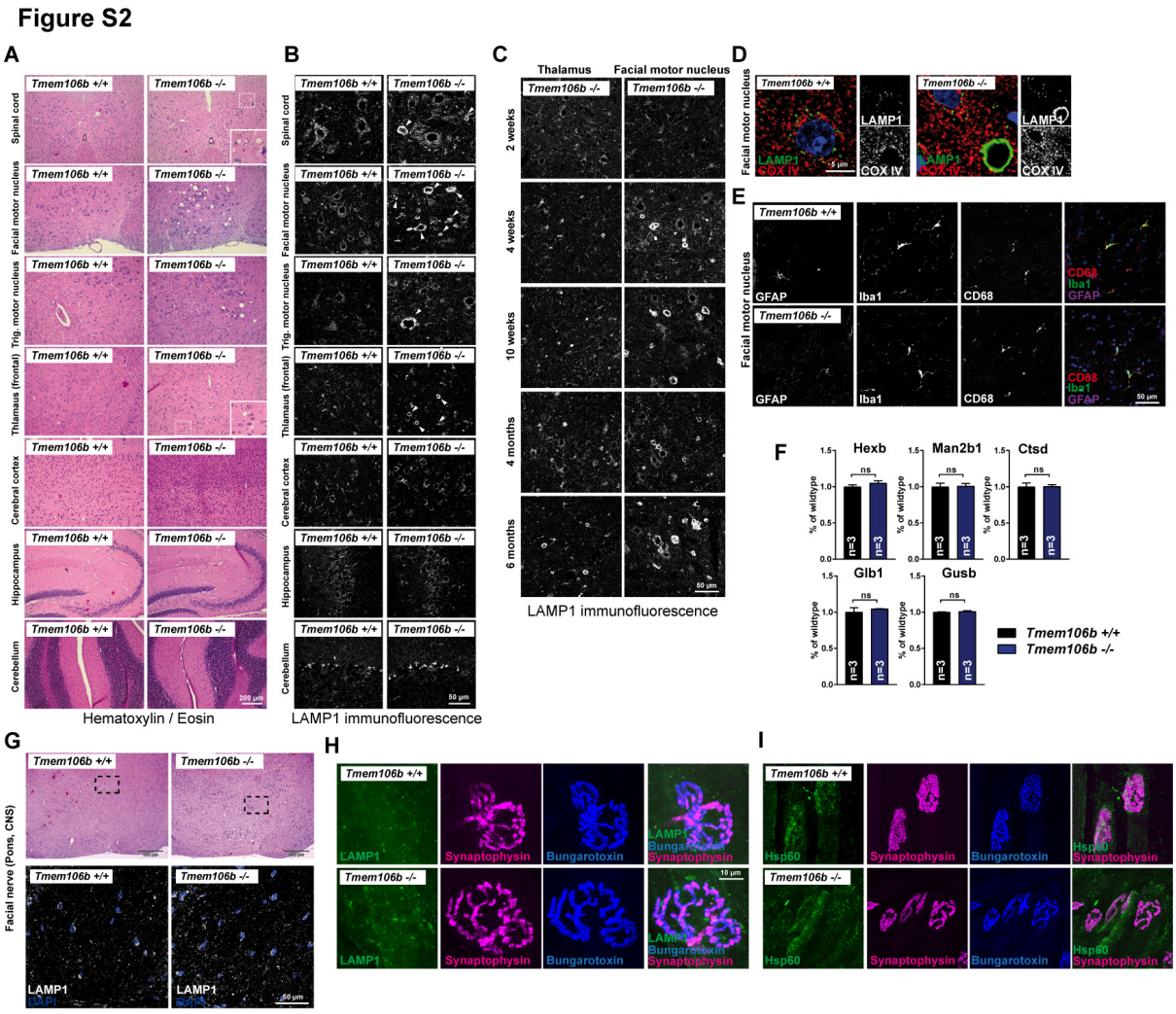

Figure S2. Related to Figure 1. Vacuolization phenotype of *Tmem106b* KO mice. (A) Hematoxylin / Eosin staining of sagittal sections of 4-months-old wildtype and *Tmem106b* KO mice of the indicated brain regions. **(B)** Immunofluorescence staining of wildtype and *Tmem106b* KO mice of the corresponding regions to (A) for LAMP1. Age: 4 months. **(C)** Immunofluorescence staining of the FMN of *Tmem106b* KO mice for LAMP1 at indicated the age. **(D)** Immunofluorescence staining for LAMP1 (green) and the mitochondria-marker COX IV (red). Nuclei are stained with DAPI (blue). The large vacuole is negative for Cox IV. **(E)** Immunofluorescence staining of CD68 (red), GFAP (magenta) and Iba-1 (green) of the FMN of 4-months-old wildtype and *Tmem106b* KO mice. Nuclei are stained with DAPI (blue). **(F)** Transcript levels of Hexb, Man2b1, Ctsd, Glb1, and Gusb determined by qPCR from wildtype and *Tmem106b* KO mice. The mean of the wildtype was set as 1 and the ratio of the average of the KO animals is depicted. Age: 6 months. (Mean ± SEM, n = 3). **(G)** Hematoxylin / Eosin staining of the Pons / Medulla of wildtype and *Tmem106b* KO mice. The compact facial

nerve is boxed. Immunofluorescence staining of the compact facial nerve for LAMP1 does not show any vacuoles in *Tmem106b* KO mice. Nuclei are stained with DAPI (blue). Age: 4 months. **(H)** (Immuno-)fluorescence staining of neuromuscular junctions (NMJ) of the orbicularis oculi muscle of six months-old *Tmem106b* KO and control animals with fluorescently labelled Bungarotoxin (blue) and antibodies against synaptophysin (magenta) and LAMP1 (green). **(I)** (Immuno-)fluorescence staining of neuromuscular junctions (NMJ) of the orbicularis oculi muscle of six months-old Tmem106b and control animals with fluorescently labelled Bungarotoxin (blue) and antibodies against synaptophysin (magenta) and Hsp60 (green).

Figure S3

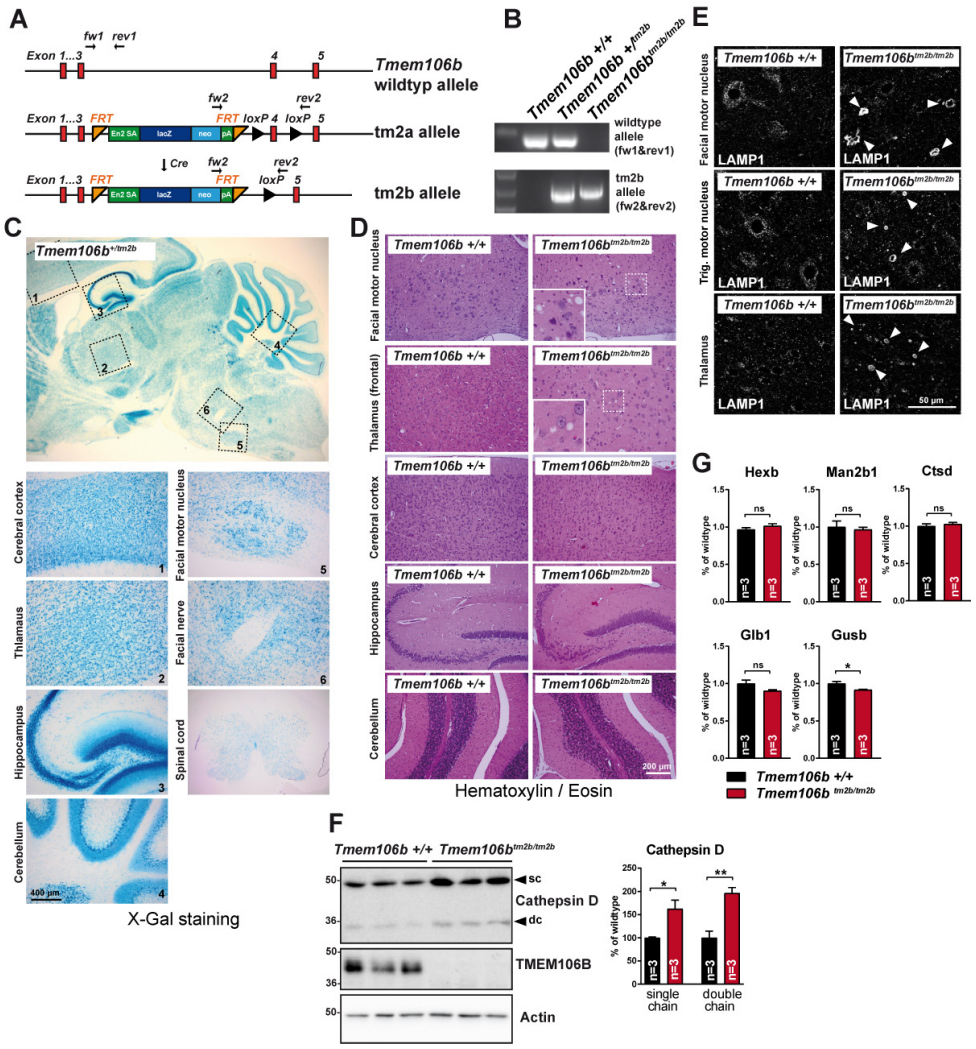

Figure S3. Related to Figure 1. Generation and characterization of *Tmem106b* KO mice generated by targeted ES-cells (*Tmem106b*^{tm2b}). (A) Schematic representation of the *Tmem106b* tm2a-targeting construct. The coding exons, recombinase sites (FRT for Flippase, Cre for Cre-recombinase) and the knockout construct containing the artificial splice-acceptor site (EN SA), LacZ, neo-cassette for selection and the polyadenylation site (pA) are indicated. The conversion of the tm2a allele to tm2b by crossing with Cre-recombinase expressing mice is indicated. **(B)** X-Gal (5-bromo-4-chloro-3-indolyl-β-D-galactopyranoside)-staining of the brain of an adult (3-month-old) old heterozygote *Tmem106b* tm2a-mouse expressing the LacZ reporter gene under the control of the endogenous *Tmem106b* promotor. **(C)** Genotyping PCR for the tm2b allele. The primer binding site is indicated in **(A)**. **(D)** Hematoxylin / Eosin staining of sagittal sections of the indicated brain regions. Age: 6 months. **(E)** Immunofluorescence staining of the indicated brain regions for LAMP1. Age: 6 months. **(F)**

Immunoblot analysis of brain lysates from 4-months-old *Tmem106b*^{tm2b} KO and wildtype control mice for cathepsin D, TMEM106B and actin as a loading control. Quantification of the cathepsin D signal (Mean ± SEM, n = 3). **(G)** Transcript levels of Hexb, Man2b1, Ctsd, Glb1, and Gusb determined by qPCR from wildtype and *Tmem106b*^{tm2b} KO mice. The mean of the wildtype was set as 1 and the ratio of the average of the KO animals is depicted. Age: 4 months. (Mean ± SEM, n = 3).

Figure S4

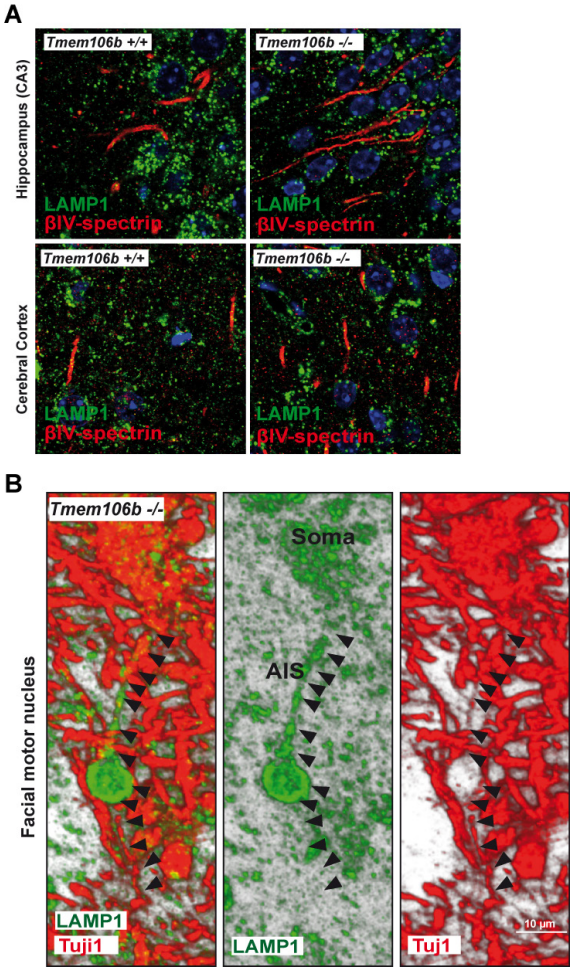

Figure S4. Related to Figure 1. Vacuolisation of facial motor neurons does not lead to axonopathy and axonal vacuoles are absent in the cerebral cortex and the hippocampus. (A) Immunofluorescence of LAMP1 (green) and β-VI Spectrin (red) of the hippocampus (CA3-region) and the cerebral cortex. Nuclei are stained with DAPI (blue). Age: two months. **(B)** Maximum intensity Z-projection of confocal stacks of LAMP1 (green) and βIII-tubulin (red) staining of the FMN. The axon of the depicted motoneuron is marked by arrowheads. Age: two months.

Figure S5

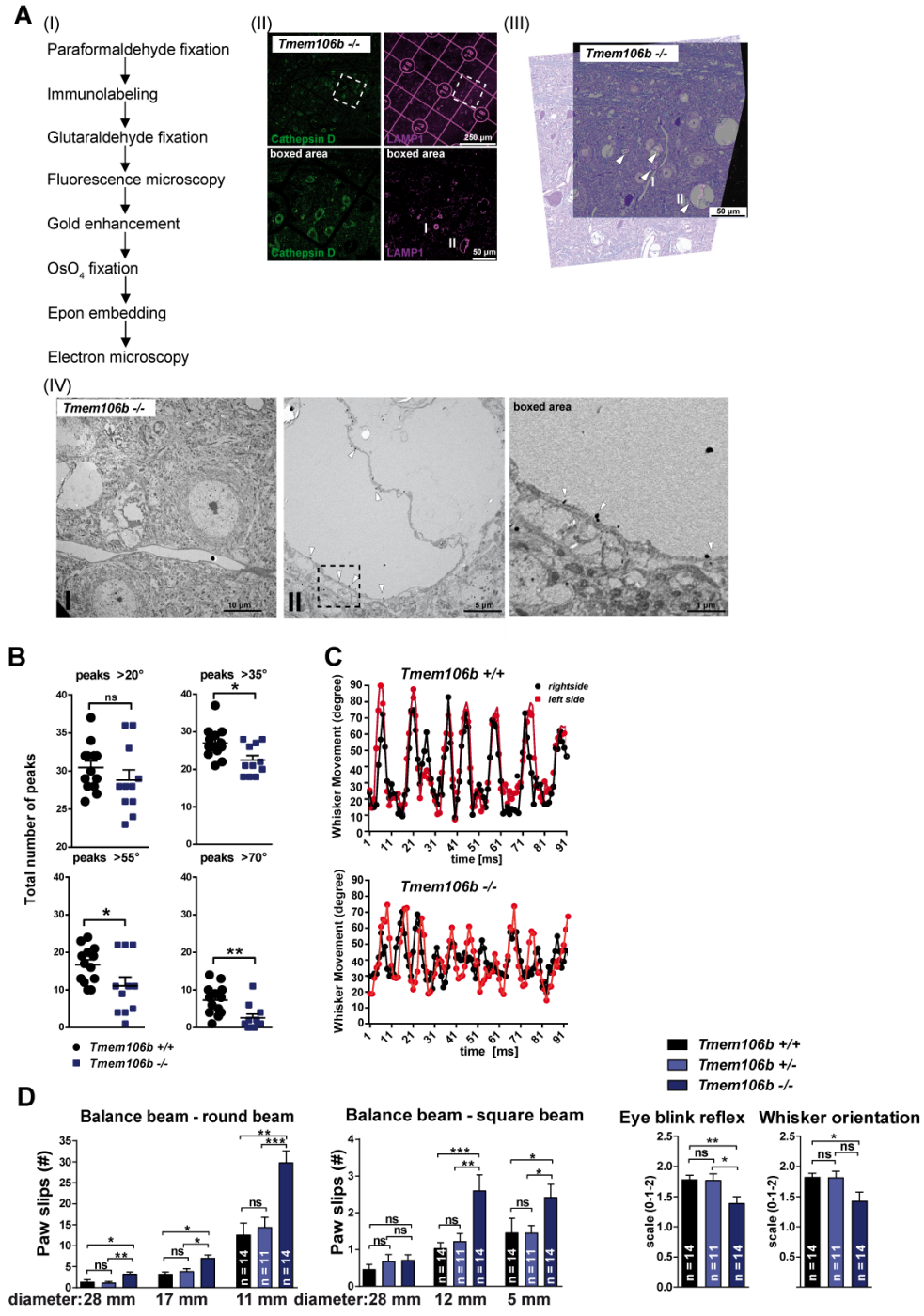

Figure S5. Related to Figure 2. Correlative light and electron microscopy and additional whisker movement data. (A) (I) Schematic overview of the workflow for correlative light and electron microscopy (CLEM). (II) Co-immunofluorescence for cathepsin D (green) and LAMP1 (magenta). The fluorescent grid for

CLEM is depicted in the magenta channel. (III) Merge of the toluidine-blue stained section and the corresponding fluorescent image. Vacuoles are labeled with arrow heads. Two vacuoles anayzed by EM are labeled with I and II. (IV) EM of the vacuoles depicted in (II). Cathepsin D immunolabeling after gold enhancement is labelled with arrowheads. **(B)** Quantification of whisker movement expressed as the total number of peaks >20°, <35°, <35° and <70° from *Tmem106B* KO mouse and wildtype control mice. The total number of peaks is depicted (n = 11-13; each point represents one animal; age: 6 months). **(C)** The whisker movement of the right and left whisker (expressed as the movement in degree over time) of a single, representative control and *TMEM106B* KO mouse is depicted. **(D)** Quantification of the eye blink and whisker-orienting reflex in *Tmem106b* +/+, +/- and -/- mice (n = 11-16). The average of 6 assessments was used for analysis. 3-point scale (0: absent – 1: reduced – 2: normal). Age: 14 months Quantification of neuromotor function: number of paw slips during balance beam traversal (square and round beams of Tmem106b +/+, +/- and -/- mice (Age 14 months); (Mean ± SEM, n = 11-16).

Figure S6

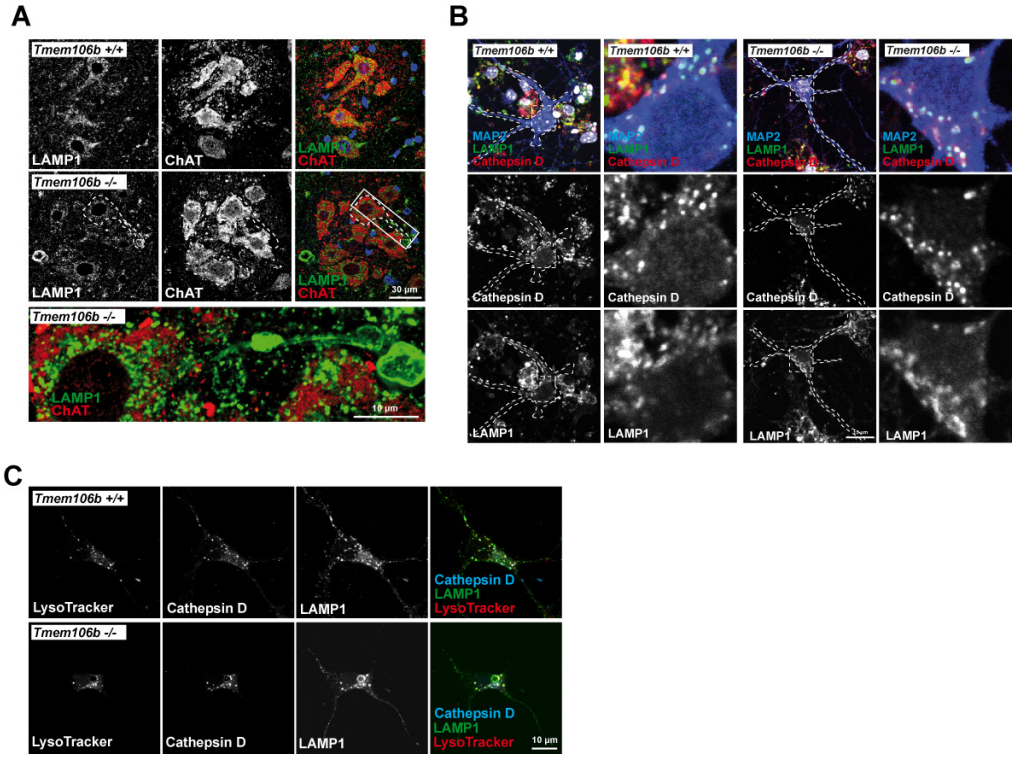

Figure S6. Related to Figure 3. Vacuoles in the spinal cord are found in ChAT-positive lower motoneurons. **(A)** Co-immunofluorescence staining of spinal cord sections (age: 10 weeks) from LAMP1

(green) and Choline acetyltransferase (ChAT) (red) from control and *Tmem106b* knockout mice. **(B)** Co-immunofluorescence staining of neurosphere-derived neurons for cathepsin D (red), LAMP1 (green) and MAP2 (blue) as a marker for neurons from control and *Tmem106b* KO mice. **(C)** Co-immunofluorescence staining of primary MN (DIV5) stained for LAMP1 (green), cathepsin D (blue) and LysoTracker (red). Nuclei are stained with DAPI (blue).

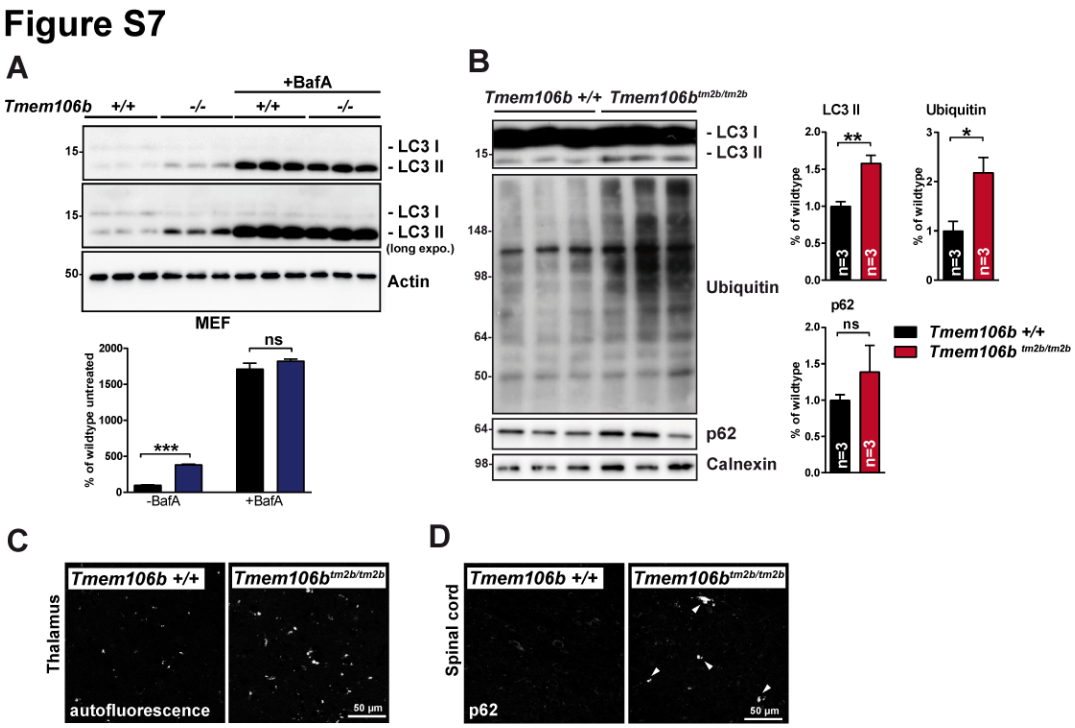

Figure S7. Related to Figure 5. Analysis of autophagic flux in wildtype and *Tmem106b* KO mouse embryonic fibroblasts and altered autophagy in *Tmem106b*^{tm2b} KO mice. (A) Immunoblot analysis of lysates from mouse embryonic fibroblasts (MEFs) prepared from CRISPR/Cas9-mediated KO mice for LC3. Three replicates of untreated and Bafilomycin A (25 nm for 4 hours) treated wildtype and *Tmem106b* KO cells are shown. **(B)** Immunoblot analysis of total brain lysates from wildtype and *Tmem106b*^{tm2b} KO mice for LC3, ubiquitin and, p62. Calnexin is depicted as loading control. Age: 4-5 months. A quantification is depicted on the right (mean ± SEM, n = 3). **(C)** Representative confocal images of autofluorescence (488 nm laser excitation) in the thalamus of *Tmem106b*^{tm2b} KO and control mice. Age: 6 months. **(D)** Immunofluorescence staining of the spinal cord for p62 of *Tmem106b*^{tm2b} KO and control mice. Age: 6 months. p62-positive aggregates are marked with arrowheads.

3 Publikation III

Opposite microglial activation stages upon loss of PGRN or TREM2 result in reduced cerebral glucose metabolism.
J. K. Götzl[*], M. Brendel[*], G. Werner[*], S. Parhizkar, L. S. Monasor, G. Kleinberger, A. V. Colombo, M. Deussing, M. Wagner, J. Winkelmann, J. Diehl-Schmid, J. Levin, K. Fellerer, A. Reifschneider, S. Bultmann, P. Bartenstein, A. Rominger, S. Tahirovic, S. T. Smith, C. Madore, O. Butovsky, A. Capell and C. Haass 2019.
EMBO Molecular Medicine 11(6):e9711. [*] Geteilte Erstautorenschaft

Alle von mir beigetragenen Ergebnisse sind in den Abbildungen 2 A,B,G,H, 3 A, EV1 A und EV1 B dargestellt (Götzl et al., 2019).

Published online: May 23, 2019

Research Article

SOURCE DATA | TRANSPARENT PROCESS | OPEN ACCESS

EMBO Molecular Medicine

Opposite microglial activation stages upon loss of PGRN or TREM2 result in reduced cerebral glucose metabolism

Julia K Götzl[1,†], Matthias Brendel[2,†], Georg Werner[1,†], Samira Parhizkar[1], Laura Sebastian Monasor[3], Gernot Kleinberger[1,4], Alessio-Vittorio Colombo[3], Maximilian Deussing[2], Matias Wagner[5,6,7], Juliane Winkelmann[5,6,7], Janine Diehl-Schmid[8], Johannes Levin[3,9], Katrin Fellerer[1], Anika Reifschneider[1], Sebastian Bultmann[10], Peter Bartenstein[2,4], Axel Rominger[2,4], Sabina Tahirovic[3], Scott T Smith[11], Charlotte Madore[11], Oleg Butovsky[11,12], Anja Capell[1,*] & Christian Haass[1,3,4,**]

Abstract

Microglia adopt numerous fates with homeostatic microglia (HM) and a microglial neurodegenerative phenotype (MGnD) representing two opposite ends. A number of variants in genes selectively expressed in microglia are associated with an increased risk for neurodegenerative diseases such as Alzheimer's disease (AD) and frontotemporal lobar degeneration (FTLD). Among these genes are progranulin (*GRN*) and the triggering receptor expressed on myeloid cells 2 (*TREM2*). Both cause neurodegeneration by mechanisms involving loss of function. We have now isolated microglia from *Grn*$^{-/-}$ mice and compared their transcriptomes to those of *Trem2*$^{-/-}$ *mice*. Surprisingly, while loss of *Trem2* enhances the expression of genes associated with a homeostatic state, microglia derived from *Grn*$^{-/-}$ mice showed a reciprocal activation of the MGnD molecular signature and suppression of gene characteristic for HM. The opposite mRNA expression profiles are associated with divergent functional phenotypes. Although loss of TREM2 and progranulin resulted in opposite activation states and functional phenotypes of microglia, FDG (fluoro-2-deoxy-D-glucose)-μPET of brain revealed reduced glucose metabolism in both conditions, suggesting that opposite microglial phenotypes result in similar wide spread brain dysfunction.

Keywords disease-associated and homeostatic microglial signatures; microglia; neurodegeneration; progranulin; TREM2

Subject Categories Immunology; Metabolism; Neuroscience

DOI 10.15252/emmm.201809711 | Received 22 August 2018 | Revised 18 April 2019 | Accepted 24 April 2019

EMBO Mol Med (2019) e9711

Introduction

While for a long time researchers distinguished only two distinct stages of microglia, the M1 and the M2 phenotype, recent evidence strongly indicates that a multitude of functionally diverse microglial populations exists in a dynamic equilibrium (Ransohoff, 2016; Keren-Shaul *et al*, 2017; Krasemann *et al*, 2017). This becomes very apparent when one compares mRNA signatures of microglia isolated from various mouse models for neurodegeneration and compares them to controls (Abduljaleel *et al*, 2014; Butovsky *et al*, 2015; Holtman *et al*, 2015; Keren-Shaul *et al*, 2017; Krasemann *et al*, 2017). In mouse models for neurodegenerative diseases, mRNA signatures were identified which are characteristic for a disease-associated microglia (DAM)/a microglial neurodegenerative phenotype (MGnD) whereas in controls a homeostatic microglial (HM) signature was observed (Butovsky *et al*, 2014, 2015; Holtman *et al*,

1 Chair of Metabolic Biochemistry, Biomedical Center (BMC), Faculty of Medicine, Ludwig-Maximilians-Universität München, Munich, Germany
2 Department of Nuclear Medicine, University Hospital, Ludwig-Maximilians-Universität München, Munich, Germany
3 German Center for Neurodegenerative Diseases (DZNE), Munich, Germany
4 Munich Cluster for Systems Neurology (SyNergy), Munich, Germany
5 Institut für Neurogenomik, Helmholtz Zentrum München, Munich, Germany
6 Institut of Human Genetics, Technische Universität München, Munich, Germany
7 Institute of Human Genetics, Helmholtz Zentrum München, Neuherberg, Germany
8 Department of Psychiatry, Technische Universität München, Munich, Germany
9 Department of Neurology, University Hospital, Ludwig-Maximilians-Universität München, Munich, Germany
10 Department of Biology and Center for Integrated Protein Science Munich (CIPSM), Ludwig Maximilians-Universität München, Munich, Germany
11 Ann Romney Center for Neurologic Diseases, Department of Neurology, Brigham and Women's Hospital, Harvard Medical School, Boston, MA, USA
12 Evergrande Center for Immunologic Diseases, Brigham and Women's Hospital, Harvard Medical School, Boston, MA, USA
*Corresponding author. Tel: +4989440046535; E-mail: anja.capell@mail03.med.uni-muenchen.de
**Corresponding author. Tel: +4989440046550; E-mail: christian.haass@mail03.med.uni-muenchen.de
†These authors contributed equally to this work

Published online: May 23, 2019
EMBO Molecular Medicine

2015; Keren-Shaul *et al*, 2017; Krasemann *et al*, 2017). MGnD upregulates a characteristic set of genes, which may initially allow microglia to respond to neuronal injury in a defensive manner. This includes the induction of pathways triggering phagocytosis, chemotaxis/migration, and cytokine release. The upregulation of genes involved in those pathways goes along with a suppression of homeostatic genes (Butovsky *et al*, 2015; Krasemann *et al*, 2017). Key genes involved in the switch of HM to MGnD are regulated by the TREM2 (triggering receptor expressed on myeloid cells 2) ApoE (apolipoprotein E) pathway (Krasemann *et al*, 2017).

A pivotal role of microglia in neurodegeneration is strongly supported by the identification of sequence variants found in a number of genes robustly or even selectively expressed within microglia in the brain, among them *GRN* (encoding the progranulin (PGRN) protein; Baker *et al*, 2006; Cruts & Van Broeckhoven, 2008; Zhang *et al*, 2014; Gotzl *et al*, 2016; Lui *et al*, 2016) and *TREM2* (Guerreiro *et al*, 2013; Jonsson & Stefansson, 2013; Jonsson *et al*, 2013; Rayaprolu *et al*, 2013; Borroni *et al*, 2014; Cuyvers *et al*, 2014; Ulrich *et al*, 2017). Mutations in the *GRN* gene (Baker *et al*, 2006; Cruts *et al*, 2006) cause frontotemporal lobar degeneration (FTLD) with TDP-43 (TAR-DNA binding protein 43)-positive inclusions due to haploinsufficiency. PGRN is a growth factor-like protein with neurotrophic properties in the brain (Van Damme *et al*, 2008). PGRN is also transported to lysosomes (Hu *et al*, 2010; Zhou *et al*, 2015) where it appears to regulate expression and activity of lysosomal proteins (Ahmed *et al*, 2010; Hu *et al*, 2010; Wils *et al*, 2012; Tanaka *et al*, 2013a,b; Gotzl *et al*, 2014, 2016, 2018; Beel *et al*, 2017; Chang *et al*, 2017; Ward *et al*, 2017; Zhou *et al*, 2017). PGRN is proteolytically processed into granulin peptides, which can be found in biological fluids (Bateman *et al*, 1990; Shoyab *et al*, 1990; Belcourt *et al*, 1993; Cenik *et al*, 2012). TREM2 is produced as a membrane-bound type-1 protein (Kleinberger *et al*, 2014), which traffics to the cell surface where it mediates signaling via binding to its co-receptor, the DNAX activation protein of 12 kDa (DAP12; Ulrich & Holtzman, 2016; Yeh *et al*, 2017). Signaling is terminated by proteolytic shedding of the TREM2 ectodomain (Kleinberger *et al*, 2014; Schlepckow *et al*, 2017). Several sequence variants associated with TREM2 cause neurodegeneration via a loss of function (Kleinberger *et al*, 2014, 2017; Schlepckow *et al*, 2017; Ulland *et al*, 2017; Song *et al*, 2018). Sequence variants of TREM2 affect a multitude of functions including chemotaxis, migration, survival, binding of phospholipids and ApoE, proliferation, survival, and others (Kleinberger *et al*, 2014, 2017; Atagi *et al*, 2015; Bailey *et al*, 2015; Wang *et al*, 2015; Yeh *et al*, 2016; Mazaheri *et al*, 2017; Ulland *et al*, 2017). Strikingly, a loss of TREM2 function locks microglia in a homeostatic state (Krasemann *et al*, 2017; Mazaheri *et al*, 2017). Instead of suppressing their homeostatic mRNA signature like mouse models of neurodegenerative disorders, in the absence of TREM2 microglia even enhance expression of homeostatic genes and fail to express the disease-associated signature (Krasemann *et al*, 2017; Mazaheri *et al*, 2017). As a result, TREM2 deficiency decreases chemotaxis, phagocytosis, and barrier function (Kleinberger *et al*, 2017; Mazaheri *et al*, 2017; Ulland *et al*, 2017). TREM2 therefore appears to play a key role as a central hub gene in the regulation of microglial homeostasis. We now investigated microglial gene expression and function in the absence of PGRN and made the surprising observation that loss of TREM2 or PGRN leads to opposite microglial activity phenotypes, which, however, both cause wide spread brain dysfunction.

Results

Opposite molecular signatures of microglia in $Grn^{-/-}$ and $Trem2^{-/-}$ mice

Loss-of-function mutations in *TREM2* are associated with various types of neurodegeneration, including a FTLD-like syndrome (Ulrich & Holtzman, 2016). Similarly, haploinsufficiency of *GRN* is associated with TDP-43-positive FTLD (Baker *et al*, 2006; Cruts *et al*, 2006; Cruts & Van Broeckhoven, 2008). At least some of the *GRN*-dependent FTLD-associated phenotypes can be mimicked in a mouse model entirely lacking PGRN (Ahmed *et al*, 2010; Yin *et al*, 2010; Wils *et al*, 2012; Gotzl *et al*, 2014). Furthermore, both, a *Trem2* knockout and the knockin of the p.T66M mutation, mimic features of a FTD-like syndrome (Kleinberger *et al*, 2017; Mazaheri *et al*, 2017). Since both proteins are preferentially expressed in microglia, we compared loss-of-PGRN-associated microglial phenotypes with those known for TREM2 deficiency (Krasemann *et al*, 2017; Mazaheri *et al*, 2017). To do so, we first purified microglia from brains of adult $Grn^{-/-}$ mice by fluorescence-associated cell sorting (FACS) using microglia-specific anti-FCRLS and anti-CD11b antibodies. We then investigated the expression pattern of gene characteristic for MGnD and HM using NanoString gene expression profiling (MG534; Butovsky *et al*, 2014; Krasemann *et al*, 2017; Mazaheri *et al*, 2017; Dataset EV1). Gene expression levels in each sample were normalized against the geometric mean of five housekeeping genes including *Cltc*, *Gapdh*, *Gusb*, *Hprt1*, and *Tubb5*. Out of 529 genes analyzed, 58 genes were significantly upregulated and 58 genes were downregulated. Strikingly, genes most strongly upregulated in $Grn^{-/-}$ microglia are those previously described for MGnD (Fig 1A; Butovsky *et al*, 2015; Holtman *et al*, 2015; Keren-Shaul *et al*, 2017; Krasemann *et al*, 2017). These include *ApoE*, as the most upregulated gene, *Ly9*, *Clec7a*, *Dnajb4*, *Cccl4*, and many others suggesting that PGRN-deficient microglia adopt the MGnD state. We then compared the $Grn^{-/-}$ microglial signature to the previously analyzed molecular signature of $Trem2^{-/-}$ microglia (Fig 1B and C; Mazaheri *et al*, 2017). Both NanoString gene expression panels overlapped in 418 genes. Out these, 359 mRNAs could be detected in both screens (Dataset EV1). In the $Grn^{-/-}$ microglia, 40 mRNAs were upregulated and 55 mRNAs were downregulated, whereas in the $Trem2^{-/-}$ microglia, 87 mRNAs were increased and 27 mRNAs were decreased (Fig 1C; left two panels). Interestingly, while only six mRNAs were equally up/downregulated in both phenotypes, 32 mRNAs showed an opposite regulation (Fig 1C; right panel). Strikingly, while in $Grn^{-/-}$ mice the neurodegenerative disease-associated signature is massively upregulated, this set of genes is suppressed in the $Trem2^{-/-}$ microglia (Fig 1B and D; Mazaheri *et al*, 2017). Similarly, the homeostatic mRNA signature is slightly but significantly upregulated in $Trem2^{-/-}$ microglia (Mazaheri *et al*, 2017) but severely suppressed in $Grn^{-/-}$ microglia (Fig 1B and D).

Confirmation of molecular microglial signatures on protein level

Expression of proteins associated with MGnDs such as ApoE, CLEC7A, TREM2, and CD68 was also increased in acutely isolated microglia (Fig 2A and B). sTREM2 was also found to be increased in brains and serum of $Grn^{-/-}$ mice (Fig 2C and D), although no increase in *Trem2* mRNA levels was observed in the NanoString analysis (Fig 1B), suggesting posttranscriptional regulation.

Published online: May 23, 2019
Julia K Götzl et al
EMBO Molecular Medicine

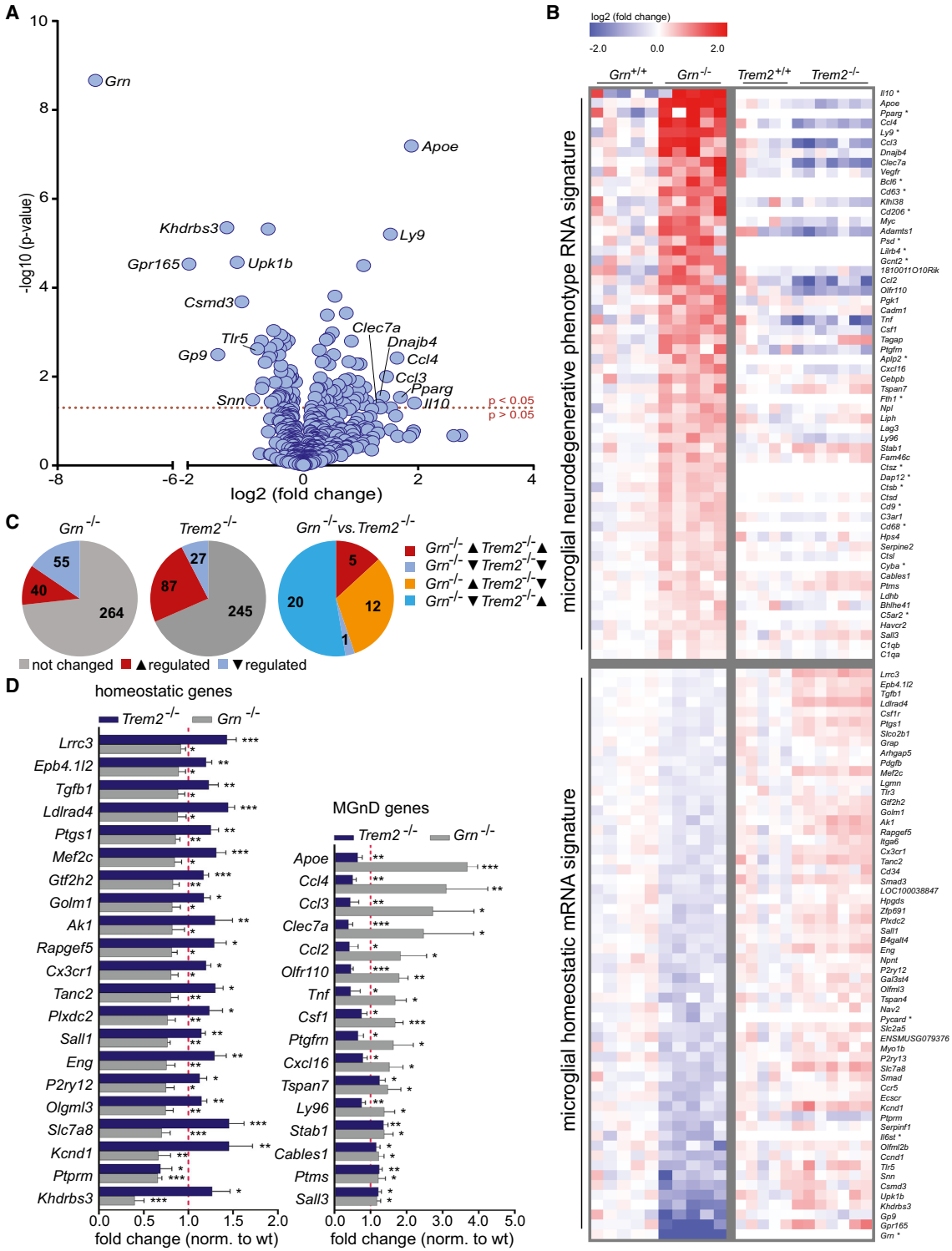

Figure 1.

Published online: May 23, 2019
EMBO Molecular Medicine Julia K Götzl et al

Figure 1. Opposite mRNA signatures of $Grn^{-/-}$/$Trem2^{+/+}$ and $Trem2^{-/-}$/$Grn^{+/+}$ microglia.

A Volcano blot representation of the differently expressed genes in FCRLS- and CD11b-positive $Grn^{-/-}$ microglia in comparison with wt microglia isolated from 5.5-month-old mice (male, n = 5). 116 genes out of 529 genes analyzed are significantly changed, and from these, 58 genes are upregulated and 58 genes are downregulated. Eight up- and down regulated genes with the highest fold change are indicated.

B Heatmap of significantly affected genes ($P < 0.05$) in FCRLS- and CD11b-positive $Grn^{-/-}$ microglia in comparison with $Grn^{+/+}$ microglia isolated from 5.5-month-old mice (n = 5 per genotype). For the significantly affected genes of the $Grn^{-/-}$ microglia, mRNA expression data of the $Trem2^{-/-}$ microglia in comparison with the corresponding wt microglia were taken from previously published data (Mazaheri *et al*, 2017). The RNA counts for each gene and sample were normalized to the mean value of wt followed by a log2 transformation ($n \geq 5$ per genotype). *labeled genes were not analyzed or below detection limit in $Trem2^{-/-}$ microglial mRNA expression dataset (Mazaheri *et al*, 2017).

C Changes in gene expression of 359 detected genes in $Grn^{-/-}$ microglia and $Trem2^{-/-}$ microglia. Note that from the 38 genes significantly altered in both genotypes, 32 genes are regulated in opposite direction.

D Expression levels of significantly altered homeostatic and MGnD genes of $Grn^{-/-}$ and $Trem2^{-/-}$ microglia from the data set in (B). Gene expression is normalized to the mean of the wt cohort in comparisons with the published normalized dataset of $Trem2^{-/-}$ microglia (Mazaheri *et al*, 2017). Data represent the mean +/− SD.

Data information: For statistical analysis, unpaired two-tailed Student's t-test was performed between $Grn^{-/-}$ microglia in comparison with $Grn^{+/+}$ microglia or $Trem2^{-/-}$ microglia in comparison with $Trem2^{+/+}$ microglia: not significant $P > 0.05$; *$P < 0.05$; **$P < 0.01$; and ***$P < 0.001$.

Furthermore, protein expression of the homeostatic *P2ry12* gene is downregulated in cortical $Grn^{-/-}$ microglia (Fig 2E and F), while cortical microglia from $Trem2^{-/-}$ mice show strongly elevated P2RY12 levels (Fig 2E and F), consistent with the finding that microglia from both mouse models are in opposite activation states. These findings were further confirmed in genetically modified BV2 microglia-like cells lacking PGRN expression, where ApoE, CLEC7A, and TREM2 were upregulated, whereas P2RY12 was downregulated (Fig 2G–I). In line with the protein expression, in PGRN-deficient BV2 cells, transcripts encoding *Apoe*, *Clec7a*, and *Trem2* were also significantly upregulated, whereas *P2ry12* was downregulated (Fig 2J) further confirming that loss of PGRN results in a microglial hyperactivation.

Increased phagocytic capacity, chemotaxis, and clustering around amyloid plaques upon loss of PGRN

Next, we investigated a series of functional phenotypes in *Grn* loss-of-function mutants, which may be differentially affected by dysregulated *Trem2* or *Grn* gene expression. First, we investigated the phagocytic capacity of PGRN-deficient BV2 cells, which recapitulate expression profile changes found in isolated $Grn^{-/-}$ microglia such as enhanced expression of ApoE, CLEC7A, and TREM2 (Fig 2). We observed a significantly increased uptake of pHrodo-labeled *Escherichia coli* (*E. coli*) in PGRN-deficient BV2 cells compared to wt (Fig 3A). Enhanced uptake of pHrodo-labeled bacteria is in strong contrast to the reduced uptake detected in *Trem2* loss-of-function mutations (Fig EV1A; Kleinberger *et al*, 2014, 2017; Schlepckow *et al*, 2017), thus demonstrating that differentially regulated mRNA signatures translate into opposite phagocytic phenotypes. In acutely isolated microglia, uptake of bacteria was also reduced upon loss of TREM2 (Fig EV1B). $Grn^{-/-}$ microglia displayed only a slight but significant increase in phagocytosis (Fig EV1B). The rather minor effect of the *Grn* knockout on increased microglial phagocytosis is most likely due to isolation-induced activation of microglia (Gosselin *et al*, 2017), which as a consequence already show a rather high uptake capacity.

Previously, we demonstrated that microglia of $Trem2^{-/-}$ mice are locked in a homeostatic state and fail to migrate (Mazaheri *et al*, 2017). Since microglia of $Grn^{-/-}$ mice express a RNA profile typical for MGnD, we investigated if that results in increased migration. To assess migration *ex vivo*, we cultured organotypic brain slices from young (P6-7) mice as recently described (Daria *et al*, 2017; Mazaheri *et al*, 2017). In line with our previous findings, we found only baseline migration of wt microglia reflected by few migrating CD68-positive cells detected mainly in the vicinity of the brain tissue (Fig 3B–D). On the contrary, the number of migrating CD68-positive cells and their distance migrated were both significantly increased in brain slices derived from the $Grn^{-/-}$ mice (Fig 3B–D). Again, this finding is in clear contrast to our previous observation in cultured

Figure 2. Expression of microglial marker protein characteristic for the homeostatic or disease-associated state.

A Immunoblot analysis of ApoE, CLEC7A, TREM2, and CD68 in lysates of acutely isolated microglia from $Grn^{-/-}$ and $Grn^{+/+}$ mice (9 months of age, n = 3 per genotype, female). IBA1 was used as loading control. The asterisk indicates an unspecific band.

B Quantification of protein expression normalized to levels of $Grn^{+/+}$ microglia (n = 3). Data represent the mean ± SD.

C ELISA-mediated quantification of sTREM2 in brain homogenates of $Grn^{-/-}$ and $Grn^{+/+}$ mice. Data are shown as mean ± SEM (n = 3–6).

D ELISA-mediated quantification of sTREM2 in serum of $Grn^{-/-}$ and $Grn^{+/+}$ mice. Data are shown as mean ± SEM (n = 4–13).

E Microglial expression of P2RY12 in cortical sections of *wt*, $Grn^{-/-}$ and $Trem2^{-/-}$ mice. (9 months of age, female). Scale bar indicates 10 μm.

F Quantification of P2RY12-positive microglia. Data are shown as mean ± SD (n = 3 per genotype, female, except one male for $Trem2^{-/-}$).

G Immunoblot analysis of secreted PGRN and ApoE ($ApoE_{med}$) in conditioned media and PGRN, ApoE, CLEC7A, P2RY12, and TREM2 in lysates of BV2 wild-type (Grn_{wt}) and PGRN-deficient ($Grn_{mu}t$) cells. Soluble amyloid precursor protein (APPs) and calnexin were used as a loading control. The asterisk indicates an unspecific band.

H Quantification of immunoblots normalized to BV2 Grn_{wt} levels (n = 3–5). Data represent the mean ± SD.

I ELISA-mediated quantification of sTREM2 in conditioned media of BV2 Grn_{wt} and Grn_{mut} cells. Data represent the mean ± SD (n = 4).

J Quantification of relative mRNA levels of *Apoe*, *Clec7a*, *P2ry12*, and *Trem2* in BV2 Grn_{wt} and Grn_{mut} cells. Data represent the mean ± SD (n = 3).

Data information: For statistical analysis, unpaired two-tailed Student's t-test was performed between Grn_{mut} or $Grn^{-/-}$ in comparison with Grn_{wt} or $Grn^{+/+}$: n.s., not significant; *$P < 0.05$; **$P < 0.01$; ***$P < 0.001$; and ****$P < 0.0001$. For (F), the one-way ANOVA with Tukey post hoc test was used.
Source data are available online for this figure.

Published online: May 23, 2019
Julia K Götzl et al
EMBO Molecular Medicine

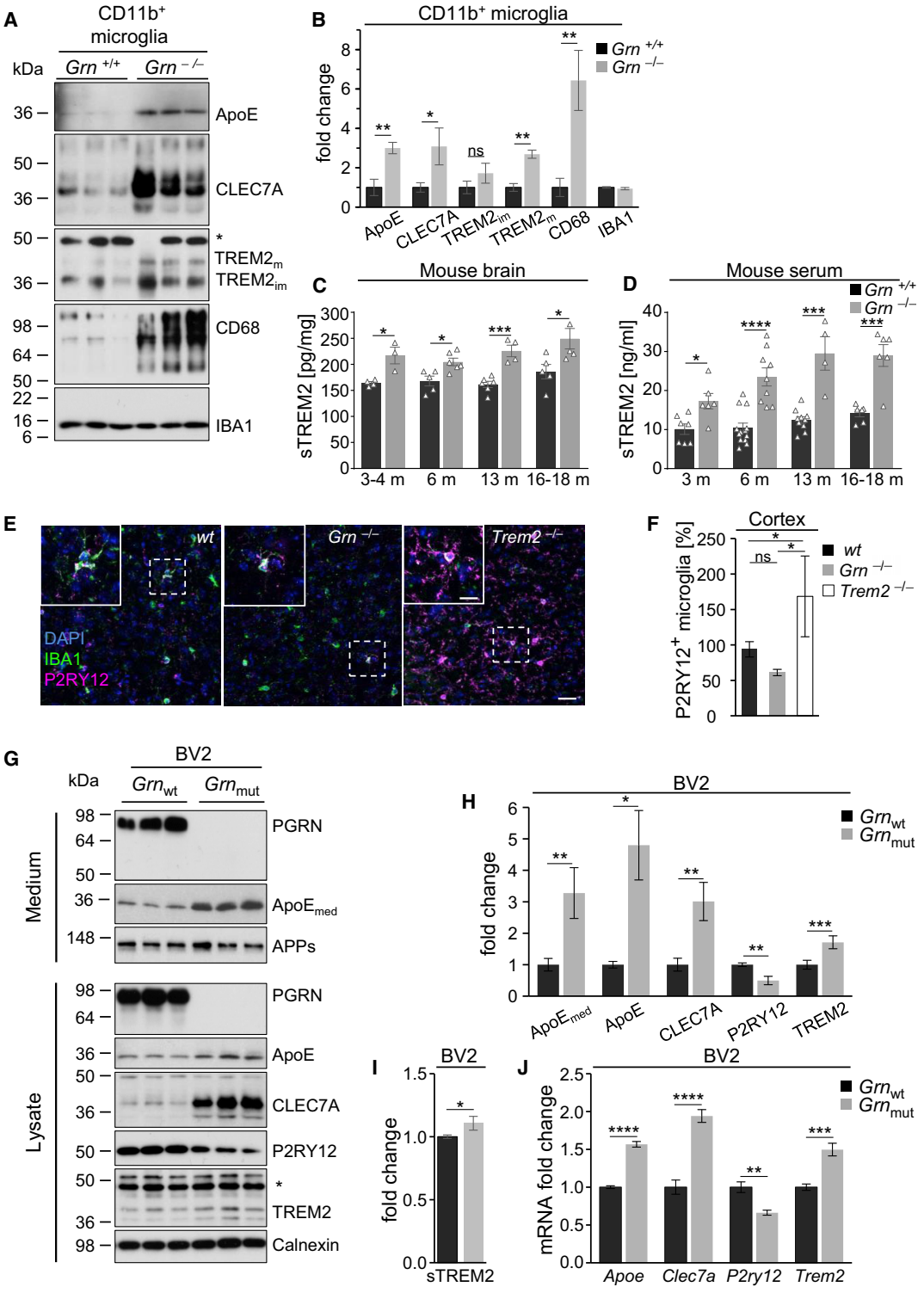

Figure 2.

Published online: May 23, 2019
EMBO Molecular Medicine

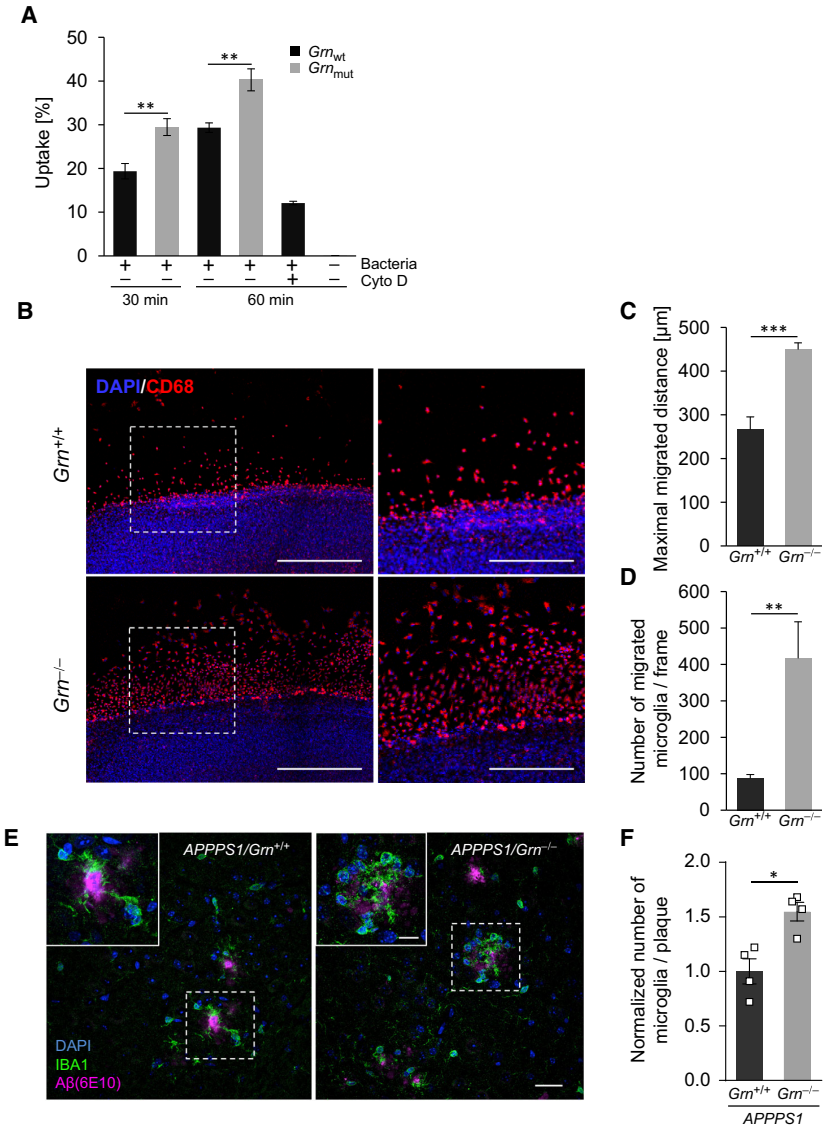

Figure 3. Enhanced phagocytosis, migration, and clustering around amyloid plaques upon PGRN deficiency.

A Flow cytometric analysis of phagocytic capacity in $BV2_{wt}$ and $BV2_{mut}$ cells using pHrodo green *E. coli* as target particles. Phagocytosis was terminated after 30 and 60 min (min) of incubation. Data are presented as mean percentage of cells positive for pHrodo uptake ± SD (n = 3).

B Enhanced migration of CD68-positive, PGRN-deficient cells in an *ex vivo* model. Immunofluorescence analysis of cultured $Grn^{+/+}$ and $Grn^{-/-}$ organotypic brain at 7 DIV immunostained using microglial marker CD68. Nuclei were counterstained using DAPI. Images of boxed regions in left panels are shown at higher magnifications in right panels. Scale bars: 500 µm (left panels), 250 µm (right panels).

C Quantitative analysis reveals that $Grn^{-/-}$ microglia migrate larger distances than $Grn^{+/+}$. Data are shown as mean ± SD (n = 3 independent experiments).

D Quantification displays an increased number of migrating $Grn^{-/-}$ cells compared to $Grn^{+/+}$ cells. Data are shown as mean ± SD (n = 3 independent experiments).

E Enhanced microglial clustering around amyloid plaques in the absence of PGRN. Left: IBA1-stained microglial clustering around X-34-positive amyloid plaque cores in 4-month-old APPPS1/$Grn^{+/+}$ mice. Right: Age-matched APPPS1/$Grn^{-/-}$ mice display microglial hyper-clustering around amyloid plaques compared with APPPS1/$Grn^{+/+}$. Dotted white boxes indicate the area that is shown at higher magnification. Scale bars indicate 10 and 3 µm in inset.

F Immunohistochemical quantification of IBA1-positive microglial cell number per plaque (APPPS1/$Grn^{+/+}$ n = 4, APPPS1/$Grn^{-/-}$ n = 4; 4-month-old; two males and two females per genotype) normalized to APPPS1/$Grn^{+/+}$ mice. Approximately 20–50 amyloid plaques were counted per mouse in 3 cortical sections to calculate the number of IBA1-positive microglia per plaque. Data are shown as mean ± SD.

Data information: For statistical analysis, unpaired two-tailed Student's t-test was performed (A, C, D) between PGRN-deficient Grn_{mut} BV2 cells or $Grn^{-/-}$ microglia and Grn_{wt} BV2 cells or $Grn^{+/+}$ microglia. For (F) the Mann–Whitney U-test, two-tailed analysis was used. Significance is indicated by *P < 0.05; **P < 0.01; and ***P < 0.001. Source data are available online for this figure.

Published online: May 23, 2019
Julia K Götzl et al EMBO Molecular Medicine

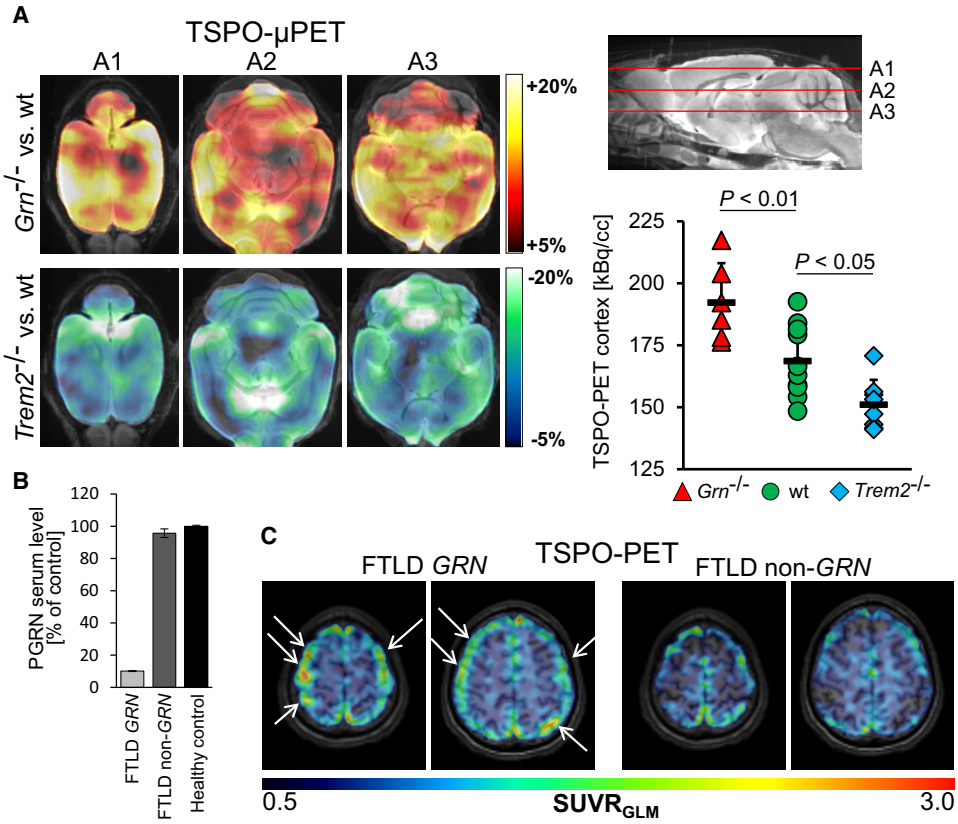

Figure 4. Enhanced microglial activity in *Grn*$^{-/-}$ mice and in a patient with *Grn* haploinsufficiency.

A TSPO-μPET in rodents: Axial slices (A1, A2, A3) of averaged %-TSPO-PET differences between *Grn*$^{-/-}$ or *Trem2*$^{-/-}$ mice and wt indicate increased microglial activity in the cerebrum of *Grn*$^{-/-}$ mice (hot color scale) and decreased microglial activity in the cerebrum of *Trem2*$^{-/-}$ mice (cold color scale). Scatter plot depicts single TSPO-μPET values deriving from a neocortical volume of interest. Data represent the mean +/− SD. μPET results are illustrated upon an MRI template; 6–10 female mice per group (*Grn*$^{-/-}$ n = 6 at 8 months, *Trem2*$^{-/-}$ n = 8 at 11 months; wt n = 10 at 8–11 months). Statistics were derived from one-way ANOVA with Tukey post hoc test.

B PGRN serum levels of the patients subjected to TSPO-PET confirmed the *GRN* mutation and non-*GRN* mutation carrier. PGRN was measured by ELISA in technical triplicates and normalized to serum levels of a healthy control. Data represent the mean +/− SD.

C TSPO-PET in human FTLD patients: Visual interpretation of axial TSPO-PET SUVR images in upper cranial layers reveals increased microglial activity in frontal and parietal cortices (white arrows) of a FTLD patient with a *GRN* loss-of-function mutation in comparison with a FTLD patient without a *GRN* mutation. PET results are illustrated upon an MRI template; 60–80 min p.i. emission recording; and global mean scaling. Both patients were low-affinity binder.

organotypic brain slices derived from *Trem2*$^{-/-}$ mice, where we found a severe inhibition of migration as compared to wt (Mazaheri *et al*, 2017). The increased migratory potential is in line with enhanced clustering of IBA1-positive microglia that we detected around amyloid plaques in APPPS1/*Grn*$^{-/-}$ versus APPPS1/*Grn*$^{+/+}$ mice (Figs 3E and F, and EV1C). Again, this finding is opposite to what was found in the absence of functional TREM2, namely impaired clustering of microglia around amyloid plaques (Wang *et al*, 2016; Parhizkar *et al*, 2019) and a general reduction of chemotaxis (Mazaheri *et al*, 2017).

Increased TSPO-PET signals in *Grn*$^{-/-}$ mice and a human patient with *GRN* haploinsufficiency

To confirm that our findings have relevance *in vivo*, we searched for differences in microglial activity between *Trem2*$^{-/-}$ and *Grn*$^{-/-}$ mice by previously established *in vivo* TSPO-μPET imaging (Liu *et al*, 2015; Kleinberger *et al*, 2017). In line with the hypothesis gained from *in vitro* experiments, we observed a striking upregulation of microglial activity throughout the cerebrum of *Grn*$^{-/-}$ mice when compared to wt (Fig 4A). Differences were pronounced in the neocortex but also present in subcortical areas. On the contrary, a reduced microglial activity was apparent in the entire cerebrum of *Trem2*$^{-/-}$ mice, fitting to our recent findings in a TREM2 loss-of-function model (Kleinberger *et al*, 2017; Fig 4A).

Furthermore, we translationally investigated a FTLD patient with a genetically confirmed *GRN* (NM_002087.2) loss-of-function mutation (c.328C>T, p.(Arg110*)). Haploinsufficiency of PGRN was proven by ELISA-mediated quantitative analysis of the patient's serum (Fig 4B). TSPO-PET imaging revealed elevated cortical microglial activity in comparison with a FTLD patient screened negative for variants in the *GRN*, *MAPT*, *C9orf72*, or the *TREM2* gene (Fig 4C).

Published online: May 23, 2019
EMBO Molecular Medicine

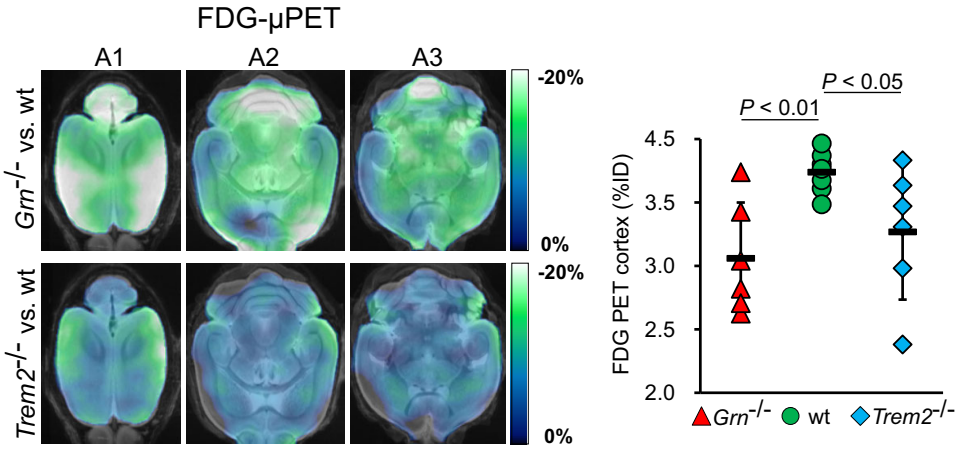

Figure 5. Cerebral hypometabolism upon loss of GRN and TREM2.

FDG-µPET in rodents: Axial slices (as indicated in Fig 4A) of averaged %-FDG-µPET differences between $Grn^{-/-}$ or $Trem2^{-/-}$ mice and wt indicate decreased glucose metabolism in the cerebrum of $Grn^{-/-}$ and $Trem2^{-/-}$ (both cold color scales) when compared to wt. Scatter plot depicts single FDG-PET values deriving from a neocortical volume of interest. Data represent the mean +/− SD. µPET results are illustrated upon an MRI template; 6–10 female mice per group ($Grn^{-/-}$ n = 6 at 8 months, $Trem2^{-/-}$ n = 6 at 11 months; wt n = 10 at 8–11 months). Statistics were derived from one-way ANOVA with Tukey post hoc test.

Cerebral hypometabolism upon loss of PGRN and TREM2

Next, we investigated whether alterations of microglial activity have an impact on synaptic brain function as assessed by *in vivo* FDG-µPET. We observed a cerebral hypometabolism not only in $Trem2^{-/-}$ mice, which had been anticipated from our previous study (Kleinberger *et al*, 2017), but even more severe in $Grn^{-/-}$ mice (Fig 5). As activated microglia itself could lead to increased energy consumption, the results in $Grn^{-/-}$ mice appear even more striking. Thus, a failure of brain function was confirmed as a consequence of both, arresting microglia in a homeostatic and a disease-associated stage.

Discussion

Taken together, our findings demonstrate that microglia lacking functional TREM2 or PGRN exhibit opposite mRNA profiles. This is consistent with the differential TSPO-PET signal observed in both animal models. While $Grn^{-/-}$ mice exhibit a hyperactivated phenotype, which is consistent with the observation that $Grn^{-/-}$ mice exhibit an exaggerated inflammation (Yin *et al*, 2010; Martens *et al*, 2012; Tanaka *et al*, 2013a; Lui *et al*, 2016) as well as induced expression of TYROBP network genes including *Trem2* (Takahashi *et al*, 2017), TREM2 loss of function results in reduced microglial activity. As a consequence, several functional assays including phagocytic capacity, migration, and chemotactic clustering around amyloid plaques revealed opposite phenotypes. Thus, loss of PGRN or TREM2 arrests microglia at the two extreme ends of a potential gradient of dynamic microglial populations (Fig 6; upper panel). Nevertheless, in both animal models we observed a dramatic reduction of glucose metabolism throughout the brain and loss of either protein causes severe neurodegeneration in humans. Reduced energy metabolism in $Trem2^{-/-}$ mice is in line with previous observations (Kleinberger *et al*, 2017; Ulland *et al*, 2017). Thus, it is tempting to speculate that microglia on the opposite ends of a large spectrum of functionally divergent microglial populations cause

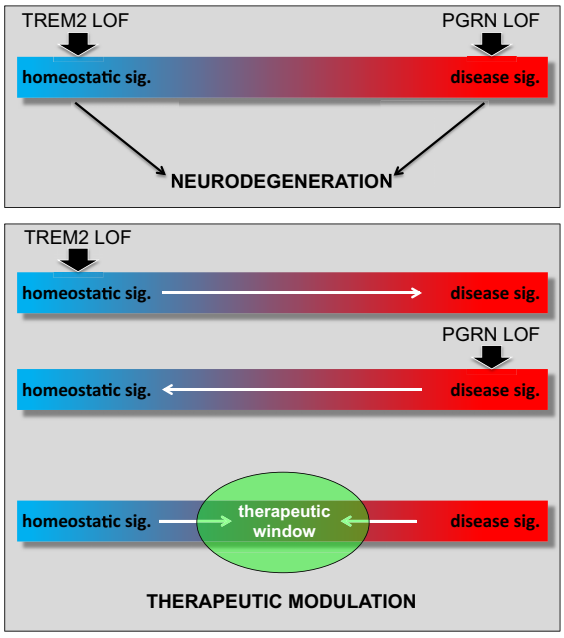

Figure 6. Modulation of microglia activity states within a narrow therapeutic window.

Schematic presentation of the disease-associated/homeostatic phenotypes observed in $Grn^{-/-}$ mice versus $Trem2^{-/-}$ and the potential consequences for a therapeutic window of microglial modulation.

Published online: May 23, 2019
Julia K Götzl et al EMBO Molecular Medicine

neurological dysfunctions that ultimately may result in neurodegeneration. In fact, disease-associated variants of TREM2 are associated with a loss of a protective function of TREM2 (Kleinberger *et al*, 2017; Song *et al*, 2018) and some mutations appear to lock microglia in a homeostatic stage (Krasemann *et al*, 2017; Mazaheri *et al*, 2017). On the other hand, during aging wild-type microglia in an AD mouse model lose their motility and phagocytic activity (Krabbe *et al*, 2013) although they express a neurodegenerative disease-associated mRNA profile (Krasemann *et al*, 2017). This may indicate that "over-activation" for a prolonged period of time may be detrimental for microglia and drive them into a loss-of-function phenotype. Our findings also indicate that arresting microglia in either a homeostatic state or a disease-associated state would be equally detrimental. This has important consequences for therapeutic strategies aiming to modulate microglial activity. Clearly, locking microglia in any of the two extreme states is detrimental (Fig 6, upper panel). Rather, microglia locked in a homeostatic state should be activated whereas microglia arrested in a disease-associated state may be silenced (Fig 6, lower panel). Nevertheless, during long-term treatment "over-activation" and "over-silencing" of microglia may both be equally detrimental, since that may drive microglia to the opposite ends of the gradient. As a consequence, the therapeutic window for microglial modulation may be rather limited (Fig 6, lower panel) and care must be taken to balance microglial activity.

Materials and Methods

Animal experiments

All animal experiments were performed in accordance with local animal-handling laws. Housing conditions included standard pellet food and water provided *ad libitum*, 12-h light–dark cycle at temperature of 22°C with maximal 5 mice per cage and cage replacement once per week, and regular health monitoring. Mice were sacrificed by CO_2 inhalation. Brain tissue, microglia, and serum were obtained from the *Grn*$^{-/-}$ mouse strain (Kayasuga *et al*, 2007), brain tissue and microglia were obtained from the *Trem2*$^{-/-}$ mouse strain (Turnbull *et al*, 2006), and brain tissue was obtained from a mouse model for amyloid pathology (APPPS1; Radde *et al*, 2006) crossed with the *Grn*$^{-/-}$ mouse strain (APPPS1/*Grn*$^{-/-}$). Experiments were performed with mice of both genders at 2–18 months of age. Organotypic brain slices were taken from postnatal days 6–7 of *Grn*$^{-/-}$ and wt mice.

Gene expression profiling

FCRLS (Butovsky *et al*, 2014)- and CD11b (BD biosciences; Clone M1/70)-positive primary microglia were isolated from mouse brains of 5.5 months of *Grn*$^{-/-}$ and wt mice (n = 5 per genotype, male) as described (Mazaheri *et al*, 2017). Total RNA was isolated using mirVanaTM miRNA Isolation Kit (Ambion) according to the manufacturer's protocol. 100 ng RNA per sample was used for gene expressing profiling using nCounter Analysis, NanoString technology as described (Butovsky *et al*, 2014, 2015). In brief, the MG534 NanoString chip was designed using the quantitative NanoString nCounter platform. Selection of genes is based on analyses that identified genes and proteins, which are specifically or highly expressed in adult mouse microglia (Butovsky *et al*, 2014) and encompasses 400 homeostatic unique and enriched microglial genes (Butovsky *et al*, 2014), 129 disease-associated genes, and 5 housekeeping genes (Krasemann *et al*, 2017).

Data normalization and analysis

NanoString data were normalized and analyzed using nSolver™ software. RNA ncounts were normalized using the geometric mean of five housekeeping genes including *Cltc*, *Gapdh*, *Gusb*, *Hprt1,* and *Tubb5* using nSolver™ Analysis Software, version 3.0 (NanoString Technologies, Inc.). A cutoff was introduced at the value two-fold of the highest negative control present on the chip. Fold changes were calculated using the average of each group. For each experiment, the fold changes were calculated comparing the experimental group to their appropriate controls. To compare the normalized gene expression levels in *Grn*$^{-/-}$ and wt mice, unpaired two-tailed Student's *t*-test was performed (*$P < 0.05$, **$P < 0.01$, ***$P < 0.001$). The volcano blot was generated employing GraphPad Prism 7 software. The heatmap was generated employing Multi Experiment Viewer v 4.9. The expression value for each gene was normalized to the mean value of wt mice followed by a log2 transformation.

sTREM2 ELISA analysis of mouse plasma and brain samples

Blood collected from *Grn*$^{-/-}$ and wt mice (3, 6, 13, 16–18 months of age, female and male mice as indicated in the source data file to Fig 2) was left at room temperature (RT) to allow the blood to clot. After centrifugation (15 min, 2,000 × *g*, RT), the supernatant (serum) was collected, snap-frozen in liquid nitrogen, and stored at −80°C.

Snap-frozen mouse brain hemispheres were homogenized by crunching the brain in liquid nitrogen to fine powder. Approximately 10–20 mg of powdered mouse brain from *Grn*$^{-/-}$ and wt mice (3–4, 6, 13, 16–18 months of age, female and male mice as indicated in the source data file to fig 2) was homogenized in Tris-buffered saline (TBS) supplemented with protease inhibitor cocktail (Sigma-Aldrich) and centrifuged for 30 min, 15,000 × *g*, 4°C. Protein concentrations of supernatants were determined using the BCA protein assay (Pierce, Thermo Scientific), and equal amount of protein was analyzed for TREM2. sTREM2 levels in mouse serum or mouse brain extracts were quantified using the Mesoscale platform essentially as described previously (Kleinberger *et al*, 2017) using 0.25 μg/ml biotinylated polyclonal goat anti-mouse TREM2 (R&D Systems; BAF1729) as capture antibody and 1 μg/ml rat monoclonal anti-TREM2 antibody (R&D Systems, MAB17291) as detection antibody. Calculation of the concentration of sTREM2 was performed with the MSD Discovery Workbench v4 software (MSD).

Cell culture and CRISPR/Cas9 genome editing in BV2 cells

The murine microglial cell line BV2 (Bocchini *et al*, 1992) was maintained in Dulbecco's modified Eagle's medium (DMEM) + GlutaMAX™- I (Thermo Fisher Scientific, 61965-026) supplemented with 10% (v/v) FBS (Sigma-Aldrich, F7524), 100 U/ml penicillin, and 100 μg/ml streptomycin. For genome editing, BV2 cells were transfected with pSpCas9(BB)-2A-GFP (PX458; gift from Feng Zhang (Ran *et al*, 2013), targeting exons 3 and 4 with the gRNA1 ATAAC GAGCCATCATCTAGA and gRNA2 GGCTTCCACTGTAGTGCAGA;

Published online: May 23, 2019
EMBO Molecular Medicine

Addgene plasmid #48138) by electroporation with the Cell Line Nucleofector® Kit T (Lonza VACA-1002) following the manufacturer's instructions. GFP-positive cells were isolated by FACS 24 h after transfection. Single-cell clones from the GFP-positive fraction were obtained by serial dilution and screened for genetic modifications in *Grn* by PCR amplification of exons 3 and 4. Media and lysates of edited clones were analyzed by Western blot for PGRN expression.

Quantitative real-time PCR (qRT–PCR)

Total RNA was prepared from BV2 cells using the QIAshredder and RNeasy Mini Kit (Qiagen) according to manufacturer's instructions. 2 μg of RNA was reverse transcribed into cDNA using M-MLV reverse transcriptase (Promega) and oligo(dT) primers (Life Technologies). The following primer sets from Integrated DNA Technologies were used: mouse *Trem2* Mm.PT.58.46092560 (Exon boundary 2 to 4b), mouse *Apoe* Mm.PT.58.33516165 (Exon boundary 1 to 3), *Clec7a* Mm.PT.58.42049707 (Exon boundary 1 to 2), and *P2ry12* Mm.PT.58.43542033 (Exon boundary 3 to 4). cDNA levels were measured in triplicates using TaqMan assays on a 7500 Fast Real-Time-PCR System (Applied Biosystems), normalized to *Gapdh* cDNA expression, and relative transcription levels of the respective sequences were analyzed using the comparative delta Ct method (7500 Software V2.0.5, Applied Biosystems, Life Technologies).

Isolation of adult primary microglia for immunoblotting

Primary microglia were isolated from adult mouse brain (9 months of age, $n = 3$ per genotype, female) using MACS Technology (Miltenyi Biotec) according to manufacturer's instructions as described previously (Gotzl *et al*, 2018).

Cell lysis and immunoblotting

Snap-frozen cell pellets were lysed in RIPA lysis buffer followed by centrifugation at 17,000 × *g*, 4°C for 20 min [RIPA lysis buffer (150 mM NaCl, 20 mM Tris–HCl pH 7.4, 1% NP-40, 0.05% Triton X-100, 0.5% sodium deoxycholate, 2.5 mM ETDA)]. Protein concentrations were determined using the BCA protein assay (Pierce, Thermo Fisher Scientific), and equal protein amounts were analyzed in SDS–PAGE. For the detection of PGRN, TREM2, CLEC7A, P2RY12, calnexin, CD68, IBA1, and APP gels were transferred on polyvinylidene difluoride membranes (Amersham Hybond P 0.45 PVDF, GE Healthcare Life Science). For the detection of ApoE, nitrocellulose membranes were used (GE Healthcare Life Science). Membranes were blocked for 1 h in I-Block™ (Thermo Fisher Scientific) and exposed to the following antibodies. In-house antibodies were as follows: PGRN (Rat 8H10 1/50; Gotzl *et al*, 2014) and TREM2 (Rat 5F4 1/50; (Xiang *et al*, 2016)). Commercial antibodies were as follows: CLEC7A (R&D Systems, AF1756, 1/2,000), P2RY12 (Abcam, [EPR18611] (ab184411), 1/1,000) and ApoE (Merck, AB947, 1/2,000), and APPs (Merck, MAB348 clone 22C11, 1/5,000). For immunoblotting in primary microglia: ApoE (HJ6.3, 1/700), kindly provided by David E. Holtzman (Kim *et al*, 2012), CD68 (Abcam, ab125212, 1/1,000), and IBA1 (GeneTex, GTX100042, 1/1,000) were used. HRP-conjugated secondary antibodies and ECL Plus (Pierce™, Thermo Fisher Scientific) were used for detection. For the quantitatively analysis, images were taken by a Luminescent Image Analyzer Vilber/Peqlab Fusion SL and evaluated with the Multi Gauge V3.0 software (Fujifilm Life Science, Tokyo, Japan).

Phagocytosis assay

Assays to determine the phagocytic capacity were carried out as described before (Kleinberger *et al*, 2014, 2017). Briefly, BV2 cells were seeded at a density of 100,000 cells per well of a 12-well dish and 1 day after seeding, incubated with pHrodo green *E. coli* for 30 and 60 min at 37°C after (pHrodo® Green *E. coli* BioParticles® Thermo Fisher). To analyze *E. coli* uptake, cells were resuspended in FACS buffer (PBS, 2 mM EDTA and 1% FBS) and subjected to flow cytometry. Data were acquired using the MACSQuant®. Cytochalasin D was used as an uptake inhibitor at a final concentration of 10 μM. Phagocytosis assays with primary microglia were performed similar to BV2 cells with the following modifications: Cells were isolated from adult mouse brain (2 months of age, $n = 3$ per genotype, male) as described above. Following isolation, primary microglia were cultivated in DMEM/F-12 (Thermo Fisher Scientific, 31330-038) supplemented with 10% (v/v) FBS (Merck, Sigma-Aldrich), 100 U/ml penicillin, 100 μg/ml streptomycin, M-CSF (10 ng/ml), and TGF-β (50 ng/ml). Four days after seeding at a concentration of 100,000 cells per well of a 24-well plate, cells were incubated with pHrodo for 45 min at 37°C. APC-Cy™7 Rat Anti-CD11b (BD Pharmingen™, M1/70, 557657, 1/100) was used as a cell population control.

Ex vivo migration assay

Organotypic brain slices from postnatal days 6–7 of $Grn^{-/-}$ and wt mice were prepared, cultured, and immunostained as described before (Daria *et al*, 2017; Mazaheri *et al*, 2017). Microglial migration was analyzed after 7 days *ex vivo* as described (Daria *et al*, 2017; Mazaheri *et al*, 2017). Quantification was performed in three independent experiments, each including three biological replicates (three independent slice culture dishes per animal and genotype). From each biological replicate, three defined image regions (775 × 775 μm) of the cortical area in the brain slice were acquired using a Leica SP5 confocal microscope with a 20× dry objective. Tile scan images were captured using a 10× dry objective. The number of migrating CD68-positive microglia and the maximum distance migrated were quantified using Fiji. The migration distance measurements (average of three length measurements per acquired image) were performed on an area defined by two manually drawn lines, one limiting the boarder of the tissue and the other surface covered by at least 90% of migrated microglial cells.

Immunohistochemistry and image analysis

Following deparaffinization and rehydration of paraffin-embedded brain sections, tissue sections mounted on slides were subjected to citric acid antigen retrieval (1 M sodium citrate in PBS, pH 6.0) and boiled in a microwave for 20 min. After cooling, sections were blocked with 5% donkey serum for 1 h at room temperature. Following this, sections were incubated with primary antibodies against IBA1 (Invitrogen, Thermo Fisher Scientific, 1/300) and β-amyloid

Published online: May 23, 2019
Julia K Götzl et al EMBO Molecular Medicine

(Biolegend, 6E10, 1/300) over two nights at 4°C. Subsequently, sections were washed and incubated with secondary antibodies (donkey anti-rabbit Alexa Fluor 488, 1/700, donkey anti-mouse Alexa Fluor 555, 1/1,000, respectively) overnight at 4°C. For the P2RY12 co-stainings, brains of 9-month-old female mice (except one male for *Trem2*$^{-/-}$, $n = 3$ per genotype) were immerse-fixed in 4% PFA for 24 h following perfusion. Brains were subsequently cryoprotected in 30% sucrose for 48 h. After freezing, 50-μm-thick microtome sections were sequentially collected in phosphate buffer saline with 15% glycerol and kept at −80°C until further use. Free-floating sections were blocked in 5% goat serum for 1 h at room temperature and then incubated in primary antibodies P2RY12 (Biolegend, 1/100) and IBA1 (Invitrogen, Thermo Fisher Scientific, 1/300) for two nights at 4°C. Sections were washed and incubated in secondary antibodies (goat anti-rat Alexa Fluor 555, 1/500, goat anti-rabbit Alexa Fluor 488, 1/500) for 3 h at room temperature. Lastly, slides were washed and stained with 4′,6-diamidino-2-phenylindole (DAPI, 5 μg/ml) before mounting coverslips with ProlongTM Gold Antifade reagent (Thermo Fisher Scientific). Images were acquired using a LSM 710 confocal microscope (Zeiss) and the ZEN 2011 software package (black edition, Zeiss). Laser and detector settings were maintained constant for the acquisition of each immunostaining. For analyses, three images were taken per slide using 20× objective (Plan-Apochromat 20×/0.8 M27) at 2,048 × 2,048 pixel resolution, with Z-step size of 1 μm at 16 μm thickness. Approximately 150 plaques per genotype were counted using FIJI software (ImageJ) to calculate the number of IBA1-positive microglia around plaques in the cortex. Microglia coverage was quantified by importing acquired images to FIJI, and data channels were separated (Image\Color\Split Channels). Gaussian filtering was used to remove noise, and intensity distribution for each image was equalized using rolling ball algorithm, which is implemented as background subtraction plug-in in FIJI. For the feasibility of the quantification, all layers from a single image stack were projected on a single slice (Stack\Z projection). Next, the microglia were segmented using automatic thresholding methods in Fiji with "Moments" thresholding setting. Subsequently, the diameter (25 or 50 μm) around each plaque was selected to calculate the sum number of positive pixels over total number of pixels within the selected area. Data for 50 μm were subtracted from 25 μm to calculate the microglia coverage in the periphery of the plaque only. Data were normalized to age-matched APPPS1/*Grn*$^{+/+}$ or *Grn*$^{+/+}$ controls (4-month-old mice; two males and two females per genotype).

Rodent μPET

All rodent μPET procedures followed an established standardized protocol for radiochemistry, acquisition, and post-processing (Brendel *et al*, 2016; Overhoff *et al*, 2016). In brief, ^{18}F-GE180 μPET with an emission window of 60–90 min p.i. was used to measure cerebral microglial activity and ^{18}F-fluordesoxyglucose (FDG) PET with an emission window of 30–60 min p.i. was used for assessment of cerebral glucose metabolism. We studied *Grn*$^{-/-}$ mice ($n = 6$; female, 8 months), *Trem2*$^{-/-}$ mice ($n = 6$–8; female, 11 months), and wt mice ($n = 7$–10; female, 8–11 months) by dual PET. Normalization of injected activity was performed by the previously validated myocardium correction method (Deussing *et al*, 2017) for TSPO-PET and by percentage of the injected dose (%-ID) for FDG-PET. Known changes in TSPO and FDG-PET during aging (Brendel *et al*, 2017) were accounted to compensate for natural age differences between individual mice. Groups of *Grn*$^{-/-}$ and *Trem2*$^{-/-}$ mice were averaged and compared against wt mice by calculation of %-differences in each cerebral voxel. Finally, TSPO and FDG-PET values deriving from a cortical target VOI (Rominger *et al*, 2013) were extracted and compared between groups of different genotype by a one-way ANOVA including Tukey post hoc correction.

Patient identification, genetic studies, PGRN ELISA, and PET

Written informed consent was obtained from all subjects prior to PET examination, and the experiments conformed to the principles set out in the World Medical Association (WMA) Declaration of Helsinki on ethical principles for medical research and the Department of Health and Human Services Belmont Report.

A female patient, 63 years at date of PET, presented with primary progressive aphasia with semantic and non-fluent features. Genetic testing was performed because of a positive family history (triplet brother with early-onset dementia). Exome sequencing from blood DNA and data analysis was performed as described before (Kremer *et al*, 2017). In brief, exonic regions were enriched using the SureSelect Human All Exon Kit V6 from Agilent followed by sequencing as 100 bp paired-end runs on an Illumina HiSeq4000 (Illumina, San Diego, CA, USA) to an average read depth of 144x. Reads were aligned to the UCSC human reference assembly (hg19) with Burrows–Wheeler algorithm (BWA v.0.5.9). More than 98% of the target sequences were covered at least 20× in all samples. Single nucleotide variants (SNVs) as well as small insertions and deletions were detected with SAM tools v.0.1.19. In-house custom Perl scripts were used for variant annotation. PGRN serum levels measured by ELISA confirmed the *GRN* mutation carrier. PGRN levels were measured and quantified using the Mesoscale platform essentially as described previously (Capell *et al*, 2011) using a biotinylated polyclonal goat anti-human PGRN antibody at 0.2 μg/ml (R&D Systems; BAF2420) as capture antibody and a monoclonal mouse anti-human PGRN antibody at 0.25 μg/ml for detection (R&D Systems, MAB2420). Calculation of the concentration of PGRN was performed with the MSD Discovery Workbench v4 software (MSD). Prior to PET in the patient, the affinity of the TSPO receptor for binding of PET radioligands was assessed by determining the genotype of the SNP rs6971 as previously described (Mizrahi *et al*, 2012; Owen *et al*, 2012).

The patient was scanned at the Department of Nuclear Medicine, University hospital of Munich, by an established TSPO-PET protocol (Albert *et al*, 2017). In brief, PET was acquired with a PET/CT scanner (Biograph 64, Siemens) 60–80 min after intravenous injection of 187 MBq of ^{18}F-GE180. A low-dose CT scan preceded the PET acquisition and served for attenuation correction. An SUVR image was generated by a global mean scaling and compared visually with TSPO-PET data deriving from a 56-year-old female patient with bvFTD, indicating no mutation in *GRN* and the same binding affinity status. This patient was scanned secondary to informed consent following the same TSPO-PET scanning procedure. In this patient, mutations in *GRN, TREM2,* and *MAPT* were excluded by panel sequencing as well as the *C9orf72* hexanucleotide expansion by repeat-primed PCR.

Published online: May 23, 2019
EMBO Molecular Medicine

The paper explained

Problem
A number of variants in genes selectively expressed in microglia within the brain are associated with an increased risk for neurodegenerative diseases such as Alzheimer's disease and frontotemporal lobar degeneration. Among these genes are progranulin (*GRN*) and the triggering receptor expressed on myeloid cells 2 (*TREM2*), which both cause neurodegeneration by a loss of function. Since many functionally different microglial population exist within the brain and since a loss of TREM2 locks microglia in a homeostatic state, we now investigated the mRNA signature of microglia derived from $Grn^{-/-}$ mice and compared the key microglial functions of $Grn^{-/-}$ and $Trem2^{-/-}$ mice.

Results
While $Trem2^{-/-}$ microglia enhance the expression of genes associated with a homeostatic state, microglia derived from $Grn^{-/-}$ mice showed a massive increase in the disease-associated signature. The opposite mRNA expression profile is reflected by completely divergent functional phenotypes. In contrast to $Trem2^{-/-}$ mice, phagocytic capacity, migration, clustering around amyloid plaques, and TSPO activation were all greatly stimulated upon loss of PGRN in mice. TSPO activation is also detected in a *GRN*-associated FTLD patient. Albeit opposite functional phenotypes, loss of PGRN and TREM2 both reduce cerebral energy metabolism.

Impact
Opposite microglial phenotypes of PGRN and TREM2 loss-of-function result in similar wide spread brain dysfunction. Thus, microglia arrested at either end of a gradient of functionally divergent microglial populations cause severe neurological syndromes. Importantly, this narrows the therapeutic window in attempts aiming to modulate microglial activity.

Statistical analysis

All data were analyzed using GraphPad Prism 7. Data are presented as mean ± SD or SEM as indicated. Statistical significance was calculated by unpaired two-tailed Student's *t*-test (Figs 1A–D and 2B, C, D, H, I and J, and 3A, C, D and EV1A and B), one-way ANOVA with Tukey's post hoc test (Figs 2F, 4A and 5) for multiple comparison, and the nonparametric two-tailed Mann–Whitney *U*-test (Figs 3F and EV1C). Statistical evaluations were displayed as follows: n.s. not significant for $P > 0.05$; statistical significance was assumed at $^{*}P < 0.05$; $^{**}P < 0.01$; $^{***}P < 0.001$; and $^{****}P < 0.0001$.

For the μPET experiments, animal numbers were calculated for a significance of 0.05 and a power of 80%. Animal numbers were not changed during the experiments, and no outliers were excluded from datasets. For all experiments, the genotype was unknown to the investigators.

Data availability

The datasets produced in this study are available in the following databases:

- Pathogenic variant in GRN: ClinVar SCV000897721.1 (https://www.ncbi.nlm.nih.gov/clinvar/?term=SCV000897721.1).
- NanoString gene sequence, raw, and processed data: Gene Expression Omnibus GSE129709 (https://www.ncbi.nlm.nih.gov/geo/query/acc.cgi?acc=GSE129709).

Expanded View for this article is available online.

Acknowledgements
This work was supported by the Deutsche Forschungsgemeinschaft (DFG) within the framework of the Munich Cluster for Systems Neurology (EXC 1010 SyNergy), the Koselleck Project HA1737/16-1, the Cure Alzheimer's fund and the NOMIS Foundation (to C.H.), by a dedicated PET imaging grant to M.B. & A. Ro. (BR4580/1-1 & RO5194/1-1) and the German Federal Ministry of Education and Research (project: FTLDc 01GI1007A; to J.D.-S.), and a PhD stipend of the Hans and Ilse Breuer Foundation to A. Re. We would like to thank Dr. M. Nishihara (Department of Veterinary Physiology, The University of Tokyo) for providing the founder of the $Grn^{-/-}$ mouse strain, Dr. David M. Holtzman (Department of Neurology, Washington University School of Medicine, St. Louis, MO, USA) for providing the ApoE antibody, Dr. Feng Zhang (Broad Institute) for providing PX458 and acknowledge the Core Facility Flow Cytometry at the Biomedical Center, Ludwig-Maximilians-Universität, München, for providing equipment and services and Christian Behrends (Ludwig-Maximilians-Universität, München) for providing assistance with flow cytometry analysis of cultivated primary microglia. The $Trem2^{-/-}$ mice were kindly provided by Marco Colonna (Washington University, School of Medicine), and the APPPS1 colony was established from a breeding pair kindly provided by Mathias Jucker (Hertie-Institute for Clinical Brain Research, University of Tübingen and DZNE-Tübingen). GE made GE-180 cassettes available through an early access model. O.B. is supported by the US National Institutes of Health (NIH) NIH-NINDS (R01 NS088137, R21 NS104609, R21 NS101673), NIH-NIA (R01 AG051812, R01 AG054672), NIH-NEY (R01 EY027921), National Multiple Sclerosis Society (5092A1), Nancy Davis Foundation Faculty Award, Cure Alzheimer's Fund Award, and Amyotrophic Lateral Sclerosis Association and Sanofi.

Author contributions
CH and AC conceived the study and analyzed the results. CH wrote the manuscript with further input from all co-authors. JKG and OB performed RNA analyses, MB. ARo, MD, and PB performed PET analyses, and LSM and ST performed *ex vivo* migration assays. GW generated and investigated CRISPR/Cas-modified BV2 cells and performed phagocytosis and Western blot assays on isolated primary microglia, N9 and BV2 cells, KF provided technical support on many experiments. SB assisted with cell sorting. A-VC and ARe performed microglial isolation and qPCR assays. JG and A-VC isolated serum from wt/$Grn^{-/-}$ mice, and GK investigated TREM2 expression in serum and brain of $Grn^{-/-}$ mice. SP provided immunohistochemical data on APPPS/$Grn^{-/-}$, $Grn^{-/-}$, and $Trem2^{-/-}$ mice; MW, JL, JW, and JD-S identified FTD patients and performed sequencing analyses. OB, STS, and CM performed the NanoString analysis and helped to interpret the data.

Conflict of interest
C.H. collaborates with DENALI, participated on one advisory board meeting of Biogen, and received a speaker honorarium from Novartis and Roche. A.R. received speaker honoraria from GE. J.L. is an advisor of Aesku, Axon neuroscience, Hexal and Ionis pharmaceuticals and received speaker fees from Bayer Vital and the Willi Gross Foundation as well as travel reimbursements from AbbVie. M.W. received speaking honoraria from Bayer Vital. O.B. collaborates and consults Sanofi, NanoString, and Cell Signaling Technology. O.B. received speaker honoraria from Sanofi and Amgen.

References

Abduljaleel Z, Al-Allaf FA, Khan W, Athar M, Shahzad N, Taher MM, Elrobh M, Alanazi MS, El-Huneidi W (2014) Evidence of trem2

Published online: May 23, 2019
Julia K Götzl et al **EMBO Molecular Medicine**

variant associated with triple risk of Alzheimer's disease. *PLoS ONE* 9: e92648

Ahmed Z, Sheng H, Xu YF, Lin WL, Innes AE, Gass J, Yu X, Wuertzer CA, Hou H, Chiba S *et al* (2010) Accelerated lipofuscinosis and ubiquitination in granulin knockout mice suggest a role for progranulin in successful aging. *Am J Pathol* 177: 311 – 324

Albert NL, Unterrainer M, Fleischmann DF, Lindner S, Vettermann F, Brunegraf A, Vomacka L, Brendel M, Wenter V, Wetzel C *et al* (2017) TSPO PET for glioma imaging using the novel ligand (18)F-GE-180: first results in patients with glioblastoma. *Eur J Nucl Med Mol Imaging* 44: 2230 – 2238

Atagi Y, Liu CC, Painter MM, Chen XF, Verbeeck C, Zheng H, Li X, Rademakers R, Kang SS, Xu H *et al* (2015) Apolipoprotein E is a ligand for triggering receptor expressed on myeloid cells 2 (TREM2). *J Biol Chem* 290: 26043 – 26050

Bailey CC, DeVaux LB, Farzan M (2015) The triggering receptor expressed on myeloid cells 2 binds apolipoprotein E. *J Biol Chem* 290: 26033 – 26042

Baker M, Mackenzie IR, Pickering-Brown SM, Gass J, Rademakers R, Lindholm C, Snowden J, Adamson J, Sadovnick AD, Rollinson S *et al* (2006) Mutations in progranulin cause tau-negative frontotemporal dementia linked to chromosome 17. *Nature* 442: 916 – 919

Bateman A, Belcourt D, Bennett H, Lazure C, Solomon S (1990) Granulins, a novel class of peptide from leukocytes. *Biochem Biophys Res Commun* 173: 1161 – 1168

Beel S, Moisse M, Damme M, De Muynck L, Robberecht W, Van Den Bosch L, Saftig P, Van Damme P (2017) Progranulin functions as a cathepsin D chaperone to stimulate axonal outgrowth *in vivo*. *Hum Mol Genet* 26: 2850 – 2863

Belcourt DR, Lazure C, Bennett HP (1993) Isolation and primary structure of the three major forms of granulin-like peptides from hematopoietic tissues of a teleost fish (*Cyprinus carpio*). *J Biol Chem* 268: 9230 – 9237

Bocchini V, Mazzolla R, Barluzzi R, Blasi E, Sick P, Kettenmann H (1992) An immortalized cell line expresses properties of activated microglial cells. *J Neurosci Res* 31: 616 – 621

Borroni B, Ferrari F, Galimberti D, Nacmias B, Barone C, Bagnoli S, Fenoglio C, Piaceri I, Archetti S, Bonvicini C *et al* (2014) Heterozygous TREM2 mutations in frontotemporal dementia. *Neurobiol Aging* 35: 934 e937–910

Brendel M, Probst F, Jaworska A, Overhoff F, Korzhova V, Albert NL, Beck R, Lindner S, Gildehaus FJ, Baumann K *et al* (2016) Glial activation and glucose metabolism in a transgenic amyloid mouse model: a triple-tracer PET study. *J Nucl Med* 57: 954 – 960

Brendel M, Kleinberger G, Probst F, Jaworska A, Overhoff F, Blume T, Albert NL, Carlsen J, Lindner S, Gildehaus FJ *et al* (2017) Increase of TREM2 during aging of an Alzheimer's disease mouse model is paralleled by microglial activation and amyloidosis. *Front Aging Neurosci* 9: 8

Butovsky O, Jedrychowski MP, Moore CS, Cialic R, Lanser AJ, Gabriely G, Koeglsperger T, Dake B, Wu PM, Doykan CE *et al* (2014) Identification of a unique TGF-beta-dependent molecular and functional signature in microglia. *Nat Neurosci* 17: 131 – 143

Butovsky O, Jedrychowski MP, Cialic R, Krasemann S, Murugaiyan G, Fanek Z, Greco DJ, Wu PM, Doykan CE, Kiner O *et al* (2015) Targeting miR-155 restores abnormal microglia and attenuates disease in SOD1 mice. *Ann Neurol* 77: 75 – 99

Capell A, Liebscher S, Fellerer K, Brouwers N, Willem M, Lammich S, Gijselinck I, Bittner T, Carlson AM, Sasse F *et al* (2011) Rescue of progranulin deficiency associated with frontotemporal lobar degeneration by alkalizing reagents and inhibition of vacuolar ATPase. *J Neurosci* 31: 1885 – 1894

Cenik B, Sephton CF, Kutluk Cenik B, Herz J, Yu G (2012) Progranulin: a proteolytically processed protein at the crossroads of inflammation and neurodegeneration. *J Biol Chem* 287: 32298 – 32306

Chang MC, Srinivasan K, Friedman BA, Suto E, Modrusan Z, Lee WP, Kaminker JS, Hansen DV, Sheng M (2017) Progranulin deficiency causes impairment of autophagy and TDP-43 accumulation. *J Exp Med* 214: 2611 – 2628

Cruts M, Gijselinck I, van der Zee J, Engelborghs S, Wils H, Pirici D, Rademakers R, Vandenberghe R, Dermaut B, Martin JJ *et al* (2006) Null mutations in progranulin cause ubiquitin-positive frontotemporal dementia linked to chromosome 17q21. *Nature* 442: 920 – 924

Cruts M, Van Broeckhoven C (2008) Loss of progranulin function in frontotemporal lobar degeneration. *Trends Genet* 24: 186 – 194

Cuyvers E, Bettens K, Philtjens S, Van Langenhove T, Gijselinck I, van der Zee J, Engelborghs S, Vandenbulcke M, Van Dongen J, Geerts N *et al* (2014) Investigating the role of rare heterozygous TREM2 variants in Alzheimer's disease and frontotemporal dementia. *Neurobiol Aging* 35: 726 e711–729

Daria A, Colombo A, Llovera G, Hampel H, Willem M, Liesz A, Haass C, Tahirovic S (2017) Young microglia restore amyloid plaque clearance of aged microglia. *EMBO J* 36: 583 – 603

Deussing M, Blume T, Vomacka L, Mahler C, Focke C, Todica A, Unterrainer M, Albert NL, Lindner S, von Ungern-Sternberg B *et al* (2017) Coupling between physiological TSPO expression in brain and myocardium allows stabilization of late-phase cerebral [(18)F]GE180 PET quantification. *NeuroImage* 165: 83 – 91

Gosselin D, Skola D, Coufal NG, Holtman IR, Schlachetzki JCM, Sajti E, Jaeger BN, O'Connor C, Fitzpatrick C, Pasillas MP *et al* (2017) An environment-dependent transcriptional network specifies human microglia identity. *Science* 356: eaal3222

Gotzl JK, Mori K, Damme M, Fellerer K, Tahirovic S, Kleinberger G, Janssens J, van der Zee J, Lang CM, Kremmer E *et al* (2014) Common pathobiochemical hallmarks of progranulin-associated frontotemporal lobar degeneration and neuronal ceroid lipofuscinosis. *Acta Neuropathol* 127: 845 – 860

Gotzl JK, Lang CM, Haass C, Capell A (2016) Impaired protein degradation in FTLD and related disorders. *Ageing Res Rev* 32: 122 – 139

Gotzl JK, Colombo AV, Fellerer K, Reifschneider A, Werner G, Tahirovic S, Haass C, Capell A (2018) Early lysosomal maturation deficits in microglia triggers enhanced lysosomal activity in other brain cells of progranulin knockout mice. *Mol Neurodegener* 13: 48

Guerreiro RJ, Lohmann E, Bras JM, Gibbs JR, Rohrer JD, Gurunlian N, Dursun B, Bilgic B, Hanagasi H, Gurvit H *et al* (2013) Using exome sequencing to reveal mutations in TREM2 presenting as a frontotemporal dementia-like syndrome without bone involvement. *JAMA Neurol* 70: 78 – 84

Holtman IR, Raj DD, Miller JA, Schaafsma W, Yin Z, Brouwer N, Wes PD, Moller T, Orre M, Kamphuis W *et al* (2015) Induction of a common microglia gene expression signature by aging and neurodegenerative conditions: a co-expression meta-analysis. *Acta Neuropathol Commun* 3: 31

Hu F, Padukkavidana T, Vaegter CB, Brady OA, Zheng Y, Mackenzie IR, Feldman HH, Nykjaer A, Strittmatter SM (2010) Sortilin-mediated endocytosis determines levels of the frontotemporal dementia protein, progranulin. *Neuron* 68: 654 – 667

Jonsson T, Stefansson K (2013) TREM2 and neurodegenerative disease. *N Engl J Med* 369: 1568 – 1569

Jonsson T, Stefansson H, Steinberg S, Jonsdottir I, Jonsson PV, Snaedal J, Bjornsson S, Huttenlocher J, Levey AI, Lah JJ *et al* (2013) Variant of TREM2 associated with the risk of Alzheimer's disease. *N Engl J Med* 368: 107 – 116

Published online: May 23, 2019
EMBO Molecular Medicine *Julia K Götzl et al*

Kayasuga Y, Chiba S, Suzuki M, Kikusui T, Matsuwaki T, Yamanouchi K, Kotaki H, Horai R, Iwakura Y, Nishihara M (2007) Alteration of behavioural phenotype in mice by targeted disruption of the progranulin gene. *Behav Brain Res* 185: 110 – 118

Keren-Shaul H, Spinrad A, Weiner A, Matcovitch-Natan O, Dvir-Szternfeld R, Ulland TK, David E, Baruch K, Lara-Astaiso D, Toth B *et al* (2017) A unique microglia type associated with restricting development of Alzheimer's disease. *Cell* 169(1276–1290): e1217

Kim J, Eltorai AE, Jiang H, Liao F, Verghese PB, Kim J, Stewart FR, Basak JM, Holtzman DM (2012) Anti-apoE immunotherapy inhibits amyloid accumulation in a transgenic mouse model of Abeta amyloidosis. *J Exp Med* 209: 2149 – 2156

Kleinberger G, Yamanishi Y, Suarez-Calvet M, Czirr E, Lohmann E, Cuyvers E, Struyfs H, Pettkus N, Wenninger-Weinzierl A, Mazaheri F *et al* (2014) TREM2 mutations implicated in neurodegeneration impair cell surface transport and phagocytosis. *Sci Transl Med* 6: 243ra286

Kleinberger G, Brendel M, Mracsko E, Wefers B, Groeneweg L, Xiang X, Focke C, Deussing M, Suarez-Calvet M, Mazaheri F *et al* (2017) The FTD-like syndrome causing TREM2 T66M mutation impairs microglia function, brain perfusion, and glucose metabolism. *EMBO J* 36: 1837 – 1853

Krabbe G, Halle A, Matyash V, Rinnenthal JL, Eom GD, Bernhardt U, Miller KR, Prokop S, Kettenmann H, Heppner FL (2013) Functional impairment of microglia coincides with Beta-amyloid deposition in mice with Alzheimer-like pathology. *PLoS ONE* 8: e60921

Krasemann S, Madore C, Cialic R, Baufeld C, Calcagno N, El Fatimy R, Beckers L, O'Loughlin E, Xu Y, Fanek Z *et al* (2017) The TREM2-APOE pathway drives the transcriptional phenotype of dysfunctional microglia in neurodegenerative diseases. *Immunity* 47: 566 – 581 e569

Kremer LS, Bader DM, Mertes C, Kopajtich R, Pichler G, Iuso A, Haack TB, Graf E, Schwarzmayr T, Terrile C *et al* (2017) Genetic diagnosis of mendelian disorders via RNA sequencing. *Nat Commun* 8: 15824

Liu B, Le KX, Park MA, Wang S, Belanger AP, Dubey S, Frost JL, Holton P, Reiser V, Jones PA *et al* (2015) *In vivo* detection of age- and disease-related increases in neuroinflammation by 18F-GE180 TSPO microPET imaging in wild-type and Alzheimer's transgenic mice. *J Neurosci* 35: 15716 – 15730

Lui H, Zhang J, Makinson SR, Cahill MK, Kelley KW, Huang HY, Shang Y, Oldham MC, Martens LH, Gao F *et al* (2016) Progranulin deficiency promotes circuit-specific synaptic pruning by microglia via complement activation. *Cell* 165: 921 – 935

Martens LH, Zhang J, Barmada SJ, Zhou P, Kamiya S, Sun B, Min SW, Gan L, Finkbeiner S, Huang EJ *et al* (2012) Progranulin deficiency promotes neuroinflammation and neuron loss following toxin-induced injury. *J Clin Invest* 122: 3955 – 3959

Mazaheri F, Snaidero N, Kleinberger G, Madore C, Daria A, Werner G, Krasemann S, Capell A, Trumbach D, Wurst W *et al* (2017) TREM2 deficiency impairs chemotaxis and microglial responses to neuronal injury. *EMBO Rep* 18: 1186 – 1198

Mizrahi R, Rusjan PM, Kennedy J, Pollock B, Mulsant B, Suridjan I, De Luca V, Wilson AA, Houle S (2012) Translocator protein (18 kDa) polymorphism (rs6971) explains in-vivo brain binding affinity of the PET radioligand [(18) F]-FEPPA. *J Cereb Blood Flow Metab* 32: 968 – 972

Overhoff F, Brendel M, Jaworska A, Korzhova V, Delker A, Probst F, Focke C, Gildehaus FJ, Carlsen J, Baumann K *et al* (2016) Automated spatial brain normalization and hindbrain white matter reference tissue give improved [(18)F]-florbetaben pet quantitation in Alzheimer's model mice. *Front Neurosci* 10: 45

Owen DR, Yeo AJ, Gunn RN, Song K, Wadsworth G, Lewis A, Rhodes C, Pulford DJ, Bennacef I, Parker CA *et al* (2012) An 18-kDa translocator protein (TSPO) polymorphism explains differences in binding affinity of the PET radioligand PBR28. *J Cereb Blood Flow Metab* 32: 1 – 5

Parhizkar S, Arzberger T, Brendel M, Kleinberger G, Deussing M, Focke C, Nuscher B, Xiong M, Ghasemigharagoz A, Katzmarski N *et al* (2019) Loss of TREM2 function increases amyloid seeding but reduces plaque-associated ApoE. *Nat Neurosci* 22: 191 – 204

Radde R, Bolmont T, Kaeser SA, Coomaraswamy J, Lindau D, Stoltze L, Calhoun ME, Jaggi F, Wolburg H, Gengler S *et al* (2006) Abeta42-driven cerebral amyloidosis in transgenic mice reveals early and robust pathology. *EMBO Rep* 7: 940 – 946

Ran FA, Hsu PD, Wright J, Agarwala V, Scott DA, Zhang F (2013) Genome engineering using the CRISPR-Cas9 system. *Nat Protoc* 8: 2281 – 2308

Ransohoff RM (2016) How neuroinflammation contributes to neurodegeneration. *Science* 353: 777 – 783

Rayaprolu S, Mullen B, Baker M, Lynch T, Finger E, Seeley WW, Hatanpaa KJ, Lomen-Hoerth C, Kertesz A, Bigio EH *et al* (2013) TREM2 in neurodegeneration: evidence for association of the p.R47H variant with frontotemporal dementia and Parkinson's disease. *Mol Neurodegener* 8: 19

Rominger A, Brendel M, Burgold S, Keppler K, Baumann K, Xiong G, Mille E, Gildehaus FJ, Carlsen J, Schlichtiger J *et al* (2013) Longitudinal assessment of cerebral beta-amyloid deposition in mice overexpressing Swedish mutant beta-amyloid precursor protein using 18F-florbetaben PET. *J Nucl Med* 54: 1127 – 1134

Schlepckow K, Kleinberger G, Fukumori A, Feederle R, Lichtenthaler SF, Steiner H, Haass C (2017) An Alzheimer-associated TREM2 variant occurs at the ADAM cleavage site and affects shedding and phagocytic function. *EMBO Mol Med* 9: 1356 – 1365

Shoyab M, McDonald VL, Byles C, Todaro GJ, Plowman GD (1990) Epithelins 1 and 2: isolation and characterization of two cysteine-rich growth-modulating proteins. *Proc Natl Acad Sci USA* 87: 7912 – 7916

Song WM, Joshita S, Zhou Y, Ulland TK, Gilfillan S, Colonna M (2018) Humanized TREM2 mice reveal microglia-intrinsic and -extrinsic effects of R47H polymorphism. *J Exp Med* 215: 745 – 760

Takahashi H, Klein ZA, Bhagat SM, Kaufman AC, Kostylev MA, Ikezu T, Strittmatter SM, Alzheimer's Disease Neuroimaging I (2017) Opposing effects of progranulin deficiency on amyloid and tau pathologies via microglial TYROBP network. *Acta Neuropathol* 133: 785 – 807

Tanaka Y, Matsuwaki T, Yamanouchi K, Nishihara M (2013a) Exacerbated inflammatory responses related to activated microglia after traumatic brain injury in progranulin-deficient mice. *Neuroscience* 231: 49 – 60

Tanaka Y, Matsuwaki T, Yamanouchi K, Nishihara M (2013b) Increased lysosomal biogenesis in activated microglia and exacerbated neuronal damage after traumatic brain injury in progranulin-deficient mice. *Neuroscience* 250: 8 – 19

Turnbull IR, Gilfillan S, Cella M, Aoshi T, Miller M, Piccio L, Hernandez M, Colonna M (2006) Cutting edge: TREM-2 attenuates macrophage activation. *J Immunol* 177: 3520 – 3524

Ulland TK, Song WM, Huang SC, Ulrich JD, Sergushichev A, Beatty WL, Loboda AA, Zhou Y, Cairns NJ, Kambal A *et al* (2017) TREM2 maintains microglial metabolic fitness in Alzheimer's disease. *Cell* 170: 649 – 663 e613

Ulrich JD, Holtzman DM (2016) TREM2 function in Alzheimer's disease and neurodegeneration. *ACS Chem Neurosci* 7: 420 – 427

Ulrich JD, Ulland TK, Colonna M, Holtzman DM (2017) Elucidating the role of TREM2 in Alzheimer's disease. *Neuron* 94: 237 – 248

Published online: May 23, 2019

Van Damme P, Van Hoecke A, Lambrechts D, Vanacker P, Bogaert E, van Swieten J, Carmeliet P, Van Den Bosch L, Robberecht W (2008) Progranulin functions as a neurotrophic factor to regulate neurite outgrowth and enhance neuronal survival. *J Cell Biol* 181: 37 – 41

Wang Y, Cella M, Mallinson K, Ulrich JD, Young KL, Robinette ML, Gilfillan S, Krishnan GM, Sudhakar S, Zinselmeyer BH *et al* (2015) TREM2 lipid sensing sustains the microglial response in an Alzheimer's disease model. *Cell* 160: 1061 – 1071

Wang Y, Ulland TK, Ulrich JD, Song W, Tzaferis JA, Hole JT, Yuan P, Mahan TE, Shi Y, Gilfillan S *et al* (2016) TREM2-mediated early microglial response limits diffusion and toxicity of amyloid plaques. *J Exp Med* 213: 667 – 675

Ward ME, Chen R, Huang HY, Ludwig C, Telpoukhovskaia M, Taubes A, Boudin H, Minami SS, Reichert M, Albrecht P *et al* (2017) Individuals with progranulin haploinsufficiency exhibit features of neuronal ceroid lipofuscinosis. *Sci Transl Med* 9: eaah5642

Wils H, Kleinberger G, Pereson S, Janssens J, Capell A, Van Dam D, Cuijt I, Joris G, De Deyn PP, Haass C *et al* (2012) Cellular ageing, increased mortality and FTLD-TDP-associated neuropathology in progranulin knockout mice. *J Pathol* 228: 67 – 76

Xiang X, Werner G, Bohrmann B, Liesz A, Mazaheri F, Capell A, Feederle R, Knuesel I, Kleinberger G, Haass C (2016) TREM2 deficiency reduces the efficacy of immunotherapeutic amyloid clearance. *EMBO Mol Med* 8: 992 – 1004

Yeh FL, Wang Y, Tom I, Gonzalez LC, Sheng M (2016) TREM2 binds to apolipoproteins, including APOE and CLU/APOJ, and thereby facilitates uptake of amyloid-beta by microglia. *Neuron* 91: 328 – 340

Yeh FL, Hansen DV, Sheng M (2017) TREM2, microglia, and neurodegenerative diseases. *Trends Mol Med* 23: 512 – 533

Yin F, Banerjee R, Thomas B, Zhou P, Qian L, Jia T, Ma X, Ma Y, Iadecola C, Beal MF *et al* (2010) Exaggerated inflammation, impaired host defense, and neuropathology in progranulin-deficient mice. *J Exp Med* 207: 117 – 128

Zhang N, Yang N, Chen Q, Qiu F, Li X (2014) Upregulated expression level of the growth factor, progranulin, is associated with the development of primary Sjogren's syndrome. *Exp Ther Med* 8: 1643 – 1647

Zhou X, Sun L, Bastos de Oliveira F, Qi X, Brown WJ, Smolka MB, Sun Y, Hu F (2015) Prosaposin facilitates sortilin-independent lysosomal trafficking of progranulin. *J Cell Biol* 210: 991 – 1002

Zhou X, Sun L, Bracko O, Choi JW, Jia Y, Nana AL, Brady OA, Hernandez JCC, Nishimura N, Seeley WW *et al* (2017) Impaired prosaposin lysosomal trafficking in frontotemporal lobar degeneration due to progranulin mutations. *Nat Commun* 8: 15277

Expanded View Figures

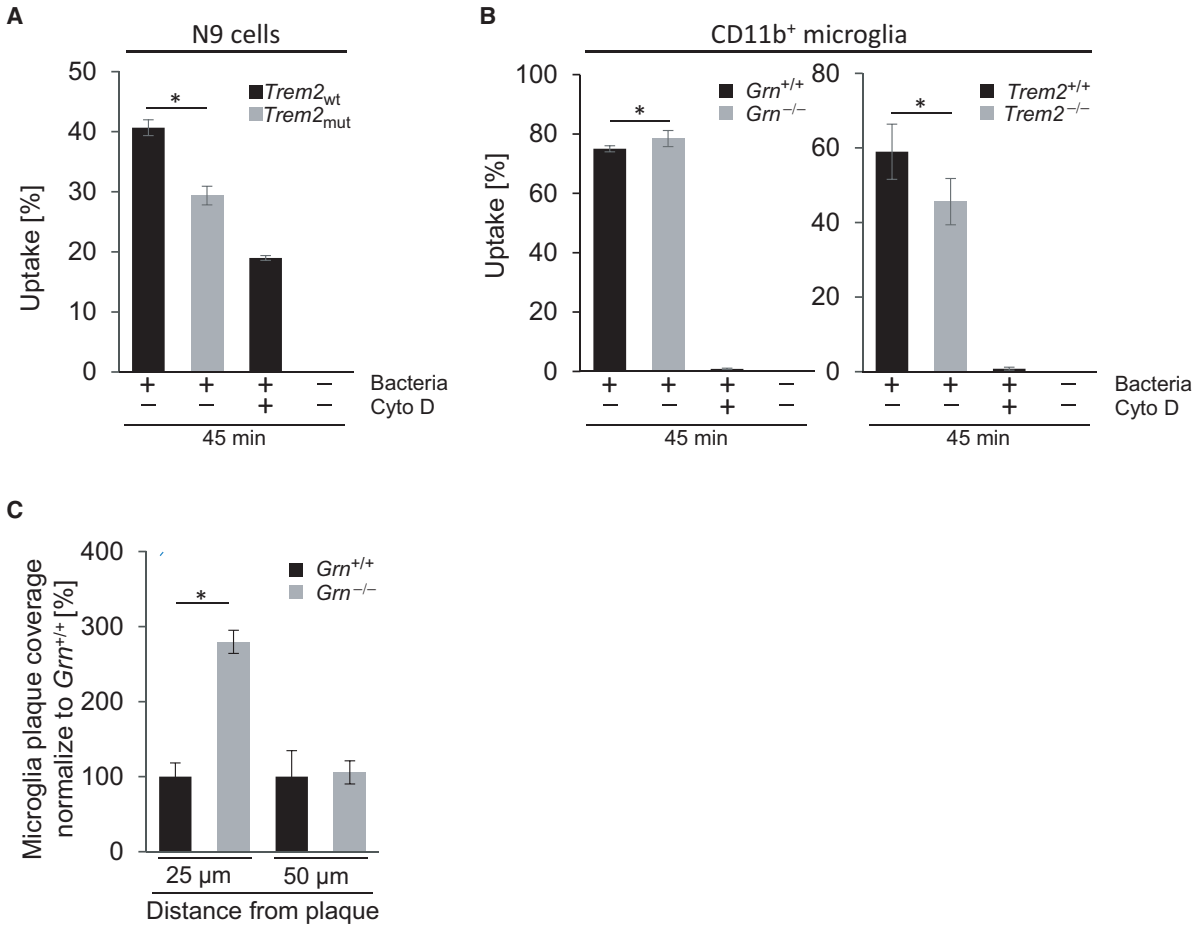

Figure EV1. Reduced phagocytosis upon TREM2 deficiency in contrast to enhanced phagocytosis and clustering around amyloid plaques in the absence of PGRN.

A Flow cytometric analysis of phagocytic capacity in N9 $Trem2_{wt}$ and N9 $Trem2_{mut}$ cells using pHrodo green *E. coli* as target particles. Phagocytosis was terminated after 45 min of incubation. Data are presented as mean percentage of cells positive for pHrodo uptake ± SD (n = 3).

B Flow cytometric analysis of phagocytic capacity of cultured primary microglia from wild-type, $Grn^{-/-}$, and $Trem2^{-/-}$ mice (2 months of age, male) using pHrodo green *E. coli* as target particles. Phagocytosis was terminated after 45 min of incubation. Left panel: Data are presented as mean percentage of $CD11b^+$ cells positive for pHrodo uptake ± SD (three biological replicates). Right panel: Data are presented as mean percentage of $CD11b^+$ cells positive for pHrodo uptake ± SD (two biological replicates).

C Percentage IBA1-positive microglia within given plaque distance quantified from immunohistochemical stainings shown in Fig 3E. Data are normalized to APPPS1/$Grn^{+/+}$ mice (n = 4; 4-month-old; two males and two females per genotype). Data are shown as mean ± SD.

Data information: For statistical analysis, unpaired two-tailed Student's t-test was performed (A, B) between TREM2 or PGRN-deficient microglia against wild-type microglia, and the Mann–Whitney U-test, two-tailed analysis (C) was performed between genotypes. Significance is indicated by $*P < 0.05$.

Source data are available online for this figure.

V. Literaturverzeichnis:

Adams, H. H., Verhaaren, B. F., Vrooman, H. A., Uitterlinden, A. G., Hofman, A., Van Duijn, C. M., Van Der Lugt, A., Niessen, W. J., Vernooij, M. W. & Ikram, M. A. 2014. TMEM106B Influences Volume of Left-Sided Temporal Lobe and Interhemispheric Structures in the General Population. *Biol Psychiatry,* 76**,** 503-508.

Ahmed, Z., Sheng, H., Xu, Y. F., Lin, W. L., Innes, A. E., Gass, J., Yu, X., Wuertzer, C. A., Hou, H., Chiba, S., Yamanouchi, K., Leissring, M., Petrucelli, L., Nishihara, M., Hutton, M. L., Mcgowan, E., Dickson, D. W. & Lewis, J. 2010. Accelerated lipofuscinosis and ubiquitination in granulin knockout mice suggest a role for progranulin in successful aging. *Am J Pathol,* 177**,** 311-24.

Alami, N. H., Smith, R. B., Carrasco, M. A., Williams, L. A., Winborn, C. S., Han, S. S. W., Kiskinis, E., Winborn, B., Freibaum, B. D., Kanagaraj, A., Clare, A. J., Badders, N. M., Bilican, B., Chaum, E., Chandran, S., Shaw, C. E., Eggan, K. C., Maniatis, T. & Taylor, J. P. 2014. Axonal transport of TDP-43 mRNA granules is impaired by ALS-causing mutations. *Neuron,* 81**,** 536-543.

Almeida, M. R., Macario, M. C., Ramos, L., Baldeiras, I., Ribeiro, M. H. & Santana, I. 2016. Portuguese family with the co-occurrence of frontotemporal lobar degeneration and neuronal ceroid lipofuscinosis phenotypes due to progranulin gene mutation. *Neurobiol Aging,* 41**,** 200 e1-5.

Andre, P., Groettrup, M., Klenerman, P., De Giuli, R., Booth, B. L., Jr., Cerundolo, V., Bonneville, M., Jotereau, F., Zinkernagel, R. M. & Lotteau, V. 1998. An inhibitor of HIV-1 protease modulates proteasome activity, antigen presentation, and T cell responses. *Proc Natl Acad Sci U S A,* 95**,** 13120-4.

Arai, T., Hasegawa, M., Akiyama, H., Ikeda, K., Nonaka, T., Mori, H., Mann, D., Tsuchiya, K., Yoshida, M., Hashizume, Y. & Oda, T. 2006. TDP-43 is a component of ubiquitin-positive tau-negative inclusions in frontotemporal lobar degeneration and amyotrophic lateral sclerosis. *Biochem Biophys Res Commun,* 351**,** 602-11.

Arrant, A. E., Filiano, A. J., Patel, A. R., Hoffmann, M. Q., Boyle, N. R., Kashyap, S. N., Onyilo, V. C., Young, A. H. & Roberson, E. D. 2019. Reduction of microglial progranulin does not exacerbate pathology or behavioral deficits in neuronal progranulin-insufficient mice. *Neurobiol Dis,* 124**,** 152-162.

Atagi, Y., Liu, C. C., Painter, M. M., Chen, X. F., Verbeeck, C., Zheng, H., Li, X., Rademakers, R., Kang, S. S., Xu, H., Younkin, S., Das, P., Fryer, J. D. & Bu, G. 2015. Apolipoprotein E Is a Ligand for Triggering Receptor Expressed on Myeloid Cells 2 (TREM2). *J Biol Chem,* 290**,** 26043-50.

Atkin, G. & Paulson, H. 2014. Ubiquitin pathways in neurodegenerative disease. *Front Mol Neurosci,* 7**,** 63.

Bailey, C. C., Devaux, L. B. & Farzan, M. 2015. The Triggering Receptor Expressed on Myeloid Cells 2 Binds Apolipoprotein E. *J Biol Chem,* 290**,** 26033-42.

Baker, M., Mackenzie, I. R., Pickering-Brown, S. M., Gass, J., Rademakers, R., Lindholm, C., Snowden, J., Adamson, J., Sadovnick, A. D., Rollinson, S., Cannon, A., Dwosh, E., Neary, D., Melquist, S., Richardson, A., Dickson, D., Berger, Z., Eriksen, J., Robinson, T., Zehr, C., Dickey, C. A., Crook, R., Mcgowan, E., Mann, D., Boeve, B., Feldman, H. & Hutton, M. 2006. Mutations in progranulin cause tau-negative frontotemporal dementia linked to chromosome 17. *Nature,* 442**,** 916-9.

Baralle, M., Buratti, E. & Baralle, F. E. 2013. The role of TDP-43 in the pathogenesis of ALS and FTLD. *Biochem Soc Trans,* 41**,** 1536-40.

Bateman, A., Belcourt, D., Bennett, H., Lazure, C. & Solomon, S. 1990. Granulins, a novel class of peptide from leukocytes. *Biochem Biophys Res Commun,* 173**,** 1161-8.

Bateman, A. & Bennett, H. P. 2009. The granulin gene family: from cancer to dementia. *Bioessays,* 31**,** 1245-54.

Beel, S., Herdewyn, S., Fazal, R., De Decker, M., Moisse, M., Robberecht, W., Van Den Bosch, L. & Van Damme, P. 2018. Progranulin reduces insoluble TDP-43 levels, slows down axonal degeneration and prolongs survival in mutant TDP-43 mice. *Mol Neurodegener,* 13**,** 55.

Beel, S., Moisse, M., Damme, M., De Muynck, L., Robberecht, W., Van Den Bosch, L., Saftig, P. & Van Damme, P. 2017. Progranulin functions as a cathepsin D chaperone to stimulate axonal outgrowth in vivo. *Hum Mol Genet,* 26**,** 2850-2863.

Bhandari, V., Palfree, R. G. & Bateman, A. 1992. Isolation and sequence of the granulin precursor cDNA from human bone marrow reveals tandem cysteine-rich granulin domains. *Proc Natl Acad Sci U S A,* 89**,** 1715-9.

Borroni, B., Ferrari, F., Galimberti, D., Nacmias, B., Barone, C., Bagnoli, S., Fenoglio, C., Piaceri, I., Archetti, S., Bonvicini, C., Gennarelli, M., Turla, M., Scarpini, E., Sorbi, S. & Padovani, A. 2014. Heterozygous TREM2 mutations in frontotemporal dementia. *Neurobiol Aging,* 35**,** 934 e7-10.

Brady, O. A., Zheng, Y., Murphy, K., Huang, M. & Hu, F. 2013. The frontotemporal lobar degeneration risk factor, TMEM106B, regulates lysosomal morphology and function. *Hum Mol Genet,* 22**,** 685-95.

Brendel, M., Kleinberger, G., Probst, F., Jaworska, A., Overhoff, F., Blume, T., Albert, N. L., Carlsen, J., Lindner, S., Gildehaus, F. J., Ozmen, L., Suarez-Calvet, M., Bartenstein, P., Baumann, K., Ewers, M., Herms, J., Haass, C. & Rominger, A. 2017. Increase of TREM2 during Aging of an Alzheimer's Disease Mouse Model Is Paralleled by Microglial Activation and Amyloidosis. *Front Aging Neurosci,* 9**,** eCollection 2017.

Brendel, M., Probst, F., Jaworska, A., Overhoff, F., Korzhova, V., Albert, N. L., Beck, R., Lindner, S., Gildehaus, F. J., Baumann, K., Bartenstein, P., Kleinberger, G., Haass, C., Herms, J. & Rominger, A. 2016. Glial Activation and Glucose Metabolism in a Transgenic Amyloid Mouse Model: A Triple-Tracer PET Study. *J Nucl Med,* 57**,** 954-60.

Briese, M., Saal-Bauernschubert, L., Luningschror, P., Moradi, M., Dombert, B., Surrey, V., Appenzeller, S., Deng, C., Jablonka, S. & Sendtner, M. 2020. Loss of Tdp-43 disrupts the axonal transcriptome of motoneurons accompanied by impaired axonal translation and mitochondria function. *Acta Neuropathol Commun,* 8**,** 116.

Bright, F., Werry, E. L., Dobson-Stone, C., Piguet, O., Ittner, L. M., Halliday, G. M., Hodges, J. R., Kiernan, M. C., Loy, C. T., Kassiou, M. & Kril, J. J. 2019. Neuroinflammation in frontotemporal dementia. *Nat Rev Neurol,* 15**,** 540-555.

Brouwers, N., Sleegers, K., Engelborghs, S., Maurer-Stroh, S., Gijselinck, I., Van Der Zee, J., Pickut, B. A., Van Den Broeck, M., Mattheijssens, M., Peeters, K., Schymkowitz, J., Rousseau, F., Martin, J. J., Cruts, M., De Deyn, P. P. & Van Broeckhoven, C. 2008. Genetic variability in progranulin contributes to risk for clinically diagnosed Alzheimer disease. *Neurology,* 71**,** 656-64.

Budini, M., Buratti, E., Morselli, E. & Criollo, A. 2017. Autophagy and Its Impact on Neurodegenerative Diseases: New Roles for TDP-43 and C9orf72. *Front Mol Neurosci,* 10**,** 170.

Buratti, E. & Baralle, F. E. 2008. Multiple roles of TDP-43 in gene expression, splicing regulation, and human disease. *Front Biosci,* 13**,** 867-78.

Busch, J. I., Martinez-Lage, M., Ashbridge, E., Grossman, M., Van Deerlin, V. M., Hu, F., Lee, V. M., Trojanowski, J. Q. & Chen-Plotkin, A. S. 2013. Expression of TMEM106B, the

frontotemporal lobar degeneration-associated protein, in normal and diseased human brain. *Acta Neuropathol Commun,* 1**,** 36.

Busch, J. I., Unger, T. L., Jain, N., Skrinak, R. T., Charan, R. A. & Chen-Plotkin, A. S. 2016. Increased expression of the frontotemporal dementia risk factor TMEM106B causes C9orf72-dependent alterations in lysosomes. *Hum Mol Genet,* 25**,** 2681-2697.

Butler, V. J., Cortopassi, W. A., Argouarch, A. R., Ivry, S. L., Craik, C. S., Jacobson, M. P. & Kao, A. W. 2019. Progranulin Stimulates the In Vitro Maturation of Pro-Cathepsin D at Acidic pH. *J Mol Biol,* 431**,** 1038-1047.

Butovsky, O., Jedrychowski, M. P., Cialic, R., Krasemann, S., Murugaiyan, G., Fanek, Z., Greco, D. J., Wu, P. M., Doykan, C. E., Kiner, O., Lawson, R. J., Frosch, M. P., Pochet, N., Fatimy, R. E., Krichevsky, A. M., Gygi, S. P., Lassmann, H., Berry, J., Cudkowicz, M. E. & Weiner, H. L. 2015. Targeting miR-155 restores abnormal microglia and attenuates disease in SOD1 mice. *Ann Neurol,* 77**,** 75-99.

Butovsky, O. & Weiner, H. L. 2018. Microglial signatures and their role in health and disease. *Nat Rev Neurosci,* 19**,** 622-635.

Cagnin, A., Rossor, M., Sampson, E. L., Mackinnon, T. & Banati, R. B. 2004. In vivo detection of microglial activation in frontotemporal dementia. *Ann Neurol,* 56**,** 894-7.

Capell, A., Liebscher, S., Fellerer, K., Brouwers, N., Willem, M., Lammich, S., Gijselinck, I., Bittner, T., Carlson, A. M., Sasse, F., Kunze, B., Steinmetz, H., Jansen, R., Dormann, D., Sleegers, K., Cruts, M., Herms, J., Van Broeckhoven, C. & Haass, C. 2011. Rescue of progranulin deficiency associated with frontotemporal lobar degeneration by alkalizing reagents and inhibition of vacuolar ATPase. *J Neurosci,* 31**,** 1885-94.

Castaneda, J. A., Lim, M. J., Cooper, J. D. & Pearce, D. A. 2008. Immune system irregularities in lysosomal storage disorders. *Acta Neuropathol,* 115**,** 159-74.

Casterton, R. L., Hunt, R. J. & Fanto, M. 2020. Pathomechanism Heterogeneity in the Amyotrophic Lateral Sclerosis and Frontotemporal Dementia Disease Spectrum: Providing Focus Through the Lens of Autophagy. *J Mol Biol,* 432**,** 2692-2713.

Chang, M. C., Srinivasan, K., Friedman, B. A., Suto, E., Modrusan, Z., Lee, W. P., Kaminker, J. S., Hansen, D. V. & Sheng, M. 2017. Progranulin deficiency causes impairment of autophagy and TDP-43 accumulation. *J Exp Med,* 214**,** 2611-2628.

Chow, C. Y., Landers, J. E., Bergren, S. K., Sapp, P. C., Grant, A. E., Jones, J. M., Everett, L., Lenk, G. M., Mckenna-Yasek, D. M., Weisman, L. S., Figlewicz, D., Brown, R. H. & Meisler, M. H. 2009. Deleterious variants of FIG4, a phosphoinositide phosphatase, in patients with ALS. *Am J Hum Genet,* 84**,** 85-8.

Ciechanover, A. & Kwon, Y. T. 2015. Degradation of misfolded proteins in neurodegenerative diseases: therapeutic targets and strategies. *Exp Mol Med,* 47**,** e147.

Cignarella, F., Filipello, F., Bollman, B., Cantoni, C., Locca, A., Mikesell, R., Manis, M., Ibrahim, A., Deng, L., Benitez, B. A., Cruchaga, C., Licastro, D., Mihindukulasuriya, K., Harari, O., Buckland, M., Holtzman, D. M., Rosenthal, A., Schwabe, T., Tassi, I. & Piccio, L. 2020. TREM2 activation on microglia promotes myelin debris clearance and remyelination in a model of multiple sclerosis. *Acta Neuropathol,* 140**,** 513-534.

Cirulli, E. T., Lasseigne, B. N., Petrovski, S., Sapp, P. C., Dion, P. A., Leblond, C. S., Couthouis, J., Lu, Y. F., Wang, Q., Krueger, B. J., Ren, Z., Keebler, J., Han, Y., Levy, S. E., Boone, B. E., Wimbish, J. R., Waite, L. L., Jones, A. L., Carulli, J. P., Day-Williams, A. G., Staropoli, J. F., Xin, W. W., Chesi, A., Raphael, A. R., Mckenna-Yasek, D., Cady, J., Vianney De Jong, J. M., Kenna, K. P., Smith, B. N., Topp, S., Miller, J., Gkazi, A., Consortium, F. S., Al-Chalabi, A., Van Den Berg, L. H., Veldink, J., Silani, V., Ticozzi, N., Shaw, C. E., Baloh, R. H., Appel, S., Simpson, E., Lagier-Tourenne, C., Pulst, S. M., Gibson, S., Trojanowski, J. Q., Elman, L., Mccluskey, L., Grossman, M., Shneider, N. A., Chung, W. K., Ravits, J. M., Glass, J. D., Sims, K. B., Van Deerlin, V. M., Maniatis, T., Hayes, S. D., Ordureau, A., Swarup, S., Landers, J.,

Baas, F., Allen, A. S., Bedlack, R. S., Harper, J. W., Gitler, A. D., Rouleau, G. A., Brown, R., Harms, M. B., Cooper, G. M., Harris, T., Myers, R. M. & Goldstein, D. B. 2015. Exome sequencing in amyotrophic lateral sclerosis identifies risk genes and pathways. *Science,* 347**,** 1436-41.

Cruchaga, C., Graff, C., Chiang, H. H., Wang, J., Hinrichs, A. L., Spiegel, N., Bertelsen, S., Mayo, K., Norton, J. B., Morris, J. C. & Goate, A. 2011. Association of TMEM106B gene polymorphism with age at onset in granulin mutation carriers and plasma granulin protein levels. *Arch Neurol,* 68**,** 581-6.

Cruts, M., Gijselinck, I., Van Der Zee, J., Engelborghs, S., Wils, H., Pirici, D., Rademakers, R., Vandenberghe, R., Dermaut, B., Martin, J. J., Van Duijn, C., Peeters, K., Sciot, R., Santens, P., De Pooter, T., Mattheijssens, M., Van Den Broeck, M., Cuijt, I., Vennekens, K., De Deyn, P. P., Kumar-Singh, S. & Van Broeckhoven, C. 2006. Null mutations in progranulin cause ubiquitin-positive frontotemporal dementia linked to chromosome 17q21. *Nature,* 442**,** 920-4.

Cuyvers, E., Bettens, K., Philtjens, S., Van Langenhove, T., Gijselinck, I., Van Der Zee, J., Engelborghs, S., Vandenbulcke, M., Van Dongen, J., Geerts, N., Maes, G., Mattheijssens, M., Peeters, K., Cras, P., Vandenberghe, R., De Deyn, P. P., Van Broeckhoven, C., Cruts, M., Sleegers, K. & Consortium, B. 2014. Investigating the role of rare heterozygous TREM2 variants in Alzheimer's disease and frontotemporal dementia. *Neurobiol Aging,* 35**,** 726 e11-9.

Dalakas, M. C., Alexopoulos, H. & Spaeth, P. J. 2020. Complement in neurological disorders and emerging complement-targeted therapeutics. *Nat Rev Neurol,* 16**,** 601-617.

Dancourt, J. & Melia, T. J. 2014. Lipidation of the autophagy proteins LC3 and GABARAP is a membrane-curvature dependent process. *Autophagy,* 10**,** 1470-1.

Darios, F. & Stevanin, G. 2020. Impairment of Lysosome Function and Autophagy in Rare Neurodegenerative Diseases. *J Mol Biol,* 432**,** 2714-2734.

Deczkowska, A., Keren-Shaul, H., Weiner, A., Colonna, M., Schwartz, M. & Amit, I. 2018. Disease-Associated Microglia: A Universal Immune Sensor of Neurodegeneration. *Cell,* 173**,** 1073-1081.

Dejesus-Hernandez, M., Mackenzie, I. R., Boeve, B. F., Boxer, A. L., Baker, M., Rutherford, N. J., Nicholson, A. M., Finch, N. A., Flynn, H., Adamson, J., Kouri, N., Wojtas, A., Sengdy, P., Hsiung, G. Y., Karydas, A., Seeley, W. W., Josephs, K. A., Coppola, G., Geschwind, D. H., Wszolek, Z. K., Feldman, H., Knopman, D. S., Petersen, R. C., Miller, B. L., Dickson, D. W., Boylan, K. B., Graff-Radford, N. R. & Rademakers, R. 2011. Expanded GGGGCC hexanucleotide repeat in noncoding region of C9ORF72 causes chromosome 9p-linked FTD and ALS. *Neuron,* 72**,** 245-56.

Deming, Y. & Cruchaga, C. 2014. TMEM106B: a strong FTLD disease modifier. *Acta Neuropathol,* 127**,** 419-22.

Dong, Y., D'mello, C., Pinsky, W., Lozinski, B. M., Kaushik, D. K., Ghorbani, S., Moezzi, D., Brown, D., Melo, F. C., Zandee, S., Vo, T., Prat, A., Whitehead, S. N. & Yong, V. W. 2021. Oxidized phosphatidylcholines found in multiple sclerosis lesions mediate neurodegeneration and are neutralized by microglia. *Nat Neurosci,* 24**,** 489-503.

Dooley, H. C., Razi, M., Polson, H. E., Girardin, S. E., Wilson, M. I. & Tooze, S. A. 2014. WIPI2 links LC3 conjugation with PI3P, autophagosome formation, and pathogen clearance by recruiting Atg12-5-16L1. *Mol Cell,* 55**,** 238-52.

Dormann, D., Capell, A., Carlson, A. M., Shankaran, S. S., Rodde, R., Neumann, M., Kremmer, E., Matsuwaki, T., Yamanouchi, K., Nishihara, M. & Haass, C. 2009. Proteolytic processing of TAR DNA binding protein-43 by caspases produces C-terminal fragments with disease defining properties independent of progranulin. *J Neurochem,* 110**,** 1082-94.

Eikelenboom, P. & Stam, F. C. 1982. Immunoglobulins and complement factors in senile plaques. An immunoperoxidase study. *Acta Neuropathol,* 57**,** 239-42.

Epelman, S., Lavine, K. J. & Randolph, G. J. 2014. Origin and functions of tissue macrophages. *Immunity,* 41**,** 21-35.

Eskelinen, E. L. 2006. Roles of LAMP-1 and LAMP-2 in lysosome biogenesis and autophagy. *Mol Aspects Med,* 27**,** 495-502.

Farias, G. G., Guardia, C. M., De Pace, R., Britt, D. J. & Bonifacino, J. S. 2017. BORC/kinesin-1 ensemble drives polarized transport of lysosomes into the axon. *Proc Natl Acad Sci U S A,* 114**,** E2955-E2964.

Feng, T., Lacrampe, A. & Hu, F. 2021. Physiological and pathological functions of TMEM106B: a gene associated with brain aging and multiple brain disorders. *Acta Neuropathol,* 141**,** 327-339.

Feng, T., Sheng, R. R., Sole-Domenech, S., Ullah, M., Zhou, X., Mendoza, C. S., Enriquez, L. C. M., Katz, Ii, Paushter, D. H., Sullivan, P. M., Wu, X., Maxfield, F. R. & Hu, F. 2020. A role of the frontotemporal lobar degeneration risk factor TMEM106B in myelination. *Brain,* 143**,** 2255-2271.

Ferrari, R., Manzoni, C. & Hardy, J. 2019. Genetics and molecular mechanisms of frontotemporal lobar degeneration: an update and future avenues. *Neurobiol Aging,* 78**,** 98-110.

Filimonenko, M., Stuffers, S., Raiborg, C., Yamamoto, A., Malerod, L., Fisher, E. M., Isaacs, A., Brech, A., Stenmark, H. & Simonsen, A. 2007. Functional multivesicular bodies are required for autophagic clearance of protein aggregates associated with neurodegenerative disease. *J Cell Biol,* 179**,** 485-500.

Finch, N., Carrasquillo, M. M., Baker, M., Rutherford, N. J., Coppola, G., Dejesus-Hernandez, M., Crook, R., Hunter, T., Ghidoni, R., Benussi, L., Crook, J., Finger, E., Hantanpaa, K. J., Karydas, A. M., Sengdy, P., Gonzalez, J., Seeley, W. W., Johnson, N., Beach, T. G., Mesulam, M., Forloni, G., Kertesz, A., Knopman, D. S., Uitti, R., White, C. L., 3rd, Caselli, R., Lippa, C., Bigio, E. H., Wszolek, Z. K., Binetti, G., Mackenzie, I. R., Miller, B. L., Boeve, B. F., Younkin, S. G., Dickson, D. W., Petersen, R. C., Graff-Radford, N. R., Geschwind, D. H. & Rademakers, R. 2011. TMEM106B regulates progranulin levels and the penetrance of FTLD in GRN mutation carriers. *Neurology,* 76**,** 467-74.

Forman, M. S., Farmer, J., Johnson, J. K., Clark, C. M., Arnold, S. E., Coslett, H. B., Chatterjee, A., Hurtig, H. I., Karlawish, J. H., Rosen, H. J., Van Deerlin, V., Lee, V. M., Miller, B. L., Trojanowski, J. Q. & Grossman, M. 2006. Frontotemporal dementia: clinicopathological correlations. *Ann Neurol,* 59**,** 952-62.

Foster, A. D. & Rea, S. L. 2020. The role of sequestosome 1/p62 protein in amyotrophic lateral sclerosis and frontotemporal dementia pathogenesis. *Neural Regen Res,* 15**,** 2186-2194.

Frakes, A. E., Ferraiuolo, L., Haidet-Phillips, A. M., Schmelzer, L., Braun, L., Miranda, C. J., Ladner, K. J., Bevan, A. K., Foust, K. D., Godbout, J. P., Popovich, P. G., Guttridge, D. C. & Kaspar, B. K. 2014. Microglia induce motor neuron death via the classical NF-kappaB pathway in amyotrophic lateral sclerosis. *Neuron,* 81**,** 1009-1023.

Gallagher, M. D., Posavi, M., Huang, P., Unger, T. L., Berlyand, Y., Gruenewald, A. L., Chesi, A., Manduchi, E., Wells, A. D., Grant, S. F. A., Blobel, G. A., Brown, C. D. & Chen-Plotkin, A. S. 2017. A Dementia-Associated Risk Variant near TMEM106B Alters Chromatin Architecture and Gene Expression. *Am J Hum Genet,* 101**,** 643-663.

Gallagher, M. D., Suh, E., Grossman, M., Elman, L., Mccluskey, L., Van Swieten, J. C., Al-Sarraj, S., Neumann, M., Gelpi, E., Ghetti, B., Rohrer, J. D., Halliday, G., Van Broeckhoven, C., Seilhean, D., Shaw, P. J., Frosch, M. P., Alafuzoff, I., Antonell, A., Bogdanovic, N., Brooks, W., Cairns, N. J., Cooper-Knock, J., Cotman, C., Cras, P., Cruts, M., De Deyn, P. P., Decarli, C., Dobson-Stone, C., Engelborghs, S., Fox, N., Galasko, D., Gearing, M., Gijselinck, I., Grafman, J., Hartikainen, P., Hatanpaa, K. J.,

Highley, J. R., Hodges, J., Hulette, C., Ince, P. G., Jin, L. W., Kirby, J., Kofler, J., Kril, J., Kwok, J. B., Levey, A., Lieberman, A., Llado, A., Martin, J. J., Masliah, E., Mcdermott, C. J., Mckee, A., Mclean, C., Mead, S., Miller, C. A., Miller, J., Munoz, D. G., Murrell, J., Paulson, H., Piguet, O., Rossor, M., Sanchez-Valle, R., Sano, M., Schneider, J., Silbert, L. C., Spina, S., Van Der Zee, J., Van Langenhove, T., Warren, J., Wharton, S. B., White, C. L., 3rd, Woltjer, R. L., Trojanowski, J. Q., Lee, V. M., Van Deerlin, V. & Chen-Plotkin, A. S. 2014. TMEM106B is a genetic modifier of frontotemporal lobar degeneration with C9orf72 hexanucleotide repeat expansions. *Acta Neuropathol,* 127**,** 407-18.

Gass, J., Cannon, A., Mackenzie, I. R., Boeve, B., Baker, M., Adamson, J., Crook, R., Melquist, S., Kuntz, K., Petersen, R., Josephs, K., Pickering-Brown, S. M., Graff-Radford, N., Uitti, R., Dickson, D., Wszolek, Z., Gonzalez, J., Beach, T. G., Bigio, E., Johnson, N., Weintraub, S., Mesulam, M., White, C. L., 3rd, Woodruff, B., Caselli, R., Hsiung, G. Y., Feldman, H., Knopman, D., Hutton, M. & Rademakers, R. 2006. Mutations in progranulin are a major cause of ubiquitin-positive frontotemporal lobar degeneration. *Hum Mol Genet,* 15**,** 2988-3001.

Glock, C., Heumüller, M. & Schuman, E. M. 2017. mRNA transport & local translation in neurons. *Curr Opin Neurobiol,* 45**,** 169-177.

Götzl, J. K., Brendel, M., Werner, G., Parhizkar, S., Sebastian Monasor, L., Kleinberger, G., Colombo, A. V., Deussing, M., Wagner, M., Winkelmann, J., Diehl-Schmid, J., Levin, J., Fellerer, K., Reifschneider, A., Bultmann, S., Bartenstein, P., Rominger, A., Tahirovic, S., Smith, S. T., Madore, C., Butovsky, O., Capell, A. & Haass, C. 2019. Opposite microglial activation stages upon loss of PGRN or TREM2 result in reduced cerebral glucose metabolism. *EMBO Mol Med,* 11**,** e9711.

Götzl, J. K., Colombo, A. V., Fellerer, K., Reifschneider, A., Werner, G., Tahirovic, S., Haass, C. & Capell, A. 2018. Early lysosomal maturation deficits in microglia triggers enhanced lysosomal activity in other brain cells of progranulin knockout mice. *Mol Neurodegener,* 13**,** 48.

Götzl, J. K., Mori, K., Damme, M., Fellerer, K., Tahirovic, S., Kleinberger, G., Janssens, J., Van Der Zee, J., Lang, C. M., Kremmer, E., Martin, J. J., Engelborghs, S., Kretzschmar, H. A., Arzberger, T., Van Broeckhoven, C., Haass, C. & Capell, A. 2014. Common pathobiochemical hallmarks of progranulin-associated frontotemporal lobar degeneration and neuronal ceroid lipofuscinosis. *Acta Neuropathol,* 127**,** 845-60.

Greaves, C. V. & Rohrer, J. D. 2019. An update on genetic frontotemporal dementia. *J Neurol,* 266**,** 2075-2086.

Guerreiro, R., Bras, J. & Hardy, J. 2015. SnapShot: Genetics of ALS and FTD. *Cell,* 160**,** 798-798 e1.

Guerreiro, R., Wojtas, A., Bras, J., Carrasquillo, M., Rogaeva, E., Majounie, E., Cruchaga, C., Sassi, C., Kauwe, J. S., Younkin, S., Hazrati, L., Collinge, J., Pocock, J., Lashley, T., Williams, J., Lambert, J. C., Amouyel, P., Goate, A., Rademakers, R., Morgan, K., Powell, J., St George-Hyslop, P., Singleton, A., Hardy, J. & Alzheimer Genetic Analysis, G. 2013a. TREM2 variants in Alzheimer's disease. *N Engl J Med,* 368**,** 117-27.

Guerreiro, R. J., Lohmann, E., Bras, J. M., Gibbs, J. R., Rohrer, J. D., Gurunlian, N., Dursun, B., Bilgic, B., Hanagasi, H., Gurvit, H., Emre, M., Singleton, A. & Hardy, J. 2013b. Using exome sequencing to reveal mutations in TREM2 presenting as a frontotemporal dementia-like syndrome without bone involvement. *JAMA Neurol,* 70**,** 78-84.

Guo, A., Tapia, L., Bamji, S. X., Cynader, M. S. & Jia, W. 2010. Progranulin deficiency leads to enhanced cell vulnerability and TDP-43 translocation in primary neuronal cultures. *Brain Res,* 1366**,** 1-8.

Guo, Q., Lehmer, C., Martinez-Sanchez, A., Rudack, T., Beck, F., Hartmann, H., Perez-Berlanga, M., Frottin, F., Hipp, M. S., Hartl, F. U., Edbauer, D., Baumeister, W. & Fernandez-Busnadiego, R. 2018. In Situ Structure of Neuronal C9orf72 Poly-GA Aggregates Reveals Proteasome Recruitment. *Cell,* 172**,** 696-705 e12.

Haack, T. B., Ignatius, E., Calvo-Garrido, J., Iuso, A., Isohanni, P., Maffezzini, C., Lonnqvist, T., Suomalainen, A., Gorza, M., Kremer, L. S., Graf, E., Hartig, M., Berutti, R., Paucar, M., Svenningsson, P., Stranneheim, H., Brandberg, G., Wedell, A., Kurian, M. A., Hayflick, S. A., Venco, P., Tiranti, V., Strom, T. M., Dichgans, M., Horvath, R., Holinski-Feder, E., Freyer, C., Meitinger, T., Prokisch, H., Senderek, J., Wredenberg, A., Carroll, C. J. & Klopstock, T. 2016. Absence of the Autophagy Adaptor SQSTM1/p62 Causes Childhood-Onset Neurodegeneration with Ataxia, Dystonia, and Gaze Palsy. *Am J Hum Genet,* 99**,** 735-743.

Hafler, B. P., Klein, Z. A., Jimmy Zhou, Z. & Strittmatter, S. M. 2014. Progressive retinal degeneration and accumulation of autofluorescent lipopigments in Progranulin deficient mice. *Brain Res,* 1588**,** 168-74.

Hakola, H. P., Järvi, O. H. & Sourander, P. 1970. Osteodysplasia polycystica hereditaria combined with sclerosing leucoencephalopathy, a new entity of the dementia praesenilis group. *Acta Neurol Scand,* 46**,** 79-80.

Hammond, T. R., Dufort, C., Dissing-Olesen, L., Giera, S., Young, A., Wysoker, A., Walker, A. J., Gergits, F., Segel, M., Nemesh, J., Marsh, S. E., Saunders, A., Macosko, E., Ginhoux, F., Chen, J., Franklin, R. J. M., Piao, X., Mccarroll, S. A. & Stevens, B. 2019. Single-Cell RNA Sequencing of Microglia throughout the Mouse Lifespan and in the Injured Brain Reveals Complex Cell-State Changes. *Immunity,* 50**,** 253-271 e6.

Harding, S. R., Bocchetta, M., Gordon, E., Cash, D. M., Cardoso, M. J., Druyeh, R., Ourselin, S., Warren, J. D., Mead, S. & Rohrer, J. D. 2017. The TMEM106B risk allele is associated with lower cortical volumes in a clinically diagnosed frontotemporal dementia cohort. *J Neurol Neurosurg Psychiatry,* 88**,** 997-998.

Harvey, R. J., Skelton-Robinson, M. & Rossor, M. N. 2003. The prevalence and causes of dementia in people under the age of 65 years. *J Neurol Neurosurg Psychiatry,* 74**,** 1206-9.

Hasegawa, M., Arai, T., Nonaka, T., Kametani, F., Yoshida, M., Hashizume, Y., Beach, T. G., Buratti, E., Baralle, F., Morita, M., Nakano, I., Oda, T., Tsuchiya, K. & Akiyama, H. 2008. Phosphorylated TDP-43 in frontotemporal lobar degeneration and amyotrophic lateral sclerosis. *Ann Neurol,* 64**,** 60-70.

Herskowitz, J. H., Gozal, Y. M., Duong, D. M., Dammer, E. B., Gearing, M., Ye, K., Lah, J. J., Peng, J., Levey, A. I. & Seyfried, N. T. 2012. Asparaginyl endopeptidase cleaves TDP-43 in brain. *Proteomics,* 12**,** 2455-63.

Hickman, S., Izzy, S., Sen, P., Morsett, L. & El Khoury, J. 2018. Microglia in neurodegeneration. *Nat Neurosci,* 21**,** 1359-1369.

Hogan, D. B., Jette, N., Fiest, K. M., Roberts, J. I., Pearson, D., Smith, E. E., Roach, P., Kirk, A., Pringsheim, T. & Maxwell, C. J. 2016. The Prevalence and Incidence of Frontotemporal Dementia: a Systematic Review. *Can J Neurol Sci,* 43 Suppl 1**,** S96-S109.

Hokkanen, S. R. K., Kero, M., Kaivola, K., Hunter, S., Keage, H. a. D., Kiviharju, A., Raunio, A., Tienari, P. J., Paetau, A., Matthews, F. E., Fleming, J., Graff, C., Polvikoski, T. M., Myllykangas, L., Brayne, C. & Collaboration, E. C. 2020. Putative risk alleles for LATE-NC with hippocampal sclerosis in population-representative autopsy cohorts. *Brain Pathol,* 30**,** 364-372.

Holler, C. J., Taylor, G., Deng, Q. & Kukar, T. 2017. Intracellular Proteolysis of Progranulin Generates Stable, Lysosomal Granulins that Are Haploinsufficient in Patients with Frontotemporal Dementia Caused by GRN Mutations. *eNeuro,* 4.

Hong, S., Beja-Glasser, V. F., Nfonoyim, B. M., Frouin, A., Li, S., Ramakrishnan, S., Merry, K. M., Shi, Q., Rosenthal, A., Barres, B. A., Lemere, C. A., Selkoe, D. J. & Stevens, B. 2016. Complement and microglia mediate early synapse loss in Alzheimer mouse models. *Science,* 352**,** 712-716.

Hosokawa, N., Sasaki, T., Iemura, S., Natsume, T., Hara, T. & Mizushima, N. 2009. Atg101, a novel mammalian autophagy protein interacting with Atg13. *Autophagy,* 5**,** 973-9.

Hu, F., Padukkavidana, T., Vaegter, C. B., Brady, O. A., Zheng, Y., Mackenzie, I. R., Feldman, H. H., Nykjaer, A. & Strittmatter, S. M. 2010. Sortilin-mediated endocytosis determines levels of the frontotemporal dementia protein, progranulin. *Neuron,* 68**,** 654-67.

Huang, M., Modeste, E., Dammer, E., Merino, P., Taylor, G., Duong, D. M., Deng, Q., Holler, C. J., Gearing, M., Dickson, D., Seyfried, N. T. & Kukar, T. 2020. Network analysis of the progranulin-deficient mouse brain proteome reveals pathogenic mechanisms shared in human frontotemporal dementia caused by GRN mutations. *Acta Neuropathol Commun,* 8**,** 163.

Huber, E. M., Basler, M., Schwab, R., Heinemeyer, W., Kirk, C. J., Groettrup, M. & Groll, M. 2012. Immuno- and constitutive proteasome crystal structures reveal differences in substrate and inhibitor specificity. *Cell,* 148**,** 727-38.

Hunt, S. E., Mclaren, W., Gil, L., Thormann, A., Schuilenburg, H., Sheppard, D., Parton, A., Armean, I. M., Trevanion, S. J., Flicek, P. & Cunningham, F. 2018. Ensembl variation resources. *Database (Oxford),* 2018.

Ito, Y., Hartley, T., Baird, S., Venkateswaran, S., Simons, C., Wolf, N. I., Boycott, K. M., Dyment, D. A. & Kernohan, K. D. 2018. Lysosomal dysfunction in TMEM106B hypomyelinating leukodystrophy. *Neurol Genet,* 4**,** e288.

Jian, J., Tian, Q. Y., Hettinghouse, A., Zhao, S., Liu, H., Wei, J., Grunig, G., Zhang, W., Setchell, K. D. R., Sun, Y., Overkleeft, H. S., Chan, G. L. & Liu, C. J. 2016. Progranulin Recruits HSP70 to beta-Glucocerebrosidase and Is Therapeutic Against Gaucher Disease. *EBioMedicine,* 13**,** 212-224.

Jonsson, T., Stefansson, H., Steinberg, S., Jonsdottir, I., Jonsson, P. V., Snaedal, J., Bjornsson, S., Huttenlocher, J., Levey, A. I., Lah, J. J., Rujescu, D., Hampel, H., Giegling, I., Andreassen, O. A., Engedal, K., Ulstein, I., Djurovic, S., Ibrahim-Verbaas, C., Hofman, A., Ikram, M. A., Van Duijn, C. M., Thorsteinsdottir, U., Kong, A. & Stefansson, K. 2013. Variant of TREM2 associated with the risk of Alzheimer's disease. *N Engl J Med,* 368**,** 107-16.

Josephs, K. A., Murray, M. E., Tosakulwong, N., Weigand, S. D., Serie, A. M., Perkerson, R. B., Matchett, B. J., Jack, C. R., Jr., Knopman, D. S., Petersen, R. C., Parisi, J. E., Petrucelli, L., Baker, M., Rademakers, R., Whitwell, J. L. & Dickson, D. W. 2019. Pathological, imaging and genetic characteristics support the existence of distinct TDP-43 types in non-FTLD brains. *Acta Neuropathol,* 137**,** 227-238.

Jun, G., Ibrahim-Verbaas, C. A., Vronskaya, M., Lambert, J. C., Chung, J., Naj, A. C., Kunkle, B. W., Wang, L. S., Bis, J. C., Bellenguez, C., Harold, D., Lunetta, K. L., Destefano, A. L., Grenier-Boley, B., Sims, R., Beecham, G. W., Smith, A. V., Chouraki, V., Hamilton-Nelson, K. L., Ikram, M. A., Fievet, N., Denning, N., Martin, E. R., Schmidt, H., Kamatani, Y., Dunstan, M. L., Valladares, O., Laza, A. R., Zelenika, D., Ramirez, A., Foroud, T. M., Choi, S. H., Boland, A., Becker, T., Kukull, W. A., Van Der Lee, S. J., Pasquier, F., Cruchaga, C., Beekly, D., Fitzpatrick, A. L., Hanon, O., Gill, M., Barber, R., Gudnason, V., Campion, D., Love, S., Bennett, D. A., Amin, N., Berr, C., Tsolaki, M., Buxbaum, J. D., Lopez, O. L., Deramecourt, V., Fox, N. C., Cantwell, L. B., Tarraga, L., Dufouil, C., Hardy, J., Crane, P. K., Eiriksdottir, G., Hannequin, D., Clarke, R., Evans, D., Mosley, T. H., Jr., Letenneur, L., Brayne, C., Maier, W., De Jager, P., Emilsson, V., Dartigues, J. F., Hampel, H., Kamboh, M. I., De Bruijn, R. F., Tzourio, C., Pastor, P., Larson, E. B., Rotter, J. I., O'donovan, M. C., Montine, T. J., Nalls, M.

A., Mead, S., Reiman, E. M., Jonsson, P. V., Holmes, C., St George-Hyslop, P. H., Boada, M., Passmore, P., Wendland, J. R., Schmidt, R., Morgan, K., Winslow, A. R., Powell, J. F., Carasquillo, M., Younkin, S. G., Jakobsdottir, J., Kauwe, J. S., Wilhelmsen, K. C., Rujescu, D., Nothen, M. M., Hofman, A., et al. 2016. A novel Alzheimer disease locus located near the gene encoding tau protein. *Mol Psychiatry,* 21**,** 108-17.

Jun, M. H., Han, J. H., Lee, Y. K., Jang, D. J., Kaang, B. K. & Lee, J. A. 2015. TMEM106B, a frontotemporal lobar dementia (FTLD) modifier, associates with FTD-3-linked CHMP2B, a complex of ESCRT-III. *Mol Brain,* 8**,** 85.

Kaneko, M., Sano, K., Nakayama, J. & Amano, N. 2010. Nasu-Hakola disease: The first case reported by Nasu and review: The 50th Anniversary of Japanese Society of Neuropathology. *Neuropathology,* 30**,** 463-70.

Kang, S. S., Kurti, A., Baker, K. E., Liu, C. C., Colonna, M., Ulrich, J. D., Holtzman, D. M., Bu, G. & Fryer, J. D. 2018. Behavioral and transcriptomic analysis of Trem2-null mice: not all knockout mice are created equal. *Hum Mol Genet,* 27**,** 211-223.

Kawakami, I., Arai, T. & Hasegawa, M. 2019. The basis of clinicopathological heterogeneity in TDP-43 proteinopathy. *Acta Neuropathol,* 138**,** 751-770.

Keren-Shaul, H., Spinrad, A., Weiner, A., Matcovitch-Natan, O., Dvir-Szternfeld, R., Ulland, T. K., David, E., Baruch, K., Lara-Astaiso, D., Toth, B., Itzkovitz, S., Colonna, M., Schwartz, M. & Amit, I. 2017. A Unique Microglia Type Associated with Restricting Development of Alzheimer's Disease. *Cell,* 169**,** 1276-1290 e17.

Kim, J., Kundu, M., Viollet, B. & Guan, K. L. 2011. AMPK and mTOR regulate autophagy through direct phosphorylation of Ulk1. *Nat Cell Biol,* 13**,** 132-41.

Kim, S. H., Shi, Y., Hanson, K. A., Williams, L. M., Sakasai, R., Bowler, M. J. & Tibbetts, R. S. 2009. Potentiation of amyotrophic lateral sclerosis (ALS)-associated TDP-43 aggregation by the proteasome-targeting factor, ubiquilin 1. *J Biol Chem,* 284**,** 8083-92.

Kimura, H., Caturegli, P., Takahashi, M. & Suzuki, K. 2015. New Insights into the Function of the Immunoproteasome in Immune and Nonimmune Cells. *J Immunol Res,* 2015**,** 541984.

Klein, Z. A., Takahashi, H., Ma, M., Stagi, M., Zhou, M., Lam, T. T. & Strittmatter, S. M. 2017. Loss of TMEM106B Ameliorates Lysosomal and Frontotemporal Dementia-Related Phenotypes in Progranulin-Deficient Mice. *Neuron,* 95**,** 281-296 e6.

Kleinberger, G., Brendel, M., Mracsko, E., Wefers, B., Groeneweg, L., Xiang, X., Focke, C., Deussing, M., Suarez-Calvet, M., Mazaheri, F., Parhizkar, S., Pettkus, N., Wurst, W., Feederle, R., Bartenstein, P., Mueggler, T., Arzberger, T., Knuesel, I., Rominger, A. & Haass, C. 2017. The FTD-like syndrome causing TREM2 T66M mutation impairs microglia function, brain perfusion, and glucose metabolism. *EMBO J,* 36**,** 1837-1853.

Kleinberger, G., Wils, H., Ponsaerts, P., Joris, G., Timmermans, J. P., Van Broeckhoven, C. & Kumar-Singh, S. 2010. Increased caspase activation and decreased TDP-43 solubility in progranulin knockout cortical cultures. *J Neurochem,* 115**,** 735-47.

Kleinberger, G., Yamanishi, Y., Suarez-Calvet, M., Czirr, E., Lohmann, E., Cuyvers, E., Struyfs, H., Pettkus, N., Wenninger-Weinzierl, A., Mazaheri, F., Tahirovic, S., Lleo, A., Alcolea, D., Fortea, J., Willem, M., Lammich, S., Molinuevo, J. L., Sanchez-Valle, R., Antonell, A., Ramirez, A., Heneka, M. T., Sleegers, K., Van Der Zee, J., Martin, J. J., Engelborghs, S., Demirtas-Tatlidede, A., Zetterberg, H., Van Broeckhoven, C., Gurvit, H., Wyss-Coray, T., Hardy, J., Colonna, M. & Haass, C. 2014. TREM2 mutations implicated in neurodegeneration impair cell surface transport and phagocytosis. *Sci Transl Med,* 6**,** 243ra86.

Klünemann, H. H., Ridha, B. H., Magy, L., Wherrett, J. R., Hemelsoet, D. M., Keen, R. W., De Bleecker, J. L., Rossor, M. N., Marienhagen, J., Klein, H. E., Peltonen, L. & Paloneva,

J. 2005. The genetic causes of basal ganglia calcification, dementia, and bone cysts: DAP12 and TREM2. *Neurology,* 64**,** 1502-7.

Kojima, Y., Ono, K., Inoue, K., Takagi, Y., Kikuta, K., Nishimura, M., Yoshida, Y., Nakashima, Y., Matsumae, H., Furukawa, Y., Mikuni, N., Nobuyoshi, M., Kimura, T., Kita, T. & Tanaka, M. 2009. Progranulin expression in advanced human atherosclerotic plaque. *Atherosclerosis,* 206**,** 102-8.

Krasemann, S., Madore, C., Cialic, R., Baufeld, C., Calcagno, N., El Fatimy, R., Beckers, L., O'loughlin, E., Xu, Y., Fanek, Z., Greco, D. J., Smith, S. T., Tweet, G., Humulock, Z., Zrzavy, T., Conde-Sanroman, P., Gacias, M., Weng, Z., Chen, H., Tjon, E., Mazaheri, F., Hartmann, K., Madi, A., Ulrich, J. D., Glatzel, M., Worthmann, A., Heeren, J., Budnik, B., Lemere, C., Ikezu, T., Heppner, F. L., Litvak, V., Holtzman, D. M., Lassmann, H., Weiner, H. L., Ochando, J., Haass, C. & Butovsky, O. 2017. The TREM2-APOE Pathway Drives the Transcriptional Phenotype of Dysfunctional Microglia in Neurodegenerative Diseases. *Immunity,* 47**,** 566-581 e9.

Kumar, S., Phaneuf, D., Cordeau, P., Jr., Boutej, H., Kriz, J. & Julien, J. P. 2021. Induction of autophagy mitigates TDP-43 pathology and translational repression of neurofilament mRNAs in mouse models of ALS/FTD. *Mol Neurodegener,* 16**,** 1.

Kundu, S. T., Grzeskowiak, C. L., Fradette, J. J., Gibson, L. A., Rodriguez, L. B., Creighton, C. J., Scott, K. L. & Gibbons, D. L. 2018. TMEM106B drives lung cancer metastasis by inducing TFEB-dependent lysosome synthesis and secretion of cathepsins. *Nat Commun,* 9**,** 2731.

Kunkle, B. W., Grenier-Boley, B., Sims, R., Bis, J. C., Damotte, V., Naj, A. C., Boland, A., Vronskaya, M., Van Der Lee, S. J., Amlie-Wolf, A., Bellenguez, C., Frizatti, A., Chouraki, V., Martin, E. R., Sleegers, K., Badarinarayan, N., Jakobsdottir, J., Hamilton-Nelson, K. L., Moreno-Grau, S., Olaso, R., Raybould, R., Chen, Y., Kuzma, A. B., Hiltunen, M., Morgan, T., Ahmad, S., Vardarajan, B. N., Epelbaum, J., Hoffmann, P., Boada, M., Beecham, G. W., Garnier, J. G., Harold, D., Fitzpatrick, A. L., Valladares, O., Moutet, M. L., Gerrish, A., Smith, A. V., Qu, L., Bacq, D., Denning, N., Jian, X., Zhao, Y., Del Zompo, M., Fox, N. C., Choi, S. H., Mateo, I., Hughes, J. T., Adams, H. H., Malamon, J., Sanchez-Garcia, F., Patel, Y., Brody, J. A., Dombroski, B. A., Naranjo, M. C. D., Daniilidou, M., Eiriksdottir, G., Mukherjee, S., Wallon, D., Uphill, J., Aspelund, T., Cantwell, L. B., Garzia, F., Galimberti, D., Hofer, E., Butkiewicz, M., Fin, B., Scarpini, E., Sarnowski, C., Bush, W. S., Meslage, S., Kornhuber, J., White, C. C., Song, Y., Barber, R. C., Engelborghs, S., Sordon, S., Voijnovic, D., Adams, P. M., Vandenberghe, R., Mayhaus, M., Cupples, L. A., Albert, M. S., De Deyn, P. P., Gu, W., Himali, J. J., Beekly, D., Squassina, A., Hartmann, A. M., Orellana, A., Blacker, D., Rodriguez-Rodriguez, E., Lovestone, S., Garcia, M. E., Doody, R. S., Munoz-Fernadez, C., Sussams, R., Lin, H., Fairchild, T. J., Benito, Y. A., et al. 2019. Genetic meta-analysis of diagnosed Alzheimer's disease identifies new risk loci and implicates Abeta, tau, immunity and lipid processing. *Nat Genet,* 51**,** 414-430.

Lang, C. M., Fellerer, K., Schwenk, B. M., Kuhn, P. H., Kremmer, E., Edbauer, D., Capell, A. & Haass, C. 2012. Membrane orientation and subcellular localization of transmembrane protein 106B (TMEM106B), a major risk factor for frontotemporal lobar degeneration. *J Biol Chem,* 287**,** 19355-65.

Lant, S. B., Robinson, A. C., Thompson, J. C., Rollinson, S., Pickering-Brown, S., Snowden, J. S., Davidson, Y. S., Gerhard, A. & Mann, D. M. 2014. Patterns of microglial cell activation in frontotemporal lobar degeneration. *Neuropathol Appl Neurobiol,* 40**,** 686-96.

Laplante, M. & Sabatini, D. M. 2009. mTOR signaling at a glance. *J Cell Sci,* 122**,** 3589-94.

Lattante, S., Le Ber, I., Galimberti, D., Serpente, M., Rivaud-Pechoux, S., Camuzat, A., Clot, F., Fenoglio, C., French Research Network On, F. T. D., Ftd, A. L. S., Scarpini, E.,

Brice, A. & Kabashi, E. 2014. Defining the association of TMEM106B variants among frontotemporal lobar degeneration patients with GRN mutations and C9orf72 repeat expansions. *Neurobiol Aging,* 35**,** 2658 e1-2658 e5.

Laurent-Matha, V., Derocq, D., Prebois, C., Katunuma, N. & Liaudet-Coopman, E. 2006. Processing of human cathepsin D is independent of its catalytic function and auto-activation: involvement of cathepsins L and B. *J Biochem,* 139**,** 363-71.

Lee, A., Rayner, S. L., Gwee, S. S. L., De Luca, A., Shahheydari, H., Sundaramoorthy, V., Ragagnin, A., Morsch, M., Radford, R., Galper, J., Freckleton, S., Shi, B., Walker, A. K., Don, E. K., Cole, N. J., Yang, S., Williams, K. L., Yerbury, J. J., Blair, I. P., Atkin, J. D., Molloy, M. P. & Chung, R. S. 2018. Pathogenic mutation in the ALS/FTD gene, CCNF, causes elevated Lys48-linked ubiquitylation and defective autophagy. *Cell Mol Life Sci,* 75**,** 335-354.

Lee, C. W., Stankowski, J. N., Chew, J., Cook, C. N., Lam, Y. W., Almeida, S., Carlomagno, Y., Lau, K. F., Prudencio, M., Gao, F. B., Bogyo, M., Dickson, D. W. & Petrucelli, L. 2017. The lysosomal protein cathepsin L is a progranulin protease. *Mol Neurodegener,* 12**,** 55.

Lewcock, J. W., Schlepckow, K., Di Paolo, G., Tahirovic, S., Monroe, K. M. & Haass, C. 2020. Emerging Microglia Biology Defines Novel Therapeutic Approaches for Alzheimer's Disease. *Neuron,* 108**,** 801-821.

Li, Q., Yokoshi, M., Okada, H. & Kawahara, Y. 2015. The cleavage pattern of TDP-43 determines its rate of clearance and cytotoxicity. *Nat Commun,* 6**,** 6183.

Li, Z., Farias, F. H. G., Dube, U., Del-Aguila, J. L., Mihindukulasuriya, K. A., Fernandez, M. V., Ibanez, L., Budde, J. P., Wang, F., Lake, A. M., Deming, Y., Perez, J., Yang, C., Bahena, J. A., Qin, W., Bradley, J. L., Davenport, R., Bergmann, K., Morris, J. C., Perrin, R. J., Benitez, B. A., Dougherty, J. D., Harari, O. & Cruchaga, C. 2020. The TMEM106B FTLD-protective variant, rs1990621, is also associated with increased neuronal proportion. *Acta Neuropathol,* 139**,** 45-61.

Liao, Y. C., Fernandopulle, M. S., Wang, G., Choi, H., Hao, L., Drerup, C. M., Patel, R., Qamar, S., Nixon-Abell, J., Shen, Y., Meadows, W., Vendruscolo, M., Knowles, T. P. J., Nelson, M., Czekalska, M. A., Musteikyte, G., Gachechiladze, M. A., Stephens, C. A., Pasolli, H. A., Forrest, L. R., St George-Hyslop, P., Lippincott-Schwartz, J. & Ward, M. E. 2019. RNA Granules Hitchhike on Lysosomes for Long-Distance Transport, Using Annexin A11 as a Molecular Tether. *Cell,* 179**,** 147-164 e20.

Ling, S. C., Polymenidou, M. & Cleveland, D. W. 2013. Converging mechanisms in ALS and FTD: disrupted RNA and protein homeostasis. *Neuron,* 79**,** 416-38.

Lu, R. C., Wang, H., Tan, M. S., Yu, J. T. & Tan, L. 2014. TMEM106B and APOE polymorphisms interact to confer risk for late-onset Alzheimer's disease in Han Chinese. *J Neural Transm (Vienna),* 121**,** 283-7.

Lui, H., Zhang, J., Makinson, S. R., Cahill, M. K., Kelley, K. W., Huang, H. Y., Shang, Y., Oldham, M. C., Martens, L. H., Gao, F., Coppola, G., Sloan, S. A., Hsieh, C. L., Kim, C. C., Bigio, E. H., Weintraub, S., Mesulam, M. M., Rademakers, R., Mackenzie, I. R., Seeley, W. W., Karydas, A., Miller, B. L., Borroni, B., Ghidoni, R., Farese, R. V., Jr., Paz, J. T., Barres, B. A. & Huang, E. J. 2016. Progranulin Deficiency Promotes Circuit-Specific Synaptic Pruning by Microglia via Complement Activation. *Cell,* 165**,** 921-35.

Lüningschrör, P., Werner, G., Stroobants, S., Kakuta, S., Dombert, B., Sinske, D., Wanner, R., Lullmann-Rauch, R., Wefers, B., Wurst, W., D'hooge, R., Uchiyama, Y., Sendtner, M., Haass, C., Saftig, P., Knoll, B., Capell, A. & Damme, M. 2020. The FTLD Risk Factor TMEM106B Regulates the Transport of Lysosomes at the Axon Initial Segment of Motoneurons. *Cell Rep,* 30**,** 3506-3519 e6.

Mackenzie, I. R. & Rademakers, R. 2008. The role of transactive response DNA-binding protein-43 in amyotrophic lateral sclerosis and frontotemporal dementia. *Curr Opin Neurol,* 21**,** 693-700.

Macosko, E. Z., Basu, A., Satija, R., Nemesh, J., Shekhar, K., Goldman, M., Tirosh, I., Bialas, A. R., Kamitaki, N., Martersteck, E. M., Trombetta, J. J., Weitz, D. A., Sanes, J. R., Shalek, A. K., Regev, A. & Mccarroll, S. A. 2015. Highly Parallel Genome-wide Expression Profiling of Individual Cells Using Nanoliter Droplets. *Cell,* 161**,** 1202-14.

Marschallinger, J., Iram, T., Zardeneta, M., Lee, S. E., Lehallier, B., Haney, M. S., Pluvinage, J. V., Mathur, V., Hahn, O., Morgens, D. W., Kim, J., Tevini, J., Felder, T. K., Wolinski, H., Bertozzi, C. R., Bassik, M. C., Aigner, L. & Wyss-Coray, T. 2020. Lipid-droplet-accumulating microglia represent a dysfunctional and proinflammatory state in the aging brain. *Nat Neurosci,* 23**,** 194-208.

Martens, L. H., Zhang, J., Barmada, S. J., Zhou, P., Kamiya, S., Sun, B., Min, S. W., Gan, L., Finkbeiner, S., Huang, E. J. & Farese, R. V., Jr. 2012. Progranulin deficiency promotes neuroinflammation and neuron loss following toxin-induced injury. *J Clin Invest,* 122**,** 3955-9.

Matcovitch-Natan, O., Winter, D. R., Giladi, A., Vargas Aguilar, S., Spinrad, A., Sarrazin, S., Ben-Yehuda, H., David, E., Zelada Gonzalez, F., Perrin, P., Keren-Shaul, H., Gury, M., Lara-Astaiso, D., Thaiss, C. A., Cohen, M., Bahar Halpern, K., Baruch, K., Deczkowska, A., Lorenzo-Vivas, E., Itzkovitz, S., Elinav, E., Sieweke, M. H., Schwartz, M. & Amit, I. 2016. Microglia development follows a stepwise program to regulate brain homeostasis. *Science,* 353**,** aad8670.

Mazaheri, F., Snaidero, N., Kleinberger, G., Madore, C., Daria, A., Werner, G., Krasemann, S., Capell, A., Trumbach, D., Wurst, W., Brunner, B., Bultmann, S., Tahirovic, S., Kerschensteiner, M., Misgeld, T., Butovsky, O. & Haass, C. 2017. TREM2 deficiency impairs chemotaxis and microglial responses to neuronal injury. *EMBO Rep,* 18**,** 1186-1198.

Mendsaikhan, A., Tooyama, I. & Walker, D. G. 2019. Microglial Progranulin: Involvement in Alzheimer's Disease and Neurodegenerative Diseases. *Cells,* 8.

Milind, N., Preuss, C., Haber, A., Ananda, G., Mukherjee, S., John, C., Shapley, S., Logsdon, B. A., Crane, P. K. & Carter, G. W. 2020. Transcriptomic stratification of late-onset Alzheimer's cases reveals novel genetic modifiers of disease pathology. *PLoS Genet,* 16**,** e1008775.

Moisse, K., Volkening, K., Leystra-Lantz, C., Welch, I., Hill, T. & Strong, M. J. 2009. Divergent patterns of cytosolic TDP-43 and neuronal progranulin expression following axotomy: implications for TDP-43 in the physiological response to neuronal injury. *Brain Res,* 1249**,** 202-11.

Monroe, K. M. & Di Paolo, G. 2021. Microglia clean up toxic lipids in multiple sclerosis. *Nat Neurosci,* 24**,** 451-452.

Moore, K. M., Nicholas, J., Grossman, M., Mcmillan, C. T., Irwin, D. J., Massimo, L., Van Deerlin, V. M., Warren, J. D., Fox, N. C., Rossor, M. N., Mead, S., Bocchetta, M., Boeve, B. F., Knopman, D. S., Graff-Radford, N. R., Forsberg, L. K., Rademakers, R., Wszolek, Z. K., Van Swieten, J. C., Jiskoot, L. C., Meeter, L. H., Dopper, E. G., Papma, J. M., Snowden, J. S., Saxon, J., Jones, M., Pickering-Brown, S., Le Ber, I., Camuzat, A., Brice, A., Caroppo, P., Ghidoni, R., Pievani, M., Benussi, L., Binetti, G., Dickerson, B. C., Lucente, D., Krivensky, S., Graff, C., Oijerstedt, L., Fallstrom, M., Thonberg, H., Ghoshal, N., Morris, J. C., Borroni, B., Benussi, A., Padovani, A., Galimberti, D., Scarpini, E., Fumagalli, G. G., Mackenzie, I. R., Hsiung, G. R., Sengdy, P., Boxer, A. L., Rosen, H., Taylor, J. B., Synofzik, M., Wilke, C., Sulzer, P., Hodges, J. R., Halliday, G., Kwok, J., Sanchez-Valle, R., Llado, A., Borrego-Ecija, S., Santana, I., Almeida, M. R., Tabuas-Pereira, M., Moreno, F., Barandiaran, M., Indakoetxea, B., Levin, J., Danek,

A., Rowe, J. B., Cope, T. E., Otto, M., Anderl-Straub, S., De Mendonca, A., Maruta, C., Masellis, M., Black, S. E., Couratier, P., Lautrette, G., Huey, E. D., Sorbi, S., Nacmias, B., Laforce, R., Jr., Tremblay, M. L., Vandenberghe, R., Damme, P. V., Rogalski, E. J., Weintraub, S., Gerhard, A., Onyike, C. U., Ducharme, S., Papageorgiou, S. G., Ng, A. S. L., Brodtmann, A., Finger, E., Guerreiro, R., et al. 2020. Age at symptom onset and death and disease duration in genetic frontotemporal dementia: an international retrospective cohort study. *Lancet Neurol,* 19**,** 145-156.

Nag, S., Yu, L., Boyle, P. A., Leurgans, S. E., Bennett, D. A. & Schneider, J. A. 2018. TDP-43 pathology in anterior temporal pole cortex in aging and Alzheimer's disease. *Acta Neuropathol Commun,* 6**,** 33.

Nagano, S., Jinno, J., Abdelhamid, R. F., Jin, Y., Shibata, M., Watanabe, S., Hirokawa, S., Nishizawa, M., Sakimura, K., Onodera, O., Okada, H., Okada, T., Saito, Y., Takahashi-Fujigasaki, J., Murayama, S., Wakatsuki, S., Mochizuki, H. & Araki, T. 2020. TDP-43 transports ribosomal protein mRNA to regulate axonal local translation in neuronal axons. *Acta Neuropathol,* 140**,** 695-713.

Nasu T, T. Y., Terayama K, Mamiya N 1970. An autopsy case of "membranous lipodystrophy" with myeloosteopathy of long bones and leucodystrophy of the brain (in Japanese).

Neary, D., Snowden, J. & Mann, D. 2005. Frontotemporal dementia. *Lancet Neurol,* 4**,** 771-80.

Nelson, P. T., Dickson, D. W., Trojanowski, J. Q., Jack, C. R., Boyle, P. A., Arfanakis, K., Rademakers, R., Alafuzoff, I., Attems, J., Brayne, C., Coyle-Gilchrist, I. T. S., Chui, H. C., Fardo, D. W., Flanagan, M. E., Halliday, G., Hokkanen, S. R. K., Hunter, S., Jicha, G. A., Katsumata, Y., Kawas, C. H., Keene, C. D., Kovacs, G. G., Kukull, W. A., Levey, A. I., Makkinejad, N., Montine, T. J., Murayama, S., Murray, M. E., Nag, S., Rissman, R. A., Seeley, W. W., Sperling, R. A., White Iii, C. L., Yu, L. & Schneider, J. A. 2019. Limbic-predominant age-related TDP-43 encephalopathy (LATE): consensus working group report. *Brain,* 142**,** 1503-1527.

Neumann, M., Kwong, L. K., Lee, E. B., Kremmer, E., Flatley, A., Xu, Y., Forman, M. S., Troost, D., Kretzschmar, H. A., Trojanowski, J. Q. & Lee, V. M. 2009. Phosphorylation of S409/410 of TDP-43 is a consistent feature in all sporadic and familial forms of TDP-43 proteinopathies. *Acta Neuropathol,* 117**,** 137-49.

Neumann, M. & Mackenzie, I. R. A. 2019. Review: Neuropathology of non-tau frontotemporal lobar degeneration. *Neuropathol Appl Neurobiol,* 45**,** 19-40.

Neumann, M., Sampathu, D. M., Kwong, L. K., Truax, A. C., Micsenyi, M. C., Chou, T. T., Bruce, J., Schuck, T., Grossman, M., Clark, C. M., Mccluskey, L. F., Miller, B. L., Masliah, E., Mackenzie, I. R., Feldman, H., Feiden, W., Kretzschmar, H. A., Trojanowski, J. Q. & Lee, V. M. 2006. Ubiquitinated TDP-43 in frontotemporal lobar degeneration and amyotrophic lateral sclerosis. *Science,* 314**,** 130-3.

Nicholson, A. M., Finch, N. A., Wojtas, A., Baker, M. C., Perkerson, R. B., 3rd, Castanedes-Casey, M., Rousseau, L., Benussi, L., Binetti, G., Ghidoni, R., Hsiung, G. Y., Mackenzie, I. R., Finger, E., Boeve, B. F., Ertekin-Taner, N., Graff-Radford, N. R., Dickson, D. W. & Rademakers, R. 2013. TMEM106B p.T185S regulates TMEM106B protein levels: implications for frontotemporal dementia. *J Neurochem,* 126**,** 781-91.

Nicholson, A. M. & Rademakers, R. 2016. What we know about TMEM106B in neurodegeneration. *Acta Neuropathol,* 132**,** 639-651.

Nicholson, A. M., Zhou, X., Perkerson, R. B., Parsons, T. M., Chew, J., Brooks, M., Dejesus-Hernandez, M., Finch, N. A., Matchett, B. J., Kurti, A., Jansen-West, K. R., Perkerson, E., Daughrity, L., Castanedes-Casey, M., Rousseau, L., Phillips, V., Hu, F., Gendron, T. F., Murray, M. E., Dickson, D. W., Fryer, J. D., Petrucelli, L. & Rademakers, R. 2018. Loss of Tmem106b is unable to ameliorate frontotemporal dementia-like phenotypes in an AAV mouse model of C9ORF72-repeat induced toxicity. *Acta Neuropathol Commun,* 6**,** 42.

Olney, N. T., Spina, S. & Miller, B. L. 2017. Frontotemporal Dementia. *Neurol Clin,* 35**,** 339-374.

Ou, S. H., Chalmers, Z. R., Azada, M. C., Ross, J. S., Stephens, P. J., Ali, S. M. & Miller, V. A. 2015. Identification of a novel TMEM106B-ROS1 fusion variant in lung adenocarcinoma by comprehensive genomic profiling. *Lung Cancer,* 88**,** 352-4.

Palmieri, M., Impey, S., Kang, H., Di Ronza, A., Pelz, C., Sardiello, M. & Ballabio, A. 2011. Characterization of the CLEAR network reveals an integrated control of cellular clearance pathways. *Hum Mol Genet,* 20**,** 3852-66.

Paloneva, J., Kestila, M., Wu, J., Salminen, A., Bohling, T., Ruotsalainen, V., Hakola, P., Bakker, A. B., Phillips, J. H., Pekkarinen, P., Lanier, L. L., Timonen, T. & Peltonen, L. 2000. Loss-of-function mutations in TYROBP (DAP12) result in a presenile dementia with bone cysts. *Nat Genet,* 25**,** 357-61.

Parhizkar, S., Arzberger, T., Brendel, M., Kleinberger, G., Deussing, M., Focke, C., Nuscher, B., Xiong, M., Ghasemigharagoz, A., Katzmarski, N., Krasemann, S., Lichtenthaler, S. F., Muller, S. A., Colombo, A., Monasor, L. S., Tahirovic, S., Herms, J., Willem, M., Pettkus, N., Butovsky, O., Bartenstein, P., Edbauer, D., Rominger, A., Erturk, A., Grathwohl, S. A., Neher, J. J., Holtzman, D. M., Meyer-Luehmann, M. & Haass, C. 2019. Loss of TREM2 function increases amyloid seeding but reduces plaque-associated ApoE. *Nat Neurosci,* 22**,** 191-204.

Paushter, D. H., Du, H., Feng, T. & Hu, F. 2018. The lysosomal function of progranulin, a guardian against neurodegeneration. *Acta Neuropathol,* 136**,** 1-17.

Peng, Q., Malhotra, S., Torchia, J. A., Kerr, W. G., Coggeshall, K. M. & Humphrey, M. B. 2010. TREM2- and DAP12-dependent activation of PI3K requires DAP10 and is inhibited by SHIP1. *Sci Signal,* 3**,** ra38.

Petkau, T. L., Blanco, J. & Leavitt, B. R. 2017. Conditional loss of progranulin in neurons is not sufficient to cause neuronal ceroid lipofuscinosis-like neuropathology in mice. *Neurobiol Dis,* 106**,** 14-22.

Petkau, T. L. & Leavitt, B. R. 2014. Progranulin in neurodegenerative disease. *Trends Neurosci,* 37**,** 388-398.

Pickford, F., Marcus, J., Camargo, L. M., Xiao, Q., Graham, D., Mo, J. R., Burkhardt, M., Kulkarni, V., Crispino, J., Hering, H. & Hutton, M. 2011. Progranulin is a chemoattractant for microglia and stimulates their endocytic activity. *Am J Pathol,* 178**,** 284-95.

Poliani, P. L., Wang, Y., Fontana, E., Robinette, M. L., Yamanishi, Y., Gilfillan, S. & Colonna, M. 2015. TREM2 sustains microglial expansion during aging and response to demyelination. *J Clin Invest,* 125**,** 2161-70.

Polson, H. E., De Lartigue, J., Rigden, D. J., Reedijk, M., Urbe, S., Clague, M. J. & Tooze, S. A. 2010. Mammalian Atg18 (WIPI2) localizes to omegasome-anchored phagophores and positively regulates LC3 lipidation. *Autophagy,* 6**,** 506-22.

Porta, S., Xu, Y., Restrepo, C. R., Kwong, L. K., Zhang, B., Brown, H. J., Lee, E. B., Trojanowski, J. Q. & Lee, V. M. 2018. Patient-derived frontotemporal lobar degeneration brain extracts induce formation and spreading of TDP-43 pathology in vivo. *Nat Commun,* 9**,** 4220.

Pottier, C., Zhou, X., Perkerson, R. B., Baker, M., Jenkins, G. D., Serie, D. J., Ghidoni, R., Benussi, L., Binetti, G., López De Munain, A., Zulaica, M., Moreno, F., Le Ber, I., Pasquier, F., Hannequin, D., Sánchez-Valle, R., Antonell, A., Lladó, A., Parsons, T. M., Finch, N. A., Finger, E. C., Lippa, C. F., Huey, E. D., Neumann, M., Heutink, P., Synofzik, M., Wilke, C., Rissman, R. A., Slawek, J., Sitek, E., Johannsen, P., Nielsen, J. E., Ren, Y., Van Blitterswijk, M., Dejesus-Hernandez, M., Christopher, E., Murray, M. E., Bieniek, K. F., Evers, B. M., Ferrari, C., Rollinson, S., Richardson, A., Scarpini, E., Fumagalli, G. G., Padovani, A., Hardy, J., Momeni, P., Ferrari, R., Frangipane, F.,

Maletta, R., Anfossi, M., Gallo, M., Petrucelli, L., Suh, E., Lopez, O. L., Wong, T. H., Van Rooij, J. G. J., Seelaar, H., Mead, S., Caselli, R. J., Reiman, E. M., Noel Sabbagh, M., Kjolby, M., Nykjaer, A., Karydas, A. M., Boxer, A. L., Grinberg, L. T., Grafman, J., Spina, S., Oblak, A., Mesulam, M. M., Weintraub, S., Geula, C., Hodges, J. R., Piguet, O., Brooks, W. S., Irwin, D. J., Trojanowski, J. Q., Lee, E. B., Josephs, K. A., Parisi, J. E., Ertekin-Taner, N., Knopman, D. S., Nacmias, B., Piaceri, I., Bagnoli, S., Sorbi, S., Gearing, M., Glass, J., Beach, T. G., Black, S. E., Masellis, M., Rogaeva, E., Vonsattel, J.-P., Honig, L. S., Kofler, J., Bruni, A. C., Snowden, J., Mann, D., Pickering-Brown, S., et al. 2018. Potential genetic modifiers of disease risk and age at onset in patients with frontotemporal lobar degeneration and GRN mutations: a genome-wide association study. *Lancet Neurol,* 17**,** 548-558.

Price, B. R., Sudduth, T. L., Weekman, E. M., Johnson, S., Hawthorne, D., Woolums, A. & Wilcock, D. M. 2020. Therapeutic Trem2 activation ameliorates amyloid-beta deposition and improves cognition in the 5XFAD model of amyloid deposition. *J Neuroinflammation,* 17**,** 238.

Prudencio, M., Jansen-West, K. R., Lee, W. C., Gendron, T. F., Zhang, Y. J., Xu, Y. F., Gass, J., Stuani, C., Stetler, C., Rademakers, R., Dickson, D. W., Buratti, E. & Petrucelli, L. 2012. Misregulation of human sortilin splicing leads to the generation of a nonfunctional progranulin receptor. *Proc Natl Acad Sci U S A,* 109**,** 21510-5.

Pu, J., Schindler, C., Jia, R., Jarnik, M., Backlund, P. & Bonifacino, J. S. 2015. BORC, a multisubunit complex that regulates lysosome positioning. *Dev Cell,* 33**,** 176-88.

Rascovsky, K., Hodges, J. R., Knopman, D., Mendez, M. F., Kramer, J. H., Neuhaus, J., Van Swieten, J. C., Seelaar, H., Dopper, E. G., Onyike, C. U., Hillis, A. E., Josephs, K. A., Boeve, B. F., Kertesz, A., Seeley, W. W., Rankin, K. P., Johnson, J. K., Gorno-Tempini, M. L., Rosen, H., Prioleau-Latham, C. E., Lee, A., Kipps, C. M., Lillo, P., Piguet, O., Rohrer, J. D., Rossor, M. N., Warren, J. D., Fox, N. C., Galasko, D., Salmon, D. P., Black, S. E., Mesulam, M., Weintraub, S., Dickerson, B. C., Diehl-Schmid, J., Pasquier, F., Deramecourt, V., Lebert, F., Pijnenburg, Y., Chow, T. W., Manes, F., Grafman, J., Cappa, S. F., Freedman, M., Grossman, M. & Miller, B. L. 2011. Sensitivity of revised diagnostic criteria for the behavioural variant of frontotemporal dementia. *Brain,* 134**,** 2456-77.

Renton, A. E., Majounie, E., Waite, A., Simon-Sanchez, J., Rollinson, S., Gibbs, J. R., Schymick, J. C., Laaksovirta, H., Van Swieten, J. C., Myllykangas, L., Kalimo, H., Paetau, A., Abramzon, Y., Remes, A. M., Kaganovich, A., Scholz, S. W., Duckworth, J., Ding, J., Harmer, D. W., Hernandez, D. G., Johnson, J. O., Mok, K., Ryten, M., Trabzuni, D., Guerreiro, R. J., Orrell, R. W., Neal, J., Murray, A., Pearson, J., Jansen, I. E., Sondervan, D., Seelaar, H., Blake, D., Young, K., Halliwell, N., Callister, J. B., Toulson, G., Richardson, A., Gerhard, A., Snowden, J., Mann, D., Neary, D., Nalls, M. A., Peuralinna, T., Jansson, L., Isoviita, V. M., Kaivorinne, A. L., Holtta-Vuori, M., Ikonen, E., Sulkava, R., Benatar, M., Wuu, J., Chio, A., Restagno, G., Borghero, G., Sabatelli, M., Consortium, I., Heckerman, D., Rogaeva, E., Zinman, L., Rothstein, J. D., Sendtner, M., Drepper, C., Eichler, E. E., Alkan, C., Abdullaev, Z., Pack, S. D., Dutra, A., Pak, E., Hardy, J., Singleton, A., Williams, N. M., Heutink, P., Pickering-Brown, S., Morris, H. R., Tienari, P. J. & Traynor, B. J. 2011. A hexanucleotide repeat expansion in C9ORF72 is the cause of chromosome 9p21-linked ALS-FTD. *Neuron,* 72**,** 257-68.

Rhinn, H. & Abeliovich, A. 2017. Differential Aging Analysis in Human Cerebral Cortex Identifies Variants in TMEM106B and GRN that Regulate Aging Phenotypes. *Cell Syst,* 4**,** 404-415 e5.

Roczniak-Ferguson, A. & Ferguson, S. M. 2019. Pleiotropic requirements for human TDP-43 in the regulation of cell and organelle homeostasis. *Life Sci Alliance,* 2.

Root, J., Merino, P., Nuckols, A., Johnson, M. & Kukar, T. 2021. Lysosome dysfunction as a cause of neurodegenerative diseases: Lessons from frontotemporal dementia and amyotrophic lateral sclerosis. *Neurobiol Dis,* 154**,** 105360.

Rosen, H. J., Gorno-Tempini, M. L., Goldman, W. P., Perry, R. J., Schuff, N., Weiner, M., Feiwell, R., Kramer, J. H. & Miller, B. L. 2002. Patterns of brain atrophy in frontotemporal dementia and semantic dementia. *Neurology,* 58**,** 198-208.

Rothaug, M., Stroobants, S., Schweizer, M., Peters, J., Zunke, F., Allerding, M., D'hooge, R., Saftig, P. & Blanz, J. 2015. LAMP-2 deficiency leads to hippocampal dysfunction but normal clearance of neuronal substrates of chaperone-mediated autophagy in a mouse model for Danon disease. *Acta Neuropathol Commun,* 3**,** 6.

Rusten, T. E. & Stenmark, H. 2010. p62, an autophagy hero or culprit? *Nat Cell Biol,* 12**,** 207-9.

Rutherford, N. J., Carrasquillo, M. M., Li, M., Bisceglio, G., Menke, J., Josephs, K. A., Parisi, J. E., Petersen, R. C., Graff-Radford, N. R., Younkin, S. G., Dickson, D. W. & Rademakers, R. 2012. TMEM106B risk variant is implicated in the pathologic presentation of Alzheimer disease. *Neurology,* 79**,** 717-8.

Safaiyan, S., Besson-Girard, S., Kaya, T., Cantuti-Castelvetri, L., Liu, L., Ji, H., Schifferer, M., Gouna, G., Usifo, F., Kannaiyan, N., Fitzner, D., Xiang, X., Rossner, M. J., Brendel, M., Gokce, O. & Simons, M. 2021. White matter aging drives microglial diversity. *Neuron,* 109**,** 1100-1117 e10.

Sakoh-Nakatogawa, M., Matoba, K., Asai, E., Kirisako, H., Ishii, J., Noda, N. N., Inagaki, F., Nakatogawa, H. & Ohsumi, Y. 2013. Atg12-Atg5 conjugate enhances E2 activity of Atg3 by rearranging its catalytic site. *Nat Struct Mol Biol,* 20**,** 433-9.

Sanchez-Martin, P. & Komatsu, M. 2018. p62/SQSTM1 - steering the cell through health and disease. *J Cell Sci,* 131.

Schlepckow, K., Kleinberger, G., Fukumori, A., Feederle, R., Lichtenthaler, S. F., Steiner, H. & Haass, C. 2017. An Alzheimer-associated TREM2 variant occurs at the ADAM cleavage site and affects shedding and phagocytic function. *EMBO Mol Med,* 9**,** 1356-1365.

Schlepckow, K., Monroe, K. M., Kleinberger, G., Cantuti-Castelvetri, L., Parhizkar, S., Xia, D., Willem, M., Werner, G., Pettkus, N., Brunner, B., Sulzen, A., Nuscher, B., Hampel, H., Xiang, X., Feederle, R., Tahirovic, S., Park, J. I., Prorok, R., Mahon, C., Liang, C. C., Shi, J., Kim, D. J., Sabelstrom, H., Huang, F., Di Paolo, G., Simons, M., Lewcock, J. W. & Haass, C. 2020. Enhancing protective microglial activities with a dual function TREM2 antibody to the stalk region. *EMBO Mol Med,* 12**,** e11227.

Schmelzle, T. & Hall, M. N. 2000. TOR, a central controller of cell growth. *Cell,* 103**,** 253-62.

Schulze, H. & Sandhoff, K. 2014. Sphingolipids and lysosomal pathologies. *Biochim Biophys Acta,* 1841**,** 799-810.

Schwenk, B. M., Lang, C. M., Hogl, S., Tahirovic, S., Orozco, D., Rentzsch, K., Lichtenthaler, S. F., Hoogenraad, C. C., Capell, A., Haass, C. & Edbauer, D. 2014. The FTLD risk factor TMEM106B and MAP6 control dendritic trafficking of lysosomes. *EMBO J,* 33**,** 450-67.

Seelaar, H., Rohrer, J. D., Pijnenburg, Y. A., Fox, N. C. & Van Swieten, J. C. 2011. Clinical, genetic and pathological heterogeneity of frontotemporal dementia: a review. *J Neurol Neurosurg Psychiatry,* 82**,** 476-86.

Seibenhener, M. L., Geetha, T. & Wooten, M. W. 2007. Sequestosome 1/p62--more than just a scaffold. *FEBS Lett,* 581**,** 175-9.

Sellier, C., Campanari, M. L., Julie Corbier, C., Gaucherot, A., Kolb-Cheynel, I., Oulad-Abdelghani, M., Ruffenach, F., Page, A., Ciura, S., Kabashi, E. & Charlet-Berguerand, N. 2016. Loss of C9ORF72 impairs autophagy and synergizes with polyQ Ataxin-2 to induce motor neuron dysfunction and cell death. *EMBO J,* 35**,** 1276-97.

Shankaran, S. S., Capell, A., Hruscha, A. T., Fellerer, K., Neumann, M., Schmid, B. & Haass, C. 2008. Missense mutations in the progranulin gene linked to frontotemporal lobar degeneration with ubiquitin-immunoreactive inclusions reduce progranulin production and secretion. *J Biol Chem,* 283**,** 1744-1753.

Shatz, O., Holland, P., Elazar, Z. & Simonsen, A. 2016. Complex Relations Between Phospholipids, Autophagy, and Neutral Lipids. *Trends Biochem Sci,* 41**,** 907-923.

Shi, Q., Chowdhury, S., Ma, R., Le, K. X., Hong, S., Caldarone, B. J., Stevens, B. & Lemere, C. A. 2017. Complement C3 deficiency protects against neurodegeneration in aged plaque-rich APP/PS1 mice. *Sci Transl Med,* 9.

Shoyab, M., Mcdonald, V. L., Byles, C., Todaro, G. J. & Plowman, G. D. 1990. Epithelins 1 and 2: isolation and characterization of two cysteine-rich growth-modulating proteins. *Proc Natl Acad Sci U S A,* 87**,** 7912-6.

Simons, C., Dyment, D., Bent, S. J., Crawford, J., D'hooghe, M., Kohlschutter, A., Venkateswaran, S., Helman, G., Poll-The, B. T., Makowski, C. C., Ito, Y., Kernohan, K., Hartley, T., Waisfisz, Q., Taft, R. J., Care4rare, C., Van Der Knaap, M. S. & Wolf, N. I. 2017. A recurrent de novo mutation in TMEM106B causes hypomyelinating leukodystrophy. *Brain,* 140**,** 3105-3111.

Sims, R., Van Der Lee, S. J., Naj, A. C., Bellenguez, C., Badarinarayan, N., Jakobsdottir, J., Kunkle, B. W., Boland, A., Raybould, R., Bis, J. C., Martin, E. R., Grenier-Boley, B., Heilmann-Heimbach, S., Chouraki, V., Kuzma, A. B., Sleegers, K., Vronskaya, M., Ruiz, A., Graham, R. R., Olaso, R., Hoffmann, P., Grove, M. L., Vardarajan, B. N., Hiltunen, M., Nöthen, M. M., White, C. C., Hamilton-Nelson, K. L., Epelbaum, J., Maier, W., Choi, S.-H., Beecham, G. W., Dulary, C., Herms, S., Smith, A. V., Funk, C. C., Derbois, C., Forstner, A. J., Ahmad, S., Li, H., Bacq, D., Harold, D., Satizabal, C. L., Valladares, O., Squassina, A., Thomas, R., Brody, J. A., Qu, L., Sánchez-Juan, P., Morgan, T., Wolters, F. J., Zhao, Y., Garcia, F. S., Denning, N., Fornage, M., Malamon, J., Naranjo, M. C. D., Majounie, E., Mosley, T. H., Dombroski, B., Wallon, D., Lupton, M. K., Dupuis, J., Whitehead, P., Fratiglioni, L., Medway, C., Jian, X., Mukherjee, S., Keller, L., Brown, K., Lin, H., Cantwell, L. B., Panza, F., Mcguinness, B., Moreno-Grau, S., Burgess, J. D., Solfrizzi, V., Proitsi, P., Adams, H. H., Allen, M., Seripa, D., Pastor, P., Cupples, L. A., Price, N. D., Hannequin, D., Frank-García, A., Levy, D., Chakrabarty, P., Caffarra, P., Giegling, I., Beiser, A. S., Giedraitis, V., Hampel, H., Garcia, M. E., Wang, X., Lannfelt, L., Mecocci, P., Eiriksdottir, G., Crane, P. K., Pasquier, F., Boccardi, V., et al. 2017. Rare coding variants in PLCG2, ABI3, and TREM2 implicate microglial-mediated innate immunity in Alzheimer's disease. *Nature Genetics,* 49**,** 1373-1384.

Sirkis, D. W., Bonham, L. W., Aparicio, R. E., Geier, E. G., Ramos, E. M., Wang, Q., Karydas, A., Miller, Z. A., Miller, B. L., Coppola, G. & Yokoyama, J. S. 2016. Rare TREM2 variants associated with Alzheimer's disease display reduced cell surface expression. *Acta Neuropathol Commun,* 4**,** 98.

Slattery, C., Beck, J., Harper, L., Adamson, G., Abdi, Z., Uphill, J., Campbell, T., Druyeh, R., Mahoney, C., Rohrer, J., Kenny, J., Lowe, J., Leung, K., Barnes, J., Clegg, S., Blair, M., Nicholas, J., Guerreiro, R., Rowe, J., Ponto, C., Zerr, I., Kretzschmar, H., Gambetti, P., Crutch, S., Warren, J., Rossor, M., Fox, N., Collinge, J., Schott, J. & Mead, S. 2014. Trem2 variants increase risk of typical early-onset Alzheimer's disease but not of prion or frontotemporal dementia. *J Neurol Neurosurg Psychiatry,* 85**,** e3.

Smith, K. R., Damiano, J., Franceschetti, S., Carpenter, S., Canafoglia, L., Morbin, M., Rossi, G., Pareyson, D., Mole, S. E., Staropoli, J. F., Sims, K. B., Lewis, J., Lin, W. L., Dickson, D. W., Dahl, H. H., Bahlo, M. & Berkovic, S. F. 2012. Strikingly different clinicopathological phenotypes determined by progranulin-mutation dosage. *Am J Hum Genet,* 90**,** 1102-7.

Song, W., Hooli, B., Mullin, K., Jin, S. C., Cella, M., Ulland, T. K., Wang, Y., Tanzi, R. E. & Colonna, M. 2017. Alzheimer's disease-associated TREM2 variants exhibit either decreased or increased ligand-dependent activation. *Alzheimers Dement,* 13**,** 381-387.

Song, W. M. & Colonna, M. 2018a. The identity and function of microglia in neurodegeneration. *Nat Immunol,* 19**,** 1048-1058.

Song, W. M. & Colonna, M. 2018b. The Microglial Response to Neurodegenerative Disease. *Adv Immunol,* 139**,** 1-50.

Stagi, M., Klein, Z. A., Gould, T. J., Bewersdorf, J. & Strittmatter, S. M. 2014. Lysosome size, motility and stress response regulated by fronto-temporal dementia modifier TMEM106B. *Mol Cell Neurosci,* 61**,** 226-40.

Stevens, B., Allen, N. J., Vazquez, L. E., Howell, G. R., Christopherson, K. S., Nouri, N., Micheva, K. D., Mehalow, A. K., Huberman, A. D., Stafford, B., Sher, A., Litke, A. M., Lambris, J. D., Smith, S. J., John, S. W. & Barres, B. A. 2007. The classical complement cascade mediates CNS synapse elimination. *Cell,* 131**,** 1164-78.

Strohm, L. & Behrends, C. 2020. Glia-specific autophagy dysfunction in ALS. *Semin Cell Dev Biol,* 99**,** 172-182.

Suh, H. S., Choi, N., Tarassishin, L. & Lee, S. C. 2012. Regulation of progranulin expression in human microglia and proteolysis of progranulin by matrix metalloproteinase-12 (MMP-12). *PLoS One,* 7**,** e35115.

Takahashi, K., Rochford, C. D. & Neumann, H. 2005. Clearance of apoptotic neurons without inflammation by microglial triggering receptor expressed on myeloid cells-2. *J Exp Med,* 201**,** 647-57.

Takeshige, K., Baba, M., Tsuboi, S., Noda, T. & Ohsumi, Y. 1992. Autophagy in yeast demonstrated with proteinase-deficient mutants and conditions for its induction. *J Cell Biol,* 119**,** 301-11.

Tan, T., Song, Z., Yuan, L., Xiong, W., Deng, X., Ni, B., Chen, Y. & Deng, H. 2016. Genetic analysis of TREM2 variants in Chinese Han patients with sporadic Parkinson's disease. *Neurosci Lett,* 612**,** 189-92.

Tanaka, Y., Chambers, J. K., Matsuwaki, T., Yamanouchi, K. & Nishihara, M. 2014. Possible involvement of lysosomal dysfunction in pathological changes of the brain in aged progranulin-deficient mice. *Acta Neuropathol Commun,* 2**,** 78.

Tanaka, Y., Matsuwaki, T., Yamanouchi, K. & Nishihara, M. 2013. Exacerbated inflammatory responses related to activated microglia after traumatic brain injury in progranulin-deficient mice. *Neuroscience,* 231**,** 49-60.

Tanaka, Y., Suzuki, G., Matsuwaki, T., Hosokawa, M., Serrano, G., Beach, T. G., Yamanouchi, K., Hasegawa, M. & Nishihara, M. 2017. Progranulin regulates lysosomal function and biogenesis through acidification of lysosomes. *Hum Mol Genet,* 26**,** 969-988.

Tayebi, N., Lopez, G., Do, J. & Sidransky, E. 2020. Pro-cathepsin D, Prosaposin, and Progranulin: Lysosomal Networks in Parkinsonism. *Trends Mol Med,* 26**,** 913-923.

Tesi, N., Van Der Lee, S. J., Hulsman, M., Jansen, I. E., Stringa, N., Van Schoor, N. M., Scheltens, P., Van Der Flier, W. M., Huisman, M., Reinders, M. J. T. & Holstege, H. 2020. Immune response and endocytosis pathways are associated with the resilience against Alzheimer's disease. *Transl Psychiatry,* 10**,** 332.

Tome, S. O., Vandenberghe, R., Ospitalieri, S., Van Schoor, E., Tousseyn, T., Otto, M., Von Arnim, C. a. F. & Thal, D. R. 2020. Distinct molecular patterns of TDP-43 pathology in Alzheimer's disease: relationship with clinical phenotypes. *Acta Neuropathol Commun,* 8**,** 61.

Turnbull, I. R., Gilfillan, S., Cella, M., Aoshi, T., Miller, M., Piccio, L., Hernandez, M. & Colonna, M. 2006. Cutting edge: TREM-2 attenuates macrophage activation. *J Immunol,* 177**,** 3520-4.

Ulland, T. K., Song, W. M., Huang, S. C., Ulrich, J. D., Sergushichev, A., Beatty, W. L., Loboda, A. A., Zhou, Y., Cairns, N. J., Kambal, A., Loginicheva, E., Gilfillan, S., Cella, M., Virgin, H. W., Unanue, E. R., Wang, Y., Artyomov, M. N., Holtzman, D. M. & Colonna, M. 2017. TREM2 Maintains Microglial Metabolic Fitness in Alzheimer's Disease. *Cell,* 170**,** 649-663 e13.

Ulrich, J. D. & Holtzman, D. M. 2016. TREM2 Function in Alzheimer's Disease and Neurodegeneration. *ACS Chem Neurosci,* 7**,** 420-7.

Ulrich, J. D., Ulland, T. K., Colonna, M. & Holtzman, D. M. 2017. Elucidating the Role of TREM2 in Alzheimer's Disease. *Neuron,* 94**,** 237-248.

Urwin, H., Authier, A., Nielsen, J. E., Metcalf, D., Powell, C., Froud, K., Malcolm, D. S., Holm, I., Johannsen, P., Brown, J., Fisher, E. M., Van Der Zee, J., Bruyland, M., Consortium, F. R., Van Broeckhoven, C., Collinge, J., Brandner, S., Futter, C. & Isaacs, A. M. 2010. Disruption of endocytic trafficking in frontotemporal dementia with CHMP2B mutations. *Hum Mol Genet,* 19**,** 2228-38.

Vaccari, I., Carbone, A., Previtali, S. C., Mironova, Y. A., Alberizzi, V., Noseda, R., Rivellini, C., Bianchi, F., Del Carro, U., D'antonio, M., Lenk, G. M., Wrabetz, L., Giger, R. J., Meisler, M. H. & Bolino, A. 2015. Loss of Fig4 in both Schwann cells and motor neurons contributes to CMT4J neuropathy. *Hum Mol Genet,* 24**,** 383-96.

Van Blitterswijk, M., Mullen, B., Nicholson, A. M., Bieniek, K. F., Heckman, M. G., Baker, M. C., Dejesus-Hernandez, M., Finch, N. A., Brown, P. H., Murray, M. E., Hsiung, G. Y., Stewart, H., Karydas, A. M., Finger, E., Kertesz, A., Bigio, E. H., Weintraub, S., Mesulam, M., Hatanpaa, K. J., White, C. L., 3rd, Strong, M. J., Beach, T. G., Wszolek, Z. K., Lippa, C., Caselli, R., Petrucelli, L., Josephs, K. A., Parisi, J. E., Knopman, D. S., Petersen, R. C., Mackenzie, I. R., Seeley, W. W., Grinberg, L. T., Miller, B. L., Boylan, K. B., Graff-Radford, N. R., Boeve, B. F., Dickson, D. W. & Rademakers, R. 2014. TMEM106B protects C9ORF72 expansion carriers against frontotemporal dementia. *Acta Neuropathol,* 127**,** 397-406.

Van Deerlin, V. M., Sleiman, P. M., Martinez-Lage, M., Chen-Plotkin, A., Wang, L. S., Graff-Radford, N. R., Dickson, D. W., Rademakers, R., Boeve, B. F., Grossman, M., Arnold, S. E., Mann, D. M., Pickering-Brown, S. M., Seelaar, H., Heutink, P., Van Swieten, J. C., Murrell, J. R., Ghetti, B., Spina, S., Grafman, J., Hodges, J., Spillantini, M. G., Gilman, S., Lieberman, A. P., Kaye, J. A., Woltjer, R. L., Bigio, E. H., Mesulam, M., Al-Sarraj, S., Troakes, C., Rosenberg, R. N., White, C. L., 3rd, Ferrer, I., Llado, A., Neumann, M., Kretzschmar, H. A., Hulette, C. M., Welsh-Bohmer, K. A., Miller, B. L., Alzualde, A., Lopez De Munain, A., Mckee, A. C., Gearing, M., Levey, A. I., Lah, J. J., Hardy, J., Rohrer, J. D., Lashley, T., Mackenzie, I. R., Feldman, H. H., Hamilton, R. L., Dekosky, S. T., Van Der Zee, J., Kumar-Singh, S., Van Broeckhoven, C., Mayeux, R., Vonsattel, J. P., Troncoso, J. C., Kril, J. J., Kwok, J. B., Halliday, G. M., Bird, T. D., Ince, P. G., Shaw, P. J., Cairns, N. J., Morris, J. C., Mclean, C. A., Decarli, C., Ellis, W. G., Freeman, S. H., Frosch, M. P., Growdon, J. H., Perl, D. P., Sano, M., Bennett, D. A., Schneider, J. A., Beach, T. G., Reiman, E. M., Woodruff, B. K., Cummings, J., Vinters, H. V., Miller, C. A., Chui, H. C., Alafuzoff, I., Hartikainen, P., Seilhean, D., Galasko, D., Masliah, E., Cotman, C. W., Tunon, M. T., Martinez, M. C., Munoz, D. G., Carroll, S. L., Marson, D., Riederer, P. F., Bogdanovic, N., Schellenberg, G. D., Hakonarson, H., Trojanowski, J. Q. & Lee, V. M. 2010. Common variants at 7p21 are associated with frontotemporal lobar degeneration with TDP-43 inclusions. *Nat Genet,* 42**,** 234-9.

Van Der Zee, J., Van Langenhove, T., Kleinberger, G., Sleegers, K., Engelborghs, S., Vandenberghe, R., Santens, P., Van Den Broeck, M., Joris, G., Brys, J., Mattheijssens, M., Peeters, K., Cras, P., De Deyn, P. P., Cruts, M. & Van Broeckhoven, C. 2011.

TMEM106B is associated with frontotemporal lobar degeneration in a clinically diagnosed patient cohort. *Brain,* 134**,** 808-15.

Van Langenhove, T., Van Der Zee, J. & Van Broeckhoven, C. 2012. The molecular basis of the frontotemporal lobar degeneration-amyotrophic lateral sclerosis spectrum. *Ann Med,* 44**,** 817-28.

Vass, R., Ashbridge, E., Geser, F., Hu, W. T., Grossman, M., Clay-Falcone, D., Elman, L., Mccluskey, L., Lee, V. M., Van Deerlin, V. M., Trojanowski, J. Q. & Chen-Plotkin, A. S. 2011. Risk genotypes at TMEM106B are associated with cognitive impairment in amyotrophic lateral sclerosis. *Acta Neuropathol,* 121**,** 373-80.

Walker, A. K., Spiller, K. J., Ge, G., Zheng, A., Xu, Y., Zhou, M., Tripathy, K., Kwong, L. K., Trojanowski, J. Q. & Lee, V. M. 2015. Functional recovery in new mouse models of ALS/FTLD after clearance of pathological cytoplasmic TDP-43. *Acta Neuropathol,* 130**,** 643-60.

Wang, S., Mustafa, M., Yuede, C. M., Salazar, S. V., Kong, P., Long, H., Ward, M., Siddiqui, O., Paul, R., Gilfillan, S., Ibrahim, A., Rhinn, H., Tassi, I., Rosenthal, A., Schwabe, T. & Colonna, M. 2020. Anti-human TREM2 induces microglia proliferation and reduces pathology in an Alzheimer's disease model. *J Exp Med,* 217.

Wang, Y., Cella, M., Mallinson, K., Ulrich, J. D., Young, K. L., Robinette, M. L., Gilfillan, S., Krishnan, G. M., Sudhakar, S., Zinselmeyer, B. H., Holtzman, D. M., Cirrito, J. R. & Colonna, M. 2015. TREM2 lipid sensing sustains the microglial response in an Alzheimer's disease model. *Cell,* 160**,** 1061-71.

Wang, Y., Ulland, T. K., Ulrich, J. D., Song, W., Tzaferis, J. A., Hole, J. T., Yuan, P., Mahan, T. E., Shi, Y., Gilfillan, S., Cella, M., Grutzendler, J., Demattos, R. B., Cirrito, J. R., Holtzman, D. M. & Colonna, M. 2016. TREM2-mediated early microglial response limits diffusion and toxicity of amyloid plaques. *J Exp Med,* 213**,** 667-75.

Ward, M. E., Chen, R., Huang, H. Y., Ludwig, C., Telpoukhovskaia, M., Taubes, A., Boudin, H., Minami, S. S., Reichert, M., Albrecht, P., Gelfand, J. M., Cruz-Herranz, A., Cordano, C., Alavi, M. V., Leslie, S., Seeley, W. W., Miller, B. L., Bigio, E., Mesulam, M. M., Bogyo, M. S., Mackenzie, I. R., Staropoli, J. F., Cotman, S. L., Huang, E. J., Gan, L. & Green, A. J. 2017. Individuals with progranulin haploinsufficiency exhibit features of neuronal ceroid lipofuscinosis. *Sci Transl Med,* 9.

Ware, J. B., Sandsmark, D. K. & Diaz-Arrastia, R. 2020. Unravelling the mechanisms of blood-brain barrier dysfunction in repetitive mild head injury. *Brain,* 143**,** 1625-1628.

Wei, F., Zhang, Y., Jian, J., Mundra, J. J., Tian, Q., Lin, J., Lafaille, J. J., Tang, W., Zhao, W., Yu, X. & Liu, C. J. 2014. PGRN protects against colitis progression in mice in an IL-10 and TNFR2 dependent manner. *Sci Rep,* 4**,** 7023.

Werner, G., Damme, M., Schludi, M., Gnorich, J., Wind, K., Fellerer, K., Wefers, B., Wurst, W., Edbauer, D., Brendel, M., Haass, C. & Capell, A. 2020. Loss of TMEM106B potentiates lysosomal and FTLD-like pathology in progranulin-deficient mice. *EMBO Rep,* 21**,** e50241.

Wils, H., Kleinberger, G., Janssens, J., Pereson, S., Joris, G., Cuijt, I., Smits, V., Ceuterick-De Groote, C., Van Broeckhoven, C. & Kumar-Singh, S. 2010. TDP-43 transgenic mice develop spastic paralysis and neuronal inclusions characteristic of ALS and frontotemporal lobar degeneration. *Proc Natl Acad Sci U S A,* 107**,** 3858-63.

Wils, H., Kleinberger, G., Pereson, S., Janssens, J., Capell, A., Van Dam, D., Cuijt, I., Joris, G., De Deyn, P. P., Haass, C., Van Broeckhoven, C. & Kumar-Singh, S. 2012. Cellular ageing, increased mortality and FTLD-TDP-associated neuropathology in progranulin knockout mice. *J Pathol,* 228**,** 67-76.

Winton, M. J., Igaz, L. M., Wong, M. M., Kwong, L. K., Trojanowski, J. Q. & Lee, V. M. 2008. Disturbance of nuclear and cytoplasmic TAR DNA-binding protein (TDP-43) induces

disease-like redistribution, sequestration, and aggregate formation. *J Biol Chem,* 283**,** 13302-9.

Woerner, A. C., Frottin, F., Hornburg, D., Feng, L. R., Meissner, F., Patra, M., Tatzelt, J., Mann, M., Winklhofer, K. F., Hartl, F. U. & Hipp, M. S. 2016. Cytoplasmic protein aggregates interfere with nucleocytoplasmic transport of protein and RNA. *Science,* 351**,** 173-6.

Wong, Y. C. & Holzbaur, E. L. 2014. Optineurin is an autophagy receptor for damaged mitochondria in parkin-mediated mitophagy that is disrupted by an ALS-linked mutation. *Proc Natl Acad Sci U S A,* 111**,** E4439-48.

Wong, Y. C. & Holzbaur, E. L. 2015. Autophagosome dynamics in neurodegeneration at a glance. *J Cell Sci,* 128**,** 1259-67.

Wu, D., Hao, Z., Ren, H. & Wang, G. 2018. Loss of VAPB Regulates Autophagy in a Beclin 1-Dependent Manner. *Neurosci Bull,* 34**,** 1037-1046.

Yan, H., Kubisiak, T., Ji, H., Xiao, J., Wang, J. & Burmeister, M. 2018. The recurrent mutation in TMEM106B also causes hypomyelinating leukodystrophy in China and is a CpG hotspot. *Brain,* 141**,** e36.

Yang, H. S., White, C. C., Klein, H. U., Yu, L., Gaiteri, C., Ma, Y., Felsky, D., Mostafavi, S., Petyuk, V. A., Sperling, R. A., Ertekin-Taner, N., Schneider, J. A., Bennett, D. A. & De Jager, P. L. 2020. Genetics of Gene Expression in the Aging Human Brain Reveal TDP-43 Proteinopathy Pathophysiology. *Neuron,* 107**,** 496-508 e6.

Yeh, F. L., Wang, Y., Tom, I., Gonzalez, L. C. & Sheng, M. 2016. TREM2 Binds to Apolipoproteins, Including APOE and CLU/APOJ, and Thereby Facilitates Uptake of Amyloid-Beta by Microglia. *Neuron,* 91**,** 328-40.

Yin, F., Banerjee, R., Thomas, B., Zhou, P., Qian, L., Jia, T., Ma, X., Ma, Y., Iadecola, C., Beal, M. F., Nathan, C. & Ding, A. 2010. Exaggerated inflammation, impaired host defense, and neuropathology in progranulin-deficient mice. *J Exp Med,* 207**,** 117-28.

Zhang, J., Velmeshev, D., Hashimoto, K., Huang, Y. H., Hofmann, J. W., Shi, X., Chen, J., Leidal, A. M., Dishart, J. G., Cahill, M. K., Kelley, K. W., Liddelow, S. A., Seeley, W. W., Miller, B. L., Walther, T. C., Farese, R. V., Jr., Taylor, J. P., Ullian, E. M., Huang, B., Debnath, J., Wittmann, T., Kriegstein, A. R. & Huang, E. J. 2020. Neurotoxic microglia promote TDP-43 proteinopathy in progranulin deficiency. *Nature,* 588**,** 459-465.

Zhang, Y. J., Xu, Y. F., Dickey, C. A., Buratti, E., Baralle, F., Bailey, R., Pickering-Brown, S., Dickson, D. & Petrucelli, L. 2007. Progranulin mediates caspase-dependent cleavage of TAR DNA binding protein-43. *J Neurosci,* 27**,** 10530-4.

Zheng, J. Q., Kelly, T. K., Chang, B., Ryazantsev, S., Rajasekaran, A. K., Martin, K. C. & Twiss, J. L. 2001. A functional role for intra-axonal protein synthesis during axonal regeneration from adult sensory neurons. *J Neurosci,* 21**,** 9291-303.

Zhou, S. L., Tan, C. C., Hou, X. H., Cao, X. P., Tan, L. & Yu, J. T. 2019. TREM2 Variants and Neurodegenerative Diseases: A Systematic Review and Meta-Analysis. *J Alzheimers Dis,* 68**,** 1171-1184.

Zhou, X., Kukar, T. & Rademakers, R. 2021. Lysosomal Dysfunction and Other Pathomechanisms in FTLD: Evidence from Progranulin Genetics and Biology. *Advances in Experimental Medicine and Biology,* 1281**,** 219-242.

Zhou, X., Nicholson, A. M., Ren, Y., Brooks, M., Jiang, P., Zuberi, A., Phuoc, H. N., Perkerson, R. B., Matchett, B., Parsons, T. M., Finch, N. A., Lin, W., Qiao, W., Castanedes-Casey, M., Phillips, V., Librero, A. L., Asmann, Y., Bu, G., Murray, M. E., Lutz, C., Dickson, D. W. & Rademakers, R. 2020. Loss of TMEM106B leads to myelination deficits: implications for frontotemporal dementia treatment strategies. *Brain,* 143**,** 1905-1919.

Zhou, X., Paushter, D. H., Feng, T., Pardon, C. M., Mendoza, C. S. & Hu, F. 2017a. Regulation of cathepsin D activity by the FTLD protein progranulin. *Acta Neuropathol,* 134**,** 151-153.

Zhou, X., Paushter, D. H., Feng, T., Sun, L., Reinheckel, T. & Hu, F. 2017b. Lysosomal processing of progranulin. *Mol Neurodegener,* 12**,** 62.

Zhou, X., Sun, L., Bastos De Oliveira, F., Qi, X., Brown, W. J., Smolka, M. B., Sun, Y. & Hu, F. 2015. Prosaposin facilitates sortilin-independent lysosomal trafficking of progranulin. *J Cell Biol,* 210**,** 991-1002.

Zhou, X., Sun, L., Bracko, O., Choi, J. W., Jia, Y., Nana, A. L., Brady, O. A., Hernandez, J. C. C., Nishimura, N., Seeley, W. W. & Hu, F. 2017c. Impaired prosaposin lysosomal trafficking in frontotemporal lobar degeneration due to progranulin mutations. *Nat Commun,* 8**,** 15277.

Zhu, J., Nathan, C., Jin, W., Sim, D., Ashcroft, G. S., Wahl, S. M., Lacomis, L., Erdjument-Bromage, H., Tempst, P., Wright, C. D. & Ding, A. 2002. Conversion of proepithelin to epithelins: roles of SLPI and elastase in host defense and wound repair. *Cell,* 111**,** 867-78.

Danksagung

Die letzten Jahre waren eine turbulente und zugleich wunderbare Zeit. Ich bin dankbar, dass ich so viel lernen durfte, meine Begeisterung für die Forschung vertiefen und viele neue Erfahrungen sammeln konnte. Deshalb möchte ich mich an dieser Stelle ganz herzlich bei vielen Menschen, die mich auf dieser Reise begleitet haben, bedanken.

Bei meinem Doktorvater Prof. Dr. Dr. Christian Haass, vielen Dank für Ihre außergewöhnliche Begeisterung an der Forschung, Ihre Unterstützung und dafür, dass Sie mir so viele spannende Projekte anvertraut haben. Danke, dass Sie meine Neugier stets unterstützt haben, es ist einfach großartig, etwas bisher Unbekanntes zu entdecken. Ich hoffe ich kann auch in Zukunft, dem schönsten Hobby auf der Welt, der Forschung, nachgehen.

Dr. Anja Capell, vielen Dank für Deine Unterstützung, die Betreuung, den kontinuierlichen Austausch im Labor. Vielen Dank für die vielen Anregungen die mich immer wieder dazu gebracht haben meine Projekte von einer neuen Seite zu betrachten und danke für die grandiosen Labor-Weihnachtsdinner!

Vielen Dank, auch allen Mitgliedern meiner Prüfungskommission, für das Durchlesen und Bewerten meiner Arbeit.

Für erfolgreiche Experimente benötigt man bekanntlich ausgezeichnete Rahmenbedingungen, und dafür braucht es den gemeinsamen Einsatz von einem super Team, deshalb ein großes Dankeschön an das gesamte Haass-Labor! Insbesondere dem AC-Team, Ramona Rodde, Claudia Thiel, Katrin Buschmann, Marvin Reich, Quirin Mühlhofer und Anika Reifschneider. Ein besonderer Dank an Julia Götzl für die Initiation des PGRN Mikroglia Projekts. Für die anregenden wissenschaftlichen Diskussionen im Casino, Yoshihiro Nihei, Gernot Kleinberger, Kai Schlepckow und Marc Suarez-Calvet. Danke an die „internen Reviewer“ Michael Willem und Sven Lammich. Jane Hettinger, Xianyuan Xiang, Ann-Katrin Bergmann, Heike Hampel, Bettina Brunner, Brigitte Nuscher, Nicole Exner, Ida Pesämaa und Fargol Mazaheri, vielen Dank Euch allen, für eine spannende und abwechslungsreiche Zeit im Labor! Sabine Odoy, danke für Deine Koordination und stetige Nothilfe mit unseren zahlreichen Laborgeräten und Bestellungen.

Danke auch an das tolle Team, von Sabina Tahirovic, Anna, Laura und Alessio, für die Antikörper, den Austausch und die Möglichkeit spannende Assays bei Euch zu lernen.
Danke auch an das gesamte Eddie Lab, ganz besonders an Martin, Mareike, Maike, Carina, Kathie, Henni, Hanne und Dieter Edbauer.
Außerdem einen großen Dank an das gesamte Behrends Lab: Laura, Alex, Susa, Karsten, Julia, und Franzi. Vielen Dank für die vielen Antikörper und die gemeinsame Zeit. Ihr seid ein tolles Autophagie Team! Und natürlich Christian Behrends, für die vielen guten Besprechungen.

Sowie Grüße in den hohen Norden nach Kiel: Danke an Paul Saftig und Markus Damme für die tolle Zeit in Kiel. Danke Markus, dass ich bei Dir so viel über „Floating Sections“ und Mausgehirne lernen durfte. Auf viele spannende TMEM-paper. Danke für die tolle

Zusammenarbeit am TMEM-Paper: Patrick Lüningschrör, Stijn Stroobants, Soichiro Kakuta, Benjamin Dombert, Daniela Sinske, Renate Wanner,Renate Lüllmann-Rauch, Rudi D'Hooge, Yasuo Uchiyama, Michael Sendtner, Bernd Knöll.
Sowie unseren anderen Kollaborationspartnern für die erfolgreiche Zusammenarbeit an so vielen spannenden Projekten: Matthias Brendel, Karin Wind, Johannes Gnörich, Maximiliam Deussing, Axel Rominger, Peter Bartenstein, Matias Wagner, Juliane Winkelmann, Janine Diehl-Schmid, Johannes Levin, Sebastian Bultmann, Peter Bartenstein, Axel Rominger, Scott T Smith, Charlotte Madore und Oleg Butovsky, vielen Dank für die Zusammenarbeit am PGRN Paper.

An das gesamte Maus-Team danke für die tolle Zusammenarbeit: Anne von Thaden, Manuela Schneider, Claudia Ihbe, Stefanie Wurster und allen anderen fleißigen Helfern.

Sowie einen großen Dank an ein paar weitere, ganz besondere Menschen: Basti, Luki, Dietmar, Benedikt, Sven, Alex, Laura (mit Alex), Karsten, Lukas, Julia, Johannes und Susa. Mit Euch kann man wirklich jedes Hindernis überwinden. Vielen Dank für Eure Freundschaft und Hilfe, zu jeder Tages- und Nachtzeit. Für Eure Geduld und Euer Verständnis, wenn es im Labor mal wieder länger gedauert hat. Zum Glück wisst Ihr ja alle selbst wie, das so ist im Labor ;-).

Meiner Familie, die mich immer unterstützt und meine Begeisterung für die Forschung gefördert hat. Danke Markus, Andrea, Martin, Michaela, Josef und ganz besonders meinen Eltern. Ich bin unglaublich glücklich, dass es Euch alle gibt und freue mich schon so sehr darauf Euch alle bald wieder zu umarmen! Zu guter Letzt meiner wundervollen Frau Nadine, danke für Deinen tollen Charakter, Deine Liebe und Deine Begeisterung am Experimentieren. Zusammen können wir alles schaffen, ich bin überzeugt es wird eine fantastische Reise!

Affidavit / Eidesstattliche Versicherung

LMU LUDWIG-MAXIMILIANS-UNIVERSITÄT MÜNCHEN | Promotionsbüro Medizinische Fakultät | MMRS

Eidesstattliche Versicherung

Werner, Georg

Name, Vorname

Ich erkläre hiermit an Eides statt, dass ich die vorliegende Dissertation mit dem Titel:

„Modulation des Progranulin-abhängigen FTLD-Risikos durch TMEM106B“

selbständig verfasst, mich außer der angegebenen keiner weiteren Hilfsmittel bedient und alle Erkenntnisse, die aus dem Schrifttum ganz oder annähernd übernommen sind, als solche kenntlich gemacht und nach ihrer Herkunft unter Bezeichnung der Fundstelle einzeln nachgewiesen habe.

Ich erkläre des Weiteren, dass die hier vorgelegte Dissertation nicht in gleicher oder in ähnlicher Form bei einer anderen Stelle zur Erlangung eines akademischen Grades eingereicht wurde.

München, 21.05.2021 — Ort, Datum

Georg Werner — Unterschrift Doktorandin bzw. Doktorand